Extracting Geodetically Useful Information From Absolute Gravimetry at a Fundamental Geodetic Station

Victoria Anne Smith

Thesis submitted for the degree of Doctor of
Philosophy of the
University College London
2018

Department of Civil, Environmental and Geomatic Engineering
University College London

Declaration

I, Victoria Anne Smith, confirm that the work presented in this thesis is my own. Where information has been derived from other sources, I confirm that this has been indicated in the thesis.

Abstract

Measuring the acceleration due to gravity at the NERC Space Geodesy Facility (SGF), Herstmonceux, provides a complimentary geodetic technique to the long established satellite laser ranging and global navigation satellite system measurements. The gravimetry measurements at the SGF were added to conform to the gravity field objective of the Global Geodetic Observing System and the European Combined Geodetic Network. Since both SLR and GNSS measurements are used in the computation of the International Terrestrial Reference Frame any un-modelled movements in the ground stations are undesirable. Gravity measurements can be used in the identification of such signals.

This thesis reports the establishment of the technique at the SGF and contains a description of the installation experiences, a maintenance guide for the instrument and a comprehensive analysis of the gravity measurements over the ten years of operation to date, from 2006-2016.

Environmentally driven influences on the gravity measurements are investigated. The precision of the measurements are shown to be seasonally dependent and of varying magnitude. The hydrological influence on the gravity data from groundwater variation is calculated to be approximately 3.14 μGal, determined from temporal measurement of groundwater depth and an estimation of soil properties. A maximum influence from soil moisture content is estimated resulting in an influence of less than a microgal, which confuses correlation studies between local tide gauge data and an intermittent periodic signal seen in the gravity data. The high frequency data taken at the SGF highlights bias corrections two explainable and one of unknown origin. The bias corrections, of magnitude +1.5, -2 and -7.33 μGal, are shown to be critical to the interpretation of the time series, and, simulated campaign style measurements, using one set of measurements on an annual basis, prove that the data would be easily misinterpreted if the bias offsets found are not applied.

Impact Statement

Geodetic stations are currently under science-driven pressure to provide observations and analyses of sufficient quality to meet global efforts to realise an international terrestrial reference frame (ITRF) at mm-levels of accuracy and 0.1mm/yr stability. Many of the most accurate and prolific observatories are upgrading and expanding their capabilities with modern versions of the traditional techniques of satellite laser ranging (SLR), very long baseline interferometry (VLBI), global navigation satellite systems (GNSS) receivers and Doppler orbitography and radio-positioning integrated by satellite (DORIS) receivers. With the advent of the International Association of Geodesy initiative to encapsulate ongoing global geodetic efforts under the single banner of a Global Geodetic Observing System (GGOS), there is a general increase in the use, and demand for, gravity measurements at these fundamental stations. The accuracy demands of GGOS are driving improvements not only in the geodetic techniques but also in prompting the measurement and understanding of site-specific un-modelled ground movements which may contaminate and compromise efforts to determine accurate coordinates of each station that contributes to the determination of the ITRF.

Recognising the GGOS initiative, the UK Space Geodesy Facility (SGF), Herstmonceux, took the opportunity to expand instrumentation to include an FG5 absolute gravimeter (AG); previous experience at Herstmonceux was based on two week-long deployments of an AG in collaboration with the National Oceanography Centre, during the 1990s. The work to integrate and begin to exploit the AG, reported in this Thesis, has therefore grown an entirely new capability for the SGF where the traditional space-geodetic techniques are now complimented by a permanently sited absolute gravimeter that is providing a unique dataset. The studies started in this work give a greater understanding of local tidal and hydrological loading effects on vertical crustal signals than previously known, which will eventually have a direct impact on the laser ranging and GNSS analyses. These results are likely to be applicable to other sites, if not directly, at least in highlighting potential shortcomings in existing models.

The SGF now provides the UK with a gravity reference site, which will be a ‘core’ station within the worldwide gravity reference frame currently under development, with the potential to provide key services such as; UK-wide monitoring of vertical signals in tide gauges, to the ability to provide overseas support to shipborne oceanic gravity surveys, by the provision of gravity reference stations.

Acknowledgements

I have so much thanks to express, to family, friends, supervisors, colleagues & to my employer. I would like to wholeheartedly thank my principal supervisor Prof. Marek Ziebart, for offering the opportunity to undertake doctoral studies &, for having the faith, perseverance and enthusiasm which carried me though. I owe particular thanks to Dr Graham Appleby, the head of the Space Geodesy Facility, to whom I owe huge thanks for giving me the responsibility for the gravimeter & his endless support and encouragement. I know I taxed you both on more than one occasion.

Thanks also to Dr. Simon Williams, for offering his expertise and knowledge & perhaps most of all for allowing me to use his processing software 'gap'. In addition I need to thank my colleagues at the SGF for providing a great working environment & allowing me to drop out of SLR observing duties whilst writing up this thesis. I'd like to say thank you to the community of absolute gravimeter users, for being such helpful, lovely people. It is a pleasure to belong to this club. Special thanks to Dr. Derek van Westrum & Dr. Tim Niebauer who have made the instrumental learning curve easier & offering assistance when needed. To all of those who endured proof reading for me I am also very grateful; Dr Appleby, Prof. Ziebart, Dr van Westrum & my brother Nicholas Smith.

To all of my friends who have been so wonderfully supportive & picked me up from dark times, I thank you. Three people who deserving a special mention are Dr. Peter Stacey, for the advice & support, my old school friend Alex Page, for being there to pick me up &, last but not least, my closest & dearest chum Clare Wilson, you are what I call fabulous.

My thanks simply would not be complete without mention of my amazing family, my mother, brother, sister-in-law, nieces & nephew, & to my dogs Tomsk and Bungo. A simple thank you is inadequate. I love you all.

I dedicate this thesis to my all of my family, those present and all of you who didn't make it this far. Miss you Mum and Dad.

Table of Contents

Title Page 1
Declaration 2
Abstract 3
Impact Statement 4
Acknowledgements 6
Table of Contents 7
List of Figures 14
List of Tables 20
Glossary of Terms, Abbreviations and Acronyms 21
Units 22

1. Introduction
1.1. Introduction 23
1.2. A Brief History of Gravity Measurement 23
1.3. A Moment About Newton 28
1.4. Geodetic Facilities 28
1.5. Absolute Gravity Measurement in Geodesy 29
1.6. Outline of Thesis Structure 30

2. The FG5 Absolute Gravimeter
2.1. Introduction 33
2.2. Principles of the Design 35
2.3. Principle Components of the FG5 37
2.3.1. Dropping Chamber 37
2.3.2. Interferometer 41
2.3.3. Laser 44
2.3.4. Super-spring 47
2.3.5. Electronics & Timing 48
2.3.5.1. Laser Controller 49

2.3.5.2. System Interface Module, Magma and System Control 50
2.3.5.3. Timing/Clock 51
2.4. Instrumental Setup 52
2.5. Vertical Alignment 52
2.6. FG5X 53
2.7. Software 55
2.7.1. 'g' software 56

3. Corrections to Absolute Gravity Measurements
3.1. Introduction 59
3.2. Tidal Corrections 59
3.2.1. Tidal Potential 60
3.2.2. Ocean-Loading 64
3.3. Polar Motion 65
3.4. Atmospheric Correction 66
3.5. Hydrological Corrections 67
3.5.1. Bouguer Free Air Correction 67
3.5.2. Bouguer Anomalies 68
3.5.3. Gravity Anomaly for a Buried Sphere 69

4. Comparisons of Absolute Gravimeters
4.1. Introduction 72
4.2. Comparisons and the Absolute Gravimetry Community 73
4.3. Method 75
4.3.1. Adjustment of the Data for Comparison 76
4.3.2. Implementation of Comparison Results 77
4.4. Comparison Sites 77
4.4.1. Walferdange Underground Laboratory for Geodynamics 78
4.4.2. Belval 80

5. The Space Geodesy Facility, Herstmonceux
5.1. Introduction 82
5.1.1. History of the Space Geodesy Facility 82
5.1.2. The Space Geodesy Facility Today 84
5.2. Absolute Gravimetry at the Space Geodesy Facility 88
5.3. Satellite Laser Ranging 89
5.3.1. Specifics of Satellite Laser Ranging at the Space Geodesy Facility 92
5.3.2. Satellite Laser Ranging Satellites 93
5.3.3. Computing Station Coordinates and Heights Using SLR
5.3.4. Measurements 95
5.3.5. Computing Stations Coordinates and Heights Using Global Navigation Satellite Systems Measurements 97
5.3.6. Vertical Height Determination Using AG Measurements 97
5.3.7. Co-Location of Geodetic Techniques at the SGF 98

6. Literary Review and Problem Statement
6.1. Introduction 100
6.1.1. Instrumental 100
6.1.2. Environmental 101
6.1.3. Tidal 102
6.1.4. Height Displacement 103
6.1.5. Previous Absolute Gravity in the UK 104
6.2. Problem Statement 105

7. Absolute Gravity at the Space Geodesy Facility
7.1. Introduction 107
7.2. Location, and Preparation for, the Absolute Gravimeter at Herstmonceux 107
7.3. Data collection and Frequency at the SGF 111
7.4. Absolute Gravimetry from 2005-2016 111
7.5. Working with Four Variants of the FG5. 114

7.6. Comparison of Absolute Gravimeters: Results between 2007 - 2015 115
7.6.1. 2007 - Walferdange, Luxembourg 116
7.6.2. 2011 - SGF, Herstmonceux 119
7.6.3. 2012 - Walferdange, Luxembourg 119
7.6.4. 2015 - Belval, Luxembourg 120
7.7. Conclusions 124

8. Operating and Maintenance Experience with the FG5
8.1. Introduction 125
8.2. Dropping chamber repair 125
8.2.1. Listening to the Dropping Chamber 127
8.2.2. Preparation for Working Inside the Dropping Chamber 127
8.2.2.1. Repair Advice 128
8.2.3. Electrical Tuning 130
8.3. Super-Spring Repairs 131
8.3.1. Example of an Electrical Fault 133
8.3.2. Super-Spring Frequency Response 135
8.4. Laser 137
8.4.1. Laser cleaning and Alignment 139
8.4.2. 5-Axis Mount 141
8.4.3. Interferometer and Polarisation 142
8.4.4. Environmental Conditions 142
8.4.5. Discussion 143
8.5. Conclusions 143

9. Software
9.1. Introduction 144
9.2. Reprocessing Data Using ‘g’ and ‘gap’ 145
9.2.1. An Assessment of ‘g’ 146
9.2.2. An Assessment of’gap’ 147
9.2.3. Summary 149

9.3. Programs Created During this Work 150
9.3.1. Hourly Data 152
9.3.2. Obtaining the Gravity Result 152
9.3.2.1. Time Convention and Conversion 154
9.3.2.2. The VxHg Hourly Results 154
9.3.2.3. Project Data 156
9.3.2.4. Critical Analysis of the VgHx Processing Software 156
9.3.3. Tide Gauge Data Extraction 158
9.4. Conclusions 159

10. Precision of the Gravity Measurements
10.1. Introduction 160
10.2. Investigation of Natural Noise Sources 160
10.2.1. Earthquake Detection 167
10.3. Anthropogenic Noise Sources at the SGF 169
10.4. Conclusions 169

11. Environmental Calculations
11.1. Introduction 170
11.2. Subsurface Investigation by the Royal Greenwich Observatory 170
11.3. Bouguer Approximations 173
11.4. Estimating Properties of the Clay Soil Around the SGF 174
11.4.1. Soil Sample Measurements 176
11.5. Environmental Influences Above and Below the Gravity Laboratory 179
11.5.1. Above the Laboratory 180
11.5.2. Below the Laboratory 181
11.5.3. Changes Affecting the Gravity Laboratory in 2015 183
11.6. Conclusions 186

12. Periodic signals 188
12.1. Short Period Signals 188

12.1.1. Ocean-Loading Model Selection 189
12.2. Tidal Investigation 192
12.3. Conclusions 196

13. The Time Series of Gravity Measurements, 2006 - 2016
13.1. Introduction 198
13.2. Introducing the Time Series of Gravity data 2006-2016 198
13.2.1. Application of the Groundwater Correction 203
13.2.2. Interpretation Using Comparison Data 209
13.3. Comparison of the Gravity Time Series with SLR Coordinate Heights 213
13.4. Simulation of Yearly Campaign Measurement at the SGF 215
13.5. Conclusions 217

14. Discussion
14.1. Introduction 219
14.2. Development of the Absolute Gravity Resource at the SGF 219
14.3. Benefits from Long-Term High Frequency Data 219
14.4. Offsets and Bias Corrections 220

15. Conclusions
15.1. Introduction 222
15.2. Principle Conclusions 222
15.3. Secondary Conclusions 228
15.4. Future Research 229

Appendix 1 Economic Appraisal of the Absolute Gravimeter 230
Appendix 2 Ordnance Survey Gravity Laboratory Stud Survey Results 234
Appendix 3 Example of Project and Set text from ‘g’ 235
Appendix 4 Yearly, Gravity Plots to show Comparison between VgHx and ‘g’ for 2006-2016 241

Appendix 5 Yearly Precision Plots from VgHx (2006-2012) and ‘g’ (2013-2016) 244
Appendix 6 Ocean-Loading Constituents used by ‘gap’ and ‘g’ 250
Appendix 7 Early Operation of the FG5 prior to the Completion of the Gravity Laboratory in 2006 251
Appendix 8 Discussion of the FG5 Timing Frequency Source 259

Bibliography 265

Table of Figures

Figure 1.1 Simple Pendulum 24
Figure 1.2 Schematic of a LaCoste and Romberg relative gravimeter 26
Figure 2.1 Trajectory time and distance diagram 35
Figure 2.2 Schematic drawing of the FG5 absolute gravimeter 36
Figure 2.3 Main components of the FG5 absolute gravimeter 37
Figure 2.4 Schematic sketch of the dropping chamber 38
Figure 2.5 Inside the bottom of the dropping chamber 39
Figure 2.6 Top view drawing of the dropping chamber lower service ring 40
Figure 2.7 The laser path diagrams inside the interferometer 42
Figure 2.8 Operational beam paths through the interferometer 43
Figure 2.9 WEO-100 laser control electronics photograph 45
Figure 2.10 Schematic drawing of the WEO-100 laser configuration 46
Figure 2.11 Basic drawing of the main components in the super-spring assembly 47
Figure 2.12 Super-spring stages 48
Figure 2.13 Photograph of the FG5 electronics rack (computer excluded) 49
Figure 2.14 Communications diagram: the primary input/output paths between components (FG5) 50
Figure 2.15 Timing process diagram 51
Figure 2.16 Interferometer verticality alignment of the FG5 53
Figure 2.17 Photograph of the FG5X 54
Figure 2.18 Communications diagram: the primary input/output paths between components (FG5X) 55
Figure 2.19 Screen shot of a gravity project in ‘g7’ 57
Figure 2.20 Example of a ‘set’ file generated by ‘g’ 58
Figure 3.1 Tidal potential geometry from the Moon 60
Figure 3.2 W_1 geometry 62
Figure 3.3 Diagram to show declination, latitude and hour angle 62
Figure 3.4 Imperfect fit of tidal models to coastline 64
Figure 3.5 Illustration of the path polar motion describes in free space 64

Figure 3.6 Surface topography and geoid relation 67
Figure 3.7 Gravity anomaly from a buried sphere 69
Figure 4.1 Inside the WULG 79
Figure 4.2 Just inside the mine 79
Figure 4.3 Inner regions of the mine 79
Figure 4.4 Belval comparison 80
Figure 5.1 Removal of the solar dome in 1981 prior to installation of the clamshell dome 83
Figure 5.2 The SGF in 2015 84
Figure 5.3 Site map of the SGF 87
Figure 5.4 Example of a retro-reflector array 89
Figure 5.5 Satellite laser ranging at night 89
Figure 5.6 Examples of geodetic satellites tracked by SLR 93
Figure 5.7 Examples of remote sensing satellites tracked by SLR 94
Figure 5.8 Examples of GNSS satellites tracked by SLR 94
Figure 5.9 LAGEOS satellite 95
Figure 5.10 Earth satellite coordinate relation, centred in a reference frame 95
Figure 5.11 CAD drawing of the SGF 99
Figure 7.1 Photographs: The SGF basement, looking south, before and after renovation 108
Figure 7.2 Photographs: The new path around the basement 109
Figure 7.3 Layout of the gravity laboratory 110
Figure 7.4 Photograph: Three generations of FG5 in the SGF gravity laboratory 115
Figure 7.5 Photograph: FG5-229 in Walferdange Underground Laboratory for Geodynamics in 2007 117
Figure 7.6 Results from the 2007 European comparison of absolute gravimeters 118
Figure 7.7 Results of the 2012 mini comparison, between FG5-229 and FG5X-216 121

Figure 7.8 Photograph: Week 1 of the international comparison of gravimeters in Belval, Luxembourg 122
Figure 7.9 Depiction of the floor in the civil engineering building, Belval, University of Luxembourg 122
Figure 7.10 Results of the 2015 regional comparison of absolute gravimeters 124
Figure 8.1 Common vacuum failure components on the lower service ring 126
Figure 8.2 Photograph: Releasing the dropping chamber snubber lock nuts 128
Figure 8.3 Photograph: Removal of the drive belt 129
Figure 8.4 Photograph: Removal of the motor assembly to access the ferrofluidic feed-through 130
Figure 8.5 Schematic drawing of the main components in the super-spring 132
Figure 8.6 Photograph: A super-spring flexure 133
Figure 8.7 Photograph: The motor spindle and a limit switch 133
Figure 8.8 Photograph: Super-spring control board within the SIMX unit 134
Figure 8.9 Photograph: Faulty pins in the super-spring LEMO socket on the SIMX 135
Figure 8.10 Oscilloscope trace to test the half-life of the super-spring 136
Figure 8.11 A failed attempt to obtain a half-life measurement of the super-spring 136
Figure 8.12 Schematic of the FG5 WEO-100 laser 138
Figure 8.13 Inside the WEO-100 laser 138
Figure 8.14 The five axis mount 141
Figure 9.1 The process of the data collection and reprocessing 146
Figure 9.2 Basic file structure used by the ‘gap’ software 149
Figure 9.3 The overall structure of the software used in this work, including ‘g’ and ‘gap’ 151
Figure 9.4 Hourly data obtained using ‘g’ and the VgHx software 155
Figure 9.5 A comparison of the hourly output from ‘g’ and VgHx software over the period of a year 155
Figure 9.6 Hourly data from ‘g’ and VgHx: uncorrected laser peak jumps with the VgHx results 157

Figure 9.7 An example of problems with the VgHx data processing..... 158
Figure 10.1 The precision of the gravity measurements plotted with local wind speed..... 161
Figure 10.2 Precision of gravity measurements with wind direction 162
Figure 10.3 The impact of a rapidly moving low pressure system on the gravity measurements..... 163
Figure 10.4 Satellite images: A rapidly moving weather front passes overhead at the SGF..... 163
Figure 10.5 The standard error of the hourly gravity measurements in 2007 164
Figure 10.6 The standard error of the hourly gravity measurements in 2010 165
Figure 10.7 Yearly averages of measurement precisions from 2006-2015 166
Figure 10.8 Precisions from the FG5X in 2013 167
Figure 10.9 Earthquake location in 2009..... 168
Figure 10.10 Detecting an earthquake in the gravity measurements..... 168
Figure 11.1 Screen shot of the boreholes around the SGF, taken by the RGO from 1940-1960..... 171
Figure 11.2 Borehole record TQ61SW9..... 171
Figure 11.3 Borehole record TQ61SW1..... 172
Figure 11.4 Photographs: The UK's Ordnance Survey's reference receiver 'HERO' 176
Figure 11.5 Photograph: A view of the semi-sunken basement from the SE corner of the SGF..... 179
Figure 11.6 Representation of the soil immediately surrounding the gravity laboratory 180
Figure 11.7 Water table depth below the gravity laboratory 182
Figure 11.8 Representation of the new dome above the gravity laboratory..... 183
Figure 11.9 Calculating the effect of the dome above the primary pier (HERG) in the gravity laboratory 185
Figure 12.1 Hourly data from 'g9' from 2013..... 189
Figure 12.2 Comparison of five ocean-loading models, obtained by extraction using 'gap'..... 190

FIgure 12.3 Ocean-loading comparison from Chalmers free ocean tide loading provider 191
Figure 12.4 Comparison of the Schwiderski ocean-loading models from Chalmers and ‘g’ 191
Figure 12.5 Ocean-loading model comparison between four models, GOT00.2, TOPEX7.2, FES2004 and CSR4.0..... 192
Figure 12.6 Hourly gravity residuals with standard errors plotted with tide gauge data from Newhaven..... 193
Figure 12.7 Ten day data set of hourly gravity values, with standard errors, plotted with corresponding tide gauge data 195
Figure 12.8 Ten day data set of hourly gravity values only, plotted with corresponding tide gauge data..... 195
Figure 12.9 Ten day data set of hourly values plotted with rainfall data from UK Met Office station at Herstmonceux..... 196
Figure 13.1 The time series of gravity data at the SGF, shown with standard deviations..... 199
Figure 13.2 Major instrumental changes are highlighted within the gravity time series..... 200
Figure 13.3 The gravity time series split into four regimes, showing similar scatter in each regime..... 201
Figure 13.4 Each regime of data has an offset from the last 202
Figure 13.5 Gravity data plotted with groundwater depth 204
Figure 13.6 A phase lag between the gravity and the groundwater depth is identified..... 204
Figure 13.7 Groundwater depth with phase lag applied..... 205
Figure 13.8 The calculated groundwater effect on gravity plotted with gravity measurements 206
Figure 13.9 The gravity data plotted with an amplified groundwater effect during the 2011 drought period..... 207
Figure 13.10 Gravity time series with calculated groundwater effect removed..... 207

Figure 13.11 Gravity time series with the calculated groundwater effect increased by a factor of two removed 208
Figure 13.12 The opposite attraction of influences 208
Figure 13.13 The comparison corrected time series, without groundwater correction..... 209
Figure 13.14 Uncorrected and corrected gravity time series of yearly regime averages..... 211
Figure 13.15 Yearly time series averages corrected with comparison results, and a bias of 7.25 for the 2013-2016 data..... 212
Figure 13.16 Gravity time series, of weekly project data, with comparison corrections and bias applied 213
Figure 13.17 Vertical height displacements from satellite laser ranging and absolute gravity 214
Figure 13.18 Vertical height displacements from gravity measurements corrected for comparisons and bias plotted with the SLR vertical displacement 214
Figure 13.19 Simulation of yearly campaign type measurements for the SGF..... 216
Figure 13.20 Campaign simulation with comparison offsets applied 216
Figure 15.1 The SGF absolute gravity time series from 2006-2016, with and without comparison offsets applied..... 224
Figure 15.2 Campaign simulation gravity data, with and without comparison offsets applied..... 225
Figure 15.3 Corrected time series of absolute gravity data 226
Figure 15.4 Opposing attraction from the changing water content of the soils above and below the gravimeter, and the attractive mass which calculations have compensated for during this work 227

Table of Tables

Table 2.1	Laser peak wavelengths	45
Table 2.2	Fringe count times and distances	51
Table 3.1	Primary tidal components	63
Table 5.1	Process of events during satellite laser ranging	90
Table 7.1	A time line of SGF gravity related activity	112
Table 7.2	Results of the 2007 European comparison of absolute gravimeters	118
Table 7.3	Results of the 2012 mini comparison at WULG	120
Table 7.4	Results of the 2015 regional comparison of absolute gravimeters	123
Table 9.1	Example of the first eight columns in the ‘gap’ logbook file	148
Table 9.2	Project gravity results from ‘g’, VgHx and ‘gap’	156
Table 9.3	An assessment of the existing reprocessing software, ‘g’ and ‘gap’	159
Table 11.1	Density levels of clay	175
Table 11.2	Results from soil sample 1	177
Table 11.3	Results from soil sample 2	178

Glossary of Terms, Abbreviations and Acronyms

AG	Absolute Gravity
BIPM	Bureau International des Poids et Mesures
BGS	British Geological Survey
BODC	British Oceanographic Data Centre
Campaign Measurement	Episodic measurement stategy
CNES	Centre National D'études Spatiales
Drop	One measured drop of the object/mass within the dropping chamber
ECAG	European Comparison of Absolute Gravimeters
IAG	International Association of Geodesy
IGS	International GNSS Service
ILRS	International Laser Ranging Service
ITRF	International Terrestrial Reference Frame
FG5	Type of Absolute Gravimeter (Classic Design)
FG5X	Type of Absolute Gravimeter (Modern Design)
GIA	Glacial Isostatic Adjustment
GGOS	Global Geodetic Observing System
GNSS	Global Navigation Satellite System
LRO	Lunar Reconnaissance Orbiter
NASA	National Aeronautics and Space Administration
NERC	Natural Environment Research Council
NOAA	National Oceanic and Atmospheric Administration
NOC	National Oceanography Centre
OS	Ordnance Survey
Project	Comprised of a specified group of sets of data

RGO	Royal Greenwich Observatory
RMS	Root Mean Square
SIM	System Interface Module
SGF	Space Geodesy Facility
Set	A data set of measurements from a group of drops of the dropping chamber
SIM	System Interface Module; a component with the electronics rack of the FG5
SLR	Satellite Laser Ranging
UTC	Universal Time Coordinated
WULG	Walferdange Underground Laboratory for Geodynamics (Luxembourg)

Units

Gal	Unit of the acceleration due to gravity: $1Gal = 0.01ms^{-2}$ $\mu Gal = 1 \times 10^{-8}ms^{-2}$
Hz	Unit of frequency: 1Hz = 1 cycle per second

Chapter 1

Introduction

1.1. Introduction

Always present, never failing, the multi-layered concept of gravity is a complicated phenomenon. It is the underlying force that binds the universe together but when discussing the real meaning, whether it is considered an acceleration, a force or a wave, largely depends upon a small change in description or a change in the profession of the user. For instance; an astronomer might commonly use the word gravity to mean the effect of gravitational force on another body in space whilst gravitation is a short form for gravitational waves, described by Einstein as ripples caused by the curvature of space-time. For geodesists, gravity is largely used to describe the effect on the surface of the planet, the local acceleration at the surface of the Earth, known as 'little g', whilst physicists will tend to use both gravitation and gravity.

This work is concerned with the measurement of gravity and the implications of the measurements for geodetic knowledge. Therefore for the purposes of this work gravity will be viewed from the geodesists' perspective.

1.2. A Brief History of the Gravity Measurement

When the topic turns to gravity it is perhaps unsurprising that many people have a tendency to think of Galileo (1564-1642) and his cannonballs, or Newton (1643-1727) and the now infamous story of the apple. It is fair to say that our modern interpretation of the definition of gravity began, and was developed, in no small part by these two founders of modern science.

Although many people associate Galileo with his experiments with dropping cannonballs, fabled to have taken place from the Tower of Pisa, or rolling cannonballs down inclined planes, it was his recognition of pendulum motion that actually lead to his study of these historical experiments. The history books say that in 1583 a young Galileo became fascinated whilst watching a candelabrum during a period of mass at the Cathedral of Pisa, wondering if the time taken for the candelabrum to describe an arc became shorter as the distance through which it travelled decreased. Using his pulse as a stopwatch he discovered that the time taken for each oscillation was independent of the size of the arc through which the object travelled (Darling, 2006). Galileo continued on to do a significant amount of work on motion by studying how objects move whilst in free-fall; most notably by studying the trajectories of cannonballs, and on inclined planes, carefully measuring distance and time intervals. These studies lead to the momentous recognition that the displacement of an object starting from rest is proportional to the square of the time that object is in motion and thus that free-fall is uniformly accelerated motion. In this connection, and his interest in pendulums, Galileo laid the foundation stones on which modern gravimetry is based, and provided the basis for measurement of gravity to be taken for over 200 years (Darling, 2006) (Torge, 1989) (Encylopaedia Britannica, 1976).

The evolution of pendulums continued after Galileo and in 1818 the reversible pendulum, by H. Kater, allowed absolute measurements of gravity to be taken to an accuracy of a few parts in 10^6 (Encylopaedia Britannica, 1976).

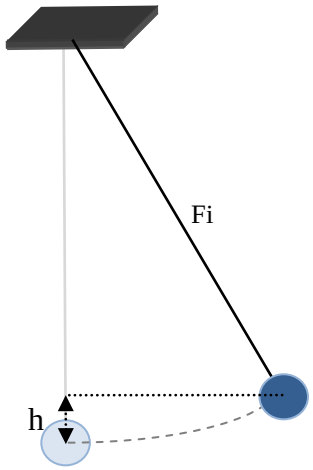

Figure 1.1 Simple Pendulum

Pendulum gravimeters are based upon the simple pendulum law:

$$P = \pi \sqrt{\frac{l}{g}}$$

and for a more accurate determination :

$$P = \pi \sqrt{\frac{l}{g}\left(1 + \frac{h}{8l}\right)}$$

Where: l is the length of the pendulum, P is the period of oscillation, g is the acceleration due to gravity and h is the height through which the point of oscillations falls during a half oscillation.

Pendulums were used for making both relative and absolute measurements of gravity. For absolute measurements both the period of oscillation and the length of the pendulum are measured to enable the calculation of g. For relative measurements the period can be measured at two locations and the ratio between locations can be derived from (Cook A. H., 1965):

$$g_1 = \frac{l\pi^2}{P_1^2} \quad \& \quad g_2 = \frac{l\pi^2}{P_2^2} \qquad \therefore \qquad \frac{g_1}{g_2} = \frac{P_2^2}{P_1^2}$$

or

$$\Delta g_{12} = g_2 - g_1 = -2g_1 \frac{P_2 - P_1}{P_2} + g_1 \frac{(P_2 - P_1)^2}{{P_2}^2}$$

Absolute measurements made with pendulums were considered more difficult than relative measurements due to the practical difficulties in obtaining an accurate enough measurement of the length of the pendulum (Hosmer, 1919), but with care a precision of 10^{-5} was achievable (Marson & Faller, 1986). Pendulum measurements for absolute gravity measurement continued until 1965 in the UK when free fall devices were sufficiently accurate to be used as an alternative (Cook A. H., 1965).

The development of spring-based gravimeters in the 1930s, for relative measurements of gravity, became popular for geophysical exploration. The instruments were smaller and

more transportable than their complex pendulum counterparts, although pendulums were still used for datum points along a calibration line. The design of the spring gravimeter was based upon the principle of spring balance, where a change in mass will produce a change in the force on the spring, according to Hooke's Law (Torge, Geodesy, 1991). In these relative gravimeters the force on a mass due to gravity is balanced by the restoring force of the spring.

LaCoste in 1934 converted a long-period seismometer for use in gravity measurements. This type of gravimeter was the first to utilise a 'zero length' spring, a spring system in which the effective length is zero when measured from a fixed point, or the initial length, corresponding to zero force (Marson & Faller, 1986) (Marson I. , 2012). This type of gravimeter, such as the LaCoste-Romberg relative gravimeter is based around the zero-length spring.

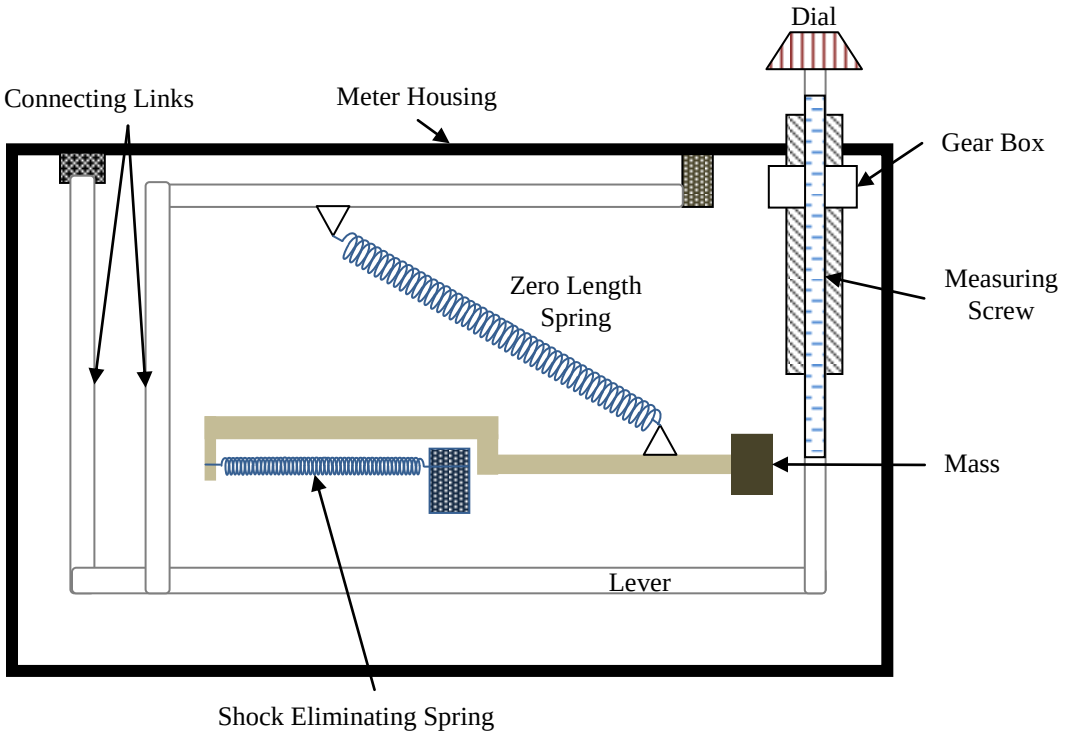

Figure 1.2 Schematic of a LaCoste and Romberg relative gravimeter (Torge, Geodesy, 1991)

In absolute gravimetry a vast amount of development has been done since the 1940s, when the ability to time, and measure the distance travelled, a free falling body became accurate

enough. Free-fall absolute gravimeters evolved as technology advanced to allow greater accuracy in the measurement of the time and distance pairs.

Development of the free-fall gravimeter began at a variety of sites around the world. One of these was the National Physical Laboratory in Teddington, UK where measurements of gravity were taken by dropping a glass sphere past two sets of slits separated vertically. One slit of either set was illuminated such that the presence of the sphere focused the light onto the second, behind which was a photomultiplier which recorded the flash of light as the sphere dropped through the slits (Cook A. H., 1965). However it is perhaps the work of R.H. Dicke and J.E. Faller at Princeton University, USA that can be said to have had the most significant impact and longevity as they developed the use of interferometry in gravity measurements. In fact, Faller had also combined the interferometric method with the newly discovered laser by 1962 (Niebauer, Hoskins, & Faller, 1986). Faller continued working on gravimeters throughout his career and by 1967 a new gravimeter, which formed the basis of modern absolute gravimeters was in operation. It incorporated interferometry, a laser, clock source and an evacuated dropping chamber (Faller, 1967). It was also Faller, working at Wesleyan University with J.A. Hammond, who designed the first portable version of the absolute gravimeter which was capable of an accuracy of 50 µGal, but which was exceedingly heavy at 880 kg.

By the 1980s Hammond et al. had modified this early design increasing the accuracy to 10-15 µGal and improving the test procedure, whilst Faller, now working at JILA (the Joint Institute for Laboratory Astrophysics, USA) with M.A Zumberge, built a machine which incorporated a ‘super-spring’, ‘drag-free’ chamber and a computer to record the fringes for the first time. Faller’s gravimeter was capable of 6-10 µGal and special attention was given to decreasing the weight of and time taken to set up the equipment; this gravimeter then achieved a survey of 12 sites in the USA in eight weeks. It should also be noted that by 1983 Tim Niebauer, the founder and current president of Micro-g LaCoste, had started working with Faller and the team at JILA (Niebauer, Sasagawa, Faller, Hilt, & Klopping, 1995). In 1985 the third generation of the JILA gravimeters, which are now known as the JILAg series, achieved an accuracy of 3-5 µGal, with some of these gravimeters still

attending absolute gravimeter comparisons (Francis, O. 2010). The culmination of these advances in technology is the FG5 absolute gravimeter, with measurement accuracy around 10^{-9}, which is explained in detail in the next chapter.

1.3. A Moment About Newton

Of course, it is impossible to cover the subject of gravity without recognition of the contribution of Newton. His work 'Principia', in 1687, changed perception of gravity entirely. His concept of attraction between all massive bodies and the idea of the inverse square law, where, for example the gravitational attractive force between the Moon and the Earth decreases as the inverse square of the distance between them. And of course Newton's law of gravity:

$$F_{12} = \frac{GM_1M_2}{D_{12}^2}$$

Where; F_{12} is the magnitude of the gravitational force acting between masses M_1 and M_2 separated by a distance D_{12}, and G is the gravitational constant.

Or, when expressed for the acceleration due to gravity on the surface of the Earth:

$$g = \frac{GM_E}{r_E^2}$$

Where, M_E and r_E are the mass and radius of the Earth respectively.

1.4. Geodetic Observatories

Geodetic observatories around the world provide a basis for studies of the Earth system, by the provision of infrastructure for a number of different observation techniques.
The techniques traditionally associated with these observatories are: Satellite Laser Ranging (SLR), Global Navigation Satellite Systems (GNSS), Very Long Baseline

Interferometry (VLBI) and Doppler Orbitography and Radio-positioning Integrated by Satellites (DORIS). Each technique employed at geodetic observatories provide very different measurements from different sources, but when combined provide a powerful tool for use in understanding geophysical processes (Boucher, Pearlman, & Sarti, 2015).
In 2003 the three fundamental areas of geodesy (Earth's shape, rotation and gravity field) were integrated under the umbrella of the Global Geodetic Observing System (GGOS), by the International Association of Geodesy (IAG). The objective of GGOS is the provision of a long-term and precise monitoring system and the basis to maintain a stable, accurate and international reference frame. Geodetic observatories have been tasked with providing the realisation of the Global Geodetic Reference Frame (GGRF, otherwise known as the ITRF) to an accuracy of 1mm and a stability of 0.1 mm yr^{-1} (Plag & Pearlman, 2009).

Gravity measurements are important as part of GGOS and observatories are encouraged to have gravity measurements taken in co-location to the other geodetic techniques. Gravimetry monitoring, via superconducting or absolute, has been actively promoted by the GGOS project at fundamental geodetic stations. One of the components of the gravity field part of GGOS includes "absolute and superconducting gravity observations at a globally distributed GGOS observations network, collocated with geometrical space geodesy sites, tied to sea-level by levelling, tide gauge and GPS observations" (Fosberg, Sideris, & Shum, 2005).

1.5. Absolute Gravity Measurement in Geodesy

Determination of the local acceleration due to gravity is important in a multitude of geophysical research topics, such as surveying, height determination, sea level variation studies, geological exploration and mining as well as being used in metrology for the definition of the kilogram. The work undertaken in this thesis has provided a long time-series of gravity observations at a fixed point on the surface of the Earth, close to an important geodetic observatory. As such, it is a unique data set.

1.6. Outline of Thesis Structure

This thesis is in two parts, in the first six chapters effectively set the scene for the study. Introducing the subject area with the technical specifics of the FG5 gravimeter, the corrections which go into the measurements and the Space Geodesy Facility, Herstmonceux, where the instrument is based.

Chapter 1: Introduction

The first chapter generally introduces the subject area of gravimetry, the measurement of Earth's gravity, and why it is important to geodesy and geodetic facilities. An outline of the thesis structure is given.

Chapter 2: The FG5 Absolute Gravimeter

The second chapter introduces the FG5 absolute gravimeter and gives a detailed account of the instrument, its principal of operation and component parts.

Chapter 3: Corrections to Absolute Gravity Measurements

The third chapter introduces the essential components which need to be removed from absolute gravity measurements to obtain an accurate measurement. Tidal corrections, polar motion and atmospheric corrections which are done for any data processing and the basis of additional environmental corrections is introduced.

Chapter 4:Comparisons of Absolute Gravimeters

The fourth chapter gives an introduction of the pseudo calibration technique used for absolute gravimeters, the concept behind the method used and European sites where they are carried out.

Chapter 5:The Space Geodesy Facility, Herstmonceux

The fifth chapter introduces the geodetic facility which houses the absolute gravimeter. The geodetic techniques employed by the Space Geodesy Facility are explained, with attention

to the satellite laser ranging technique. The derivation of the vertical height product from SLR is described, as if the transfer from gravity measurements into vertical heights.

Chapter 6:Literary Review and Problem Statement

The sixth chapter gives an overview of the main bodies of literature available on absolute gravimetry that are relevant to the studies conducted with this thesis.

The second part of the thesis (chapters 7 to 15) describes the establishment of the FG5 at the SGF, and the processes and calculations done to extract, and test, the results of the gravity measurements.

Chapter 7:Absolute Gravity at the Space Geodesy Facility

The seventh chapter provides an overview of the work done in absolute gravity at the SGF in the time period encompassing this study. Early technical problems are described with the establishment of the gravity laboratory and the evolution of the gravity facility at the SGF. Results of international or European comparisons of gravimeters are for the FG5 used in this study are presented for the FG5 used for this study.

Chapter 8:Operating and Maintenance Experience with the FG5

The eighth chapter details the instrumental experiences gained during this study. This chapter can be used as a technical guide to new, or inexperienced, users of FG5s.

Chapter 9: Software

The ninth chapter provides a review of the available data processing software, and sets out to detail some advantages and disadvantages of the software. The rationale for adding to the existing software is explained and the programmes written by the author of this thesis are outlined.

Chapter 10:Precision of the Gravity Measurements

The tenth chapter investigates the precision of the gravity measurements at the SGF, describing known and suspected noise sources and reveals trends within the data.

Chapter 11:Environmental Calculations

The eleventh chapter describes the investigation into the environmental surroundings of the SGF and gives an assessment of the subsurface soils. The influence to gravity measurements are calculated for the varying hydrology around the gravity laboratory and a correction factor attained.

Chapter 12:Periodic Signals

The twelfth chapter investigates residual periodic signals in the gravity measurements after standard corrections have been removed. The hourly data showing the periodic signal detected is examined for tidal similarity.

Chapter 13:The Time Series of Absolute Gravity Measurements 2006-2016

The thirteenth chapter introduces the entire, daily, time series of gravity measurements for the first time and seeks to describe discontinuities within the data and display how different interpretations of the data can be made. The correction for hydrological influence calculated in chapter eleven is removed from the gravity time series and the results are discussed.

Chapter 14 Discussion

The fourteenth chapter provides a avenue to explore some conclusions and thoughts regarding the results of this study.

Chapter 15:Conclusions

The final chapter gives a concise statement of the principal findings of this study, providing evidence for each. Secondary conclusions are also drawn and some future research topics are described.

Chapter 2

The FG5 Absolute Gravimeter

2.1. Introduction

This chapter describes the mechanisms and components of the FG5 absolute gravimeter. The chapter is organised in sections as follows:

- **Introduction**
- **Principles of the Design**
- **FG5 Components**
  - *Dropping Chamber*
  - *Interferometer*
  - *Laser*
  - *Super-Spring*
  - *Electronics*
    - *Laser Controller*
    - *System Interface Module, Magma and System Controller*
    - *Timing/Clock*
- **Instrumental Set Up**
  - *Physical and Optical alignment*
- **FG5X**
- **Processing Software**
  - *'g' Software*

The FG5 absolute gravimeter came about as a result of a cooperative effort which included academia, government and the private sector in the U.S.A. The target for the instrument was to make improvements in operation and reliability from the previously available absolute gravimeters, the JILAg series, whilst aiming for an instrumental accuracy of 1 µGal (Niebauer, Sasagawa, Faller, Hilt, & Klopping, 1995).

The FG5 absolute gravimeters are currently the most advanced instruments for the measurement of gravity acceleration at the Earth's surface. The gravity measurement is considered absolute since the determination of gravity can be traced to metrological standard of time and length, through the independent calibrations of the laser and reference clock (Marti, 2014) (Timmen, 2010) (Micro-g LaCoste).

The FG-5 is a ballistic, or free-fall, device where the measurement of gravity is derived by dropping an object and 'tracking' it through a known distance using interferometric means. The instrument is capable of obtaining gravity measurements to an accuracy of 2 µGal ($2 \times 10^{-8}\, ms^{-2}$), which can be equated to approximately 10 mm of vertical displacement by using the flat plate bouguer conversion (see Chapter 3), and to a precision of approximately 1 µGal in 3.75 minutes at a quiet site (Micro-g LaCoste, 2005).

The first FG5 (FG5-101) built for commercial sale was available in 1993 and included major improvements over the design of the JILAg. Known instrumental error sources of the JILAg series, such as tilt coupling errors in the optical systems, were eliminated (Sasagawa, 1995). Since 1993 the basic design concept of the FG5 has remained whilst modifications and improvements have gradually been made over the years to various components. The latest evolution was introduced in 2011 (Niebauer, Billson, Mason, van Westrum, & Klopping, 2011) with the introduction of the FG5X variant. This chapter will set about to explain the design and features of the FG5 and will explain the most notable differences found between the 2006 version of the FG5 and the FG5X variant.

2.2. Principles of the Design

The principle of operation of the FG5 is relatively straightforward. An object situated inside a vacuum chamber is dropped through a known distance and the trajectory of the object whilst in free-fall is measured. The trajectory information provides time and distance pairs of measurements throughout the drop interval that are used to determine the acceleration due to gravity using a least squares fit to the equation:

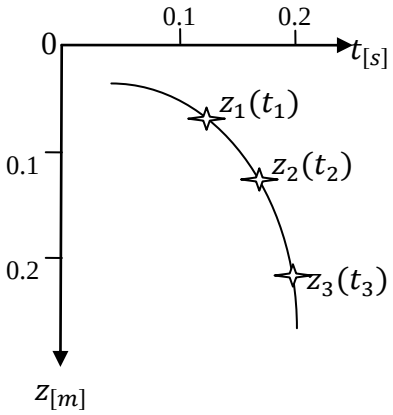

Figure 2.1 Trajectory time and distance diagram (Torge, 1989)

$$x_i = x_0 + v_0\tilde{t}_i^2 + \frac{g_0\tilde{t}_i^2}{2} + \frac{\gamma x_0\tilde{t}_i^2}{2} + \frac{\gamma v_0\tilde{t}_i^3}{6} + \frac{\gamma g_0\tilde{t}_i^4}{24} \qquad \tilde{t} = t_i - \frac{(x_i - x_0)}{c}$$

$$x_i, t_i, i = 1, \ldots\ldots, 700$$

x_0, v_0, g_0 , the initial position, velocity and acceleration at t = 0, are all free parameters to be fitted, γ, the vertical gravity gradient, is also a free parameter but is provided a-priori since it is poorly determined over the length of the drop.

The retarded time: $\tilde{t} = t_i - \frac{(x_i - x_0)}{c}$ is used since the object is tracked using a laser and the finite speed of light gives a correction for the calculated gravity signal. Due to the fact that the time-distance pairs are generated some time after the light bounces off of the dropped object. (Niebauer, Sasagawa, Faller, Hilt, & Klopping, 1995) (Van Camp, 2003).

The trajectory time-distance pairings are obtained by optical fringes which have been compared to an atomic clock. The optical fringes are generated by the recombination of the specialised, Iodine stabilised Helium-Neon laser beam, which has been split within an interferometer to provide two optical arms. One of the optical arms is known as the reference beam and travels a fixed distance through the interferometer. The second arm, the test beam, is reflected upwards within the interferometer towards the object in the vacuum

chamber. The object is comprised of a motorised cart assembly which contains a retro-reflector, or corner cube, to reflect the laser arm back through the interferometer into the super-spring assembly.

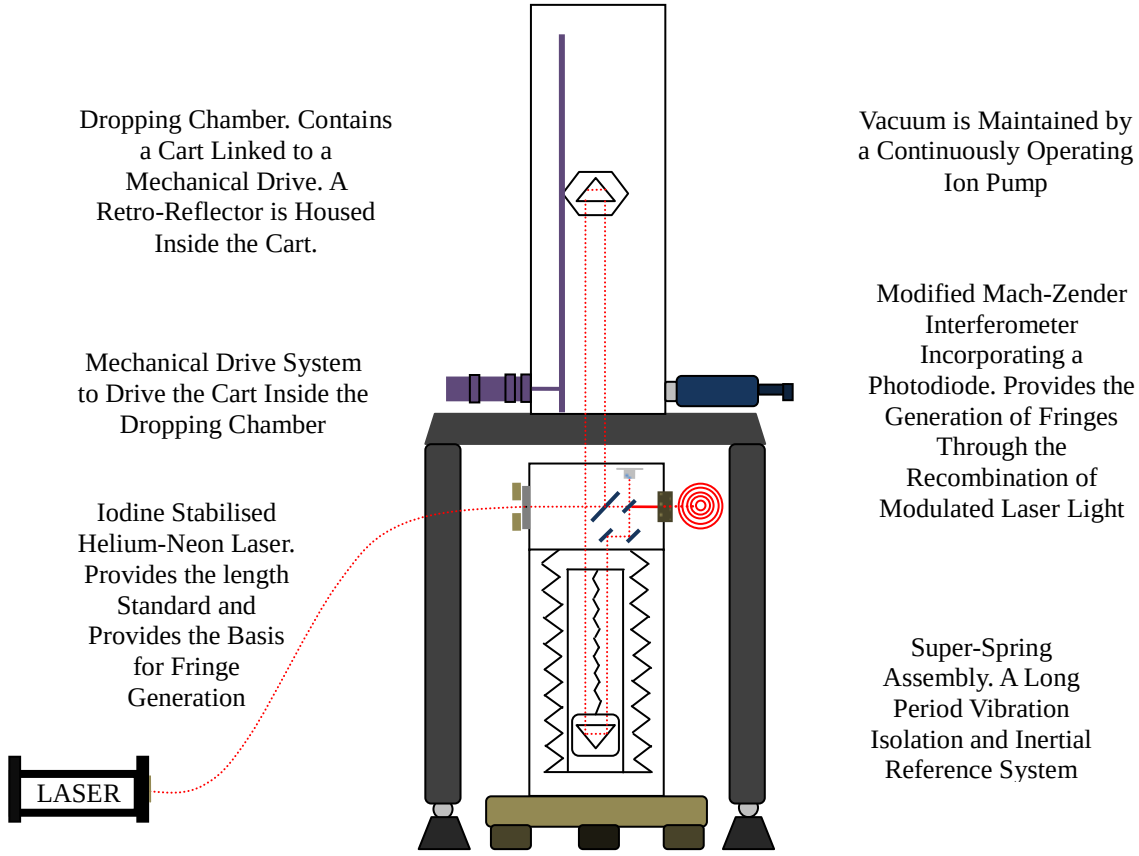

Figure 2.2 Schematic drawing of the FG5 absolute gravimeter

Situated in the centre of the spring assembly is a retro-reflector which directs the test beam back towards the interferometer. The recombination of the test and reference beams generates the optical fringes each time the object in the vacuum chamber falls through a distance of 316 nm, or half of the wavelength of the laser (Neibauer, 2011). A photodiode detects the fringe output converting each fringe zero crossing into an electrical TTL* output signal to be compared to a 10 MHz clock source frequency. An over-constrained solution to the equation of motion is provided by the hundreds of time-distance pairings provided by each drop of the object (Niebauer, Sasagawa, Faller, Hilt, & Klopping, 1995).

* TTL is a square wave electrical signal of 5V amplitude, TTL stands for transistor-transistor logic

2.3. Principle Components of the FG5

The FG5 absolute gravimeter is comprised of five principal components; the dropping chamber, interferometer, super-spring assembly, laser and electronics rack.

The operational organisation of the components is shown schematically in Figure 2.3. To isolate the super-spring and interferometer from the vibrations of the dropping chamber two tripods are used. The assembled gravimeter is approximately 1.3 metres high and has a footprint on the ground of around 1 m^2.

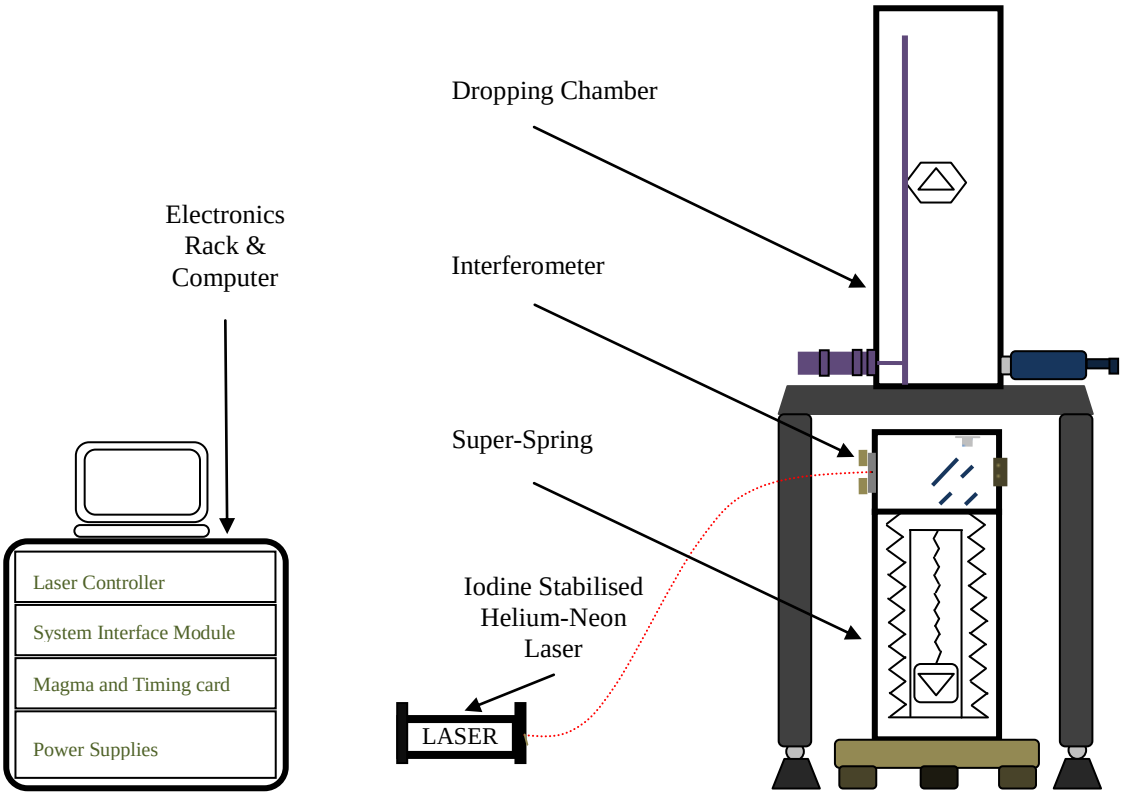

Figure 2.3 Main components of the FG5 absolute gravimeter

2.3.1. Dropping Chamber

The retro-reflector is housed within a test mass assembly within the cart. The cart is connected to a vertical drive mechanism. During operation, after the cart is raised to the top of the chamber it is held for a period of five seconds (this is the default value) to ensure the

cart, and test mass assembly, are completely at rest before being ‘dropped’. After the five seconds has elapsed the cart is mechanically driven away from the test mass assembly, to allow the assembly to fall freely, purely under the influence of gravity. Near the bottom of the drop distance, the cart slows to ‘catch’ the test mass assembly as gently as possible before coming to a rest.

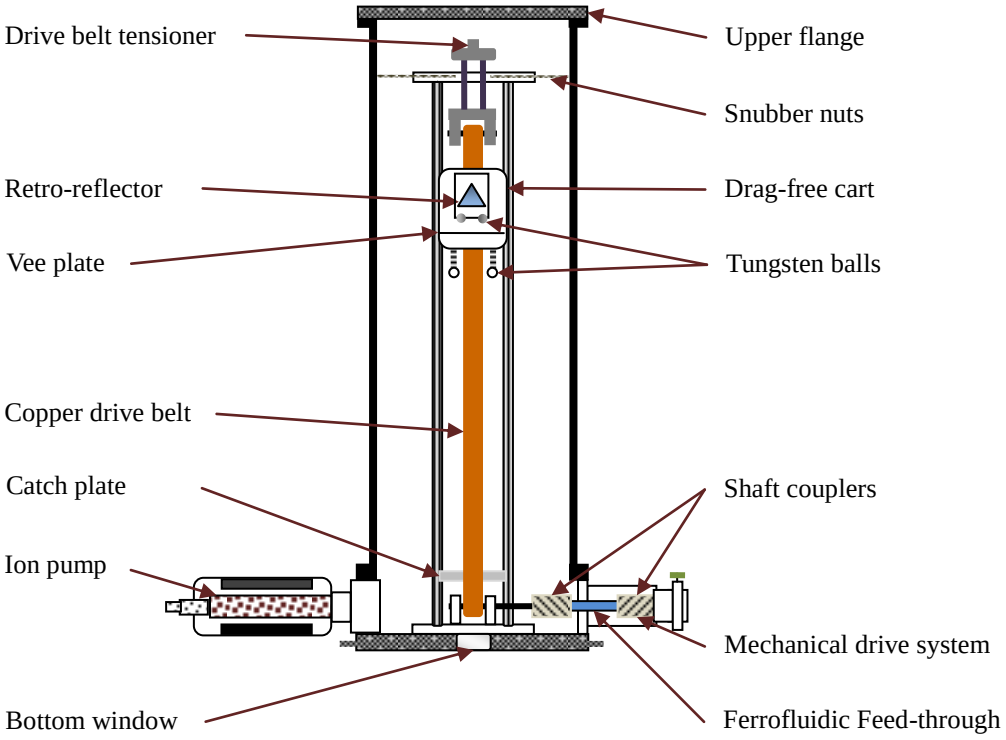

Figure 2.4 Schematic sketch of the dropping chamber

The orientation of the resting position test mass assembly is dictated by 'balls and vee's' on the bottom of the cart and the top of the catch-plate respectively; this positioning system is used to minimise any rotational effect which might translate into the dropping sequence, as well as ensuring the start orientation is always the same. The balls, situated on the bottom of the test mass assembly are made of tungsten, whilst the vee plate is located within the cart. There are additional balls and vee’s on the bottom of the cart and above the mechanical drive of the cart to catch and orientate the cart.

The mechanical drive system to control the cart comprises a copper belt, attached to the cart, which is driven by a motor on the outside of the chamber. The linkage which allows the drive mechanism to operate through the vacuum/atmospheric pressure divide is provided by a connector called a ferrofluidic feed-through.

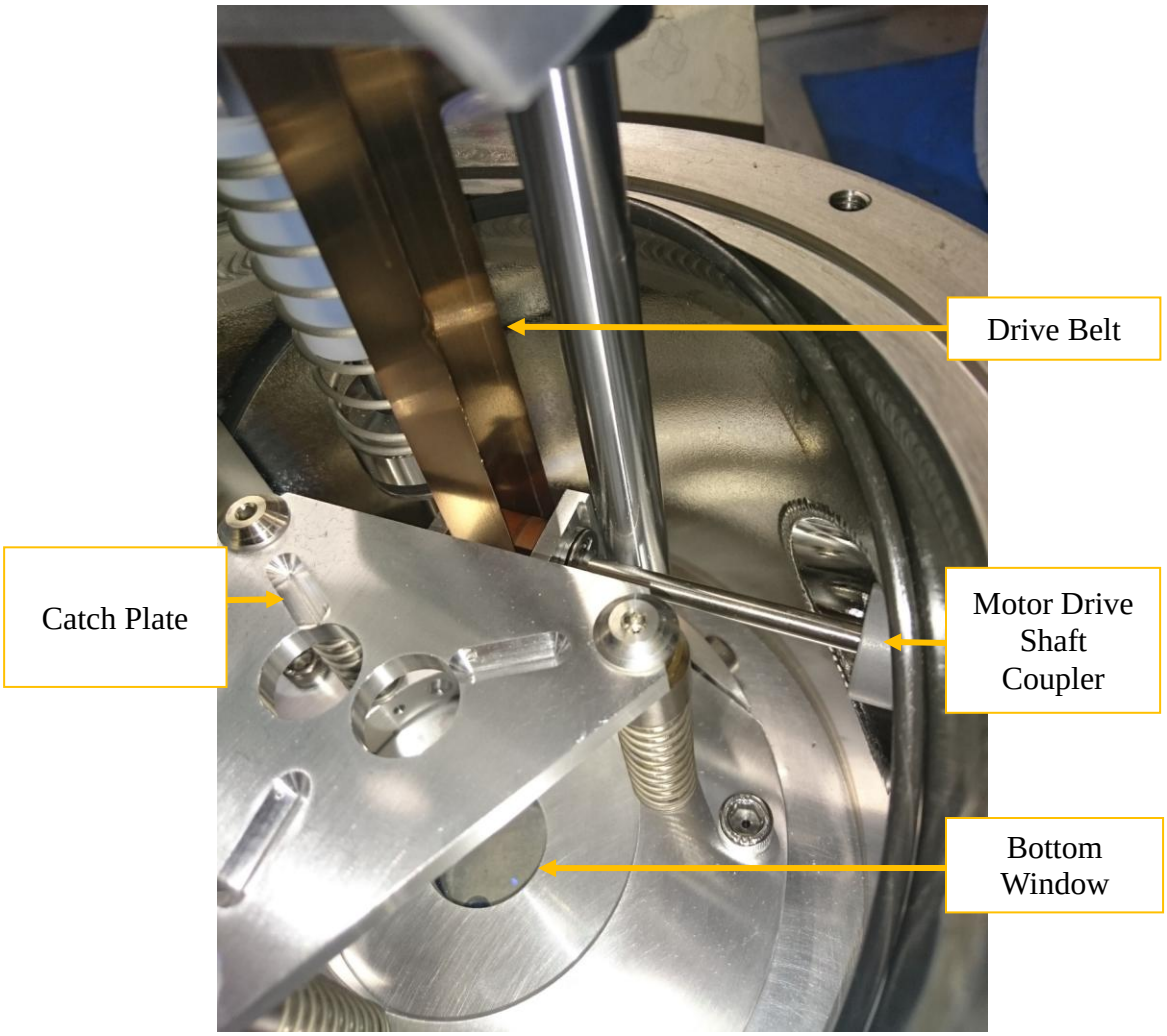

Figure 2.5 Inside the bottom of the dropping chamber

The instrument is always aligned North-South. A bubble level situated on the super-spring tripod allows the orientation of the FG5 to be correctly achieved.

The vacuum within the dropping chamber is obtained by use of a rotary pump, which is attached to the chamber by a dedicated port in the lower service ring (see Fig. 2.6). A baffle plate in the port is moved into the correct position via a screw thread to allow the rotary

pump to connect to the chamber. When a sufficient vacuum has been achieved the baffle plate is moved back to shut off access to the chamber and the rotary pump is switched off in preference for an ion pump, which will take over and continue to improve the vacuum in the chamber.

The ion pump maintains the vacuum in the dropping chamber at a pressure of $1x10^{-6}\ Torr$ (Micro-g LaCoste, 2006). The ion pump controller electronics includes an integrated battery backup to prevent vacuum loss during a power-cut situation. The battery backup will sustain power to the ion pump for around four hours.

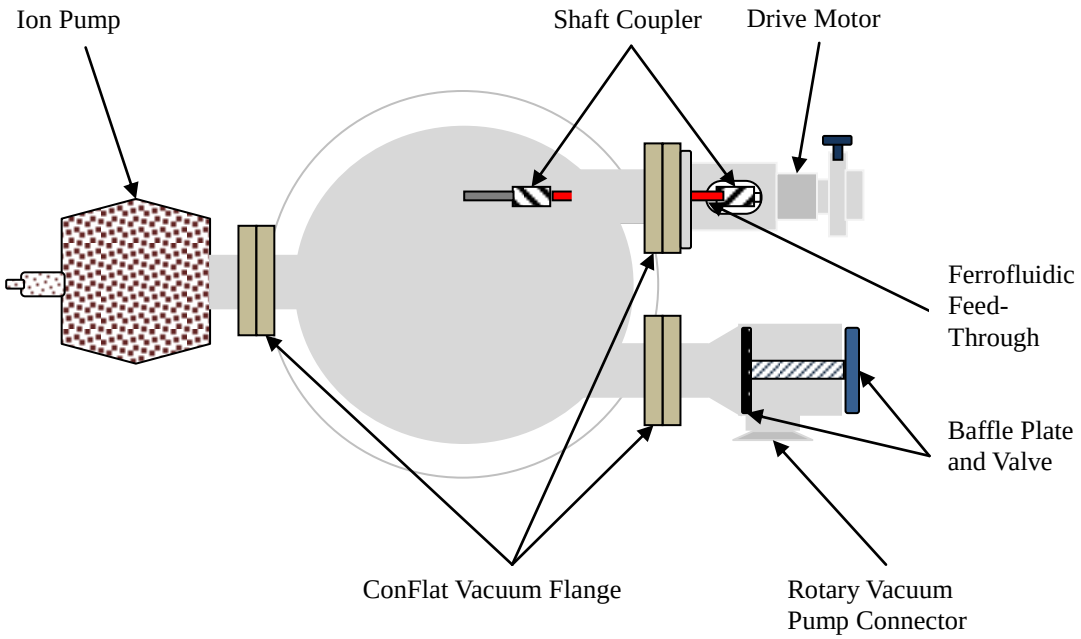

Figure 2.6 Top view drawing of the dropping chamber lower service ring

The dropping chamber sits upon its own tripod, to isolate it from the rest of the system and most importantly from the super-spring component of the FG5. The vibrations created within the chamber, through the drop and catch of the cart/object, are significant. The recoil from the floor, due to the vibration of the dropping chamber tripod can be seen in the individual drop residuals, however this recoil was been significantly reduced in the newer design of the FG5X dropping chamber.

In the older FG5 dropping chamber the drop length was 20 cm, the internal design was a-symmetric and the cart drive system was a single copper belt. In the newer FG5X the dropping distance has been increased by 75% to 35 cm. The internal design is symmetrical around one axis and the drive system for the cart is via two copper belts and is counterweighted to reduce the mechanical recoil of the cart. The recoil, or oscillation of the system as the test mass is dropped, causes two primary effects:

- Vibration through the tripod to be imparted into the floor, risking increased measurement noise
- Air-gap modulation, where 'the fraction of the total optical path of the laser beam travelling in ambient air compared with that occurring in the vacuum changes' (Neibauer, 2011)

In addition, improvements in material selection of the test mass reduces interaction with external magnetic fields, whilst the counterbalanced drive system reduces horizontal velocities and rotation of the test mass as it is being released at the start of the drop.

2.3.2. Interferometer

Below the dropping chamber and central to the design of the FG-5 is a modified Mach-Zender interferometer. A collimated continuous wave 633 nm laser beam enters into the side of the interferometer and is split into two optical arms, one of which goes through the beam splitter to generate a reference arm. The other arm is reflected up into the dropping chamber to be reflected off of the retro-reflector before travelling to the other retro-reflector within the 'super-spring' assembly for subsequent recombination with the reference beam inside the interferometer. These recombined arms of laser light generate the interference fringes that form the basis of the determination of gravity.

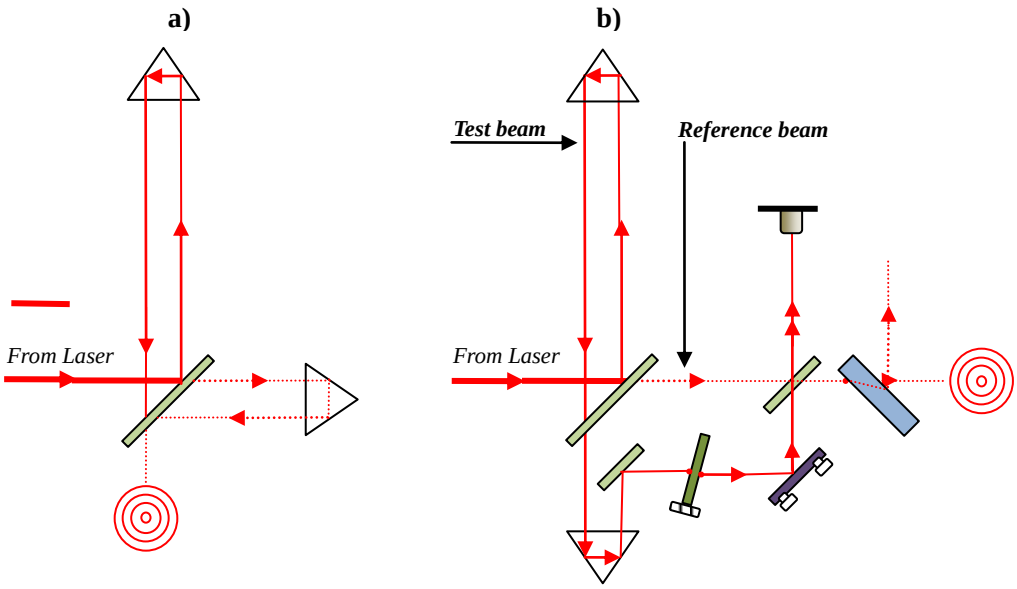

Figure 2.7 The laser path in the interferometer..Diagram a) shows a simplified diagram, a beam path commonly found in Michelson's interferometers. Diagram b) shows the beam path in the FG5 interferometer, a Mach-Zender interferometer.

If the fringes are viewed on an oscilloscope, as modulating sine wave which passes from positive to negative, each time they cross the zero point a TTL pulse is produced which is recorded in the electronics. In reality the fringes are scaled such that although around 70000 fringes should be produced and detected during the 20 cm drop (in the older FG5), just 700 are actually recorded to be married with a clock signal from the 10 MHz source.

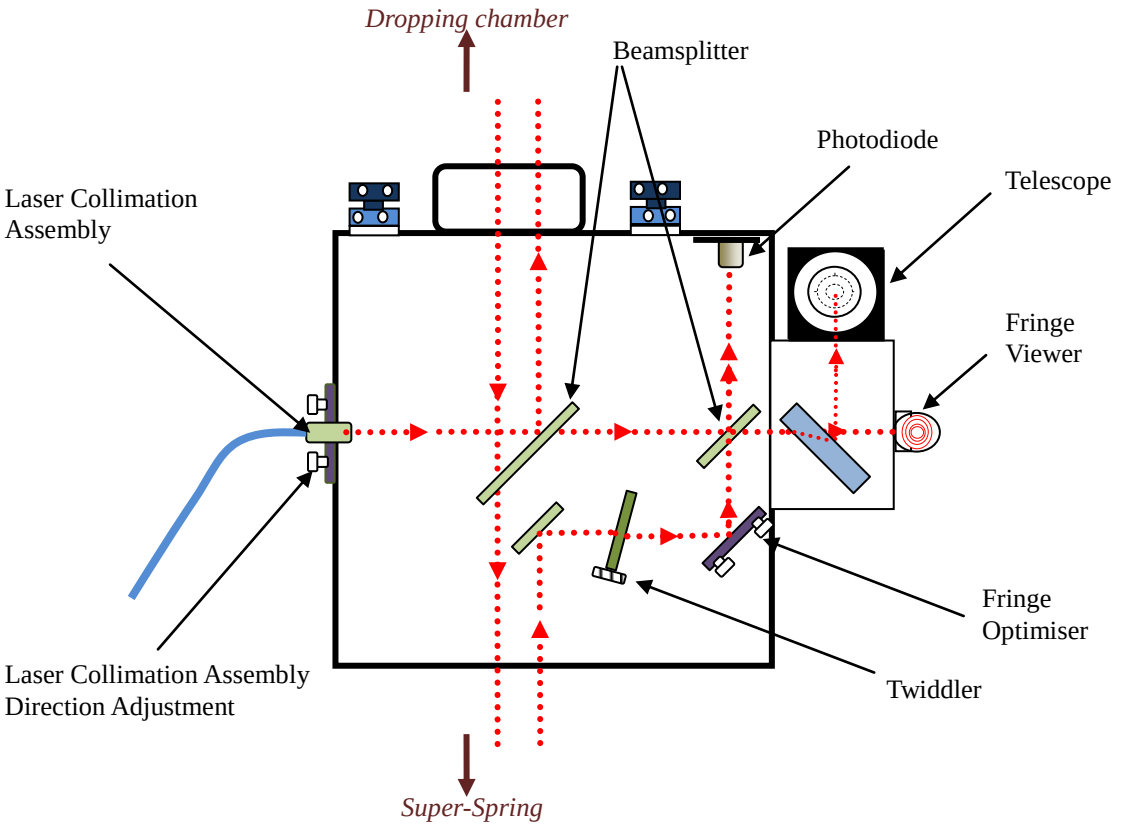

Figure 2.8 Operational beam paths through the interferometer

The optical path inside the interferometer includes three essential elements: it provides the essential input to the photodiode, where both reference and test beams recombine; the alignment telescope, situated on the side of the interferometer, and the fringe viewer, which is located beneath the telescope. Both telescope and fringe viewer are used in the vertical alignment procedure: the telescope is used to align the pointing of the test and reference beams (and is set to infinity to allow the parallel beams to overlap) to minimise any error in the vertical alignment. The fringe viewer optimises the overlap of the beams to optimise the signal to the photodiode. The alignment procedure is explained in section 2.4.

In addition to the optical outputs the interferometer also provides two electrical outputs; a TTL timing signal, and an analogue signal. The TTL signal, produced by the conversion of the photodiode output, is compared by the time interval analyser with the clock source to

provide the time-distance pairings that are used in the equation of motion. The analogue signal is used in conjunction with the fringe optimiser adjustment, during the FG5 setup procedure, to determine and optimise the amplitude of the fringe signal. The amplitude of the fringe output signal is important since it should ideally be set to between 400-250 mV.

2.3.3. Laser

Coupled to the interferometer via a fibre optic cable is a highly specialised laser, a WEO-100 laser manufactured by Winters Inc, USA. It was designed in collaboration with the national standards laboratory of France, BIPM* in Paris (Winters Electro-Optics Inc., 2004). It is one of the most common absolute optical frequency standards in use today with an absolute accuracy of 2.5 parts in 10^{11} (Niebauer, Sasagawa, Faller, Hilt, & Klopping, 1995).

The specialised laser is necessary to obtain the 2 μGal accuracy of the FG5 through the exceedingly stable and discrete wavelengths of the iodine transition peaks. The laser provides traceability of the FG5 to the SI† primary length standards (Van Camp, 2003).

The WEO-100 is a Helium-Neon continuous wave laser with an iodine cell between the rear mirror and the He-Ne tube. Iodine is used in lasers due to its strength and narrowness of the transition lines and the abundance of transition lines throughout the visible spectrum.

The WEO-100 uses the hyperfine lines of the R(127)11-5 transition of $^{127}I_2$ around the He-Ne 633 nm wavelength (Winters Electro-Optics, 2000). The peak wavelength for each laser transition line is given an alphabetic label ‘A’ to ‘J’, not all of which are used in the FG5. The laser peaks and corresponding emission wavelength is given in table 1. The table copies information held within the FG5 control software ‘g’ which is explained in the software section of this chapter.

* Bureau international des poids et Mesures

† The international system of units

2.1 Laser peak wavelengths

Laser Peak	Wavelength (nm)
D	632.991177539
E	632.991194728
F	632.991212588
G	632.991230227
H	632.991368898
I	632.991398220
J	632.991427042

The laser controller, situated in the electronics rack, allows the user to manually select which peak the laser is set to work on. This control allows the photo-diode, situated at the rear of the laser chassis, to give a photovoltaic output corresponding to each peak. This voltage output must be entered into the 'g' software since the selection of which laser peak to use has a significant impact on the measurement due to the wavelength difference.

Figure 2.9 WEO-100 Laser control electronics within the gravimeter electronics rack

The primary outputs, other than laser power and control, are:

- Peak lock indication
- Cavity and Cell temperature outputs
- Laser power output
- Photovoltaic output associated with each transition peak.

The FG5 commonly uses the E-peak for measurements, though any peak may be used. Should the laser lose lock on the selected peak and lock onto a different peak then an offset in the recorded gravity will occur unless adjusted for. The offset is predictable according to the change in the discrete wavelength and can be set to be automatically detected by the Micro-g LaCoste software 'g', which is discussed later in this chapter.

The laser is mounted at one end of the Micro-g LaCoste chassis, at the other end of which is a faraday isolator. The isolator is situated outside the WEO-100 laser and is used to provide a stable polarisation vector into the fibre optic. Inside the WEO-100 laser a cavity spacer provides spatial separation between the Helium-Neon tube, the iodine cell and the rear mirror.

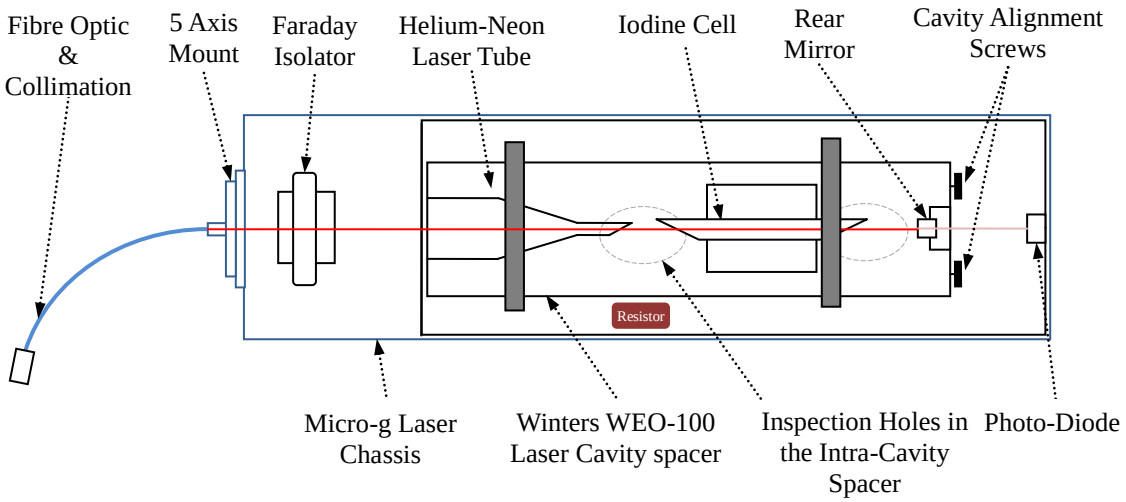

Figure 2.10 Schematic drawing of the WEO-100 configuration

The cavity spacer provides access to the Brewster windows at the end of the iodine cell and the He-Ne laser tube and the front face of the rear mirror via two inspection holes. Cleaning of the internal optics is carried out through these holes in the spacer. In a space between the rear mirror and the back of the laser the mirror alignment screws and the electronics are situated. The alignment screws allow careful adjustment of the angular displacement of the rear mirror. Within the electronics at the back of the laser a photodiode provides feedback information on power output of the laser, which can be displayed on the control electronics.

Full details of the laser can be found in the WEO-100 operators manual.

2.3.4. Super-Spring

To provide an inertial reference frame and vibration isolation from the high frequency natural micro-seismic activity of the planet, the FG-5 has a unique super-spring component (or assembly). The super-spring sits on a tripod base and is coupled to the interferometer which sits above it.

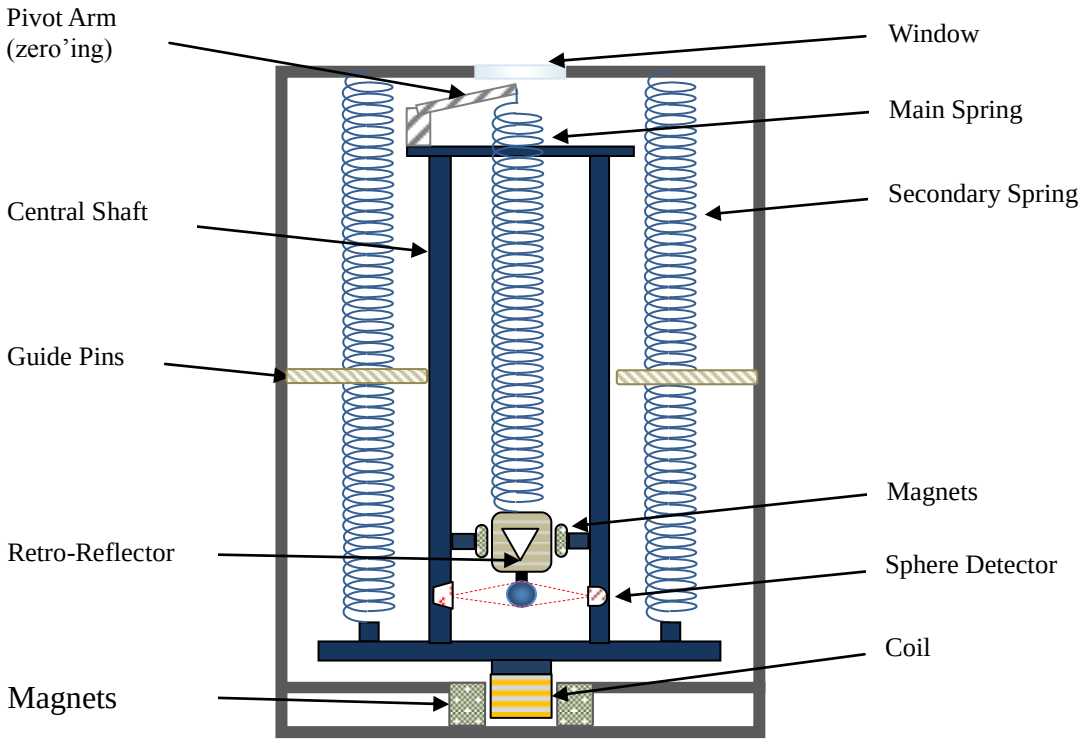

Figure 2.11 Basic drawing of the main components in the super-spring assembly

The super-spring is a electromechanical assembly with an active servo control. If considered as a two stage system: the first stage consists of the secondary springs and the active servo control, whilst the second stage consists of the main spring, mass, and retro-reflector, with magnets either side of the mass to provide some oscillation dampening. A device to provide positioning feedback, known as the sphere detector system, is situated below the mass/retro-reflector. It works by shining light from an LED*, situated on the

* LED - Light Emitting Diode

second stage, through a glass sphere situated on the bottom of the second stage, into a photo-detector, again positioned on the first stage.

The first stage is actively servo controlled to cancel the motion of the retro-reflector via the position feedback from the sphere detector system in the second stage. The combination of both stages results in a system which has a period of between 30 to 60 seconds which tends to remove the micro-seismic noise of the Earth with frequencies above 20 mHz.

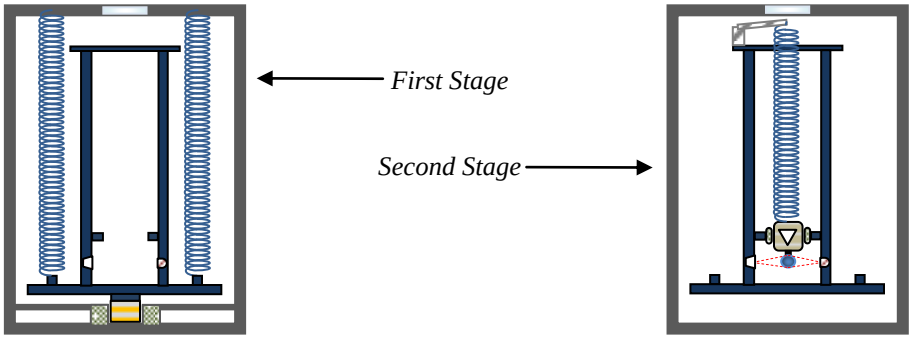

Figure 2.12 Super-spring stages

Although the system is able to compensate for the seismic frequency band mentioned, it is unable to compensate for larger seismic activity such as those generated from earthquake events, extreme weather over oceans and a variety of other sources, mainly man-made.

The super-spring is finely engineered and is easy to damage in transit; it therefore has a transit locking system and must be 'zero'd' before use. The zero'ing procedure ensures that the base of the spring system is taken to an equilibrium point, via the pivot arm, which will prevent it from coming into contact with any other surface under normal seismic conditions.

2.3.5. Electronics and Timing

The electronics rack and computer provide the communications, control, power, timing, barometric readings and data acquisition for the FG5. The computer is the system controller of the gravimeter and although not physically part of the electronics rack is best described in conjunction with it as it interfaces, via the Magma communications module, with the rest

of the systems. The Magma unit is a PCI expansion bus. Perhaps the next key component within the electronics rack is the SIM (system interface module), which provides, much as the name suggests, the central interface for information to be disseminated to the other components either through inputs or outputs. Other components are the power distribution module, within which the 10 MHz Rubidium clock is situated, the laser control electronics module, the Magma communications unit and the time interval card.

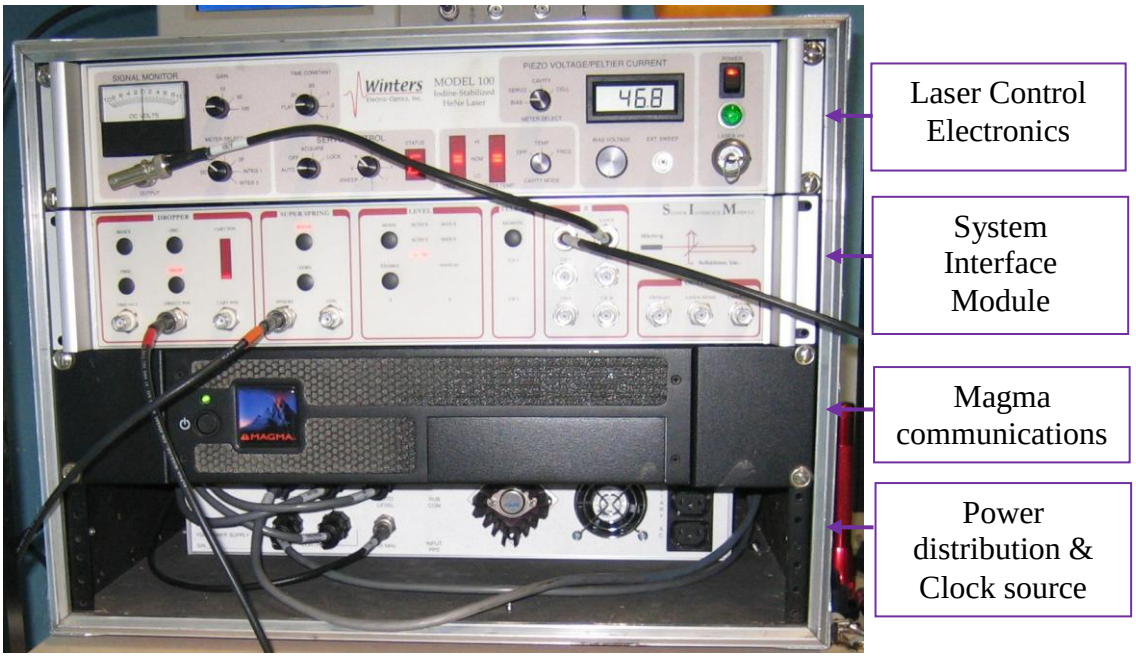

Figure 2.13 Photograph of the FG5 electronics rack (external computer excluded)

2.3.5.1. Laser Controller

The laser controller provides an interface which is primarily used by an operator to select a transition peak as well as the determination of the associated voltages of each transition peak, which is required to be inputted into the 'g' software. Whilst the gravimeter is in operation the voltage output of the selected peak is supplied to the system interface unit. This ensures the gravimeter operating software always knows which peak the laser is operating from and therefore compensates for the wavelength; see section 2.3.3 for further information.

2.3.5.2. System Interface Module, Magma and System Control

As mentioned above the system interface module provides the interface for the majority of signals that are passed, via the Magma module, to the system controller. In addition to this, the SIM also houses the dropping chamber control electronics, super-spring control electronics and the system barometer.

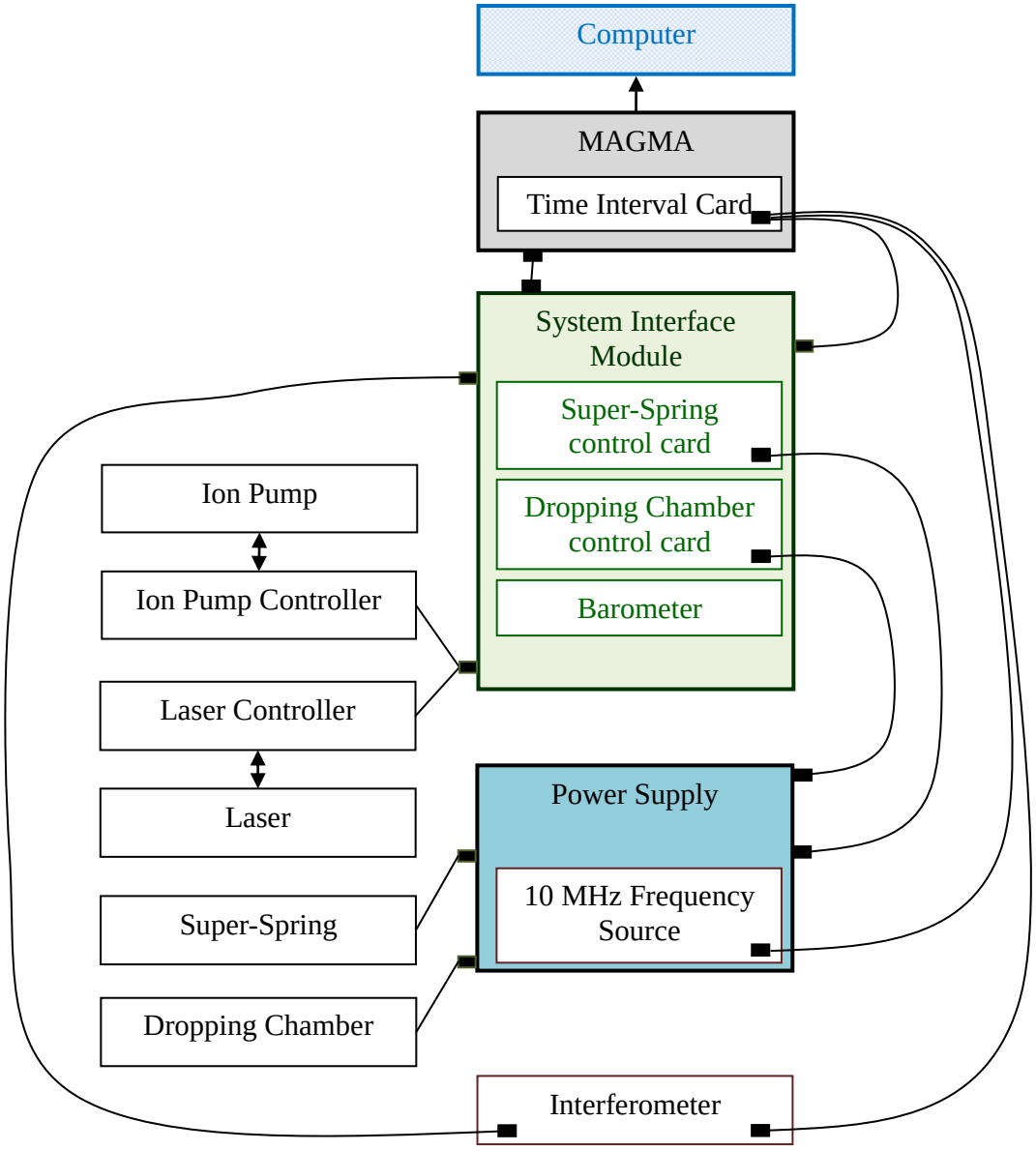

Figure 2.14 Communications between components, inputs and outputs included within the electronics rack ((FG5)

2.3.5.3. Timing/Clock

The fringe signal detected by the diode in the interferometer is converted into a TTL pulses. The TTL pulses are then scaled down so that around 700 can be compared to the 10 MHz clock pulses by the time interval analyser.

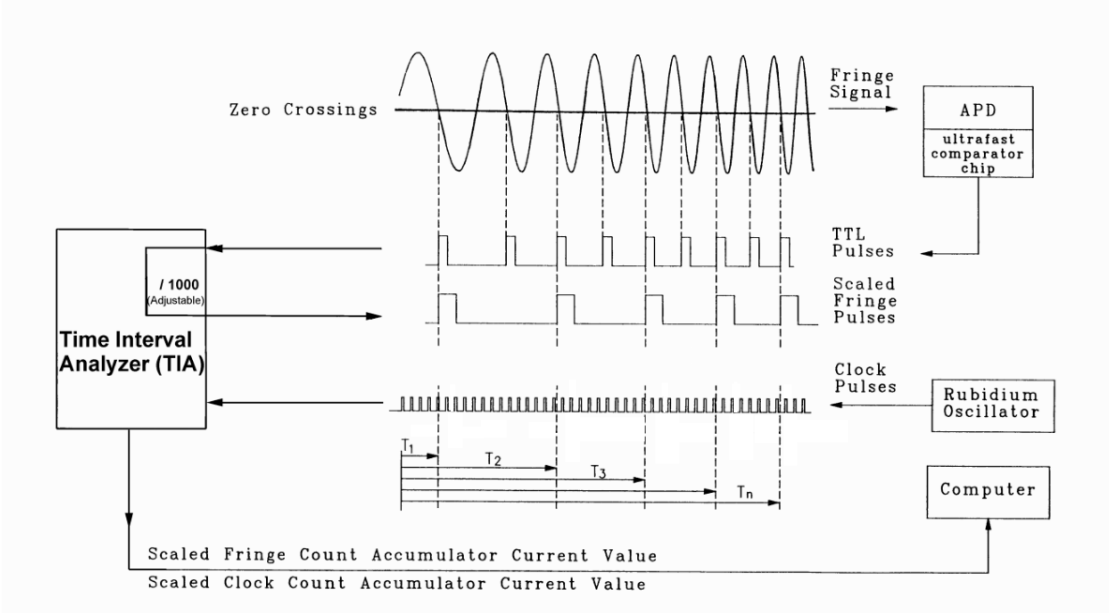

Figure 2.15 Timing process diagram, courtesy of Micro-g LaCoste

Table 2.2 Fringe count times and distances

Recorded Fringe number	Actual number of fringes	Time (s) T	Distance (mm) X
1	1	0.00025	0.0003
2	1001	0.00780	0.3000
3	2001	0.01110	0.6000
…	…	…	…
…	…	…	…
700	700001	0.20700	210.0000

(Micro-g LaCoste, 2006)

The scaled fringe times, from the time interval analyser, of 700 fringe counts, is then passed onto the computer and its software to store and calculate the associated value of g.

2.4. Instrumental Setup

Before each data set can be taken the FG5 must be set up carefully, both physically and electronically. The reference heights, the physical separation between floor and super-spring base and the interferometer and dropping chamber, must be taken and noted in the software.

The upper and lower tripods must be carefully levelled using the bubble levels provided on the super-spring and the top of the dropping chamber before the optical alignment, 'verticality' described in the next section, can be performed. The super-spring must be 'zero'd' to ensure the mass is hanging freely using the electronic control in the SIM unit. The voltaic output associated with the laser peak transitions must also be updated within the software (see section 2.3.3), along with the current polar rotation value. Following verticality the fringe peak-to-peak output must also be checked to ensure it is in operational range (between 250 mV – 400 mV).

2.4.1. Vertical Alignment

To ensure the drop is aligned correctly to the reference vertical, or plumb line, a pool of alcohol is placed within the interferometer. The optical path is changed by alcohol pool, the resulting beam path is shown in Figure 2.16. The split laser beam is now directed at the telescope, focussed at infinity, on the side of the interferometer. Each beam is seen as a spot of red light within the crosshairs within the telescope. Careful alignment of these spots must be made to ensure both spots overlap exactly. This is done by adjustment of the collimation assembly mount screws on the side of the interferometer. An error of half a spot, one spot overlaps the other by its radius, will result in an instrumental measurement error of 4 μGal.

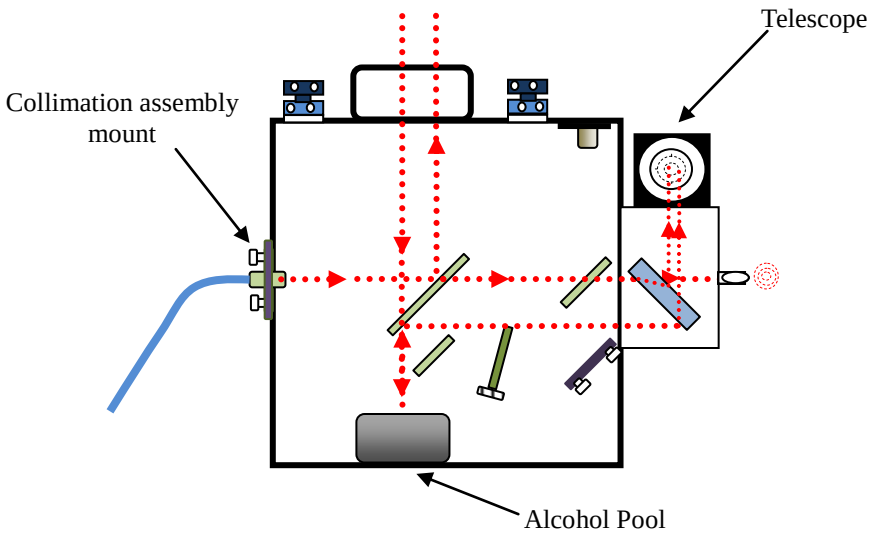

Figure 2.16 Interferometer verticality alignment of the FG5

2.5. FG5X

The FG5X is the new incarnation of the FG5. It is very similar to the older variants but features a longer dropping chamber, which is symmetrical around one axis, and is the dropping mechanism is now counterweighted, to reduce mechanical recoil and air gap modulation (Micro-g LaCoste, 2014). The counterweighted design reduces the mechanical recoil of the dropping system which can impart a pulse into the floor on which the gravimeter is situated.

The new drive system, featuring much larger drive pulley wheels and double drive belts (copper beryllium), is designed to reduce the wear on these components and improve the drop lifetime of the chamber (this is the anticipated total number of drops the chamber can perform before service is required) by four fold, the chamber has an anticipated drop lifetime of one million drops rather than the quarter of a million of the old chamber and drive system. Visually the new dropping chamber is aesthetically pleasing as the outer sheath is now glass and therefore the inner components are visible.

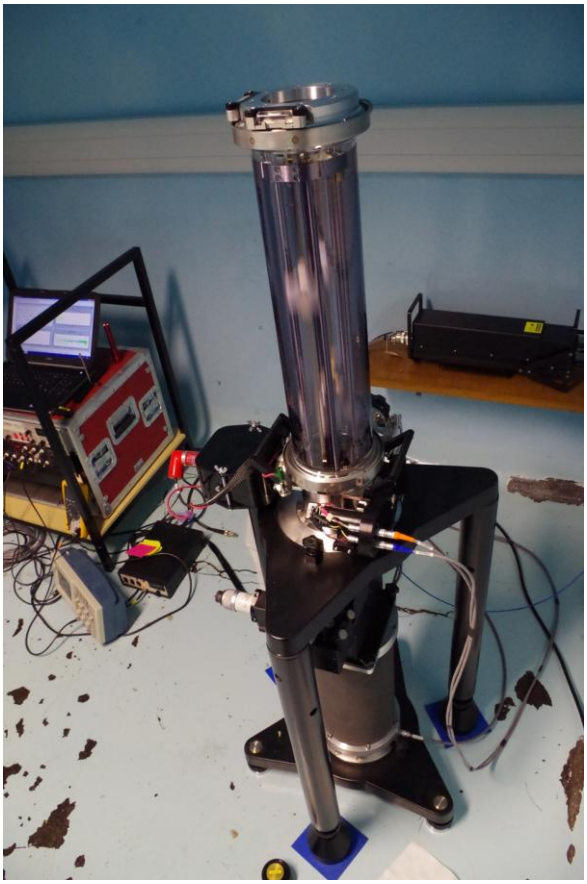

Figure 2.17 The FG5X: with the object within the dropping chamber in the process of being dropped.

Additionally the electronics have been improved and have eliminated a rack unit from the 2005 version of the FG5. In the FG5X the electrical leads to each component interface with the new SIM(X), frequency source switching is clearly labelled and the computer interface with the SIM(X) has been improved. Full details of the improvements can be found on the Micro-g LaCoste web pages.

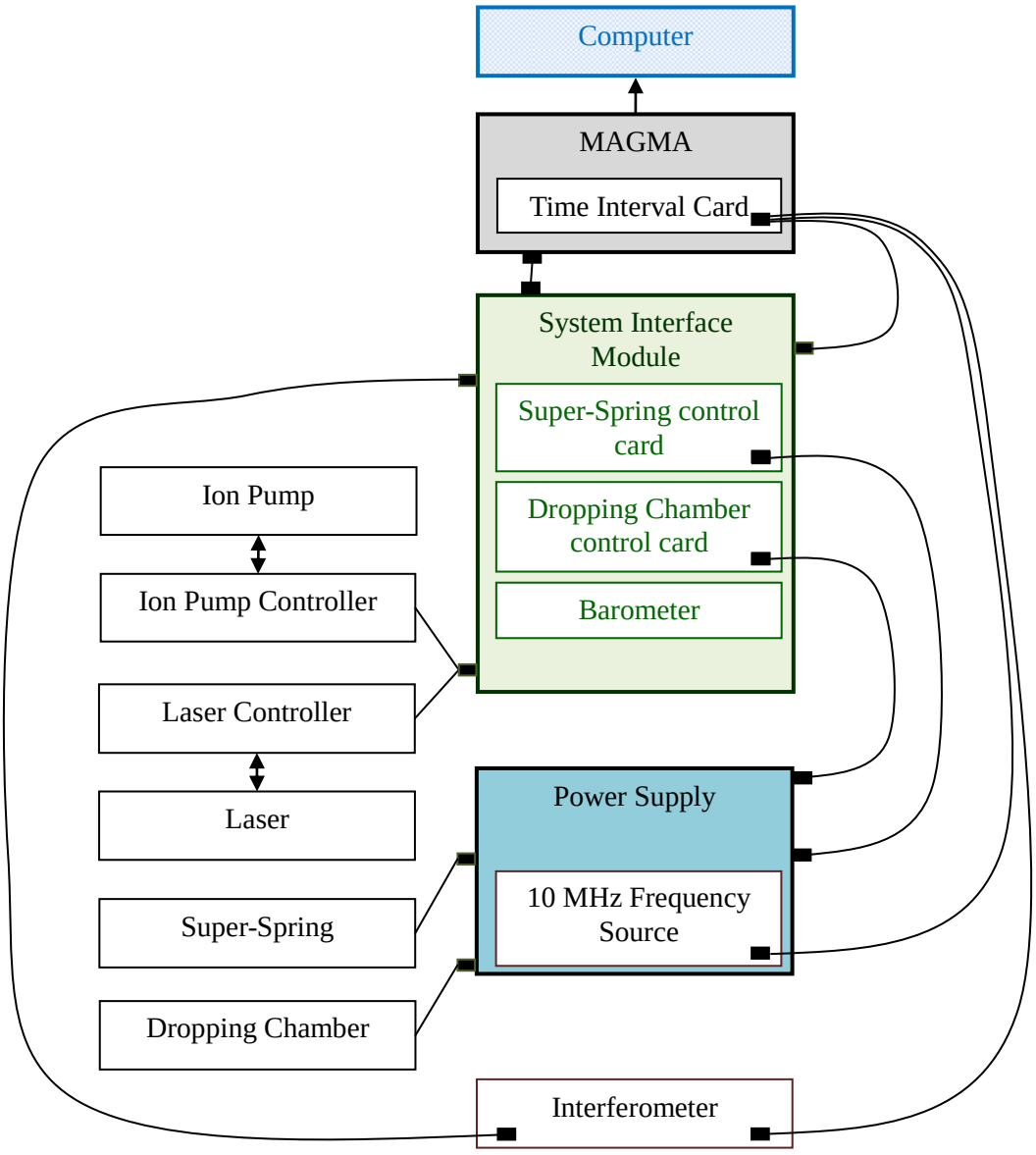

Figure 2.18 Communications between components, inputs and outputs included within the electronics rack (FG5X)

2.6. Software

A computer running the data acquisition software ‘g’ provides the gravimeter system control, as well as the data collection, processing and analysis of the results (Micro-g LaCoste, 2006). There have been numerous incarnations of ‘g’. During the period 2005 - 2016 versions g6, g7, g8 and g9 have been available.

In addition to ‘g’, supplied by the manufacturer, Dr Simon Williams, of the UK’s National Oceanography Centre - Liverpool, has developed a post processing software package named ‘gap’ which uses the binary output files generated by ‘g’. The ‘gap’ program is used later in this work and will be discussed in Chapter 9.

2.6.1. ‘g’ Software

The software governs the operation of the FG5 and allows the user to customise the data acquisition and operational running parameters. The software also processes the data and corrects for geodetic parameters; Earth tide, ocean-loading and polar motion.

The operational parameters ‘g’ allows the user to adjust fall into three main categories: those to be altered with each set up, those to be altered when the gravimeter has been moved to a new location, and those which are generally left untouched; which are considered standard for that instrument unless an instrumental parameter changes or some data tuning is desired.

- The first category, elements to be changed or adjusted on each setup, includes such things as polar rotation values, laser peak voltages and project details, including the duration and timing of the measurements.
- The second category includes geodetic coordinates, instrument set up heights* and a ‘tidal correction, which must be run for each site.
- The final category, standard parameters, include; fringe window (the interval timing during the drop over which gravity is calculated), frequency of the 10 MHz source† and configuration details of computer interface cards.

* The instrumental set up height of the FG5, which is comprised of the gap between floor and the base of the super-spring tripod and the gap between the interferometer and the base of the dropping chamber.

† The frequency of the rubidium clock has a nominal frequency of 10 MHz but the actual frequency must be calibrated and entered into the software.

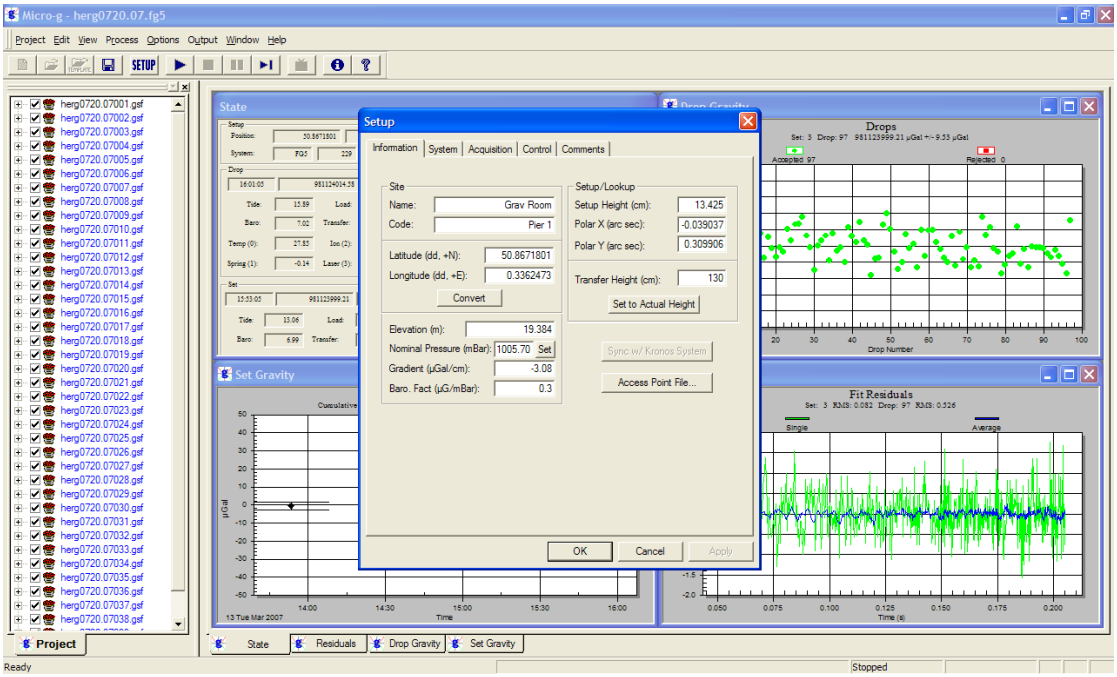

Figure 2.19 Screen shot of a gravity project in g7: to show the Setup tab, in which values can be adjusted

The data is processed rapidly and corrections applied with each drop, after each set and finally at the end of the project. If any changes need to be made to the setup information, for example: polar rotation or ocean-loading, the project will need to be reprocessed.

The project consists of a number of 'sets' which are comprised of a number of drops of the cart in the dropping chamber. The start-time of the sets and the number of drops per set can be set in the 'g' software. Standard procedure is to produce one set each hour of between 100 or 200 drops, the latter of which would result in a measurement duration for each set of approximately 25 minutes in each hour.

For each drop of the test mass within the dropping chamber a total of 700 time-position pairs are recorded. The data acquisition software performs a least square fit of the trajectory data using the equation:

$$x_i = x_0 + v_0\tilde{t}_i^2 + \frac{g_0\tilde{t}_i^2}{2} + \frac{\gamma x_0\tilde{t}_i^2}{2} + \frac{\gamma v_0\tilde{t}_i^3}{6} + \frac{\gamma g_0\tilde{t}_i^4}{24}$$

Where $\tilde{t} = t_i - \frac{(x_i - x_0)}{c}$ and $x_i, t_i, i = 1, \ldots\ldots, 700$

x_0, v_0, g_0 are the initial position, velocity and acceleration at t = 0. γ is the vertical gravity gradient and c is the speed of light. The gravity gradient is provided a-priori.

Statistical outlier criteria can be set by the user, the default value is set as three times the standard deviation. Outliers are rejected on a drop by drop basis where any drop outside the rejection criteria is removed and a new standard deviation is calculated, which is iterated until the set has completed. The remaining drops give the set values. The project gravity is the weighted average of the set values where the weights are $\frac{1}{\sigma_i^2}$ σ is the standard deviation of each set.

As already mentioned the software corrects for polar motion, Earth tides, ocean loading and barometric pressure as well as other variables which can be selected, such as the fringe selection used in the formulation of g for each drop. However it does is cumbersome to use if large data sets require reprocessing or re-evaluation for any reason.

The 'g' software outputs the raw observation information for each drop in a set in a binary file format, labelled with a 'gsf' extension. These files contain the raw information including time of drop, fringe times and sensor data (temperature, pressure, ion pump voltage, super-spring deflection voltage and laser wavelength). Additionally a two text files are generated, one containing the data for each set and the final project file.

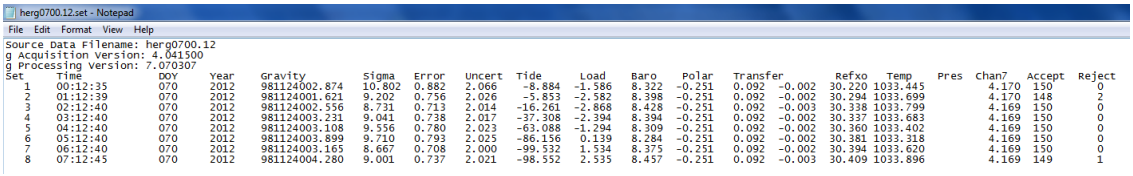

herg0700.12.set - Notepad

File Edit Format View Help

Source Data Filename: herg0700.12
g Acquisition Version: 4.041500
g Processing Version: 7.070307

Set	Time	DOY	Year	Gravity	Sigma	Error	Uncert	Tide	Load	Baro	Polar	Transfer	Refxo	Temp	Pres	Chan7	Accept	Reject
1	00:12:35	070	2012	981124002.874	10.802	0.882	2.066	-8.884	-1.586	8.322	-0.251	0.092 -0.002	30.220	1033.445		4.170	150	0
2	01:12:39	070	2012	981124001.621	9.202	0.756	2.026	-5.853	-2.582	8.398	-0.251	0.092 -0.002	30.294	1033.699		4.170	148	2
3	02:12:40	070	2012	981124002.556	8.731	0.713	2.014	-16.261	-2.868	8.428	-0.251	0.092 -0.003	30.338	1033.799		4.169	150	0
4	03:12:40	070	2012	981124003.231	9.041	0.738	2.017	-37.308	-2.394	8.394	-0.251	0.092 -0.002	30.337	1033.683		4.169	150	0
5	04:12:40	070	2012	981124003.108	9.556	0.780	2.023	-63.088	-1.294	8.309	-0.251	0.092 -0.002	30.360	1033.402		4.169	150	0
6	05:12:40	070	2012	981124003.899	9.710	0.793	2.025	-86.156	0.139	8.284	-0.251	0.092 -0.002	30.381	1033.318		4.169	150	0
7	06:12:40	070	2012	981124003.165	8.667	0.708	2.000	-99.532	1.534	8.375	-0.251	0.092 -0.002	30.394	1033.620		4.169	150	0
8	07:12:45	070	2012	981124004.280	9.001	0.737	2.021	-98.552	2.535	8.457	-0.251	0.092 -0.003	30.409	1033.896		4.169	149	1

Figure 2.20 Example of a '.set' file generated by 'g'

Chapter 3

Corrections to Absolute Gravity Measurements

3.1. Introduction

This chapter introduces those gravitational influences that are routinely removed from absolute gravity measurements. These include Earth system variables such as tidal deformations, polar motion, atmospheric corrections and the Bouguer free air correction. Gravity anomalies are also introduced, for both hydrological interpretations and to quantify the effect of masses above or below a measurement site.

3.2. Tidal Corrections

The largest signals to be removed from gravity data are the tidal effects. A varying gravitational attraction on Earth is induced by the orbital movements of planetary bodies, primarily the Moon and Sun, which causes deformation of the whole Earth system. This deformation can be broken down into three components; the solid Earth body tide, the magnitude of which is position dependent and of order 30 cm in site displacement, can be described by the tidal potential on the rigid Earth, given in Section 3.2.1 of this chapter. Additionally, the oceanic tide, of varying magnitude from a few to several metres, is not directly related in phase or periodicity to the body tide since it is dependent on a number of factors such as topography of the oceanic floor, ocean depth, interaction with land masses and the rotational interaction between Earth and water. Finally ocean-loading is a secondary effect caused by the loading effect upon the Earth's crust from the rising and falling oceanic tide (Hopewell, 1999) (Torge, 1991); the magnitude of the effect is greatly dependent upon distance from the ocean. In the southern UK the ocean loading effect is a large 6 cm in the West (Cornwall), to 1 cm at Herstmonceux. Herstmonceux is a so-called nodal point, where

to a large degree the ocean-loading induced by the North Sea is cancelled by the out-of-phase impact of the loading from the English Channel.

For ground-based measurements of the local acceleration due to gravity, the solid Earth and ocean-loading displacements are the primary signals that are expected to be found in the observations, the direct acceleration sensed by the gravimeter due to water displacement driven by the ocean tidal change is extremely small, being an acceleration for all instruments that are not on the shoreline close to normal to the vertical path of the test-mass.

3.2.1. Tidal Potential

The tidal generating potential effect of celestial bodies upon the Earth can be described by terms involving the positions of the celestial body in question and the latitude and longitude of a position upon the Earth (Charles, 1995).

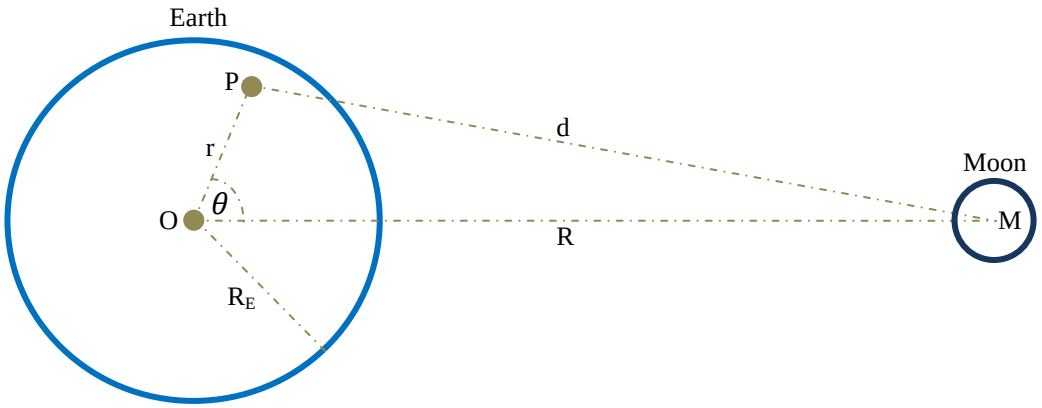

Figure 3.1 Tidal potential geometry from the Moon

The gravitational potential at a point P on the Earth's surface is defined to be:

$$V = \frac{GM}{d}$$

Where G is the gravitational constant and M the mass of the Earth.

The cosine law for the triangle OMP: $d^2 = r^2 + R^2 - 2rRcos\theta$

Therefore:

$$V = GM(r^2 + R^2 - 2rRcos\theta)^{-\frac{1}{2}}$$

So:

$$V = \frac{GM}{R}\left(1 + \frac{r^2}{R^2} - 2\frac{r}{R}cos\theta\right)^{-\frac{1}{2}}$$

However since the radius of the Earth is approximately $\frac{1}{60}th$ the distance of R: $\frac{r}{R} \ll 1$, therefore using the Binomial expansion: $(x + a)^n = \sum_{k=0}^{n} \binom{n}{k} x^k a^{n-k}$

$$V = \frac{GM}{R}\left(1 + \frac{r}{R}cos\theta - \frac{r^2}{2R^2} + \frac{3}{8}\left(4\frac{r^2}{R^2}cos^2\theta\right) + \cdots\right)$$

$$\therefore V = \frac{GM}{R}\left(1 + \frac{r}{R}cos\theta - \frac{r^2}{2R^2} + \frac{r^2}{R^2}(3cos^2\theta - 1) + \cdots\right)$$

$$\therefore V = \frac{GM}{R} + W_1 + W_2 + \cdots$$

Where $W_1 = \frac{GMr}{R^2}cos\theta$ and $W_2 = \frac{GMr^2}{R^3}(3cos^2\theta - 1)$

Most tidal work stop at W_2 since expressions above this account for only 1-2% of the tide varying potential.

The first term of the potential $\frac{GM}{R}$ is a constant and therefore produces no force and can thus be ignored.

The second term: $W_1 = \frac{GMr}{R^2} cos\theta$ can be written

$$W_1 = \frac{GM}{R^2} x$$

$$\text{Force} = \nabla W_1 = \frac{\delta}{\delta x}\frac{GM}{R^2} = \frac{GM}{R^2}$$

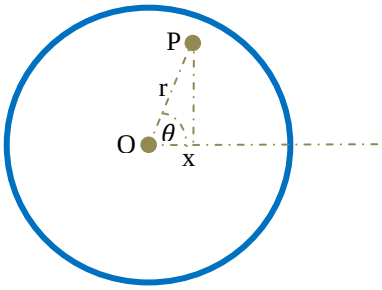

Figure 3.2 W_1 geometry

Every point P has the force acting upon it in a direction parallel to the line between the centre of the Earth and the Moon, therefore W_1 gives no differential forces within the Earth and therefore does not generate tides. The first term to give differential forces and from which the main tidal potential is obtained is W_2.

$$W_2 = \frac{GMr^2}{R^3}(3cos^2\theta - 1)$$

Spherical trigonometry, for Figure 3.3, gives:

$$cos\theta = sin\varphi\, sin\delta + cos\delta\, cos\varphi\, cosH$$

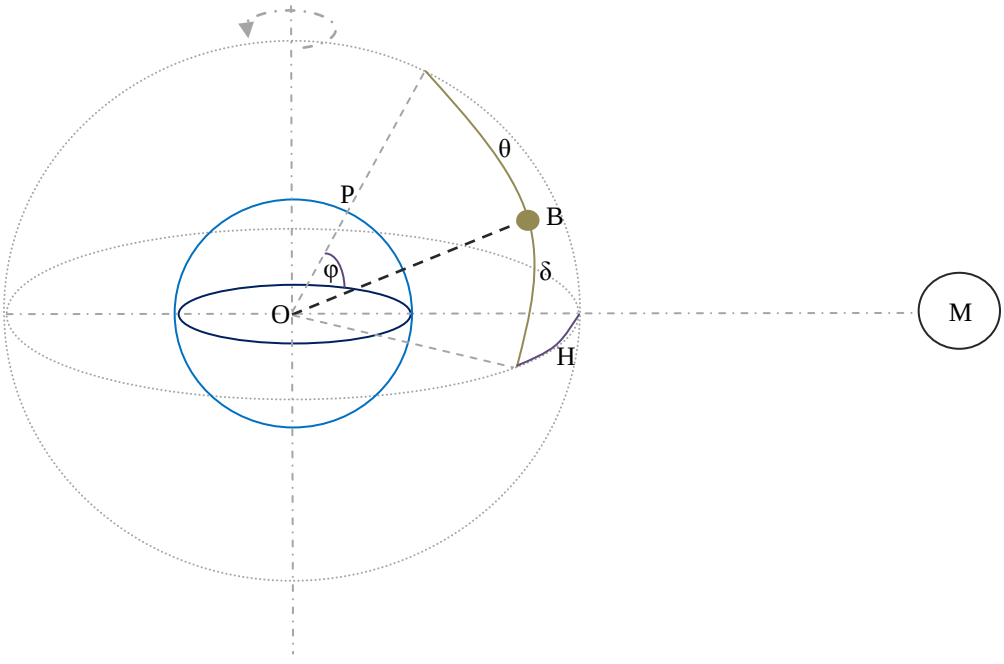

Figure 3.3 Diagram to show declination, latitude and hour angle

When this is substituted into the equation for W_2:

$$W_2 = \frac{3GMr^2}{4R^3}\left(cos^2\varphi\, cos^2\delta\, cos2H + sin2\varphi\, sin2\delta\, cosH + 3\left(sin^2\varphi - \frac{1}{3}\right)\left(sin^2\delta - \frac{1}{3}\right)\right)$$

The first two terms in brackets in this equation is dependent on the hour angle, H, and therefore produce two different tides. The cos2H and cosH terms give rise to semi-diurnal and diurnal tides respectively. The last term in brackets has no dependency on H and produces long period tides. Some primary tidal constituents are given in Table 3.1.

Table 3.1 Primary Tidal Components (Baker, 1984) (NOAA, 2013) (Torge, 1989)

	Name	Nature	Period	Amplitude of gravity tide to the rigid Earth (φ = 45°, H=0) (μGal)
M_2	Principle lunar	Semi-diurnal	12.42	37.56
S_2	Principle solar	Semi-diurnal	12.00	17.48
N_2	Major lunar elliptical	Semi-diurnal	12.66	7.19
K_2	Luni-solar declinational	Semi-diurnal	11.97	4.75
K_1	Luni-solar declinational	Diurnal	23.93	43.69
O_1	Principle lunar	Diurnal	25.82	31.06
P_1	Principle solar	Diurnal	24.07	14.46
Q_1	Major lunar elliptical	Diurnal	26.87	5.95
M_f	Lunar fortnightly	Long term	13.66d	3.19
M_m	Lunar monthly	Long term	27.55d	1.68
S_{sa}	Solar semi-annual	Long term	182.62d	1.48

The elastic response of the Earth to the tidal potential is small and can thus be treated as a linear. The radial displacement, δr, caused by the tide-generating potential W_2 is proportional to W_2 and the subsequent potential, U_{def}, from the deformation caused by δr is also proportional to W_2 thus:

$$\delta r \propto \frac{W_2}{g} \quad \text{and } U_{def} \propto W_2$$

However since the elasticity and density of the Earth need to be considered, from Love's numbers h and k which themselves depend on the spherical harmonic expansion of the tidal deformation) (Torge, 1989):

$$\delta r = \frac{hW_2}{g} \text{ and } U_{def} = kW_2$$

The total tidal effect, from a celestial body, upon gravity can be described by three factors;

- The direct gravitational attraction of the celestial body itself, g_{attr}
- The deformation of the Earth's crust, g_{def}
- The redistribution of the Earth's mass, g_{rm}

The sum of which gives an equation for the total variation in gravity as:

$$g = g_{attr} + g_{def} + g_{rm} = \frac{2W_2}{R_E}\left(1 + h + \frac{3k}{2}\right)$$

3.2.2. Ocean-Loading

Global tidal models are formulated in grids, usually of fixed spacing's of latitude and longitude, the spatial resolutions of which are dependent on the model being used, but are usually between 0.125° and 0.25° (for example FES2004 and GOT00.2 respectively). The models can be a computation of the global oceans or an amalgamation of a few ocean basins which are stitched together (Bos, 2011). Problems with using tidal models are commonly found at coastal sites where the large grid cells do not match the coastlines, as shown in Figure 3.4.

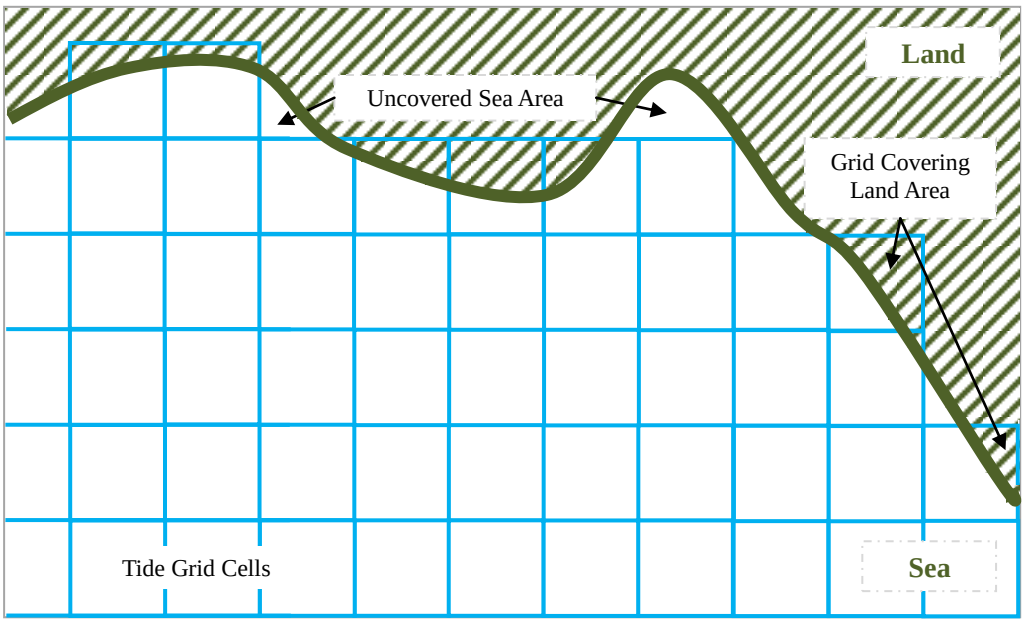

Figure 3.4 Imperfect fit of tidal model to coastlines

If problematic one way to overcome this mismatch can be the insertion of a higher resolution grid into the global model. Or, for gravity sites, instruments to measure the tidal effects can be installed.

3.3. Polar Motion

Polar motion is the motion of the rotation axis of the Earth relative to a fixed, time invariant, rotational axis, which is defined as the average pole position between 1900.0 and 1906.0 (Torge, 1989). A compensation for the change in centripetal acceleration must be made to the gravity data as the Earth wobbles on its axis and the distance from that axis to the gravity station changes. (Taylor, 1997).

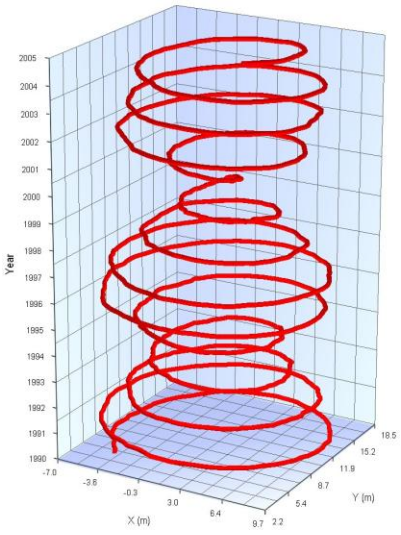

Figure 3.5 Illustration of the path polar motion describes in free space

The equation used is:

$$\delta g = -1.164 \times 10^{8}\left(2a\omega^{2} Sin\varphi Cos\varphi (xCos\lambda - ySin\lambda)\right)$$

Where: δg is the polar motion correction in μGal, ω is the Earth's angular rotational velocity in radians per second, a is the semi-major axis of the reference ellipsoid, φ & λ are the geodetic latitude and longitude in radians and x & y are the polar coordinates in the IERS system, also in radians. (Micro-g LaCoste, 2006).

The polar motion coordinates, or Earth observation data can be obtained from the International Earth Rotation and Reference Systems Service (IERS)*.

3.4. Atmospheric Correction

Variable atmospheric pressure will affect the measured value of gravity at a site due to changing Newtonian atmospheric-mass attraction on the dropping test-mass. It is thus necessary to remove this time-dependent effect by normalising measured gravity to a standard value of atmospheric pressure. In order to facilitate this, the FG5 is equipped with a barometric pressure sensor within the system interface module, which is used to apply the pressure correction. The observed gravity for each drop is normalised to the nominal pressure, supplied for each site in the software setup parameters, by the application of a barometric correction factor, C_p :

$$C_p = A \cdot (P_0 - P_n)$$

Where: A is the barometric admittance factor (approximately -0.35 μGal hPa^{-1}) , P_0 is the observed barometric pressure and P_n is the nominal barometric pressure (Micro-g LaCoste, 2006).

* https://www.iers.org/IERS/EN/DataProducts/EarthOrientationData/eop.html

3.5. Hydrological Corrections

The Bouguer free air correction is used in gravimetry as a default gravity gradient when the real value is unknown. Calculating the gravitational attraction of a mass beneath the surface of the Earth from a measurement point above the mass is based on a well documented theory. Some of the simple examples include an infinite flat plate anomaly (Bouguer correction), and a buried sphere.

3.5.1. Bouguer Free Air Correction

A correction must be made to gravity measurements when not observed at the geoid (for this purpose we can also use mean sea level), this being known as the 'free-air' correction and is based upon the assumption that only the elevation of a gravimeter is important, not the (usually unknown) mass between it and the geoid.

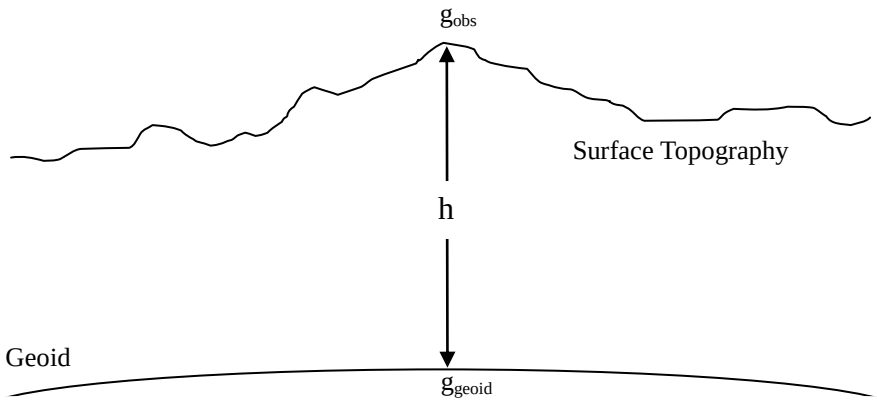

Figure 3.6 Surface topography and geoid relation

From the first term in the spherical harmonic expansion for the Earth's gravitational field:

$$U = \frac{GM}{R}\left(1 - \sum_{n=2}^{\infty} J_n \left(\frac{R}{r}\right)^n P_n sin\delta\right)$$

Only the first term is important for acceleration, so with respect to the distance between the measurement point and the geoid (Figure 3.5):

$$\frac{\partial g}{\partial h} \approx \frac{\partial}{\partial h}\left(\frac{GM}{(R+h)^2}\right) = -2G\frac{M}{(R+h)^3}$$

Then since R>>h, and $g = \frac{GM}{R^2}$

$$\frac{\partial g}{\partial h} \approx -2\frac{g}{R}$$

Therefore to correct a value of observed gravity (g_{obs}) to height h from the geoid the free air correction must be added to the measurement.

$$\delta g_{freeair} = \frac{2g}{R}h$$

This term is commonly used when using FG5 absolute gravimeters to convert the measured height to a standardised height. If the mean acceleration due to gravity across the world is used for g_o the $\frac{2}{R}g$ term becomes a constant and therefore:

$$\partial g = 3.086h\ \mu Gal\ cm^{-1}$$

3.5.2. Bouguer Anomalies

The Bouguer anomaly is used for local corrections to gravity measurements. The Bouguer infinite slab correction calculates the gravitational effect of a homogenous horizontal plate of thickness, h, and infinite extension.

$$\Delta g = 2\pi G\rho h$$
$$\therefore \Delta g = 0.0419\rho h \quad \mu ms^{-2}$$

Where ρ is the density of the disturbing mass in kgm^{-3} and h is the distance to the slab in metres.

This gives a first approximation for flat plate changes in a homogeneous layer, but this can be altered slightly when considering either a change in gravity due to soil moisture level or

by a change in the thickness of the groundwater layer. Such that: The effect on the gravity value for a change in *soil moisture* is:

$$\delta g_{sm} = 2\pi GH\rho_w \delta P = 4.2H\delta P$$

And, the effect on the gravity value for a change in the thickness of the *ground water* is:

$$\delta g_{gw} = 2\pi GP\rho_w \delta H = 4.2P\delta H$$

where: δg_{gw} is the change in gravity due to a change in ground water, G is the gravitational constant, δH is the change of thickness of the groundwater layer, $\rho_w$is the density of water and P is the water filled pore space. δg_{sm} is the change in gravity due to soil moisture, H is the thickness of the soil moisture layer, $\rho_w$is the density of water (Torge, 1989).

3.5.3. Gravity Anomaly for a Buried Sphere

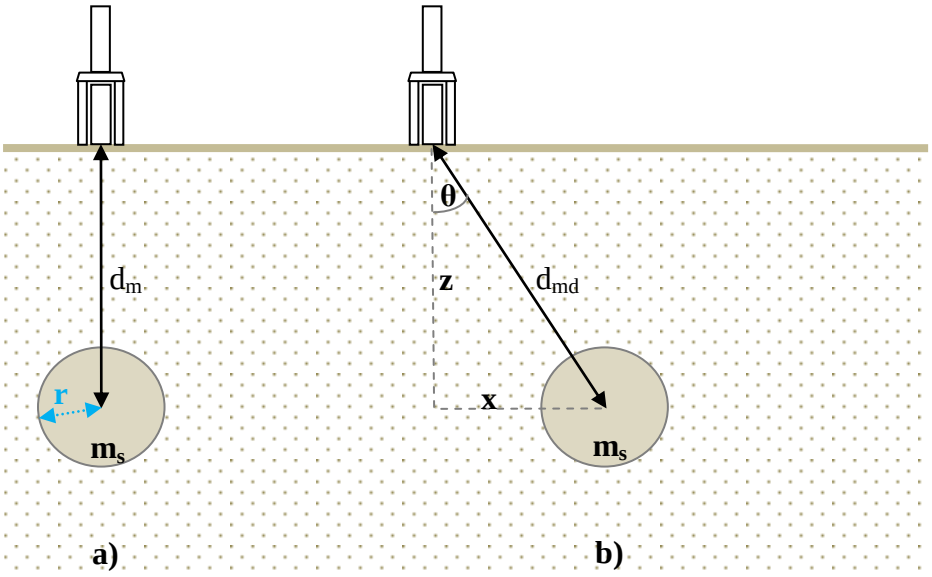

Figure 3.7 Gravity anomaly from a buried sphere

Analogous to the attraction of the Earth on some point in space, a buried sphere follows from the same basic equation :

$$g = \frac{GM}{R^2}$$

But instead of considering the whole Earth as the mass we are considering a change in mass of a buried sphere from the material surrounding it, as shown in Figure 3.7, which results in a change in gravity. Using the configuration shown in the figure above:

$$\Delta g = \frac{G\Delta m}{{d_m}^2}$$

Since $m = \rho V$ & $\Delta m = \Delta \rho V$

$$\Delta g = \frac{G\Delta \rho V}{{d_m}^2}$$

Since in this case $V = \frac{4}{3}\pi R^3$

$$\Delta g = \frac{G\Delta \rho}{{d_m}^2} \cdot \frac{4}{3}\pi R^3$$

This equation gives the result for example ‘a’ in Figure 3.7, where the mass is directly below the gravimeter. However if the mass is not directly beneath the gravimeter then both the horizontal and vertical components must be taken into consideration, Figure 3.7 case ‘b’.

Since ${d_{md}}^2 = z^2 + x^2$ then:

$$\Delta g = \frac{4G\pi R^3 \Delta \rho}{3} \cdot \frac{1}{(z^2 + x^2)}$$

also, since $\Delta g = \Delta g cos\theta$, and $cos\theta = \frac{z}{r}$:

$$\Delta g = \Delta g cos\theta = \frac{4G\pi R^3 \Delta\rho}{3} \cdot \frac{1}{(z^2 + x^2)} \cdot \frac{z}{r}$$

$$\Delta g = \frac{4G\pi R^3 \Delta\rho}{3} \cdot \frac{1}{(z^2 + x^2)} \cdot \frac{z}{(z^2 + x^2)^{1/2}}$$

$$\Delta g = \frac{4G\pi R^3 \Delta\rho}{3} \cdot \frac{z}{(z^2 + x^2)^{3/2}}$$

Substituting for $\frac{4}{3}\pi G$:

$$\Delta g = 2.79 \times 10^{-10} \frac{R^3 z \Delta\rho}{(z^2 + x^2)^{3/2}} \quad ms^{-2}$$

This brief summary of the basic theory will be used in Chapter 11 to correct observed values of gravity at Herstmonceux for the effects of structural change and for hydrological variations below and above the instrument.

Chapter 4

Comparisons of Absolute Gravimeters

4.1. Introduction

Scientific measurement instruments require regular checks in the form of calibrations or comparisons to ensure they are operating within performance specifications; this is true for a vast array of instruments ranging from oscilloscopes, dosimeters, micrometers or practically any measurement sensor (such as those for temperature or humidity).

Generally, for calibrations/comparisons an instrument called a reference standard is used, which is calibrated in a chain of measurements that can be traced back to international standards, such as the volt, ampere, metre or watt, against which an instrument can be tested under strict protocols. Such testing either results in the device under test being adjusted to conform with the standard or, more commonly in high-accuracy devices, an offset from the standard being obtained and recorded.

However, the method described above is not suitable for absolute gravimeters (AGs) since the measurement of the acceleration due to the Earth's gravity (g) is not dependent on the instrumentation alone but also on spatial and temporal variables. In fact, the term 'calibration' is generally avoided within the absolute gravimetry community since it is impossible for measurements to be taken in the same location at the same time. Estimation of how accurate the gravimeters are to a true value of g is beyond the bounds of possibility; all that can be quantified is the relative offset of gravimeters from one another (Francis, et al., 2013).

Since we cannot make simultaneous measurements at the same site, a comparison of AGs must be conducted with multiple AGs that are run at the same epochs in different, but well known, locations within a laboratory (Sasagawa, et al., 1995) (Robertsson, et al., 2001). The ability to transfer temporally and spatially independent observations of a particular location makes the choice of site for a comparison especially important; therefore, sites are generally chosen where a number of factors, such as gravity gradient, seismic noise and environmental changes, are either known or known to be minimal.

The first International Comparison of Absolute Gravimeters (ICAG) held at the International Bureau of Weights and Measures (BIPM) in 1981 involved JILAg absolute gravimeters, as it predated the first FG5 absolute gravimeter (1993, see Chapter 2) by nearly a decade. Comparisons were held by the BIPM at near 4-year intervals until 2009 (Jiang, et al., 2012), when BIPM ceased their support of ICAG meetings at Sèvres. Nowadays the primary location for comparisons within Europe, and arguably the world, is the Walferdange Underground Laboratory of Geodesy in the grand duchy of Luxembourg, which first hosted the ICAG in 2013, but was first used as a comparison site in 2003, for a European Comparison of Absolute Gravimeters (ECAG) (Ruess, 2011), and has hosted regular ECAG's since. The Walferdange laboratory has a large advantage over the BIPM site due to the ability to host a maximum of 16 absolute gravimeters simultaneously, whereas only 3-5 piers were used during comparisons at the BIPM site (Robertsson, et al., 2001) (Jiang, et al., 2012) (Vitushkin, et al., 2002).

4.2. Comparisons and the Absolute Gravimetry Community

AG users comprise both geodesists and metrologists, each with slightly different objectives from AG measurements and therefore also slightly different desired outcomes from a comparison. National Metrology Institutes (NMIs) are generally more concerned with the traceability of the gravity measurement to SI base units (Marti, et al., 2014) and commonly use an AG for the determination of standards based upon the kilogram and for the watt balance experiment (Francis, et al., 2013). In contrast, geodesists use AG measurements for monitoring geodynamic processes over a period of decades and therefore are most

interested in the overall performance of a gravimeter, especially in terms of reproducibility and repeatability.

Two distinct types of comparison have been adopted to best suit the requirements of each community of users. Metrologists must follow strict metrological rules to participate in a Key Comparison, which is only available for the metrological community to signatories of the CIPM (the international committee for weights and measures) Mutual Recognition Arrangement (CIPM MRA) and laboratories officially designated by those institutes (Francis, et al., 2013). The second type of comparison is known as a 'Pilot Study' and is available for both geodesists and metrologists.

There was no strict agreement between the communities until 2014, when a common strategic document was agreed upon between the 2 user communities. The common strategic document came about from a meeting held in 2013 between the president of the Consultative Committee for Mass and Related Quantities (CCM) and the president of the International Association of Geodesy (IAG), Commission 2 (Gravity Field), during which it was agreed in principle. The resulting document was reviewed by both communities during 2014 and was accepted by the IAG in 2015. The following is an excerpt from the IAG's letter (International Association of Geodesy, 2015) to the 2 committees involved:

> 'This initiative does improve the traceability of absolute gravity measurements, and ensures the continuation of future comparison and calibration activities and procedures. This document is most relevant, and important, for the IAG as it will assist in the establishment of a global gravity reference system. Furthermore it is a contribution to the Global Geodetic Observing System (GGOS). The IAG Executive Committee therefore accepts the current document "CCM-IAG Strategy for Metrology in Absolute Gravity".

It should be noted that both the frequencies of the laser and the frequency of the reference clock in free-fall devices, such as the FG5, can be independently traced to the SI (Marti, et al., 2014).

4.3. Method

The basic requirement for any comparison is that multiple AGs are used, and ideally simultaneous measurements are taken with each gravimeter located on an independent pier, for which the associated coordinates are known. Each pier can either be a mechanically isolated platform designed to decouple the interferometer subsystem from building vibrations, or simply a location marker on the floor.

Generally a comparison is taken over a number of sequential days with each participating AG occupying several of the available piers over the duration, each measured for a period of 12 or more hours. Some users might also use the scheduled start operation facility available in the ‘g’ software to ensure all operators are absent from the measurement room and therefore outside noise is limited to a minimum.

Over the last 10 years, comparisons have been conducted using up to 22 gravimeters, mostly FG5s (including the FG5X) but including 4 other different types (Francis, et al., 2013). In these large comparisons, the occupation of gravimeters and piers was carefully planned to ensure that each gravimeter could be compared with the maximum number of instruments, and a protocol by the comparison laboratory was issued prior to the meeting.

In addition to a programme of measurement for each gravimeter, the technical protocol for the comparisons held at Walferdange since 2007 has also included geographical coordinates, a determination of the vertical gravity gradient for each measurement pier and a set of observed tidal parameters to be used in the reduction process.

During the duration of the comparison, each instrument is swapped around the scheduled piers; depending on the facilities available at a comparison, a determination of rubidium clock frequency, barometer and laser collimation may be available (Schmerge, et al., 2012) (Francis & vanDam, 2010).

4.3.1. Adjustment of the Data for Comparison

Following completion of the comparison, the data are usually supplied to an organising laboratory or committee, who will analyse the data. Prior to 2007, the emphasis was placed with the organising laboratory, to which raw data were supplied to be reduced and compared. However, since the ECAG comparison in 2007, the responsibility has shifted to ensure each participant is generally responsible for producing a data point with associated uncertainty for each pier. Only then are the data passed along to the organiser as usual to be compared to results from the other participating absolute gravimeters. An uncertainty budget for each gravimeter is also provided, an example of which is detailed in the technical protocols for each comparison. Since 2009, when the first Key Comparison in absolute gravimetry was held, an estimation of the self attraction of the gravimeter or the diffraction effect was considered in the final results; more information on both can be found in Chapter 6.

The statistical method used in each comparison has varied over the decades, most significantly by the move away from transferring all measurements to one pier via ties provided by relative gravimeter measurements in 2001 (Jiang, et al., 2012). Since then, the results have been processed by using some form of least squares analysis to generate different solutions, as required, for independent results for relative gravimeters, absolute gravimeters or combined results (Vitushkin, et al., 2002).

Regardless of the detail of the least squares adjustment of the data employed, the basis is to use the observational data from each site or pier, whilst allowing each AG, simultaneously in the solution, to have its own intrinsic offset (or bias) that is independent of the sites visited. A constraint is placed upon the solution, such that the mean of all of the offsets is equal to zero to provide the relative offsets between the AGs; the constraint ensures that the problem is numerically stable, giving limited results rather than the infinite set of solutions that would be generated without the condition.
For the ECAG of 2007 and the NACAG of 2010 (the north American comparison of absolute gravimeters) the least square observation equation was:

$$g_{ik} = g_k + \delta_i + \varepsilon_{ik}$$

with the condition $\sum_i \delta_i = 0$

Where g_{ik} is the gravity value at the site k given by the instrument i, g_k is the adjusted gravity value at the site k, δ_i is the offset of the gravimeter i and ε_{ik} is the stochastic error (Francis & vanDam, 2010) (Francis, et al., 2014) (Palinkas, et al., 2015). This equation was also used in the NACAG 2010 but a different sign convention is shown in the relevant paper (Schmerge, et al., 2012). Data processing involved the use of observed vertical gravity gradients and the tidal parameters obtained from the superconducting gravimetry measurements at each site.

4.3.2. Implementation of Comparison Results

The aim of comparisons is to provide knowledge that each gravimeter is operating within specification. The end result provides each gravimeter with an offset from a mean value, obtained from the observation equation, and an associated uncertainty in the offset.

In geodesy comparisons are essential to ensure consistency between observations which span decades, but the offset values are not always used to correct time series. The use of any offset may be dependent on whether it falls outside the accuracy parameters of the instrument. In this way the geodetic use of the comparison data is not regimented.

4.4. Comparison Sites

There have been a variety of comparison sites used since the early 1980s for large comparisons, including the BIPM in France, the Table Mountain Geodetic Observatory (TMGO) in the USA, the Walferdange Underground Laboratory for Geodynamics (WULG) in Luxembourg and Belval, which is also in Luxembourg (see section 4.4.2), but smaller comparisons have been conducted at many different sites around the world, including at Micro-g's factory. The sites in Luxembourg are the focus of this study as the results from these sites are reported in Chapters 7 and 13.

It should be noted that the first formal comparison measurement outside of the European Union was conducted at TMGO for the first North American comparison of absolute gravimeters in 2010 (Schmerge, et al., 2012).

4.4.1. Walferdange Underground Laboratory for Geodynamics

The small town of Walferdange is situated just outside the city of Luxembourg, in the grand duchy of Luxembourg, and is home to the WULG and the European Centre for Geodynamics and Seismology (ECGS).

Although the gravimeters were installed within the WULG as far back as 1967, the dedicated gravimetry room (dedicated to the former astronomer Paul Melchior), which is now regularly used by the gravimetry community, was not added until 1999 (European Centre for Geodynamics and Seismology, n.d.). The gravimetry room was purpose-built on 3 levels of concrete flooring, each with 5 piers (surveyed location studs), and has the largest capacity for conducting comparisons in the world. In addition to the AG room, the capability at the WULG includes a super-conducting gravimeter, which is considered a great advantage in a comparison location due to its continuous measurement and the increased level of knowledge this type of gravimeter can provide about a site, and also an assessment of the laser frequencies compared to a standard.

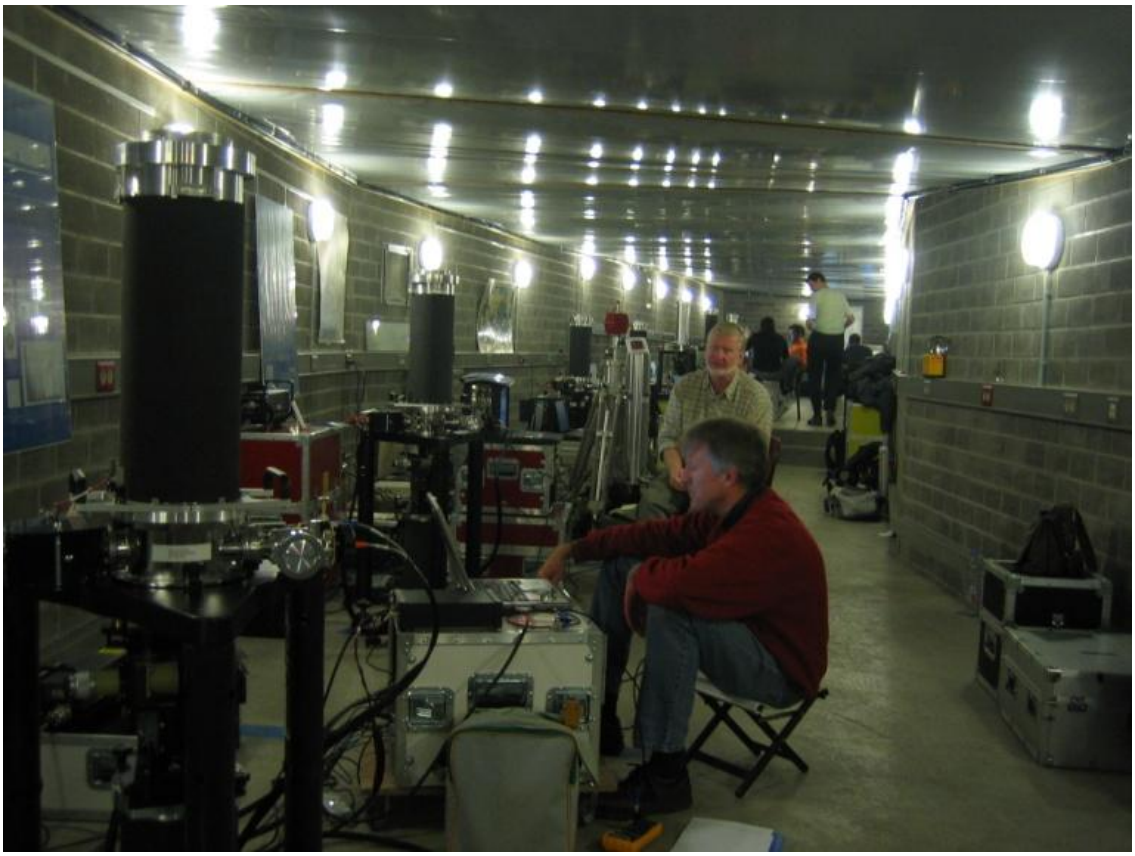

Figure 4.1 Inside the WULG

The WULG is located within a former gypsum mine with the gravimetry room approximately 300 metres from the entrance and 100 metres below the surface. The site came about under the GRAVILUX project, the aim of which was to establish a gravity reference site with low seismic noise and that was constantly monitored (Melchior, 2005).

Figure 4.3 Just inside the mine

Figure 4.2 Inner regions of the mine

The WULG has desirable properties for a gravity laboratory, having low seismological noise, excellent environmental stability (temperature and humidity), low anthropogenic noise and easy access (European Centre for Geodynamics and Seismology, n.d.).

The entrance of the mine provides easy access from a dirt track leading from the main road, and transportation of equipment to the mine is simplified by the availability of an electric cart and trailer. The 300-metre access into the laboratory runs through different structures within the mine, from the supported outer regions, which have metal supports (Figure 4.2), side baffles to contain debris and many side shafts running horizontally from the main corridor, into the unsupported bedrock, in which drill holes from the original mining can still be seen (Figure 4.3).

4.4.2. Belval

The comparison at WULG has grown in popularity since approximately 2003 and comparisons in recent years have necessitated the comparison organiser (usually Professor O. Francis of Luxembourg University) to arrange a schedule to include 2 batches of AGs to arrive, such that for 15 available measurement locations, a total of 30 AGs were scheduled to participate in the comparison in 2011 (CCM and WGG, 2013). The number of those wishing to participate has undoubtedly increased due to an expansion in the number of countries sending participants, the gradual increase in the number of AGs in the world and the capabilities of the laboratory.

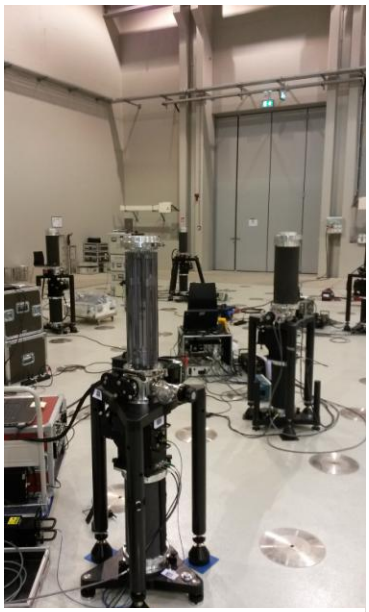
Figure 4.4 Belval comparison

For the EURAMET (European Association of National Metrology Institutes) 2015, a health and safety inspection closed access to the mine and an alternative site was found in the new Belval campus of the University of Luxembourg. Built in grounds that were once home to Luxembourg's largest steel foundry, the new campus is projected to house

almost the entire university by 2019 (University of Luxembourg, 2015). One of the new buildings designed for use by the civil engineering department was chosen to host the ICAG. Seventeen gravimeters from seventeen institutes participated in the comparison. (Palinkas, et al., 2015).

Chapter 5

The Space Geodesy Facility, Herstmonceux

5.1. Introduction to the Space Geodesy Facility

The Space Geodesy Facility (SGF) is situated just outside of the South Downs National Park, near the south coast of the British Isles, and within the grounds of Herstmonceux Castle. The facility is a legacy of the ownership and occupation of the castle and its grounds by the Royal Greenwich Observatory (RGO) for a period spanning five decades. The role of the SGF is to support Earth observation, in geodetic and geophysical research, by the provision of high precision geodetic data. Three complimentary co-located geodetic techniques are operated at the facility: Satellite Laser Ranging (SLR), Global Navigation Satellite Systems (GNSS) and Absolute Gravimetry (AG).

The SGF is owned and run by the British Geological Survey (BGS) on behalf of the Natural Environment Research Council (NERC) and the Ministry of Defence (MOD), and contributes to the international scientific communities of the International Laser Ranging Service (ILRS), the International GNSS Service (IGS) and the absolute gravity database (AGRAV).

5.1.1. History of the Space Geodesy Facility

The Royal Greenwich Observatory moved to Herstmonceux Castle from Greenwich in 1948 due to deteriorating conditions in London, although the move itself took 9 years to complete in its entirety (Dolan, 2014-15). In 1949, the solar dome became the RGO's first purpose-built building to be completed at Herstmonceux, although the basement to the

building was completed later in 1951. It was subsequently home to the solar department, which was based at the dome from the 1950s until 1977 (Wilkins, 2009).

The demise of the solar department at Herstmonceux and formal transfer of the sunspot monitoring programme to the Heliophysical Observatory in Hungary in 1977 (Graham-Smith, 1978) was followed by the approval by the science and engineering research council (SERC) of plans, by the RGO Almanacs and Time Division to build a satellite laser ranging station. The rationale for developing a laser ranging capability was to continue the involvement of the RGO in international efforts to monitor Earth rotation parameters (UT - UTC, its derivative length-of-day and polar motion), which had hitherto been accomplished by optical stellar observations (which was called project MERIT, (Wilkins, 2009)). After a few years of planning the process which would transform the use of the solar building into an SLR station, work effectively started in 1981 with the replacement of the solar dome by a clamshell, or eyelid, type of dome and the installation of the SLR 50 cm Cassegrain telescope. The first laser returns from a satellite pass were obtained by the SLR on March 31st 1983 (Appleby, 1998).

Figure 5.1 Removal of the solar dome in 1981 prior to installation of the clamshell dome.

Later, when the RGO moved from Herstmonceux to Cambridge in the 1990's, the SLR was the only building to retain its operation. Subsequently, when the RGO was formally shut down in 1998, the Natural Environment Research Council (NERC) became directly responsible for the SLR.

In recognition of its growing geodetic capability, beyond that of solely monitoring the Earth's rotation vector, in 2001 the SLR team leaders recommended to NERC that its name be changed to the Space Geodesy Facility, Herstmonceux. In 2012 the management of the facility was moved into NERC's British Geological Survey, within the Earth Hazards and Observatories Directorate.

5.1.2. The Space Geodesy Facility Today

Over its thirty-year lifetime, the SLR has seen numerous changes in its daily operation. Although still tracking artificial satellites the number of those satellites to be tracked on a daily basis increased significantly over the years. There are now over fifty satellites tracked by the SGF on a daily basis, whereas there were only two satellites (named Starlette and LAGEOS) available in the early days of the 1980s. To support the increase numerous

Figure 5.2 The SGF in 2015

changes in hardware and software have been required to take place, including installation of an additional laser in 2006. The SGF is now one of the most productive SLR stations in the world and has been ranked in the top ten stations in the ILRS for over twenty years*.

Since the 1980s, the geodetic capability of the SGF has been expanded to now include two GNSS receivers known as HERS, which was added in 1992, and HERT, which was added in 2003. HERS is the UK's primary IGS receiver and is situated on top of a seven-metre latticed mast in close proximity to the SLR. Around 130 metres due west of both the SLR and HERS, the HERT receiver is situated on top of an old brick-built water tower built by the RGO. HERT is part of the EUREF network and provides real-time data to EUREF and the IGS. Both HERS and HERT have undergone changes in both antenna and receiver over their lifetimes, details of which can be found in the SGF site log held on the IGS and ILRS websites.

An FG5 absolute gravimeter was added to the geodetic capability in 2006 which, housed in the gravimetry laboratory in the basement of the facility, provides the SGF with a satellite-independent geodetic technique. Further details of the installation and results from the gravimeter are given in part 2 of this thesis. The economic appraisal application made to NERC for the gravimeter is reviewed in the next section.

In addition to the geodetic measurements, the SGF operates a growing number of environmental measurement systems. High accuracy meteorological instruments record temperature, pressure and humidity at 5-minute intervals, along with groundwater levels that are automatically recorded from the borehole. In addition, a visiometer monitors the atmospheric horizontal visibility and a sun photometer measures the concentration of aerosols in the atmosphere. The SLR system can also be used to take atmospheric elastic LiDAR measurements, the primary function of which is to detect variations in the density and aerosol make-up of the atmosphere above the SGF; such variations include the differentiation of different height cloud cover and of aircraft condensation trails. The

* Full information regarding station performance can be found through the International Laser Ranging Service: http://ilrs.gsfc.nasa.gov/index.html

system was used to monitor the ash cloud from the Eyjafjallajökull in 2010, in collaboration with the UK's Met Office (Potter, 2015).

The SGF now also houses two instruments which are remotely managed and operated by external personnel or agencies: a BGS broadband seismometer, housed in the north of the basement (with the hydrogen MASER), and an Ordnance Survey GeoNet 'zero-order' GNSS reference station.

In 2010, the SGF started taking precise levelling data on a monthly basis between the gravimetry laboratory, the SLR and the GNSS monuments, in an effort to further understand any small-scale local movement of the site, especially between the locations recorded in the survey.

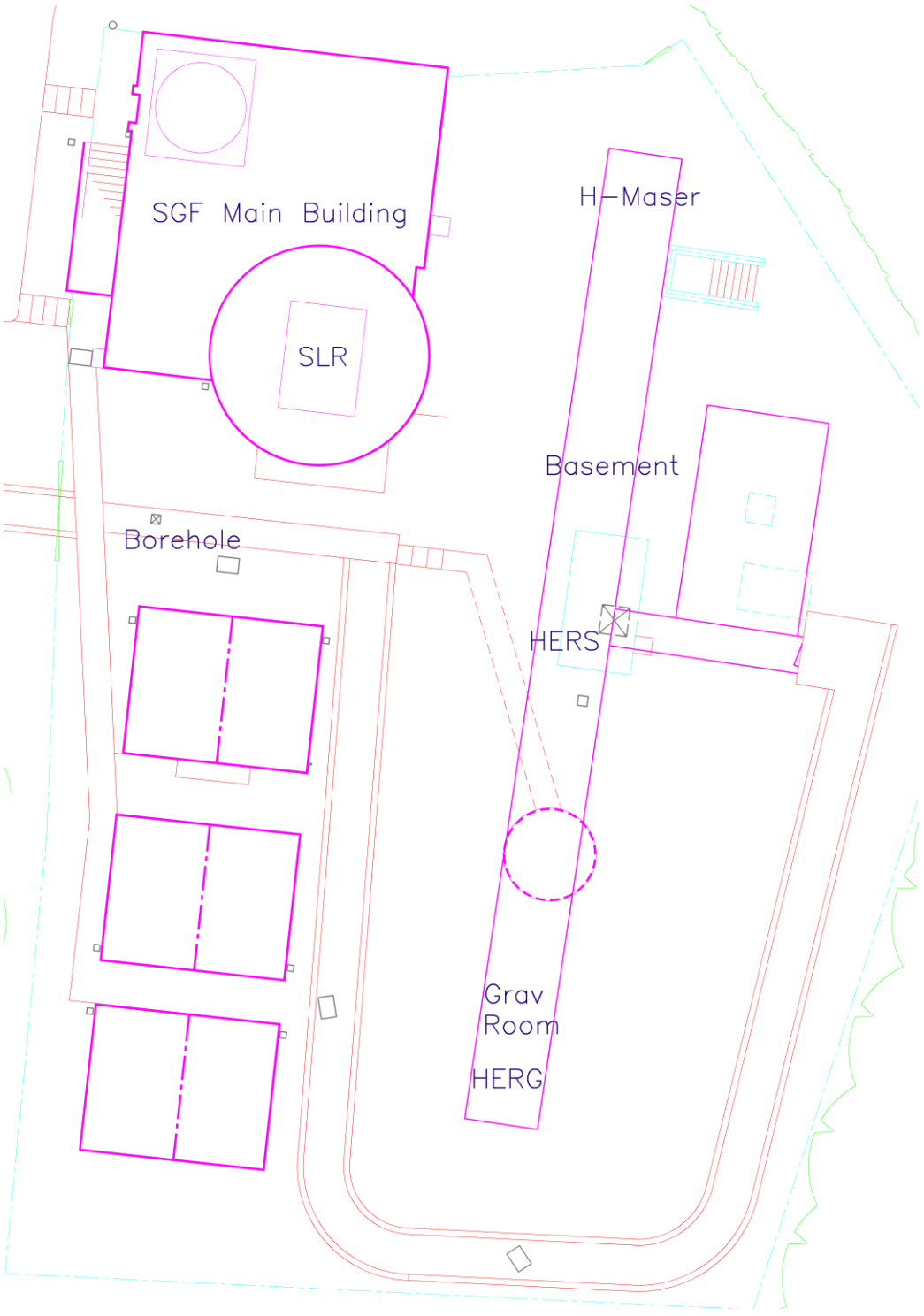

Figure 5.3. Site map of the SGF, courtesy of the SGF

5.2. Absolute Gravimetry at the Space Geodesy Facility

The addition of the absolute gravimetry technique to the SGF capability marked the largest capital investment in the site since the conception of the satellite laser ranger. The purchase of the gravimeter was approved by NERC Services and Facilities management, with funds from the capital budget of the NERC services and facilities made available to the SGF during August 2004. Following this, an advertisement in the notices section of the Official Journal of the European Union (OJEC) was submitted on September 15th 2004, and Micro-g LaCoste was awarded the contract for the gravimeter by December 2004.

Rationales supporting the purchase of the AG were highlighted in a brief scientific assessment (given in Appendix 1) written for NERC Services and Facilities management by Dr G. Appleby (SGF Head of Service) and in collaboration with the Proudman Oceanographic Laboratory, Liverpool (now NOC Liverpool), which highlighted that an AG would:

- Address a perceived weakness in the breadth of scientific techniques at the SGF and aid the inclusion of the facility into the European Combined Geodetic Network (ECGN)
- Strengthen the AG work within the UK via collaboration with the Proudman Oceanographic Laboratory
- Provide a capability for AG comparisons
- Provide an independent technique used to check on any systematic errors in the vertical crustal movement derived from SLR or GNSS measurements
- Measure glacial isostatic adjustment
- Provide information on the seasonal variation in station height seen in the SLR and GNSS measurements at the SGF

During refurbishment work carried out at the SGF during 2005-6 the southern end of the basement was segmented to create a room for gravimetry work with four location markers installed to indicate gravimetry ‘piers’. To conform with the monument names of other local techniques (where HERL is the SLR and HERS is a GNSS receiver) the piers were

designated HERG (for the southern most marker and otherwise known as pier 1), HERH, HERI and HERJ. In early 2006 the piers were surveyed, kindly at no cost to NERC, by the Ordnance Survey of the UK, for inclusion into the local SGF network. The survey results are given in Appendix 2. Later the same year the gravimeter was installed in the new gravity laboratory of the facility. Further information on the gravimeter installation and results are covered in Chapters 7-14.

5.3. Satellite Laser Ranging

A time-of-flight measurement of a laser pulse can be used to provide an accurate distance to an artificial satellite equipped with a retroreflector. SLR stations can provide distance measurements throughout the entire arc of the satellite orbit seen by the SLR ground station and these measurements can be combined with similar data from other international SLR stations to provide precise orbit determination of the satellite to the mm scale.

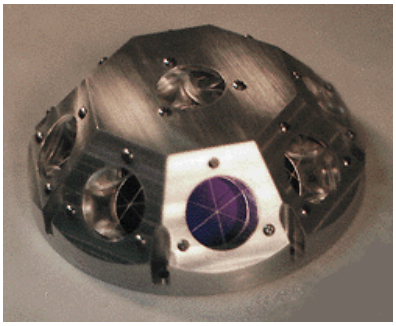

Figure 5.4. Example of a retro-reflector array

SLR utilises short-pulse lasers to illuminate a satellite as it passes within range of the ground station. The laser light transmitted by an SLR station is reflected back towards the same station by a retroreflector, or array of retroreflectors, where accurate station clocks measure the time interval between transmission and detection of the light pulse. Each two-way time-of-flight measurement τ is converted into one-way range r to the satellite by $r = c\tau/2$, where c is the speed of light in vacuum. As the satellite passes over the station, range measurements can

Figure 5.5 Satellite laser ranging at night

be taken many times a second, which can provide many thousands of range measurements over the duration of the pass. Atmospheric delay of the laser pulse is removed from the measured range using an accurate zenith delay model and elevation-dependant mapping function developed by Mendes and Pavlis (2004). The delay model is accurate to better than 1 mm for elevations greater than 15°, requiring only that atmospheric temperature, pressure and humidity be measured to high precision at the station at the time of the satellite pass.

Table 5.1 Process of events during satellite laser ranging

Orbit prediction
• Calculation of epoch and vector of satellite
Tracking sequence
• Telescope and radar in position and slewing
Laser fire
• Timers started • Pulse transmitted from telescope • Detector armed for each pulse
Satellite reflects laser pulse
• The laser pulse is directed back towards the SLR station • Photons will be scattered by atmosphere on each journey, the percentage dependent on sky conditions
Photon detection
• Telescope collects and focuses returning photons from each pulse onto single photon avalanche detector • Timers stopped

When the collected pass data is processed, the predicted range is fitted to the measured range values by adjustment of orbital parameters that are equivalent to time and range bias, in order to remove systematic trends due to imperfect a-priori predictions and remove

outliers using a 3σ rejection scheme. By then calculating the differences between the observed and predicted range values, de-trended range residuals are formed. The observational equation used can be expressed:

$$R_{obs} - R_{calc} + \varphi = \sum_{i=1}^{n} \left(\frac{\partial R}{\partial p_i} \Delta p_i \right)$$

where φ is a value to be minimised by least squares regression analysis. p_i are the correction parameters, R_{obs} is the observed range and R_{calc} is the predicted range for any observational instant (Appleby, PhD, 1996).

$$Range_{obs-comp} + \varphi = \frac{\partial R}{\partial xyz_{st}} \cdot \Delta xyz_{st} + \frac{\partial P^m}{\partial P^m} \Delta P^m + \frac{\partial A^r}{\partial A^r} \Delta A^r + \frac{\partial E^t}{\partial E^t} \Delta E^t + \cdots$$

Finally, the de-trended observational residuals are used to form compressed 'normal points' (NP). Each normal point is equivalent to a short time-slot of data from the satellite pass, being a single range value and an associated precision, derived from the fitted function and the residuals.

The duration of the normal point time-slot is satellite height-dependent; for example, two minutes is standard for the LAGEOS satellites, it being argued that no information is lost by using one measurement every two minutes since at LAGEOS' heights the force models, primarily the gravity field of the Earth, may be considered constant during that time span. The formula for producing independent normal points that greatly reduced the volume of 'full-rate' range data, and conveniently filtered the data, was developed by a technical group during the fifth International Workshop on Laser Ranging Instrumentation held in 1984 at Herstmonceux (International Laser Ranging Service, 1984). Additional details can be found on the ILRS website:
http://ilrs.gsfc.nasa.gov/data_and_products/data/npt/npt_algorithm.html

The accuracy of satellite laser ranging measurements is dependent on numerous factors, not least high precision environmental readings for each site to determine the refraction through the atmosphere, the accuracy of the timing system used, satellite signature, satellite centre of mass correction used and consistent and frequent calibrations of the system.

5.3.1. Specifics of Satellite Laser Ranging at the Space Geodesy Facility

The SGF SLR operates a single photon ranging system where the return rate of photons into the specialised single photon avalanche detector (SPAD) is statistically controlled to no more than one photon for each pulse of the laser. The orbital equations of motion of a satellite refer to the behaviour of its mass centre in the presence of all the forces acting upon it. Except for a very few special satellites the phase centres of the laser corner cubes are not located at this mass centre, but for instance for spherical geodetic satellites (Section 5.3.2) are located within the surface some tens of cm away. Therefore, the laser range measurements need to be referred to the mass centre by the addition of a so-called 'centre of mass' correction. Early work at Herstmonceux (Appleby G.M, 1999) showed that very accurate models could be built of the response of spherical satellites from which centre of mass values are obtained on the assumption that the measurements are at single photon levels.

Since 2007, the SGF has had a dual laser system capability, permitting the choice of laser most suited to the type and orbit of the satellite. This allows either a fast repetition rate (1 or 2 kHz) short pulse laser (10 ps*) or the more conventional 13 Hz longer pulse length (100 ps) laser to be used for tracking. Switching between the lasers is done via computer interface and can be achieved in approximately 40 seconds. Both lasers have distinct advantages; the 2 kHz system allows fast acquisition of satellites at a higher precision than the longer pulse length 13 Hz system, whilst the 13 Hz laser allows the station to be able to participate ranging to missions such as NASA's lunar reconnaissance orbiter (LRO) (Planet Earth Online, 2009), as well as the time-transfer experiment onboard the satellite JASON-2 (primarily an altimetry satellite built and run by a collaboration of NASA, CNES, EUMETSAT and NOAA).

* ps - picoseconds, $1x10^{-12}$seconds

5.3.2. Satellite Laser Ranging Satellites

The SGF uses a dynamic list of satellites that are ordered in priority by the ILRS network. The types of satellites tracked fall into four main categories: gravity, altimetry, geodetic and navigation satellites. Some current and previous satellites for each category are given below.

The name of the satellite is followed by the operational years within the ILRS and the satellite altitude above sea level (International Laser Ranging Service, 2013):

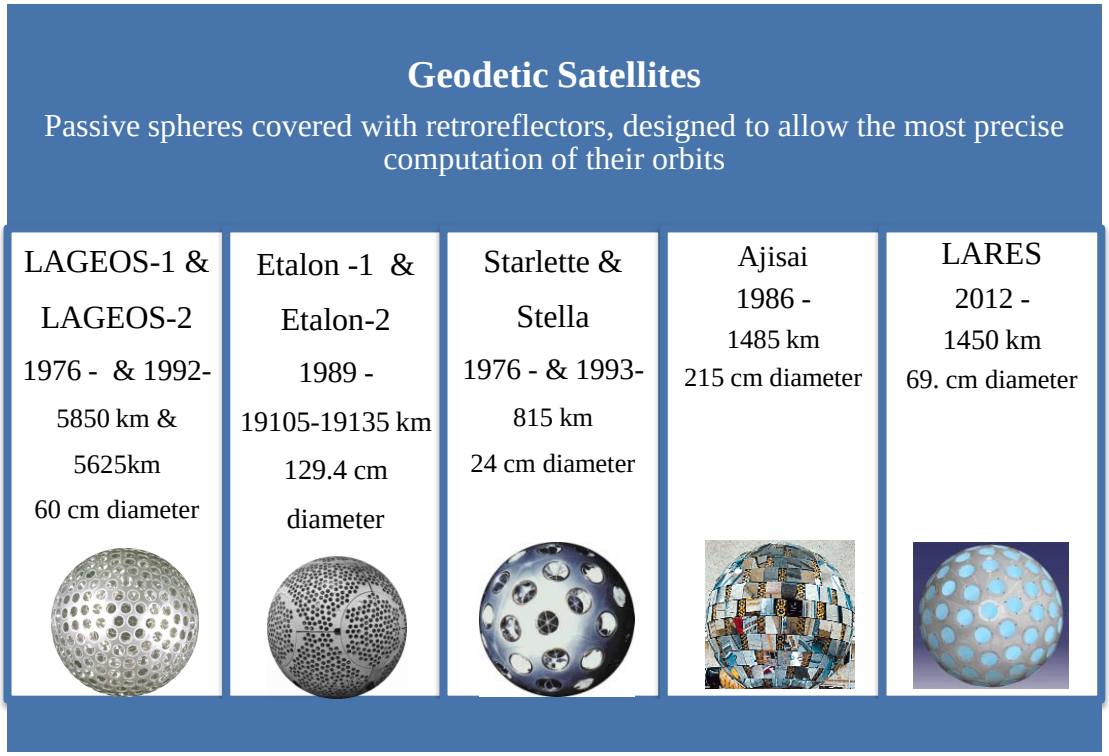

Figure 5.6 Examples of geodetic satellites tracked by SLR

Remote Sensing Satellites

Carry payloads that measure the processes of the dynamic Earth system

Altimetry Satellites	Gravity Satellites	Other Satellites
JASON-1 2003-2012	GRACE-A 2002 -	Swarm A 2013 -
JASON-2 2008 -	GRACE B 2002 -	Swarm B 2013 -
JASON-3 2015 -	Champ 2000 - 2010	Swarm C 2013 -
ERS-1 1991 - 2000	GOCE 2009 - 2013	Tandem-X 2010 -
ERS-2 1995 - 2011	Gravity Probe B 2004 - 2006	Terrasar-X 2007 -
TOPEX 1992 - 2005		STSAT-2C 2013 -
ENVISAT 2002 - 2012		SpinSat 2014 -
Cryosat-2 2010 -		Reflector 2001-2004
Sentinel 3A 2016 -		

Figure 5.7 Examples of remote sensing satellites tracked by SLR

Global Navigation Satellite Systems

Constellations of satellites providing accurate positioning on any surface of the Earth

GPS (USA)	Glonass (RU)	Galileo (EU)	Compass (CN)	IRNSS (IN)
1993 -	1993 -	2006 -	2012 -	2013 -
20300-20195 km	17300-25900 km	23220 km	21528-42164 km	42164 km

Figure 5.8 GNSS satellites tracked by SLR

Source – the website of the International Laser Ranging Service

The precise orbits generated by satellite laser ranging tracking of the Earth observation remote sensing satellites can be used for a vast range of products, such as the study of ice-caps, ocean velocities, currents and temperatures, deforestation, tectonic plate movement, the Earth's gravity and surveying the Earth's geomagnetic field.

Specifically designed to act as point-mass objects for the most accurate determination of their precise orbits, geodetic satellites have a small area-to-mass ratio to minimise the effect of non-conservative forces, an example of which is solar radiation pressure. The most important of the geodetic satellites are the LAGEOS and Etalon pairs, both of which have exceedingly stable orbits above the point where either variations in the gravitational field of the Earth or atmospheric drag would have a dominant effect. The orbital altitudes of this pair are complimentary and form the basis of the scale used in the formulation of the International Terrestrial Reference Frame (ITRF).

Figure 5.9 LAGEOS satellite

The precise orbit determination of the geodetic satellites is used by ILRS analysis centres to produce information such as orbital data quality checks, Earth orientation parameters and SLR station coordinates, the latter of which is relevant to the work in this thesis and is referenced in chapter 15.

5.3.3. **Computing Station Coordinates & Heights Using SLR Measurements**

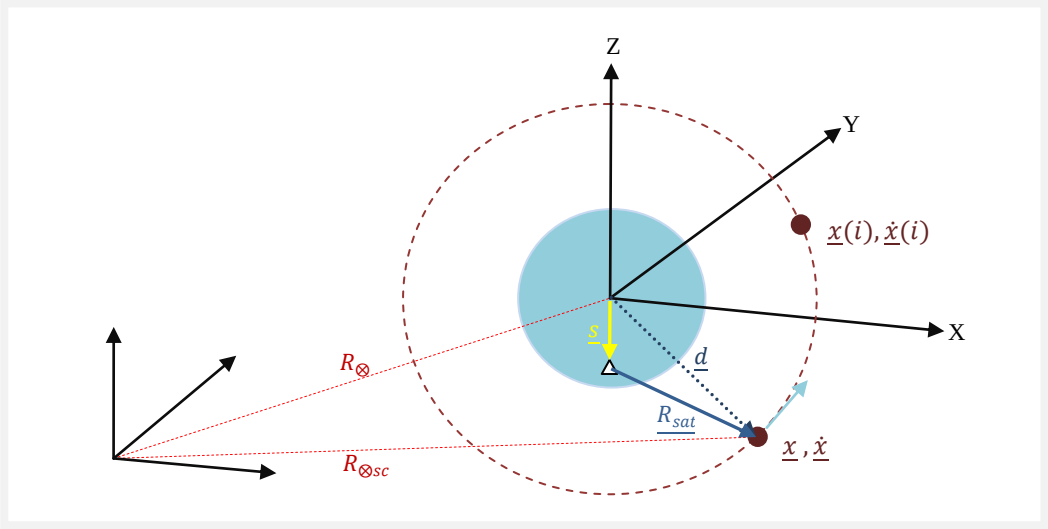

Figure 5.10 Earth to satellite coordinate relation, centred in a reference frame. Where _(R_sat) = topocentric coordinates of satellite, _(d_geo) = geocentric coordinates of satellite and _s = geocentric coordinates of observing station. R_⊗ and R_(⊗sc) indicate relative to an Earth centred reference frame.

The range to the satellite for any epoch is obtained from $\underline{R_{sat}} = \underline{d} - \underline{s}$

$$Range\ to\ Satellite = r = \underline{|R_{sat}|} = \ \left|\underline{d} - \underline{s}\right|$$

therefore to obtain the $\frac{\partial R}{\partial xyz_{st}} \cdot \Delta xyz_{st}$ components of $R_{obs} - R_{calc} + \varphi = \sum_{i=1}^{n} \left(\frac{\partial R}{\partial p_i} \Delta p_i\right)$

$$r = \ [(x - x_{st}) + (y - y_{st}) + (z - z_{st})]^{0.5}$$

then taking partial derivatives of the range with respect to each geocentric coordinate component gives:

$$\frac{\partial r}{\partial x_{st}} = -\frac{(x - x_{st})}{r} \qquad \frac{\partial r}{\partial y_{st}} = -\frac{(y - y_{st})}{r} \qquad \frac{\partial r}{\partial z_{st}} = -\frac{(z - z_{st})}{r}$$

Normal point range measurements from the ILRS tracking stations may then be used to generate precise orbits for the satellites, along with reference frame solutions (tracking station coordinates, Earth orientation parameters) in a least squares adjustment. The solutions are carried out by computing via numerical integration of the equations of motion weekly orbital arcs of the satellites using estimated initial position and velocity. In a subsequent least squares adjustment scheme, world-wide SLR observations taken during each week are used to solve for improved values of the satellites' initial state vectors as well as those of the stations' coordinates and of Earth rotation parameters. The observation equation used is of the form:

$$Range_{obs-comp} + \varphi \ = \frac{\partial R}{\partial xyz_{st}} \cdot \Delta xyz_{st} + \frac{\partial P^m}{\partial P^m} \Delta P^m + \frac{\partial A^r}{\partial A^r} \Delta A^r + \frac{\partial E^t}{\partial E^t} \Delta E^t + \cdots$$

where (xyz_{st}) station coordinates, polar motion (P^m), Earth tides (E^t), ocean-loading, orbit parameters, atmospheric drag & solar radiation pressure, etc., are solved-for iteratively

The SGF Herstmonceux is an ILRS-certified Analysis Centre (AC, ilrs.gsfc.nasa.gov/analysisCenters/index.html) and is responsible for computing daily and weekly reference frame solutions and precise orbits of the LAGEOS and Etalon satellites

that are subsequently made freely available to the community via ILRS Data Centres. The SGF AC contributed multi-year solutions towards the realisation of the International Terrestrial Reference Frame for the past ten years (e.g., ITRF2014, (Altamimi, Rebischung, Metivier, & Collilieux, 2016)). Further, recent research carried out at Herstmonceux (Appleby, Rodriguez, & Altamimi, 2016) has shown that subtle systematic effects at each station can be determined simultaneously with the reference frame; the SGF observations are second-to-none, with an estimated absolute accuracy better than 2 mm. The weekly time series of the height of the SGF laser tracking system obtained for the period 1993-2015 during this analysis is used later in the thesis for comparison with the AG time series in Chapter 13.

5.3.4. Computing Station Co-ordinates Using Global Navigation Satellite System Measurements

To compute station coordinates GPS observations from the international GNSS service can be obtained for hundreds of GNSS stations, amongst which are HERS and HERT. Similar to the SLR processing not all stations need be used to compute co-ordinates for a single station though a well-distributed selection of the stations is advised. There are various analysis packages available, such as GAMIT, which can produce station coordinates via a least squares adjustment similar in principle to that used to process SLR data, or a station time-series can be obtained from the centre for orbit determination in Europe (CODE). At the SGF loosely constrained site co-ordinates are estimated by the use of GAMIT using IGS final solution orbits, satellite navigation files and Earth rotation parameters from USNO and a-priori station positions taken from the ITRF (Appleby G. , 2010).

5.3.5. Vertical Height Determination Using Absolute Gravimetry Measurements

Absolute gravity measurements allow an independent, and non space-based determination of the vertical movement of the site. A scaling factor, based upon a near-Bouguer plate approximation, can be calculated for a site in order to convert the local acceleration due to gravity into equivalent changes in height.

The conversion factor can be calculated for a specific site if the density of the subsurface soil is known exactly. In cases where the density is not known the conversion is based upon two calculations; the Bouguer model where the mass in the upper mantle forms an infinite plate and the Bouguer free air model, where no addition of mass is assumed (Hopewell, 1999). These are:

$$\frac{\delta g}{\delta h} = \frac{2g}{R} + 2\pi G\rho = -1.7\ \mu Gal\ cm^{-1}$$

$$\frac{\delta g}{\delta h} = \frac{2g}{R} = -3.086\ \mu Gal\ cm^{-1}$$

where R is the radius of the Earth, G is the gravitational constant and ρ is the density of the mantle, which is taken as 3.3 Mgm^{-3}. The total height conversion factor is (B. Richter, 2004), (Bilham, 2016), (Torge, 1989) obtained from the inverse of the sum of the infinite plate model and the free air model, such that;

$$\frac{1}{-(3.086 + 1.7)} = 0.2\ \mu\text{Gal cm}^{-1}$$

However, this does not take into account any mass changes above or below the gravity station, such as varying hydrological signals and changes in atmospheric pressure. The direct effect of variable atmospheric mass attraction on the AG test mass is removed from the gravity measurements by referring them to a location dependent standard atmospheric pressure (Nicolas, et al., 2006).

5.3.6. Co-Location of Geodetic Techniques at the Space Geodesy Facility

The close proximity of the geodetic techniques at the SGF is unusual for a geodetic station, but is in line with GGOS recommendations for core geodetic sites. The separation between the SLR, AG and the GNSS receivers HERS and HERT is no more than 122 metres, if HERT is discounted then the maximum separation falls to just under 25 metres.

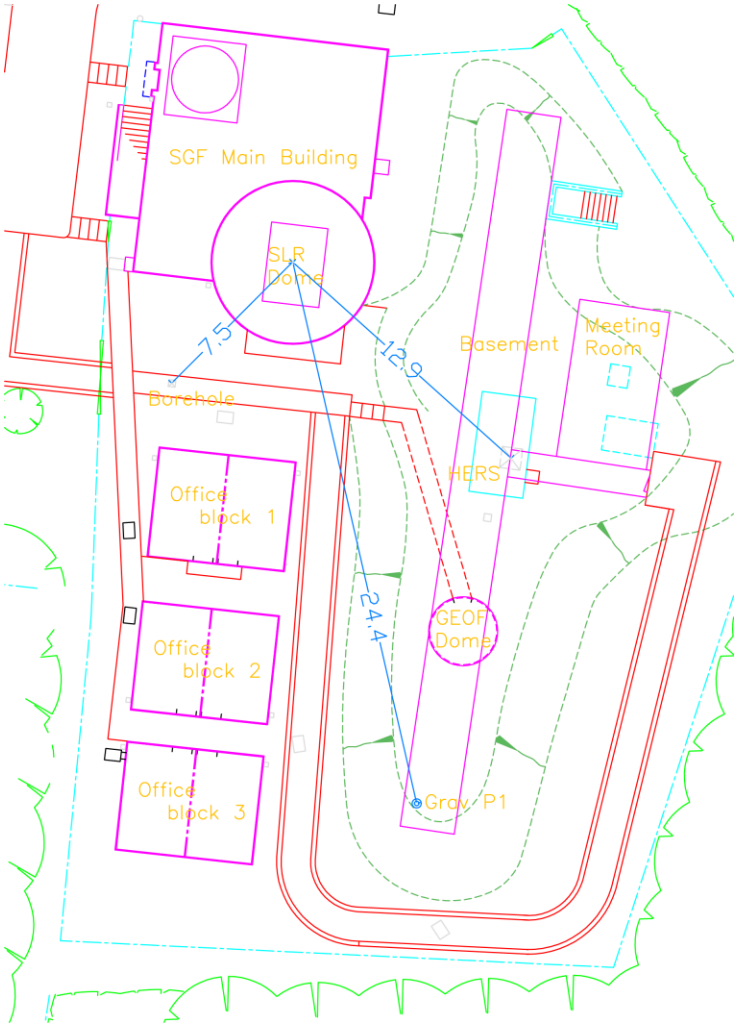

Figure 5.11 CAD drawing of the SGF, courtesy of the SGF

From the vertical axis of the SLR telescope; the absolute gravimeter is 24.4 ± 0.5 m, the HERS GNSS antenna is 12.9 ± 0.2 m, the borehole is 7.5 ± 0.2 m. Distances obtained from the CAD drawing and were verified via laser rangefinder in August 2015.

Chapter 6

A Review of the Relevant Literature

6.1. Introduction

This chapter discusses the literature available on the subject of absolute gravimetry since the 1990's and the birth of the FG5 absolute gravimeter. The applicable scientific papers mostly cover four main topic areas.

- Instrumental
- Environmental
- Tidal
- Height displacement

The latter three classifications are all location specific, as each site must be investigated to understand signals held within gravity measurements. In addition to these four categories, absolute gravity work in the UK is added. The instrumental review does not include instrument comparisons as this has been covered in the previous chapter.

6.2. Instrumental

The first FG5 absolute gravimeters were operational by February 1993, were designed with the objective of achieving 1 μGal accuracy and were based upon a previous instrument called a JILA. The design specifics of the FG5 have been well documented (Niebauer, 1995) (Torge, 1991) (Micro-g LaCoste, 2007) (Van Camp, 2003) (Hopewell, 1999) (Charles, 1995). Since 1993, a variety of publications have covered measurement analysis, such as (Van Camp, et al., 2005) and (Nagornyi, 1995), whilst others have discussed instrumental corrections or improvements. The two most prominent instrumental

corrections stem from diffraction of the laser beam and the self-attraction of the instrument. The diffraction correction, required because the laser beam is a Gaussian waveform rather than a plane wave, is dependent on the diameter of the laser beam and is typically between 1-5 µGal (Van Westrum. D, 2003) (Robertsson, 2007). Self-attraction is the gravitational attraction of the body of the gravimeter upon the mass inside the dropping chamber; the effect produces a systematic offset in the measurements of -1.5 ±0.1 µGal for the classic FG5 and -1.2±0.1 µGal for the FG5X (Niebauer, et al., 2013). The evolution from the classic FG5 to the FG5X, with recoil-compensated dropping chamber and improved electronics, is covered in papers by Micro-g LaCoste (Niebauer, et al., 2011) (Micro-g LaCoste, 2013).

6.3. Environmental

The most prolific topic for environmental studies of gravimetry data is investigations involving hydrological influences. Groundwater and soil moisture form a pivotal correction which should be applied to the gravity measurements, and probably the most recognised of authors in this area is J. Makinen of the Finnish Geodetic Institute, from his work in the 1980s with S. Tattari (Makinen & Tattari, 1990). The extent of hydrological influence on gravity measurements is very different from station to station (Harnisch & Harnisch, 2006), dictated, primarily, by the topography, sub-surface soil structure, climate, and location of the station (above or below ground). In addition to temporal measurements of soil moisture and precipitation (from rainfall or snow for instance), groundwater is also a large factor (Breili & Pettersen, 2009).

Whilst gravity stations above ground can see hydrological signals that are several tens of microgal in amplitude (Naujoks, et al., 2010), stations situated in underground laboratories generally face a more complex problem to remove the hydrological signals. This is due to the fact that two influences are acting upon the gravity measurements, from both above and below the instrument. In some studies attractions from groundwater and soil moisture have been shown to have a cancellation effect, effectively reducing the amplitude of the impact on the gravity measurements (Longuevergne, et al., 2009), whilst others show that

precipitation i.e. rainfall or snow, have a dominant influence on the gravity data. Where the effect from subsurface layers is minimal in comparison to the Newtonian attraction of the water accumulating above the gravimeter, rainfall is associated with a decrease in gravity value. (Imanishi, et al., 2006) (van Camp, et al., 2006) (Meurers, et al., 2007).

For some sites the local hydrological modelling does not account for much of the gravity residual and in some cases regional and even global modelling for atmospheric and hydrological effects have also been considered. This type of analysis was done at the Grasse geodetic station where the global model accounted for some 70% of the annual and semi-annual signals detected in the SLR and GPS data; however the AG data is of little use since it was used on a campaign mode and only occupied the site 14 times in 6 years (J. Nicolas, 2006).

In addition to local hydrological influences, various studies have shown marked variation in gravity measurements due to regional sources including aquifers and nearby rivers (Naujoks, et al., 2010), (Van Camp, et al., 2006) (Lampitelli & Francis, 2010) (Pfeffer, et al., 2011) (Demoulin, et al., 2007).

6.4. Tidal

Validation of tidal models for use in gravimetry studies has been an area of study for many gravity stations. Tidal signals are often seen in data from coastal gravity stations. This is largely due to the fact that such stations are susceptible to tide modelling errors due to the relatively course grid spacing used in the models. Typical ocean tide models are provided on grids with a separation of (0.125°, 0.25° or 0.5°) and therefore do not fit coastal areas fully (Penna, et al., 2008) and hence give rise to detection of un-modelled signals within gravity data. One way to resolve this issue is to compute a local ocean-loading model, with a closer grid spacing, which is inserted into a global model (Williams, 2009) (Llubes, et al., 2008).

Trevor Baker, of the Proudman Oceanography laboratory, is well known for oceanography and tidal studies. His study of inland sites that exhibit small ocean-loading signatures using satellite altimetry and gravity measurements, assessed the quality of existing Earth tide models. He later assessed various ocean-loading models using data from a number of different gravity stations (relative stations using spring or super-conducting gravimeters). In this study, phase variance between model and observed tide were seen for stations within Europe (Baker & Bos, 2003). Errors due to ocean-loading models were found to be largest in coastal sites, especially from the M2 component, giving errors of up to 20% for sites with complicated coastlines and shallow seas.

Of particular interest to this study are the results from studies in Canada, where coastal sites have been assessed in detail and where one in particular is using absolute data from an underground laboratory. In that investigation residual tidal signals, seen in gravity data, were reduced by the implementation of a correction to ocean-loading models and a remaining tidal component was considered to be due to direct attraction of the water mass (Lambert, et al., 2006).

In addition to the ability to study tides, absolute gravimetry plays a significant role in sea level change using tide gauge analysis. To understand true sea level variations from tide gauge data, the movement of the land on which the tide gauge is situated must be extracted. This can be achieved using space geodetic observations, but the data can usefully be constrained by use of precise gravity measurements (Zerbini, et al., 2002) (Teferle, et al., 2007).

6.5. Height Displacements

Absolute gravity measurements have long been considered an important tool for the measurement of crustal deformation, since gravity measurements are sensitive to the vertical motion of the crust as well as mass changes around the gravimeter. Therefore the technique provides a complimentary measurement tool against space based geodetic techniques, which can help identify the mechanism responsible for the motion (Niebauer, et

al., 1986)(Larson & van Dam, 2000). Land subsidence can be extracted from the combination of various surveying or height measurement techniques, such as: GNSS, levelling and absolute gravity (Hwang, et al., 2010) (Aldiss, et al., 2014). A number of sites studied for crustal motion display seasonal height variations linked to hydrological changes and/or atmospheric changes (J. Nicolas, 2006) (Demoulin, et al., 2007).

Probably the principal area of study for crustal deformation is estimation of the crustal movement due to glacial isostatic adjustment, otherwise known as postglacial rebound (GIA), where the Earth is adjusting to the retreat of loading ice following the last glacial period and the subsequent redistribution of mass. GIA estimates have been made using absolute gravity measurements at multiple gravity stations around the world. Amongst these are: Norway (Ophaug, et al., 2016), Sweden (Timmen, et al., 2015), Alaska (Sato, et al., 2012) and the UK (F.N. Terferle, 2009).

Absolute gravimeters also provide a valuable gravity datum for relative gravimeter measurements (Sugihara, 2003)

6.6. Previous Absolute Gravity in the UK

Gravity measurements using FG5 absolute gravimeters have been conducted in the UK since 1993, when the Proudman Oceanography Laboratory purchased FG5-103. Two PhD studies were conducted between 1993-1999 by K. Charles and H. Hopewell, both based at the University of Edinburgh. Charles used AG measurements to control relative gravity measurements for the formulation of the British Precise Network (BPN) of 1993 (Charles, 1995), whilst Hopewell, again using relative and absolute measurements, studied and improved ocean-loading corrective amplitudes at 69 sites in the BPN. Hopewell took absolute gravity measurements at eight sites around the UK during his work, one of which was the SGF at Herstmonceux (Hopewell, 1999). FG5-222 was purchased by the Proudman Oceanographic Laboratory in 2002 and joined FG5-103 to conduct campaign measurements at a few stations around the UK, including: Newlyn, Eskdalemuir, Aberdeen, Edinburgh and Lerwick (S.D.P. Williams, 2001). Both gravimeters were based in Liverpool

until 2012. Results from UK campaign measurements have been used primarily with tide gauge data and GNSS data (S.D.P. Williams, 2001), (F.N. Terferle, 2009) (Teferle, et al., 2007).

The NOC gravity data has also been used as a component for instrumental investigations including data noise and observational precision (M. Van Camp, 2005), the basis of internal NOC comparisons (Williams, 2006) and assessment of the effect of the drift of the internal 10MHz Rubidium clock (Williams, 2001).

6.7. Problem Statement

The current level of scientific demand upon geodetic observatories is extremely challenging; the geodetic community is charged with realising a global geodetic reference frame (ITRF) with an accuracy of 1mm and stability of 0.1 mm yr^{-1} (GGOS, 2009). Science drivers include determination of un-biased estimates of global sea level rise, and estimates of ice-mass loss in the polar regions. Observations from a global network of prolific laser ranging and VLBI stations together determine the scale of the reference frame and the laser observations its origin at the mass-centre of the Earth. A powerful and complementary observational technique that is emerging at so-called core geodetic sites is the very accurate measurement of local gravity. Gravity data is sensitive both to site vertical motion and to changes in mass above and below the site, the space geodetic techniques being sensitive only to the vertical motion.

The majority of absolute gravimeters are commonly used for gravity survey work, where episodic measurements are taken, or benchmarking of tide gauge locations rather than use at geodetic core sites. Gravimetric surveys or benchmarking are reliant on well defined, calibrated, instrumentation and each measurement location will be subject to environmental changes, such as hydrological influences or vertical land movements, for example by glacial isostatic adjustment. Uncorrected instrumentation bias or environmental change will, of course, impact directly on the quality and validity of the results for each location.

The overall aim of this study is to establish a gravity laboratory at the Space Geodesy Facility, produce an accurate gravity time series from a fixed, well-instrumented location, and to begin to investigate environmental, geophysical and instrumental signals within the data. It is expected that there will be a strong water-table hydrological signal in the observations that will be understood and removed during the course of the data analysis. The unique nature of the occupation at the SGF, as a near-permanent location with high frequency of measurements will eliminate some of the instrumentation errors which can be made in the movement of the instrument and will provide an assessment tool for the potential benefit and addition of gravity measurements at other core geodetic sites worldwide.

Chapter 7

Absolute Gravity at the Space Geodesy Facility

7.1. Introduction

Following the successful application for capital funds from the Natural Environment Research Council (NERC) Services and Facilities group (discussed previously in Chapter 5), the Space Geodesy Facility (SGF) received delivery of the FG5 absolute gravimeter on June 2nd 2005.

This chapter describes the evolution of gravimetry measurements at the SGF, from preparation for arrival of the instrument through major events in the years of occupation at the SGF. The objective is to provide a review of events and decisions which have influenced the gravimetry measurements undertaken at the SGF.

7.2. Location of, and Preparation for, the Absolute Gravimeter at Herstmonceux

A new laboratory for absolute gravimetry sensors would ideally be located in a seismically quiet location, away from natural and anthropogenic noise sources, and include mechanically isolated concrete piers on which each sensor would be located. The laboratory should also be located in a stable environment, where no large scale changes will be made to the environment, such as new buildings being erected. Inside the laboratory the electrical supply should be isolated from any external power fluctuations, especially surges or power spikes and uninterruptable power supplies would be placed to protect the sensors as much as possible. Temperature and humidity levels are also important to minimise instrumental failures, ideally they should be relatively stable and within the operational range quoted by the manufacturer.

The SGF encompasses a relatively small environment where only the original building and basement are of a solid and permanent construction; therefore, the possible locations to site an FG5 were exceedingly limited. The laser room of the Satellite Laser Ranger (SLR) was considered as it offered the best readily available environmental conditions, with a very stable temperature and good cleanliness, but due to the limited availability of space and significant probability of accidental damage, it was dismissed as a viable option. Other locations, such as offices, a sub-terrain corridor (linking the basement to the laser room)

Figure 7.1Photographs of the SGF basement, looking south, before and after renovation

and alternative buildings external to the SGF (but within the Herstmonceux Castle grounds), were also considered but deemed unsuitable. It was eventually decided that the 100-foot basement, originally used for the focusing of sunlight for the photography of sunspots, which had lain unused since the decommissioning of the solar observatory, should be converted for use. The South section of the basement could be walled off to provide a laboratory dedicated to gravity. Unused for 27 years, other than for storage, the basement was known to leak and occasionally suffer flooding.

The renovation and conversion of the basement began in 2004 and included the introduction of a new access door into the basement, via an old heating plant room modified into a meeting room, removal of concrete benches from the entire length of the basement, and a new access path. Due to constraints of the physical gradient of the path it

could only be constructed to the South of the basement, and SLR. The process involved disturbing soils which had been untouched since the inception of the solar department. Concerns were raised over the building of the path since it bracketed the gravimetry room on three sides meaning that the ground around the south of the basement would take time to thoroughly stabilise following the work.

Figure 7.2 The new path around the basement. Photographs were taken from the South edge of the path looking North. The photograph on the left is on the East side of the gravimetry room, the West view is on the right.

As previously mentioned, the south end of the basement was chosen to be partitioned off to become the new gravimetry room. This laboratory space was designed to provide intercomparison facilities for four absolute gravimeters in total and supplied with air-conditioning and a carefully considered electrical outlet distribution, allowing ample power for the four gravimeter locations.

Following the completion of the basement, four location studs (hereafter known as piers) were installed and surveyed into the SGF local site by the UK Ordnance Survey, the results

of which can be found in Appendix 2: Coordination of RGO Absolute Gravimeter at Herstmonceux.

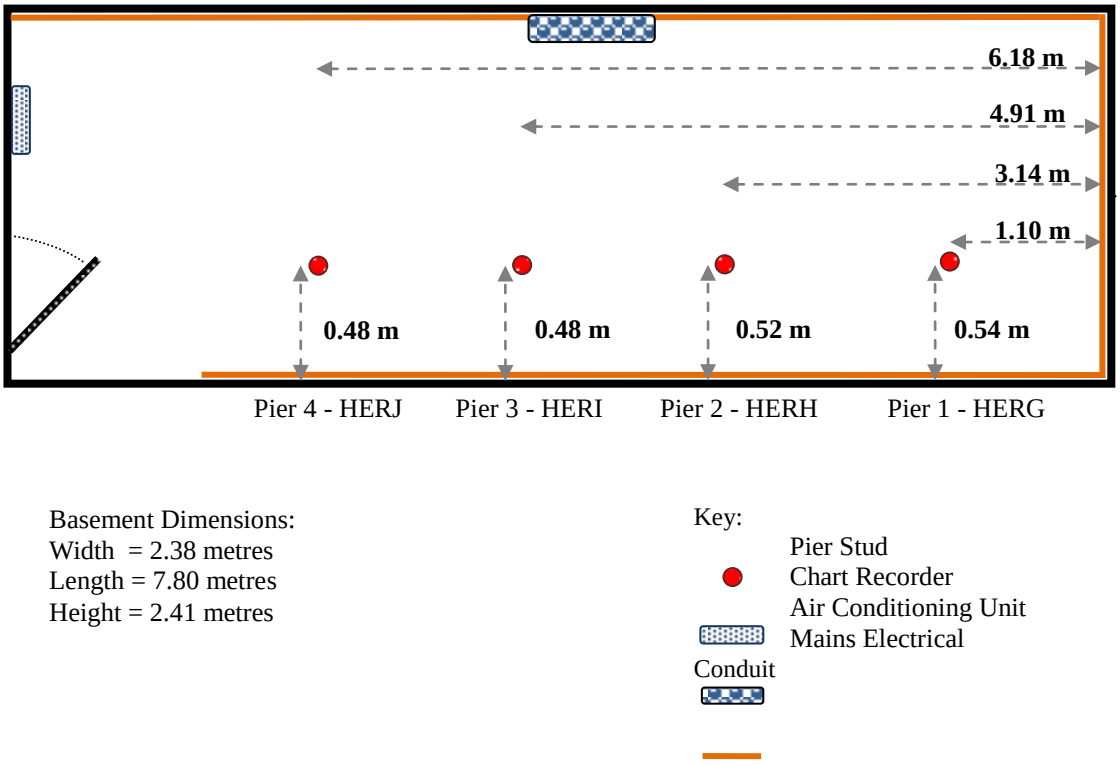

Figure 7.3 Layout of the gravity laboratory, showing distances of the piers from the South and West walls of the laboratory

The position of the pier marker studs are less than ideal due to their close proximity to the outer wall, however the choice of each position was influenced by the flooring throughout the room. Due to the removal of the concrete benches, which were used when the building was home to the solar department for focussing sunlight to obtain photographs of sunspots, the floor is a combination of new asphalt, and original asphalt, laid in the 1950's. Since there is a slight height differential between the new/old asphalt the location of all piers were chosen to enable the SGF FG5 to be able to occupy all piers on the original 1950's asphalt. Unfortunately as a consequence of locating the piers in close proximity to the wall and the larger footprint of the older FG5 variant manufactured in 1993, with bulk interferometer and diagonal legs, only Pier 1 (HERG) is able to accommodate the older FG5 with all tripod feet on the older asphalt, Piers 2-4 require this type of gravimeter to straddle both ages of flooring.

7.3. Data Collection Frequency at the SGF

The decision to take measurements over 24 hours on a weekly basis was taken before delivery of the FG5 at the SGF, Herstmonceux. The objective at the start of the installation of the instrument was to compare height results with the other geodetic techniques, although the SLR was to be the main comparison, to observe un-modelled environmental components at the site.

The middle of the Global Navigation Satellite Systems (GNSS) week was chosen as an ideal time over which the gravimeter should take measurements. This period was also convenient since it is also the middle of the SLR 7-day orbital solutions; thus the gravimeter was scheduled to operate from midnight each Wednesday until past midnight on Thursday to provide hourly data sets over 24 hours.

The mid-week operating criterion was maintained from 2006 until 2007 but was slightly modified there afterward in an effort to keep the signal noise as low as possible. Therefore from 2008 onward the operational day was shifted as necessary, dependant on the weather forecast for the week ahead. The change in operating criteria and the impact of meteorological environmental factors on the precision of the measurements at the SGF is discussed further in Chapter 10.

7.4. Absolute Gravimetry from 2005 until 2016

In the years of operation at the SGF the gravimeter has undergone many repairs (which are discussed in Chapter 8), been serviced by Micro-g LaCoste twice, been to two formal intercomparisons and one informal intercomparison (details are given in section 7.6), taken measurements in Scotland and been upgraded into an X variant of the FG5. A timeline of events from inception of the gravimetry idea through to 2015 is given below. Some history of early attempts to operate the gravimeter before the gravimetry laboratory was finished, as well as early operation problems in the laboratory is given in Appendix 7.

In 2013 the SGF took delivery of two additional FG5 gravimeters, FG5-103 and FG5-222, on loan from the National Oceanographic Centre (NOC).

Table 7.1 A time line of SGF gravity related activity

2004 to 2006

2004

- Scientific case for AG and finances approved
- Plan room layout designed
- Gravimeter ordered

2005

- Basement renovations begin
- Attended FG5 training course at Micro-g LaCoste

June

- Gravimeter delivered & installed in the Old Physics block
- Gravimeter removed to SE office

August

- Laser returned from Micro-g LaCoste.
- Temperature related problems in operating in the SE office

September - November

- Gravimeter SIM and dropping chamber returned to Micro-g LaCoste. Fault found on dropping control card at Micro-g LaCoste

2006

April

- Basement completed
- Chart recorder installed in gravimetry laboratory
- Gravimeter moved into basement

May

- *2nd* - Temperature = 13 °C with 98% humidity
- Air-con switched on to 'dry' mode
- *8th* - Temperature = 13 °C with 92% humidity
- Heater added to room
- *9th* - Temperature = 16.5 °C with 74% humidity
- *10th* - Temperature == 19 °C with 69.5% humidity
- Official commissioning of FG5 by Micro-g at the SGF begun
- Synchronicity problems found
- UPS installed
- SIM returned to Micro-g LaCoste for electrical modification

June

- Temperature = 20 °C with 60% humidity
- SIM re-fitted to gravimeter
- Gravimeter run successfully but synchronicity problems continue

July

- Ordnance Survey of Gravimetry laboratory (and SGF) and location studs installed to indicate Piers 1 to 4
- Differential voltage found in the electrical mains supply between the Earth and the Neutral (1.6-2.2 V)
- Isolating transformer with Earth and Neutral connected (reducing the differential to 0.1 V) installed after UPS, with an Earth line choke after the transformer

September

- Attended gravimetry workshop at Micro-g where synchronicity problems were discussed

November

- New SIM installed by Micro-g during a second visit to commission the instrument
- Gravimeter working as expected. Synch problems fixed

2007 to 2010

2007

March

- Dropping chamber drive belt replaced

April

- Confirmed the emptying of the septic tank, located to the East, and beneath the level of, the North end of the basement, has no impact on gravity value

November

- Attended ECAG Walferdange with the gravimeter
- Laser died at the end of the comparison but cleaned up with extensive cleaning

2008

July

- FG5 Service at Micro-g LaCoste, Colorado
- Manufacturer replaced components:
  -Ferrofluidic Feedthrough
  -Laser Tube
  -Dropping chamber retroreflector (old one cracked)

2009

January

- Laser sent to Micro-g LaCoste - tube replaced

March

- Laser returned to SGF

August

- Laser problems again, returned under warranty to Micro-g LaCoste
- New tube installed

October

- Laser installed at SGF

November

- NOC-L NOC-L = National Oceanographic Centre, Liverpool delivered FG5#222 to the SGF for the purpose of mini-comparison
- Drop scatter very noisy returned to NOC-L without usable data being obtained

2010

January

- Dropping chamber drive belt replaced due to wear

August

- Dropping chamber drive belt tightened and bottom window cleaned. Due to excessive noise, bad drops and ion pump observed to he struggling over drops.

September

- Dropping chamber drive belt replaced
- Low laser power

2011 to 2013

2011

January
- Laser sent to Micro-g LaCoste
- UPS replaced

March
- Laser returned to SGF

October
- 10MHz source timing tests

November
- NOC-L at SGF with FG5#103
- FG5#103 obtaining drop scatters four times the value of #229. Visit abandoned without usable data being obtained

2012

June
- Gravimeter taken to Walferdange for informal comparison with Prof. O. Francis FG5
- Returned to SGF & required a laser clean

August
- Laser power down, no improvement from cleaning

October
- Gravimeter sent to Micro-g LaCoste for second service and upgrade into the FG5X variant

December
- FG5X gravimeter delivered at SGF

2013

January-July
- Connection problems with Super-spring - see chapter 9
- High levels of noise in the gravity measurements
- Increased gravity value by 6μ Gal
- SIM-X swapped for replacement

September
- FG5's #222 and #103 delivered from NOC-L
- Gravimeters assessed for operational capacity
- #103 found to be working
- #222 not operational due to problems attaining a vacuum in the dropping chamber

2014 to 2015

2014

February
- Undertook a week of campaign measurements in Eskdalemuir, Scotland using #229

March
- Reference WEO-100 laser purchased

April
- #103 Leant to the National Physical Laboratory (NPL).
- #222 Ferrofluidic feedthrough replaced

August
- Reference laser found to be misaligned, required full cavity alignment due to very low power - Power does not show on laser controller DC power read out or on the laser power metre, red light only just visible at collimation assembly and pulsing on and off. Regained to 10 VDC, 174 μW of power at the exit of the laser (before the faraday isolator), iodine cell detuned to decrease fringe voltage
- Rotated polarisation vector in collimation assembly to enable the laser to be used in the interferometer of #229
- Tests conducted with both lasers to ensure no error induced by the polarisation change
- Tests conducted to check the frequency of the Rubidium clock inside #229 against the SGF Hydrogen MASER
- #222 copper gaskets replaced around ferrofluidic feedthrough. Ion pump replaced, O-rings greased and bottom window (of dropping chamber) cleaned

November
- #222 set up on Pier 2 (HERH) in gravimetry laboratory
- #222 ion pump controller fails due to battery backup - replaced
- #229's laser cleaned and optimised
- #222 - computer communication problems with internal card
- #222 - problem with loose shaft coupler inside the dropping chamber. Chamber stripped stripped to tighten coupler

December
- First data obtained from #222 - check date but with high measurement noise

2015

January
- #229's laser cleaned and optimised due to low power
- Power outputs of #222 and #229's laser compared:
- 229 - 85% power loss from laser exit to collimation assembly
- 222 - 82% power loss from laser exit to collimation assembly
- #229 with 12 μW at collimation assembly = 250 mV fringe voltage, with 5 μW at collimation assembly = 160 mV fringe voltage

February
- Super-spring 'ring down' tested on #222 and #229 due to concerns over high measurement noise since delivery
- #222 polarisation vector rotated at collimation assembly to optimise intensity in all optics in the interferometer
- High measurement noise from #222, consistently 3-5 times higher than that measured by #229
- #222 - Refurbished super-spring controller received from Micro-g LaCoste
- Measurement noise improved to twice that from #229

April
- #229 - Laser tube failure, laser swapped to the reference laser

May
- Tuning of #222 super-spring attempted

August
- #229 sent to Micro-g LaCoste for comparison with other gravimeter regarding the gravity value. #222's super-spring and controller sent back for tuning

October
- #229 received back from Micro-g LaCoste - perfect comparisons with FG5's in Colorado
- #222's superspring returned fully tuned

November
- Attended international comparison of gravimeters in Luxembourg. Zero offset from the average of the attendee's gravimeters
- Tests conducted to compare #222 with #229
- Electromagnetic field tested in gravimetry laboratory

7.5. Working with Four Variants of the FG5

Four different variants of the FG5 have been housed at the SGF between 2006 - 2016. The SGF's own gravimeter was manufactured during 2005 and subsequently upgraded in 2012, to the FG5X. In addition to these two variants of the SGF FG5 the SGF has been home to two gravimeters from the UK's National Oceanographic Centre (NOC) since 2013, these are FG5-103, which was manufactured in 1993 and FG5-222, manufactured in 2002.

FG5-103 is the earliest model and stands out visually from the design of the three others largely due to the following factors;

1. The dropping chamber tripod
    1.1. larger base
    1.2. mounted on diagonal legs
2. The lower section is significantly different than the others since it has
    2.1. a bulk interferometer with integrated laser
    2.2. the super-spring assembly suspended to hang below the interferometer

FG5's 222,229 and 229X are all visually appear similar as they all have the same combination of components. Visual changes from the earlier version include;

1. Vertical legs on the dropping chamber tripod
2. Floor mounted super-spring tripod, on top of which is the super-spring and interferometer
3. The laser is mounted in its own chassis with heat sink and connected to the interferometer via fibre optic cable.

Visual differences aside there are large variations in the electronic components and capabilities between the four generations. FG5's 103 and 222 share similar electronics, with, amongst other things, an electronically tracked cart, individual controllers for the super-spring and dropping chamber, a patch panel to connect each unit and a computer which houses the timing card and to which the fringe, trigger and clock signals are connected directly. Whilst for both generations of FG5-229 a system interface module

(SIM) houses both controllers, dispenses the need for the patch panel, takes in all gravimeter connections and communicates to a laptop via a Magma PCI unit, and the timing card is timing card is housed in the electronics rack behind the SIM. The experiences of using the two NOC owned gravimeters are not contained in this thesis but some results from FG5-222 may be mentioned in brief. The differences between the variants have little impact on the accuracy or precision capabilities of the instruments.

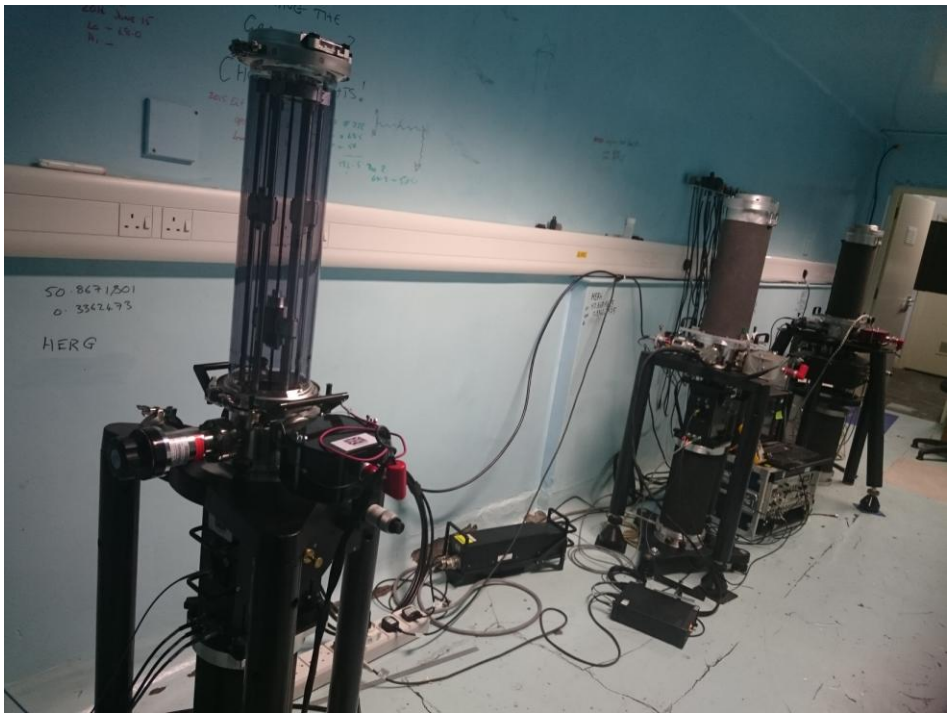

Figure 7.4 Three generations of FG5 in the SGF gravity laboratory. The FG5X is situated in the foreground with the FG5 classic variants in the background

7.6. Comparisons of Absolute Gravimeters Results between 2007-2015

To ensure absolute gravimeters are in full working order and that the measured value of gravity is comparable to other absolute gravimeters comparisons between instruments have to be carried out on a regular basis. This is especially important for a long time series of data from any one location.

Comparison of the SGF gravimeter with other FG5's has unfortunately fallen short of the ideal due to illness and the infrequency of international comparisons. However the effect of the lack of regularity in comparison information is, perhaps, mitigated since the gravimeter is permanently located at the SGF and, unlike the majority of FG5s in existence, is not used for campaign measurements which involve transportation and the instrument being used in non-ideal environments.

A total of four comparisons have been carried out since 2006 which have involved between one and 22 other gravimeters. These comparisons were carried out in Walferdange, Luxembourg, in 2007 and 2012, Micro-g LaCoste, Colorado USA, in 2015 and Belval, Luxembourg in 2015. The lack of comparison between 2007 and 2012 was due to the illness of the writer. An additional comparison was attempted in 2011 but did not produce useable data.

The results of comparisons are important for gravimeters, not only to verify that the gravimeter is operating well and within specification but also, arguably, to be able to implement offsets to a time line of gravimetry data. The two communities using comparisons tend to treat the comparisons in different ways; whereas the NMI's* formally use the offset the geodetic community tend to view the results as a guideline, or a verification that the gravimeter is operating within the stated instrumental accuracy of 2 µGal. Later in this work, in Chapter 12, the implementation of the various comparison offsets are discussed.

7.6.1. 2007 - Walferdange, Luxembourg

Twenty gravimeters from fifteen countries participated in the 2007 comparison held in the Walferdange underground laboratory for geodynamics (WULG). Of the participating gravimeters seventeen were FG5's. The comparison was officially held over a period of three days and involved each gravimeter measuring on a 'pier' (the WULG consists of three levels of concrete slab with five locations each for gravimeters) on each level. Therefore

* NMI's - National Metrological Institutes

the planned rotation meant that each gravimeter did not measure more than one pier in commonality with any other gravimeter. In reality FG5-229 was on site longer than the recommended three days and therefore occupied six piers in total.

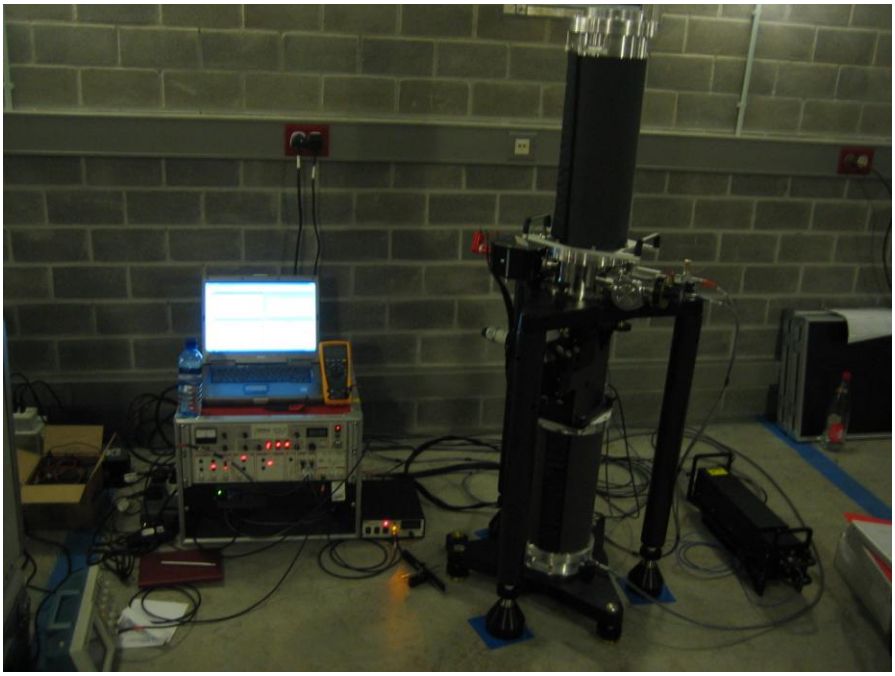

Figure 7.5 FG5-229 in Walferdange underground laboratory for geodynamics in 2007

The ‘piers’ are simply studs placed within the concrete at near regular intervals. It should be noted that one of the draw backs of the construction of this room is the non-bonding of the concrete to the rock strata, in fact a plastic sheet separates the two, which results in rebound effect of the concrete which can be seen in the residual drop data.

Table 7.2 Results of the 2007 European comparison of absolute gravimeters. Taken from the published paper by Prof. Francis of the University of Luxembourg (Francis, 2010).

Gravimeter	Final Results				
	Offset (µGal)	Standard Deviation (µGal)	Gravimeter	Offset (µGal)	Standard Deviation (µGal)
FG5-101	2.2	0.9	FG5-222	1.0	1.1
FG5-202	2.7	1.1	FG5-226	-3.4	1.2
FG5-206	-1.6	1.1	FG5-228	-0.3	1.3
FG5-211	2.2	1.1	FG5-229	-1.5	0.8
FG5-215	0.8	0.9	FG5-230	0.0	1.2
FG5-216	1.8	0.8	FG5-232	1.5	0.8
FG5-218	-4.1	1.2	FG5-233	1.0	0.9
FG5-220	2.5	1.1	FG5-234	-0.5	1.1
FG5-221	0.1	1.1			

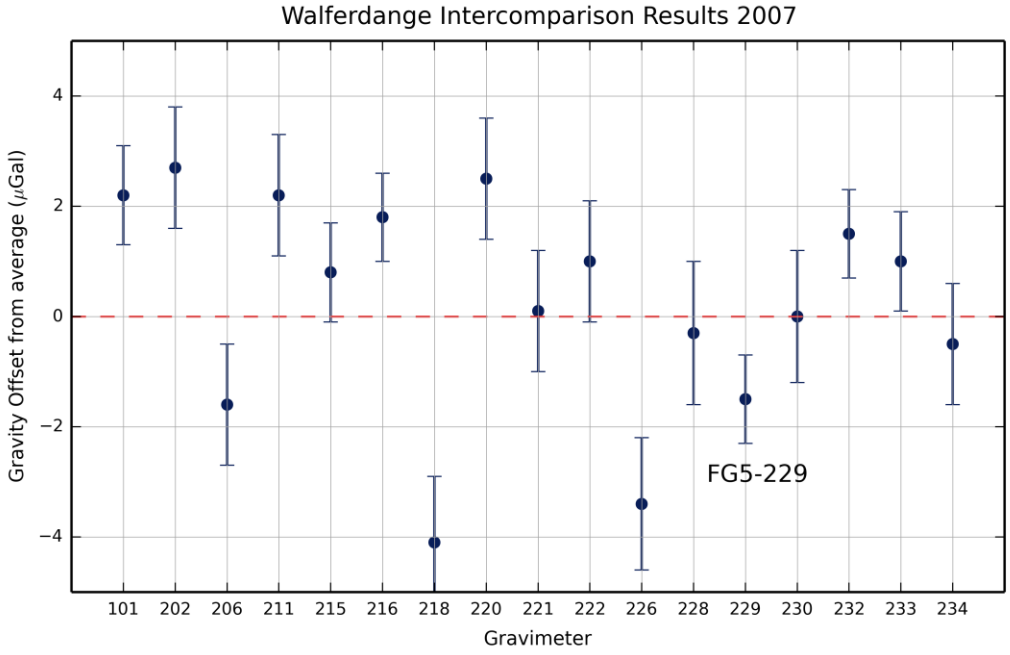

Figure 7.6 Results from the 2007 European comparison of absolute gravimeters. The serial number of each FG5 gravimeter is given with its associated offset and standard distribution. The SGF gravimeter (FG5-229) is shown with an offset of 1.5 µGal lower than the average result.

Since the approach taken by Prof. Francis has been used for various comparisons since this comparison, the values obtained by his solution will be used later on in this work.

7.6.2. 2011 - SGF, Herstmonceux

Since illness prevented attendance of the ECAG comparison in Walferdange in 2011, gravimeter FG5-103, operated by the National Oceanography Centre, Liverpool, visited the SGF whilst returning from the comparison. The objective was to provide a link into the ECAG 2011 by measuring against a participating gravimeter. Both gravimeters would have operated on piers 1 and 2 to attain a loose comparison. Unfortunately the results from FG5-103 were considered to be of such poor quality whilst measuring on P2, FG5-103 measuring 36 microgal below the expected value and with high drop scatter, the comparison was abandoned by the visiting operator of FG5-103. No useable results were produced.

The comparison was abandoned due to a belief that the gravimeter had developed a problem with the super-spring whilst en-route back from the ECAG. However, the problem may well have been a set up error induced by the fact that FG5-103 was set up in a position which one of the dropping chamber feet straddled the new/old floor boundary in the gravity laboratory; there is a level change between the new asphalt and the older, more stable, asphalt. A 3mm shim was used to steady the leg of the gravimeter between the flooring levels. Gravimeter FG5-229 was moved onto P2 a few days later, no problems were found, the data was tight and produced the expected value.

7.6.3. 2012 - Walferdange, Luxembourg

Due to the fact that the ECAG-2011 was missed and the upgrade of the SGF gravimeter to the FG5X variant was scheduled a comparison was deemed essential in 2012, prior to the upgrade. A mini comparison at Luxembourg was organised between the SGF gravimeter

and the gravimeter of Prof. Francis; FG5X-216*. A total of three piers in the WULG were measured during this mini comparison by both gravimeters.

Table 7.3 Results of the 2012 mini comparison at WULG.

Gravimeter	Pier	Gravity	Standard Error of the Mean	Offset ($g_{FG5216} - g_{FG5229}$)
FG5-229	A4	980964189.97	0.37	-2.54
FG5X-216		980964187.43	0.87	
FG5-229	B3	980964065.87	0.61	-0.12
FG5X-216		980964065.75	0.70	
FG5-229	C3	980963945.81	0.41	+0.27
FG5X-216		9809643946.08	1.63	

The results show good agreement between the two gravimeters, with the exception of the value obtained on pier A4. If we assume an error was made during the setup of FG5-229 on pier A4, any FG5 setup error forces the observed gravity value to be low, then it is reasonable to treat the results from A4 to be an outlier and therefore exclude it from the mini comparison. If the results from the piers B3 and C3 only are used the measurement difference between these two gravimeters is negligible.

* Prof. Francis is from the University of Luxembourg and is organiser of the 2007 and 2011 ECAG comparisons.

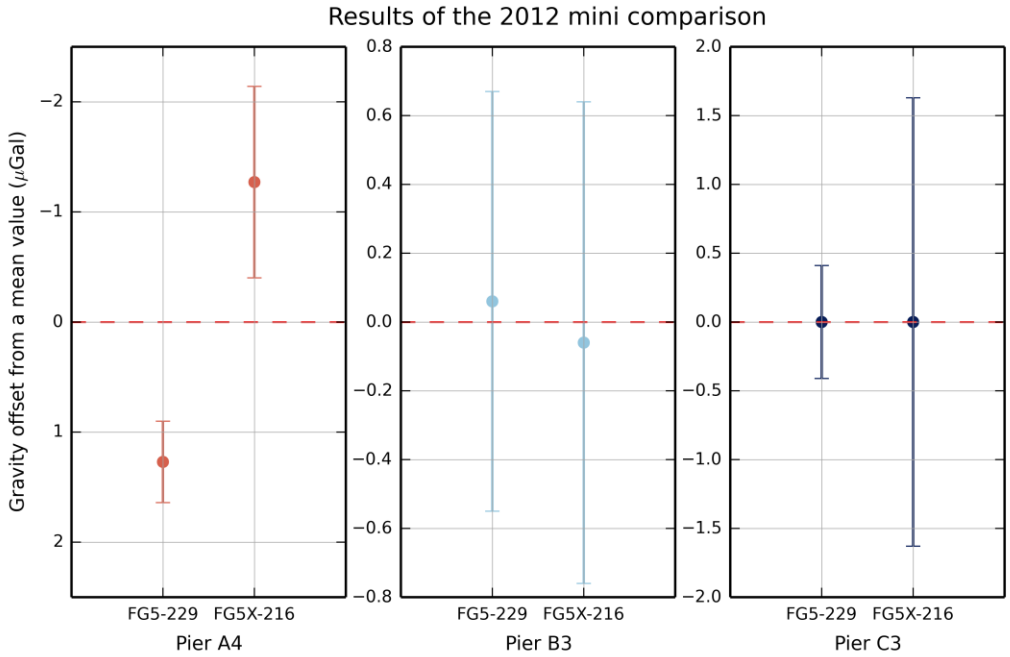

Figure 7.7 Results of the 2012 mini comparison, between FG5-229 and FG5X-216. The plot shows the residual value taken from a mean of the observed from both gravimeters.

Further, since the results of the 2011 international comparison of gravimeters show that FG5X-216 was +2 µGal higher than the mean it could be concluded that FG5-229 would have also read +2 µGal higher than the mean if it had participated in that comparison.

7.6.4. 2015 - Belval, Luxembourg

The location of the 2015 international comparison of gravimeters was moved to the new Belval campus of the University of Luxembourg due to the closure of the WULG mine due to health and safety considerations. The Belval measurement site utilised one half of a new building belonging to the engineering department. A total of nine piers (measurement sites) were available.

Figure 7.8 Week 1 of the international comparison of gravimeters in Belval, Luxembourg

The comparison was undertaken over a two week period involving seventeen participants. The floor at the comparison site is a slab 15 m wide, 10 m long and 1 m thick supported by three girders 3m high by 10m long (see Figure 8.12), and the void underneath the floor results in large differences in gravity gradient at each pier. Because of this the organisers of the comparison took relative gravity gradients for each pier prior to the comparison.

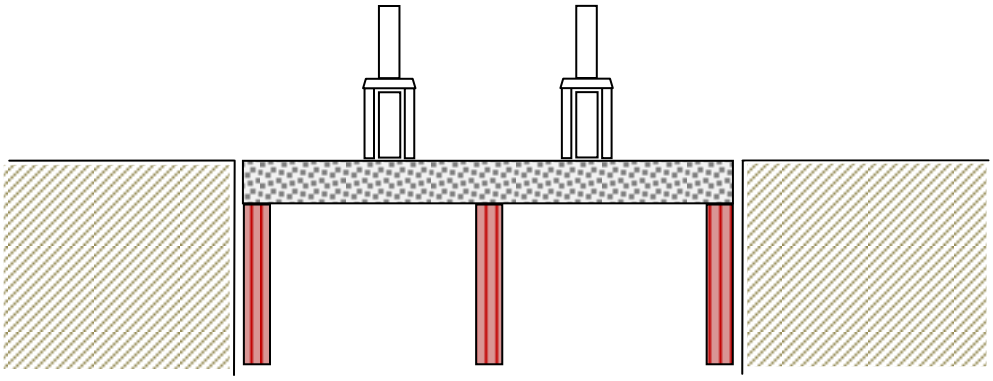

Figure 7.9 Depiction of the floor in the civil engineering building, Belval, University of Luxembourg. Showing a large cavity underneath the measurement piers

In addition to the variation of gravity gradients the site at Belval was considered less than ideal due to its close proximity to roads and construction work, (which included the neighbouring building). However the high level of anthropogenic noise allowed for a good test of the noise response of the SGF gravimeter away from Herstmonceux.

The results from the comparison have been analysed and will be published soon (Palinkas, 2015), in this paper the results have been analysed using three techniques, one using an

non-weighted constraint, one using a weighted constraint, where the weights are the RMS* values of the uncertainty of the gravity measurements, and one where the weights are also considered by the RMS value of the uncertainties but where those uncertainties have been adjusted to be in line with those supplied by the participants of the key comparison (NMI's). Since the results from the second and third techniques are near identical the results from the third method have been taken as the final result. The offset results are presented here for consistency with the results from the 2007 comparison:

Table 7.4 Results of the 2015 regional comparison of absolute gravimeters. Taken from the draft results (Palinkas, 2015).

Gravimeter	Final Results				
	Offset (µGal)	Standard Deviation (µGal)	Gravimeter	Offset (µGal)	Standard Deviation (µGal)
FG5-202	4.49	0.77	FG5X-102	0.15	0.79
FG5-215	3.82	0.54	FG5X-216	-1.42	0.50
FG5-218	0.45	0.75	FG5X-220	5.11	0.69
FG5-230	-3.18	0.79	FG5X-221	-2.19	0.59
FG5-233	2.51	0.87	FG5X-229	0.08	0.80
FG5-234	4.52	0.8	FG5X-247	-3.87	1.38
FG5-238	3.72	2.0	FG5X-302	1.06	0.61
FG5-301	0.16	0.74			

The SGF gravimeter (FG5X-229) with a near zero offset from the average. The intercomparison results and possible implementation of them on the SGF gravity time series is discussed later, in Chapters 13.

* Root mean square

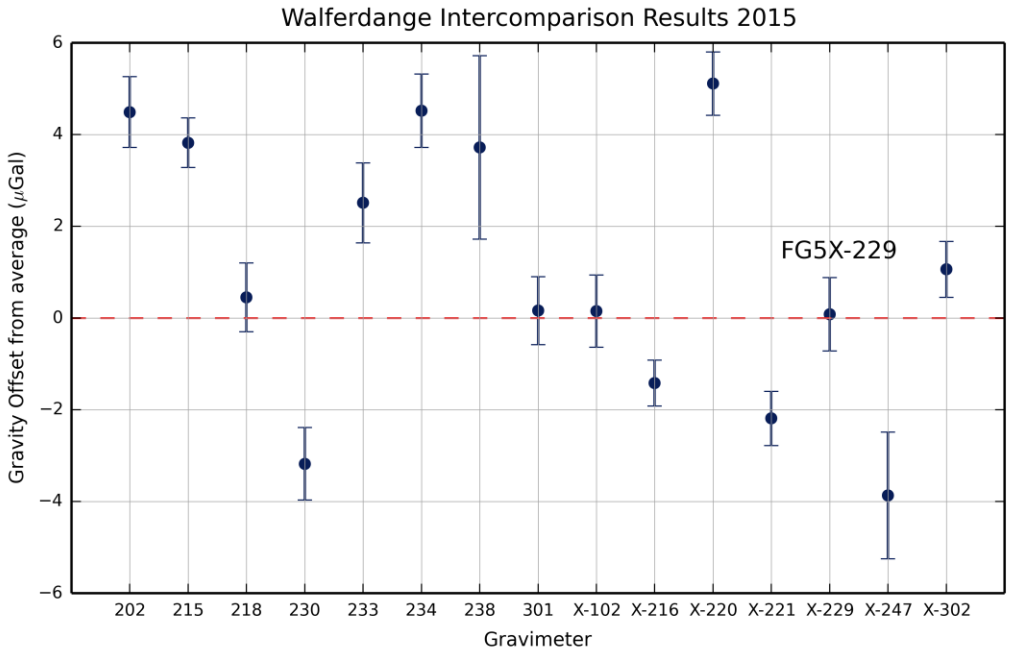

Figure 7.10 Results of the 2015 regional comparison of absolute gravimeters. The serial number of each FG5 gravimeter is shown on the x-axis, with the differentiation between the standard FG5 and the FG5X indicated. The results give the offset of each gravimeter with its associated standard uncertainty.

7.7. Conclusions

The initial attempts to operate the gravimeter outside the gravity laboratory have shown that the conversion of the basement for this use was justified. The laboratory has proved to be a useful space now able to house all the gravimeters currently owned by the UK.

Comparison data is essential for determining the accuracy of the instrument as it changes through use or servicing. All comparison results indicate that the FG5 was operating within the accuracy specification of ±2 µGal. The use of the comparison offsets are discussed further in Chapter 13.

Chapter 8

Operating and Maintenance Experience with the FG5

8.1. Introduction

This chapter derives from the author's personal experiences of maintaining FG5's. The purpose of this chapter is to inform the reader of specific problems which may need to be overcome to produce a long time series of accurate and precise data using an FG5.

The instrument knowledge described here has been obtained from working with FG5's over the time period 2005 - 2015 and includes some information from three generations of FG5. The majority of experience has been obtained from working upon the SGF FG5 numbered FG5-229, which was upgraded in 2011 into the FG5X. Additional experience has been obtained on FG5-222 and FG5-103, which have been housed at the SGF since 2013 but are property of the National Oceanography Centre (NOC). Unless specified the experiences set out within this chapter refer to working with the older type of FG5 rather than the FG5-X model.

The user manual (Micro-g LaCoste, 2007) written by the manufacturer of the FG5, Micro-g LaCoste, should always be consulted when working on the instrument. A 2007 version of the users' manual is available on line at:
http://www.microglacoste.com/pdf/FG5Manual2007.pdf

8.2. Dropping Chamber Repair

Maintenance of the dropping chamber is necessary over time to maintain the functionality and minimise errors. Basic operation of the dropping chamber is reliant on the drive belt

and maintaining a good vacuum ($1.3x10^{-4}$ Pa, (Hopewell, 1999)) in the chamber. Failure of the drive belt is critical, the drive belts wear and snap over time and number of drops rendering the dropping chamber inoperable. Both the ferrofluidic feed-through and ion pump are common points of failure of the vacuum system.

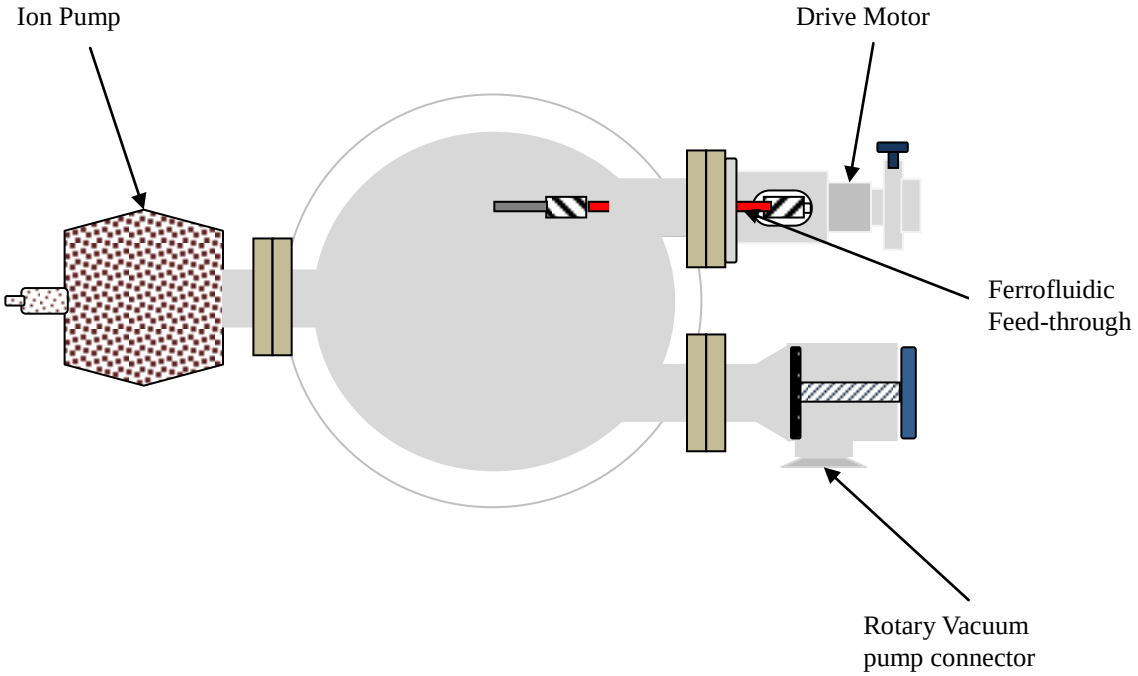

Figure 8.1 Common vacuum failure components on the lower service ring

Failure of the ferrofluidic feed-through, which couples the mechanical drive situated on the outside of the chamber to the drive inside, is likely to be a gradual process but the degree of loss is likely to be dependent on the number of drops used and the length of the project. The deteriorating vacuum will impact the measurements in poor fit residuals (or may show a sinusoidal signal, or a higher percentage of rejected drops). Problems with the ion pump can be hard to differentiate from failure of the ferrofluidic feed-through.

Mechanical or electrical work carried out on the dropping chamber includes the replacement of the ion-pump, drive-belt, ferrofluidic feed-through and tuning of the dropper control card. These components have been described in the previous chapter.

8.2.1. Listening to the Dropping Chamber

The sound produced by the dropping chamber is a useful indicator of an approaching, or current problem with one or more elements associated with this component of the FG5. For instance:

- A ‘hum’ from the motor can indicate incorrect or imperfect tuning of the dropping controller board
- An intermittent knock, which may be faint, may be signalling that the drive belt has reached the end of its lifetime and may be about to fail
- A loud crash, with a spring noise, is an obvious tell that the lift/drop/oscillate has failed and the cart has just smashed into the base plate.

8.2.2. Preparation for Work Inside the Dropping Chamber

When a repair or cleaning work has to be carried out inside the dropping chamber the first task is to open the vacuum chamber to enable working at atmospheric pressure. As stated in the manual the chamber should not be opened rapidly, a slow increase of pressure inside the chamber is desirable. Since the opening valve is a baffle plate which travels past a vacuum flange (ConFlat type), and the thread associated with it is long, the precise location at which the valve will open is variable between instruments; care is advised. The use of nitrogen is recommended in the manual as this will reduce contamination of the chamber by high velocity air particles or water molecules which will stick to the chamber walls. The time taken to re-attain a good vacuum is affected by the level of contamination in the chamber. Nitrogen has never been used at the SGF.

Before the vacuum is destroyed it is advisable to have everything to hand which may be required ready for the repair. Since work inside the chamber and the pump down process (to obtain a vacuum) can be onerous it is also advisable to have on hand any components which might be reaching the end of lifetime and any items which might be damaged in the repair process; such as o-rings or gaskets. To reduce the level of contamination in the chamber the objective should be to carry out all of the repair work in one go. Minimising

the time spent at atmospheric pressure for the internal components should reduce ingress of water molecules and particle contamination and therefore reduce the time taken to pump the chamber back down to a workable vacuum.

Working with equipment which has to be under vacuum means that the following precautions should be taken:

- All tools which will touch the surfaces inside the chamber should be cleaned to remove residual oils. It is worth creating two sets of tools, 'dirty tools' for the outside of the chamber, and 'clean tools' for inside.
- Gloves should be worn at all times when touching any surface within the vacuum chamber to prevent the natural oil on fingertips transferring. During vacuum pumping any transferred fingerprint oil can outgas water vapour and other molecules which will have an impact on the attainable vacuum level within the vacuum chamber.
- Should any oil, for any reason, contact with the surfaces inside the chamber then wiping down with a lint free cloth or optical tissue with pure acetone, or isopropyl alcohol (HPLC* grade is used at the SGF) is recommended.
- A roll of kitchen aluminium foil should be kept with lab supplies.
- Long hair should be tied back to prevent stray hairs, hairs which fall across gaskets/o-rings will result in imperfect seals and therefore a loss of vacuum pressure.

8.2.2.1. Repair Advice

Most repairs carried out inside the dropping chamber, such as replacement of the drive belt, ferrofluidic feed-through or ion pump, will involve removal of the chamber outer casing

Figure 8.2 Releasing the dropping chamber snubber lock nuts

* HPLC - High Purity Low Carbon

which itself involves the removal of the upper flange and relaxation of the guide supports (described as ‘snubber lock nuts’ in the manual). Removed components should be kept as clean as possible, covering the flange surfaces with aluminium foil is advised as aluminium foil does not require any cleaning prior to use.

Figure 8.3 Removal of the drive belt

When changing the drive belt the belt must be cleaned prior to installation with acetone and only handled with gloved hands afterwards.
When changing the ion-pump or ferrofluidic feed-through it is advisable to have plenty of spare copper gaskets for the ConFlat vacuum range ready, they are a one use item and reuse is not advisable. A 3/8” ratchet set with additional extension bar is recommended for a faster removal of the flexible coupling and motor attachment on the outside of the chamber.

Whilst the chamber is exposed to air, for any reason, the opportunity should be taken to clean the window on the bottom of the chamber to remove the particle build up resulting from the friction of the drive belt and ejecta from the impact of the balls & vee’s. An invaluable tool for the safe removal of the window, which has the added advantage that it will not damage the o-rings, is a pen-vacuum device which can be obtained from most good optical suppliers.

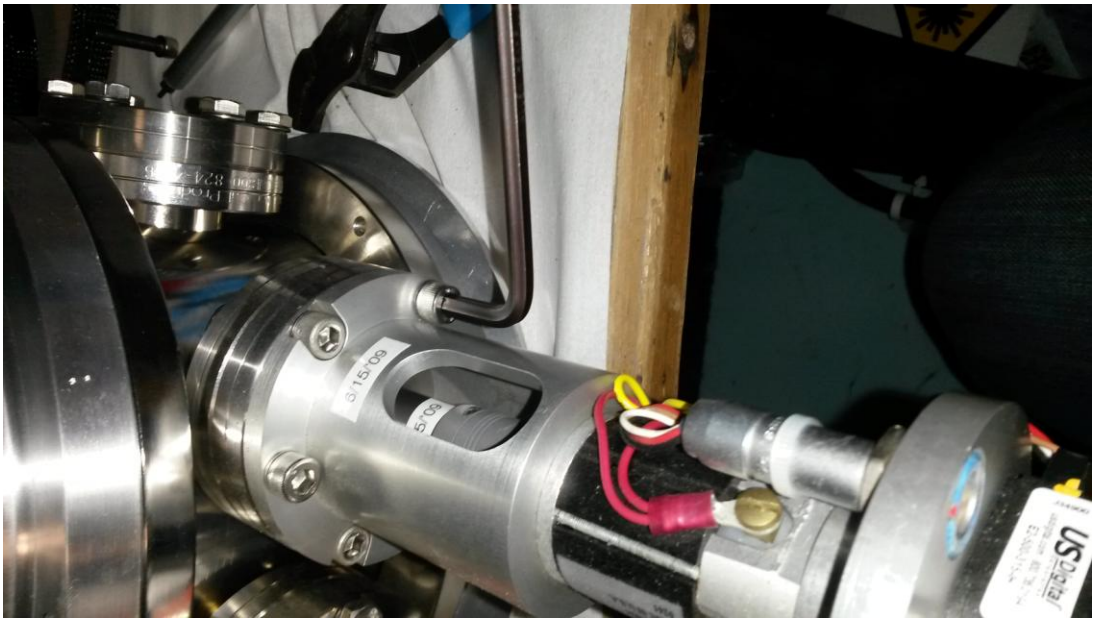

Figure 8.4 Removal of the motor assembly to access the ferrofluidic feed-through

After internal repair of the dropping chamber it is very important to follow instructions in the user manual regarding bubble level alignment and use of an 'X-Y detector' to avoid incorrect alignment of the chamber bubble levels due to a change in the internal alignment of the guide rods to chamber housing. Failure to do so may impact the gravity value the instrument will measure.

The guide rods are not required to be perfectly straight or perpendicular to the base of the dropping chamber, it is only important that the position of the cart at the top of the drop is directly above the position at the bottom of the drop.

8.2.3. Electrical Tuning

The tuning of the dropping controller board dictates the amount of power supplied to the drive motor inside the dropping chamber to enable it to lift, hover, and drop and catch the retro-reflector smoothly. The composite configuration desired from the adjustment of each potentiometer dictates the power supplied for each movement, or stage, and each should operate smoothly and quietly. This process of tuning the dropping chamber cart is a complicated and delicate process of balancing the potentiometers on the control card to get

the drop trace to match a model trace shown on an oscilloscope as well as possible whilst listening to the mechanics of the lifting and dropping cart.

Correct tuning of the dropper will ensure smooth operation of the cart. If the card is tuned incorrectly at hover phase at the top of the drop the cart may be released before it should, or the motor may struggle to maintain position inducing a vibration or rotation to the falling object. Either of which will impact on the quality of the data taken during the drop. If the drop phase is incorrectly tuned the cart may not release the object to free-fall or fail to catch the object correctly. Poor tuning may cause the cart to impact the base plate of the dropping chamber at high velocity, this will result in: unnecessary damage to the tungsten balls at the bottom of the cart and the base plate, which will cause more particles to be ejected, making the ion pump work harder, which will theoretically decrease the lifetime of the ion pump. The resulting particle ejecta will also coat the bottom window of the dropping chamber, particle build up on the window will eventually lead to a decrease in the attainable fringe voltage which can only be cured by the cleaning of the optic. The result may also cause the failure of the system causing a reset in the electronics.

Repeated high impact events of the cart may cause permanent damage to the retro-reflector. The first service of FG5-229 at Micro-g LaCoste found a cracked retro-reflector, which may have been a result of the testing of the gravimeter in the South East office at Herstmonceux described in the previous chapter. The tuning of the FG5X is done entirely by firmware changes, removing the requirement for guide card tuning.

8.3. Super-Spring Repairs

The super-spring is arguably the most sensitive component of the FG5, and as such great care should be taken when attempting any repair or make adjustments to the spring system.

Unnecessary damage to the spring assembly can largely be avoided by ensuring the spring is on a levelled platform for any action which requires the cover to be removed. The spring tripod is perfect; it is usually unnecessary to use an alternative levelling plate. The

clearance between the guide pins and the centre tube assembly, inside which the main spring hangs, is directly related to the positioning of the flexure rods. The clearance should be between 0.0762 mm - 0.127 mm. Once on a well levelled platform the travel lock should remain locked until the outer casing of the spring has been removed.

Problems with the super-spring, either mechanically or electronically (tuning), can have a large impact on the quality of the data produced by the gravimeter. Snagging of the springs inside the chamber, bent flexures or poor tuning will generally increase the inherent noise of the measurements drop to drop.

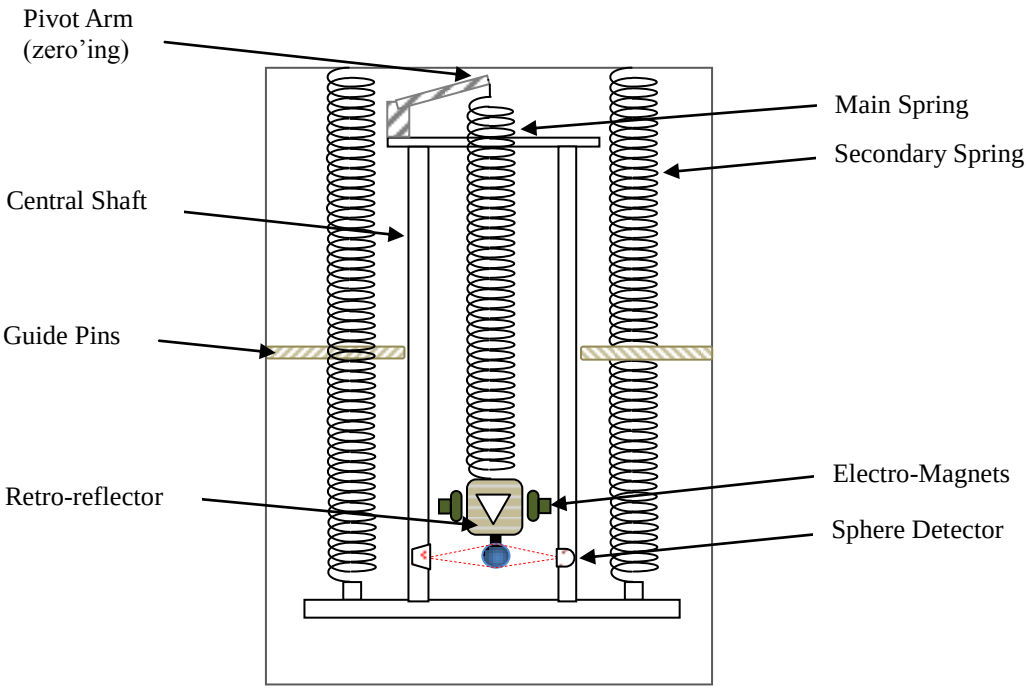

Figure 8.5 Schematic drawing of the main components in the spring assembly

In the nine years of operating an FG5 at the SGF the outer casing of the super-spring has required removal on a handful of occasions, usually after transit, when there is a suspicion the measurement noise is much greater than expected; i.e. when the standard deviation of

drops is over 70 μGal. On each occasion the flexure rods, or delta bars, were checked to ensure they remained undistorted. The flexures consist of a brass triangular section in the centre with straight wires either end which attach to the body of the spring assembly. A visual check of the flexure ends (wires) is generally enough to determine if the flexure is damaged, see Figure 8.6.

Figure 8.6 A Super-Spring flexure

Diagnosis of any fault of a more complicated origin is best handled in consultation with Micro-g to prevent unnecessary complications, or accidental damage, unless the operator has previous experience.

8.3.1. Example of an Electrical Fault

The position of the super-spring sphere, located at the bottom of the assembly (see Chapter 3), can be checked by use of a multimeter plugged into the sphere position feedback on the SIM* unit. The sphere position gives a voltage feedback to the user to indicate the vertical deflection from a median position of the sphere within the housing. A negative and unchanging voltage is generally obtained when the spring is still clamped or locked for transit. When the spring is released the voltage should start to oscillate immediately

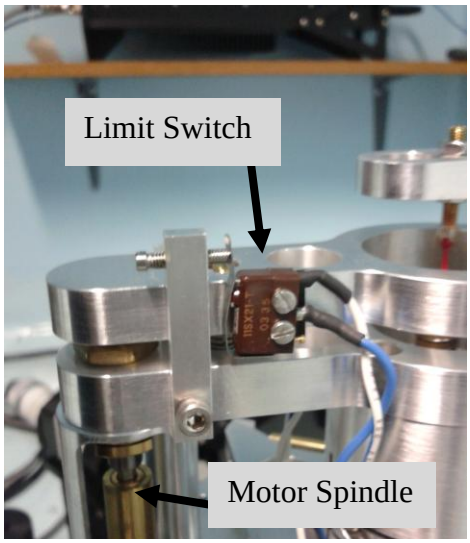

Figure 8.7 The motor spindle, on the left, and one of the limit switches

* SIM - System Interface Module

giving a largely varying voltage, generally in the hundreds of millivolt scale. When the spring starts to settle the voltage feedback will also steady, dependent on site noise, giving a reading of V = 0 ±10 mV. An offset from zero in the voltage feedback indicates that the spring needs to be reset into its median position by use of the ‘zero’ function on the SIM.

On one occasion a serious fault with the spring presented as an inoperative ‘zero’ function. The ‘zero’ button is located on the SIM and optimises the position of the spring to ensure the mass is hanging in the centre of the oscillation space. With the travel lock released the spring position voltage read a steady -0.98 V and remained unchanged when attempts were made to use ‘zero’.

However by tracing the connectivity from the control board (see Figure 8.8) to the super-spring it was established that the motor control signal, from the board to the motor within the spring assembly (see Figure 8.7), was not connecting.

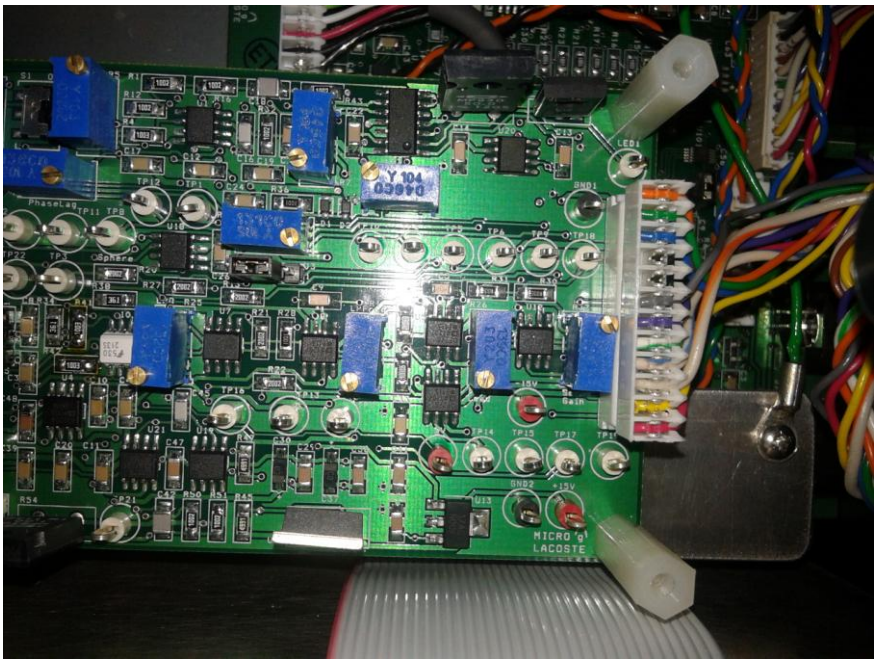

Figure 8.8 Super-spring control board within the SIMX unit

With the lack of connectivity established the fault was found on the cable socket on the rear of the SIMX*, where the pin for the motor drive was pushed back and loose in its housing, see Fig 8.9, therefore it unable to contact with the cable plug, essentially terminating communication from the controls to the spring motor. The problem necessitated replacement of the LEMO† socket.

Figure 8.9 Faulty pins in the super-spring LEMO socket on the SIMX

If an electrical fault of this type was ignored and the FG5 were to be set up to operate would result in the spring hanging outside the median location which in turn might cause:

- The electromagnets trying to 'pull' the spring into an unnatural position
- Causing contact with a surface inside the super-spring housing

8.3.2. Super-Spring Frequency Response

The oscillation half-life‡ of the spring can be checked to determine if the spring is behaving as it should. This is done by disabling the electrical servo and monitoring the spring position using an oscilloscope (a 40 mV - 1 V vertical scale with a time base of either 2 or 4 seconds can be used). After the travel lock is quickly released the half life of the oscillation from the first sign of dampening can be estimated. The half life should be around 12 seconds. Testing the half-life of the spring is a check that the mechanical components are aligned and working correctly. Any misalignment increases the friction within the assembly and increases the damping rate.

The ability to obtain a clear trace showing the ring down of the spring can be difficult, is rather subjective, as the result depends on how smoothly the travel lock ring is turned as well as how hard the locking collar is released. Tests carried out on springs from two gravimeters showed one reacted best to the locking collar being gently repositioned whilst

* FG5X System Interface Module
† A type of push fit electrical connector
‡ Half-life is the time required for the oscillation amplitude to decrease by half

the other required the collar to be 'snapped' back into location. Examples of a successful test for ring down and a failed attempt are shown in Figures 8.10 & 8.11 respectively.

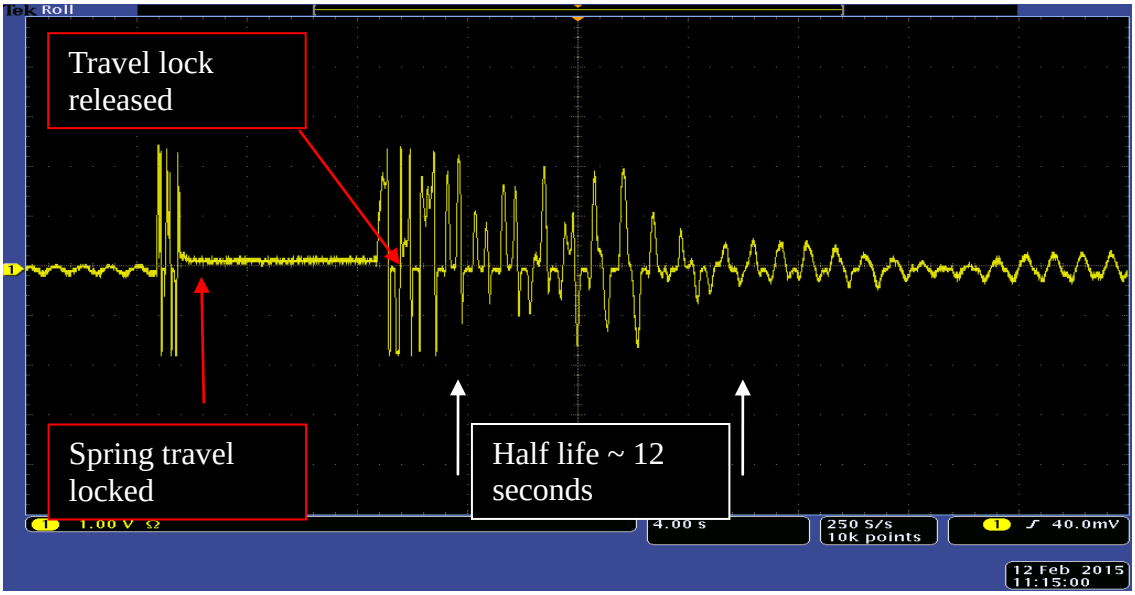

Figure 8.10 Oscilloscope trace to test the half-life of the super-spring

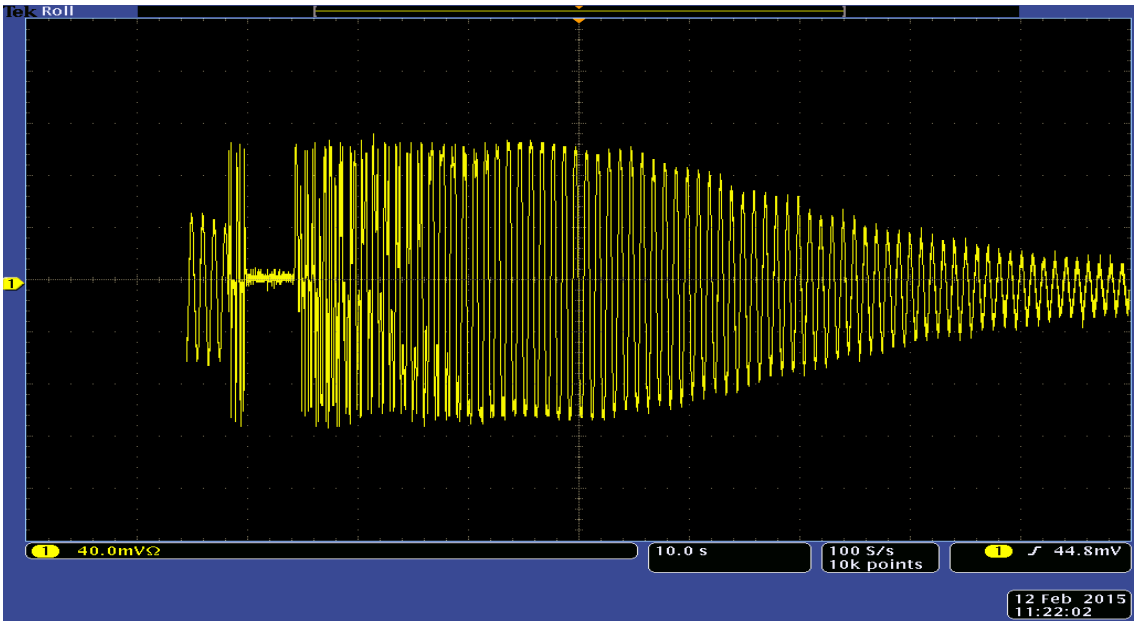

Figure 8.11 A failed attempt to obtain a half-life measurement of the super-spring

8.4. Laser

The laser supplied with the FG5 is a WEO-100 manufactured by Winters Inc. which has been discussed in Chapter 3. It is supplied mounted on a chassis supplied by Micro-g which has a fibre optic coupling for use with the FG5 (however FG5-103 is an older design where the laser is integrated with the interferometer and has no fibre optic).

The laser power output from both the tube and the collimation assembly is of interest to an FG5 operator and as with most laser systems it is a good idea to track the power output from the start, as such, to the end of the optical chain. In this case the power output of the laser may be measured, at least in the first instance, in three places:

a) Through the photo detector situated behind the rear mirror, the current output of which is converted to the laser power output in Volts D.C. and can be monitored from a signal monitor dial on the laser control electronics or via plugging in a multimeter into a BNC* output.
b) By using a power meter at the laser output from the cavity, before the faraday isolator.
c) By using a power meter to monitor the output coming out of the collimation assembly which plugs into the side of the interferometer.

* BNC = British Naval Connector and is a quick release electrical connector commonly used with co-axial cables.

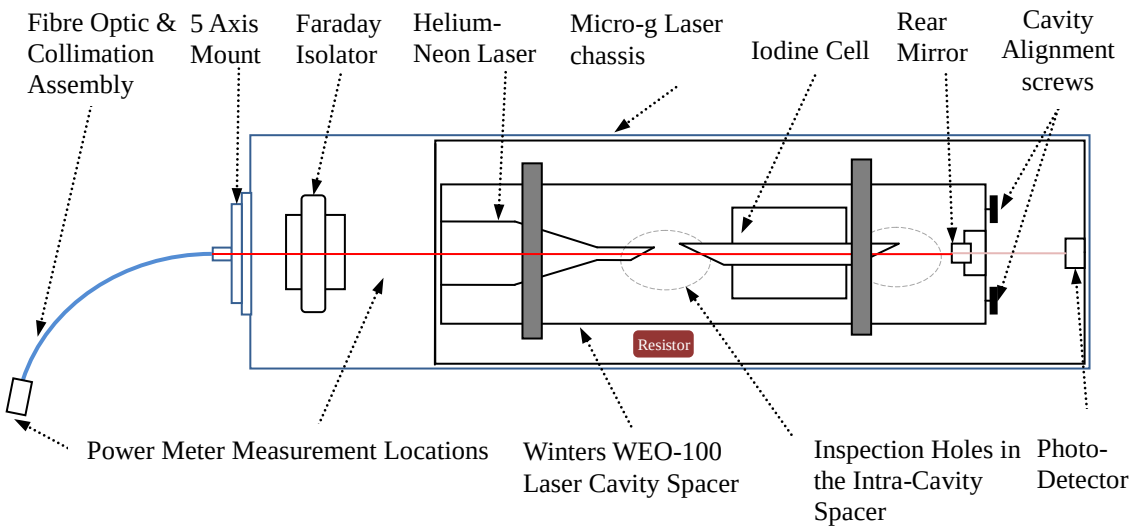

Figure 8.12 Schematic of the FG5 WEO-100 laser

Arguably one of the negatives of the design of the WEO-100 is the placement of a large resistor, covered in heat tape, which is situated directly beneath the inspection hole in the laser cavity spacer. The hole in the spacer allows access to the Brewster windows at the end of the He-Ne laser tube and at one side of the iodine cell. The resistor generates significant heat which causes the heat tape to outgas which in turn coats both the tube cover and causes contamination to the Brewster windows. A Brewster window is a glass window, set on or very near to the Brewster angle, which transits light of the proper linear polarisation with effectively no reflection loss at either side of the glass interface.

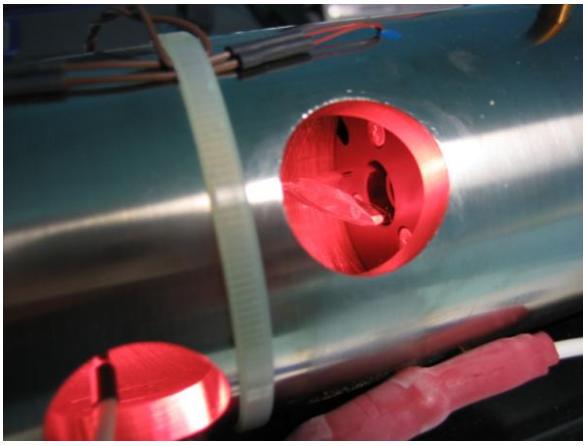

Figure 8.13 Inside the WEO-100 laser. The resistor is shown at the bottom right of the photograph. Discolouration above the resistor shows resultant contamination. The Iodine cell

This contamination as well as dust causes the laser to require frequent cleaning, when in the gravimetry room at the SGF cleaning is generally required on a three monthly basis, but can be required more frequently from other factors, such as tube deterioration with age or contamination of the acetone solvent used for cleaning the optics.

The operational lifetime of the laser at the SGF has been an area of concern, with the average lifetime of the laser tube being approximately only three years. It was theorised that since weekly measurements of 'g' are taken the laser was, generally, permanently on. However it is now thought that the lifetime of the laser tube is independent of usage.

8.4.1. Laser Cleaning and Alignment

When cleaning the laser caution and patience need to be exercised. To clean the laser the laser head cover requires removal and results in the user having access to both the high voltage and laser radiation. Extreme caution should be taken when doing cavity alignments or cleaning since the laser starting voltages are in excess of 8 kV and can be lethal (Winters Electro-Optics, 2000).

The cleaning of the laser optics should be carried out with high grade acetone. It is wise to buy the acetone in small containers since any contamination in the acetone will be detrimental to the objective and may cause power output to fall instead of improve.

The cleaning of the laser is best carried out with the power meter a position shown in Fig.8.12 and where the user is able to monitor the signal output and the peak status on the front of the laser controller. When the power meter is in place the removal of the laser head cover will cause the power output to destabilise momentarily, it often drops at a little due to the loss of thermal cushion and is likely to momentarily lose the 'peak lock'. The cleaning of the Brewster windows should be carried out according to the instructions in either the FG5 manual or the manual supplied by Winters Inc. and each optic cleaned in sequence.

Each optic is swiped with a clean lens tissue which has been wetted with 1-2 drops of acetone, each time this is done the user must wait for the laser to re-lock on the laser peak before continuing. It is worth noting that whilst cleaning of the windows may only take a few swipes of the acetone if the contamination is bad cleaning may take several dozen swipes of the acetone.

The two Brewster windows situated above the resistor require the most frequent cleaning due to the accumulation of particulate contamination from the heated tape. Since they do not suffer the same build up of particulate matter the rear mirror and last Brewster window require relatively infrequent cleaning and tend to be cleaned only if the power output of the laser has not been improved sufficiently by either cleaning of the other windows, by an alignment or by optimisation of the iodine cell.

Angular adjustment of the iodine cell can provide a coarse adjustment to the power output, it is a fast and relatively coarse adjustment which can be used to either increase or reduce the power output on certain occasions. For instance; if the laser is producing too much power output, which may produce undesirable fringe voltages in excess of 400 mV, the cell can be used to ‘detune’ the laser, perhaps in concert with adjustment to the focus on the 5 axis mount.

If cleaning has not improved the power output on the meter or signal monitor significantly an adjustment to the cavity alignment may be required. This is done by small adjustments to the two cavity alignment screws situated on the back of the laser tube. However if significant cleaning has been required a gap of a few hours has been found to be beneficial before attempting to make any adjustment to the cavity alignment.

Although the laser output can be tweaked in a variety of ways the amplitude of the fringe voltages is usually directly related to the laser power output. The quickest way, though not the most useful, to determine the laser output is the use of the signal monitor on the laser controller situated in the electronics rack, generally when this voltage drops below 4 volts (DC) the laser needs attention. When the laser power falls below 3V the fringe signal is

likely to be too low to provide reliable signals to the photo-detector in the interferometer causing cessation in data collection or an unusable gravimeter.

8.4.2. 5-Axis Mount

The five axis mount controls the positioning of the laser beam into the fibre optic. It allows both coarse and fine adjustment of the alignment and allows the power density of the beam going into the optic to be controlled, by use of a 'focus' screw.

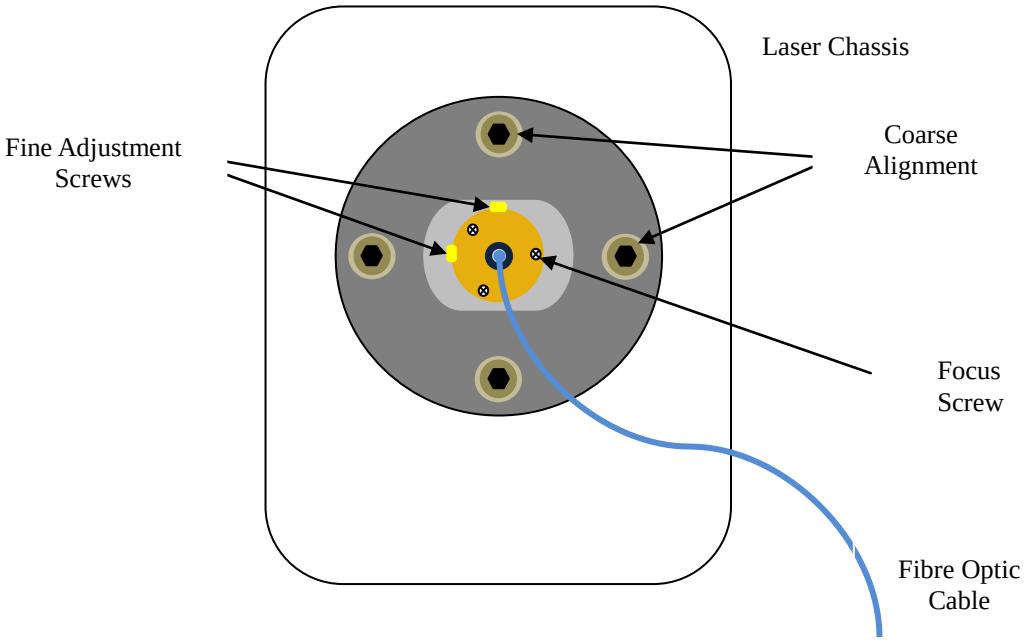

Figure 8.14 The five axis mount. Which is situated on the front of the laser chassis

If for any reason the laser beam is losing a large amount of power when going through the fibre, ascertained by measurement post cavity and at the end of the collimation assembly, an adjustment of the mount is likely to be required. If the laser is making it through the fibre but the output is low then the fine adjustment screws on the top and side of the mount can be used in conjunction with the 'focus' screw to improve power output. If no laser is making it through the fibre, or the fine screws do not improve the situation sufficiently, then the coarse adjustments must be made. Unfortunately the coarse adjustments are made

by sliding the whole head of the mount in x and y by loosening the grip screws such that the washers allow some degree of freedom but only just enough. Care is recommended as too much movement will result in entire 'loss' of the beam through the fibre.

8.4.3. Interferometer & Polarisation

Prior to the 5 axis mount and after the beam exits the cavity it passes through a Faraday isolator, to control the polarisation vector. The linear polarisation of the beam is critical both for the transmission through the fibre optic and into the interferometer.

Incorrect polarisation in the interferometer can result in a large disparity between the intensity of the 'test' and 'reference' beams (see Chapter 2) and can result in a low fringe signal voltage. Changing the polarisation of the assembly can be done by rotating the inner core of the assembly from the outer however the divergence of the laser, which should be as parallel as possible, is also dependent on the positioning of the core so extreme care should be taken when dealing with this component. Diffraction patterns seen in the laser beam through the telescope of the interferometer can be due to contamination on optics, such as finger prints or dust.

8.4.4. Environmental Conditions

Like most lasers built for specific scientific uses the alignment of the WEO-100 is critical to the operation and power output of the laser. Sudden mechanical shocks endanger the optical alignment and have the potential to dramatically reduce power output, sometimes critically.

Operation of the laser may become difficult in humid conditions since rapid changes in humidly or very high humidity can cause problems with misting of optics and affect the ability to attain/maintain lock on a transition peak (explained in Chapter 2.1.1). The laser should also be protected from prolonged periods of a cold environment. Leaving a laser turned off in temperatures of 10-20 degrees for months could result in prolonged

reactivation, where the tube operates and both cavity and cell temperatures attain operational temperature but no laser light is generated for a period of days (a period of up to ten days has been observed at the SGF).

8.4.5. Discussion

One distinct negative of the laser, for this user, is the lack of repair facility in the European community, sending the laser back to the US for any repair is a time consuming and costly enterprise. Also, since lasers of the type used in the FG5 are susceptible to misalignment from vibration shock, it is common for a laser which has been returned from the U.S.A. to have a low power output. Requiring alignment adjustments to return it to full power.

It is considered that the placement of the resistor underneath the inspection windows and in close proximity to the two Brewster windows is undesirable, due to the contamination and associated cleaning required. Improvement could be attained by either the simple movement of the resistor, or encapsulating it in a material which does not cause particulate contamination due to heat/age.

8.4.6. Conclusions

The FG5 is a highly accurate and sensitive instrument which required regular maintenance to keep in fully operational condition. Since the return of any component or the entire instrument to the American manufacturer is expensive comprehensive knowledge has been acquired during the ten years of operating the FG5 at the SGF. It is hoped some of the knowledge contained within this chapter may be useful to inexperienced users required to maintain the instrument.

Chapter 9

Software

9.1. Introduction

The ‘g’ software, introduced in Chapter 2, provides control of the instrument, data collection and analysis of collected data. The values of gravity provided by the FG5 are derived from the observations, and are processed, and stored, in real time, or can be obtained by reprocessing the stored data. Reprocessing of the stored observation data is common and can be done to modify numerous processing parameters which have been used in the original data collection, for example; polar rotation values, latitude and longitude and the gravity gradient. Reprocessing of the data can be performed using the ‘g’ software or the ‘gap’ processing software. ‘g’ has been introduced in Chapter 2 and is a product of Micro-g LaCoste. ’gap’ was written by Dr Simon Williams of the National Oceanographic Centre (NOC) Liverpool.

The objective of this chapter is to give an overview of the two software packages, including the perceived advantages and disadvantages of both, to provide a basis for the analysis programs written by the author for the work described in this thesis. The rationale and objectives of each program are discussed.

Terminologies commonly used within this chapter are: drop data, hourly drop data, sets and projects. Drop data contains the raw information obtained from each individual drop of the mass i.e. approximately 700 time and distance position pairs, t_i and x_i. Hourly drop data is a combination of all the drop sets collected during an hour, the start of which is defined by the time of the first drop. Sets are comprised of a number of drops and are usually, although not restricted to be, hourly data. Projects are comprised of a single, or a group, of sets.

9.2. Reprocessing Data Using ‘g’ and ‘gap’

The reprocessing of any data is often done to correct certain parameters used in the original data collection. The software packages by Micro-g LaCoste and Dr Williams have both proved useful due advantages of one over in particular scenarios.

When storing data from the data collection phase ‘g’ generates files labelled with the name of the project, chosen when the gravimeter is set up, with three principle file extensions.

- Binary format files - the ‘gsf’ files. Contain the individual drop information for each drop within a set of data, one ‘gsf’ file is generated for each set within a project
- A text file - the project file. Contains setup information, such as the ocean-loading parameters used, the number of drops per set, the setup height of the instrument and the overall project results, which include the gravity over the project with associated error and uncertainties. An example project file is included in Appendix 3,
- A text file - the set file. Contains information for each set recorded during a project, including the time, gravity measurement for the set, the standard deviation and standard error, the earth tide, the ocean tide, the barometer reading. An example set file is also included in Appendix 3.

The ‘gsf’ files are used for any reprocessing required, as they contain the raw drop information; if the project is reprocessed with ‘g’ the text files are overwritten, or can be saved using a different filename. The file data can also be exported in an ASCII* format, though this is not done automatically done.

* ASCII - American Standard Code of Information Interchange

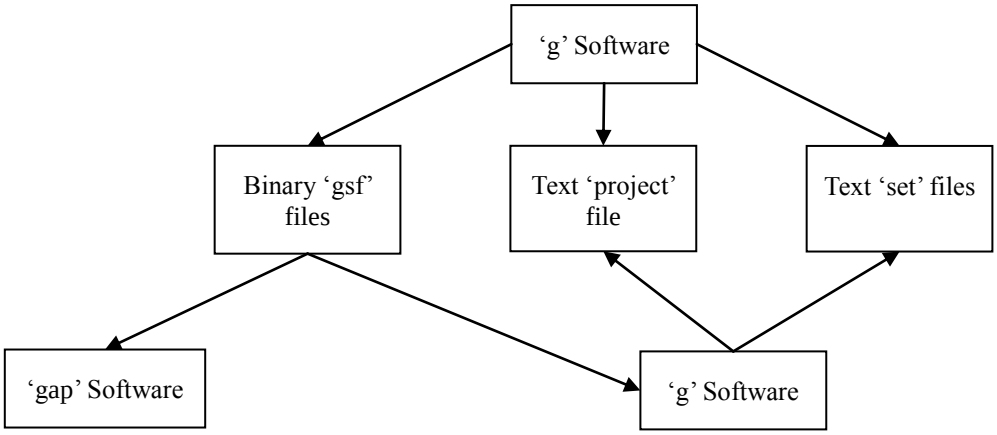

Figure 9.1 The process of the data collection and reprocessing. The output files from 'gap' are shown in Figure 9.2.

9.2.1. An Assessment of 'g'

'g' is a user friendly, graphical user interface, Windows based and encapsulated software package with help functions and a manual which is available from Micro-g LaCoste. The software allows the user great flexibility to view a range of different graphical outputs, adjust a variety of parameters and view the data in real time or whilst being reprocessed at higher speed than the data is collected. Only parameters used for data acquisition are removed from user intervention when a project is reloaded for post-processing or viewing. The key parameters which are discussed in the scope of this work are: the polar motion, tidal correction and fringe window. The fringe window is the number of fringes which are counted in the measurement of the drop; fringes occur throughout the dropping process, but those at the start and end are discounted since the object is not in free-fall. The polar motion values entered into the software pre-data acquisition are predicted values, reprocessing is required to take advantage of the real, measured values when they become available from space geodesy analysis centres. The tidal correction consists of both the earth tide correction and the ocean-loading correction, the latter of which is discussed further in Chapter 12. 'g' provides two choices for tidal corrections, Berger or ETGTAB. Only ETGTAB has been used at the SGF and therefore the Berger model will not be discussed further. ETGTAB uses the earth tide model by Yoshiaki Tamura and offers five options for ocean-loading; Schwiderski, FES2004, CSR3.0, none or a user defined file.

One perceived weakness of ‘g’ is the usage of computer memory and memory allocation, which causes the program to fail after several projects are reprocessed. ‘g has an inability to reprocesses more than one file at a time and reprocessing more than one project can be labourious since each file must be loaded, selected parameters changed, and then reprocessed.

9.2.2. An Assessment of ‘gap’

The ‘gap’ software is command line based software written in the C programming language. It allows great flexibility in accessing results and performing corrections, if the user knows how. There is no manual available for ‘gap’ so the user is dependent on Dr Williams for the initial instruction of how to use it.

Due to the fact that ‘gap’ can reprocess multiple projects of data with one command (the entire ten years of gravity data from the SGF for instance) the user must supply ‘gap’ with an input logbook file, which must contain an expected layout of information which includes the project information; name, year, day of year (all of which are contained in the project name), as well as additional information including whether or not the user wants the file to be processed and the fringe voltage. Additional processing files which are required to be filled in include information on instruments, such as gravimeter serial number, year of manufacture or change (service or upgrade), and the number of fringes used during data collection and measurement location; name of pier, address, latitude and longitude, elevation, gravity gradient and nominal acceleration due to gravity on the pier. Extra input files are required for the pre-processing and post processing of data. The pre-processing file for the SGF includes only laser peak information, as ‘gap’ must be manually instructed where the peak ‘jumps’ away from E peak (laser peak transitions are previously discussed in Chapter 2).

The ‘gap’ software is not as intuitive to the user as ‘g’, since it was written for specific use rather than a generic wrap around for operation of the FG5. However it supplies the user

with a greater ability to interrogate the data without the need to specifically command the generation of output files for each project.

Table 9.1 . Example of the first eight columns in the 'gap' logbook file

Project Name	Year	Day of Year	Data flag	Data processing flag	Pier Name	FG5 Serial Number	A to D card Information	Maximum Fringe Value (mV)
herg1680.06	2006	168	y	y	herg	FG5-229	ad9696	320
herg1690.06	2006	169	n	n	herg	FG5-229	ad9696	350
herg0440.08	2008	044	y	y	herg	FG5-229	ad9696	290
herg0770.12	2012	077	y	y	herg	FG5-229	ad9696	400

The main output file gives the project measurement values calculated by ‘gap’. The file is located in a products/sitename directory and contents include; the date, in year fraction and MJD*, gravity value (in ms^{-2}) and the standard deviation, the gravity value and the total number of drops used in the measurement. Other output files, which are of the most interest in this work, are located with the processed data, as indicated in Figure 9.2, include the ‘gtmp’ file and ‘etmp’ file. The two files contain the environmental and gravity factors which go into generating a value for g, a total of 19 variables for each drop.

Another bonus to batch reprocessing is that ‘gap’ can be instructed to retrieve polar motion values automatically so that the data is quickly processed with more accurate information. The IERS† Earth orientation parameters finals‡ data is used, and the data matched to the epoch of the gravity project files.

A bonus of batch reprocessing, especially at a near coastal location, is the ability to quickly process the data using different ocean loading models, in work shown later in Chapter 12 a selection of data is reprocessed using four ocean loading models.

* Modified Julian Date

† International Earth Rotation and Reference Systems Service

‡ The EOP file can be found at https://www.iers.org/IERS/EN/DataProducts/EarthOrientationData/eop.html

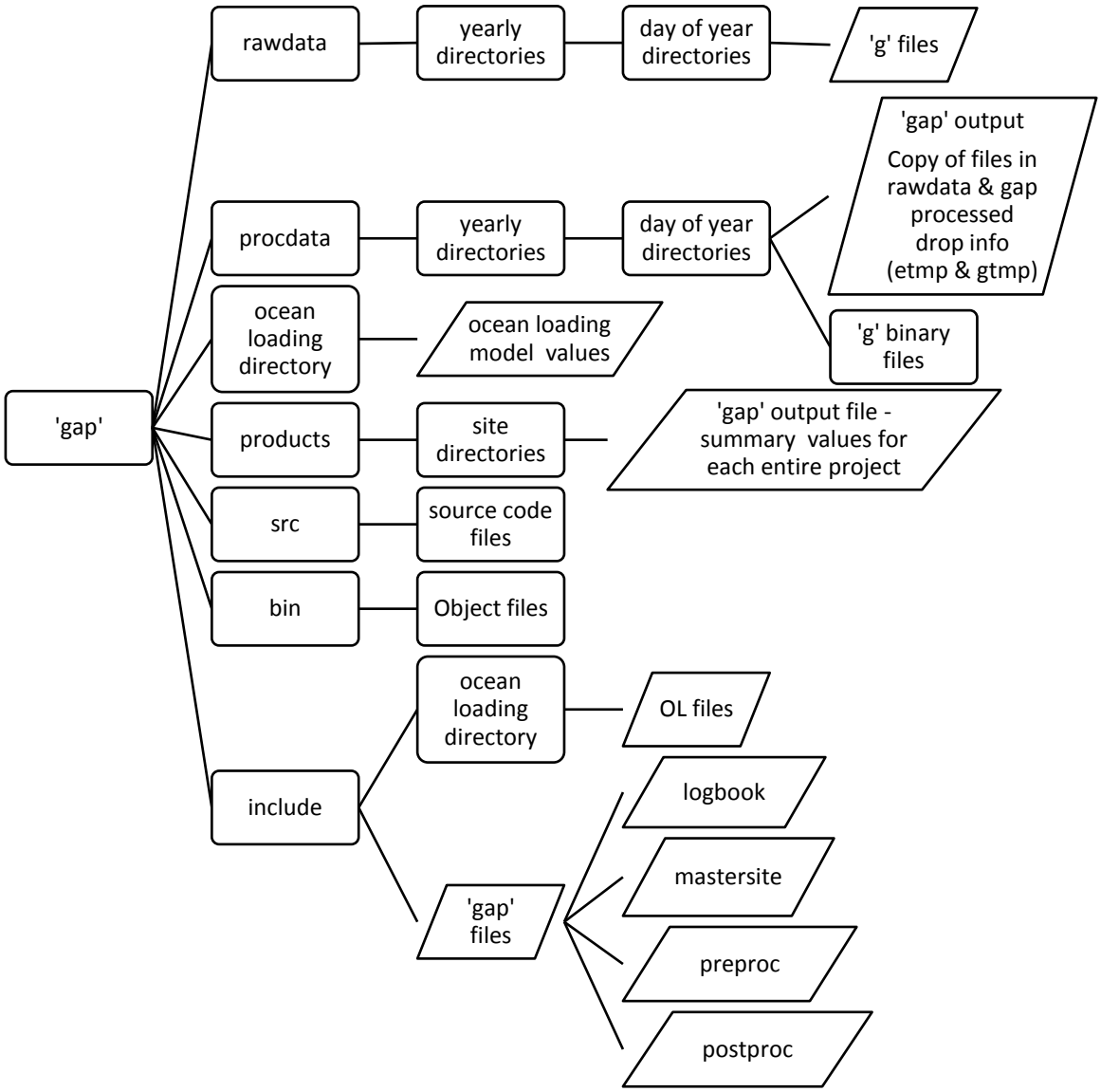

Figure 9.2 Basic file structure used by the 'gap' software

9.2.3. Summary

Both ‘g’ and ‘gap’ have associated advantages and disadvantages. The user friendliness of ‘g’, the graphical interface and range of sensor values available to view at the touch of a button are all desirable attributes. However, the necessity to manually ask for a raw output dump to obtain access to the drop data in an easy format, which might fail on older computers due to computer memory usage, is not appealing. The beauty of ‘gap’ is the knowledge the reprocessing of a large group of projects would take minutes with any

changes made to the processing parameters implemented in one swift stroke, rather than the individual reprocessing required in ‘g’. The downside is the manual interface, necessity for the input files and analysis and reprocessing of files containing laser-peak jumps and the fact no hourly information is generated. The processing by ‘gap’ is also reliant on the file format supplied in the files created by ‘g’. Format changes between ‘g7’, ‘g8’ and ‘g9’ have meant that ‘gap’ has required modification to operate on files generated by these variants of ‘g’. Unfortunately since the change to ‘g9’ the ‘gap’ software has not yet been modified, and is written in a language the author has been unable to successfully alter, some work in this thesis has only been processed using ‘g’.

9.3. Programs Created During this Work

The programs written in the course of this work have been done so primarily due to the use of the two software packages and the early decision to concentrate on using the gravity results as processed by ‘gap’. This decision meant that the primary objectives for the creation of new programs became:

- To generate hourly data from the raw drop information provided by ‘gap’
    - To provide an alternative inter-daily analysis than ‘g’, to enable comparison with:
        - Tide gauge data
        - Met Office wind speed data
        - Comparison with hourly data from ‘g’
        - Inter-daily periodic signal analysis
- To analyse the project data, from ‘g’ and ‘gap’, for construction of a time line of data, to be used for enabling comparison and analysis with:
    - The SGF borehole ground water depths
    - The temporal changes in the height component of the SLR coordinate positions
    - Investigation of any long period signals

All programs by the author were written using the Python programming language, and will be hitherto referred to as the VgHx processing software. An overview of the program and data structure is shown in Figure 9.3.

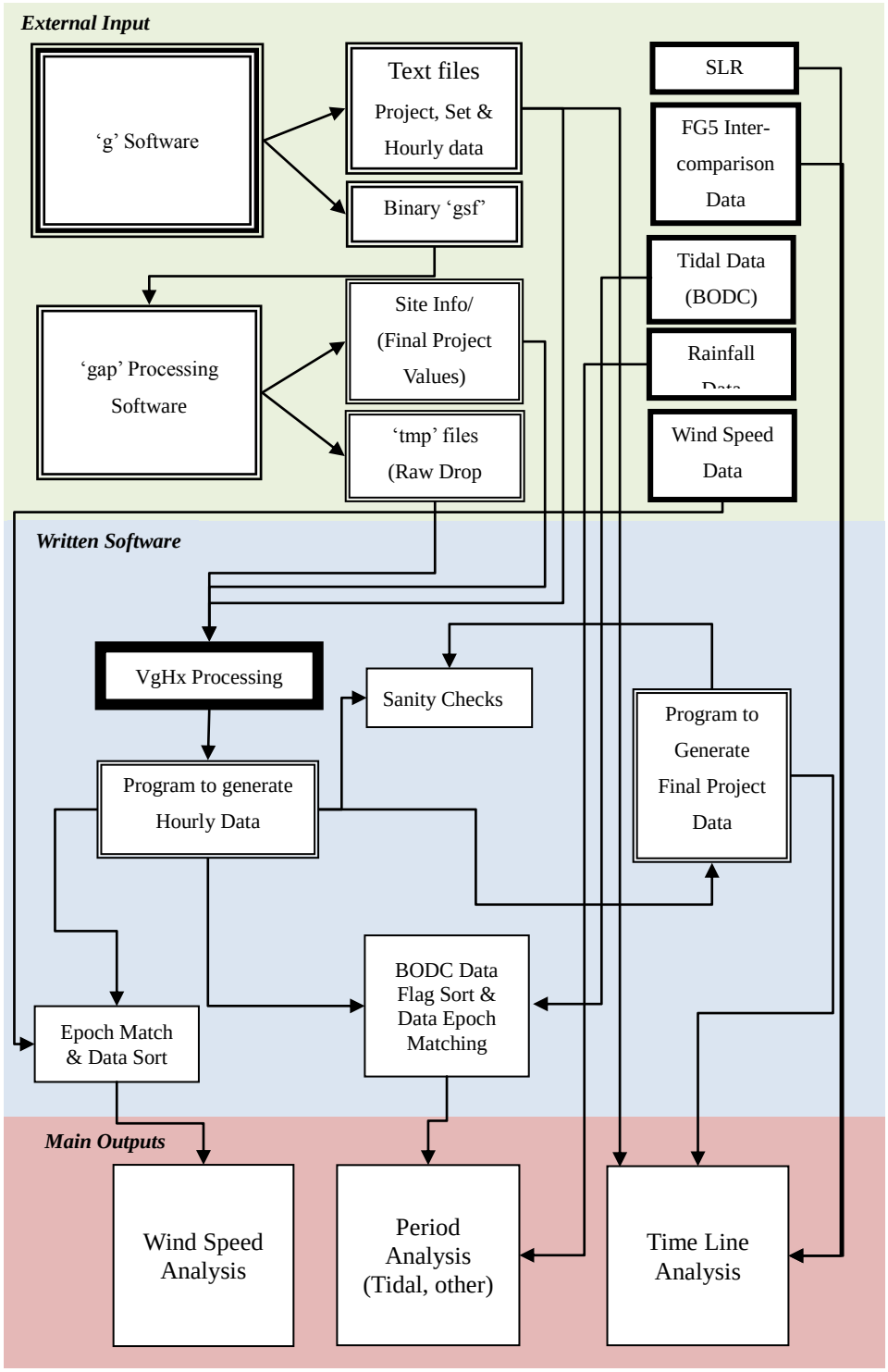

Figure 9.3 The overall structure of the software used in this work, including 'g' and 'gap'.

9.3.1. Hourly Data

The 'etmp' and 'gtmp' files generated by 'gap' contain the individual drop data required to perform investigation of the data. The 'gtmp' files contain the uncorrected gravity measurement and components which comprise full information for each drop:

$$gtmp = s_0, d_0, MJD, 1, g_0, v_0, z_0, \delta g_0, \delta v_0, \delta z_0, pr, tt, pm, rz, cr$$

Where: $s_0$is the set number, $d_0$is the drop number, MJD is the modified Julian date, 1 is a constant, $g_0 v_0$ and z_0 are the acceleration, velocity and position, at the start of the drop and $\delta g_0, \delta v_0, \delta z_0$ are the associated measurement errors for each. pr is the barometric pressure, tt is the total tide (solid earth tide and tidal ocean-loading), pm is the polar motion, rz is the height correction* and cr is the comparator response†. The units for each of the components of 'gtmp' are metres per second squared, with the exception of s_0 & d_0 which are integer numbers, MJD and the constant 1.

The 'etmp' files contain the sensor information collected by the FG5 for each drop:

$$etmp = set, drop, time, temperature, super - spring, \\ ion\ pump\ voltage, laser\ voltage, pressure$$

9.3.2. Obtaining the Gravity Result

The corrected gravity for each drop is obtained by using an equation to recombine the variable gravity component factors using the 'gtmp' file. The 'gtmp' file contains the information to reconstruct the gravity measurement from the using the least squares fit of the gravitational acceleration equation, quoted in Chapter 2:

* rz is the difference between the actual height of the instrument (factory instrument height plus setup heights) and the measurement height, in this case 1.3m above the floor.

† The comparator converts the signal from the photodiode in the interferometer into digital pulses which are counted and timed in the electronics rack (Niebauer, 1995).

$$x_i = x_0 + v_0\tilde{t}_i^2 + \frac{g_0\tilde{t}_i^2}{2} + \frac{\gamma x_0\tilde{t}_i^2}{2} + \frac{\gamma v_0\tilde{t}_i^3}{6} + \frac{\gamma g_0\tilde{t}_i^4}{24} \qquad \text{Where:} \quad \tilde{t} = t_i - \frac{(x_i - x_0)}{c}$$

$$x_i, t_i, i = 1, \ldots\ldots, 700$$

x_0, v_0, g_0 are the initial position, velocity and acceleration at t = 0. γ is the vertical gravity gradient (since we do not know the gravity gradient at the SGF 3.086 µGal/cm is used) and c is the speed of light.

The second method uses the recombination of corrections to obtain the values, in this case g can be determined by correcting the uncorrected gravity (g_0) by removing the effects of Earth tides, polar motion, comparator response and by reducing to standard atmospheric pressure and reference height. However, the equation which should be used in this case was unknown by the author and was, therefore, determined using a best fit principle; where the final derived result for both set and project value gave the least variance from the results obtained using 'g', and also compared to the project value determined by 'gap'.

The combination of correction terms which gave the least variance was found to be:

$$g = g_0 - pr - tt - pm - rz - cr$$

The final hourly value of gravity determined in 'g'* is obtained by from a iterated mean of the drop values, with a three sigma rejection criteria applied (van Westrum, 2012), therefore the same has been used in the VgHx program.

To validate the results from VgHx, the hourly values were tested against results produced by 'g', for individual days and were plotted for comparison using a year of data. The results for 2011 are shown in Figure 9.4. Some variance between the two sets of data is expected due to different parameters used, such as tidal correction and polar motion values, in the processing by 'g' and 'gap'.

* This is the default rejection criteria within 'g'.

9.3.2.1. Time Convention and Conversion

The time stamp convention used in ‘g’, in both the project text file and the set text file, is to output the year, day of year and time of day in separate columns or rows, with the hours, minutes and seconds of the day separated by colons. The time of day given in both the project and set files is the median of the set times and the median of the drop times respectively. Time stamping in ‘gap’ is given as a modified Julian date. The VgHx programs convert both the ‘g’ and ‘gap’ timestamps either to a year with fraction of year or day of year for ease of use. Since the time stamp is important for data consistency and comparison with other sources of data careful attention was paid to the conversion and consistency checks between format changes.

9.3.2.2. The VxHg Hourly Results

The program was produced to enable processing on a yearly basis. To process the data for a year it must first find the folders contained within the relevant directory (procdata/year/) then process the individual drop results for each project in turn. When it has completed the project it stores the output in a common directory which is used for all the VxHg results, using a similar file structure to the data origin. To check the results the hourly data from VxHg was compared to the hourly data from the set text file, generated by ‘g’. Figures 9.4 and 9.5 show comparisons of the outputs, the first is an example of a comparison of one single project, in this case 25 hours, and the second an example of an entire year plotted together. Examples for each year are shown in Appendix 4.

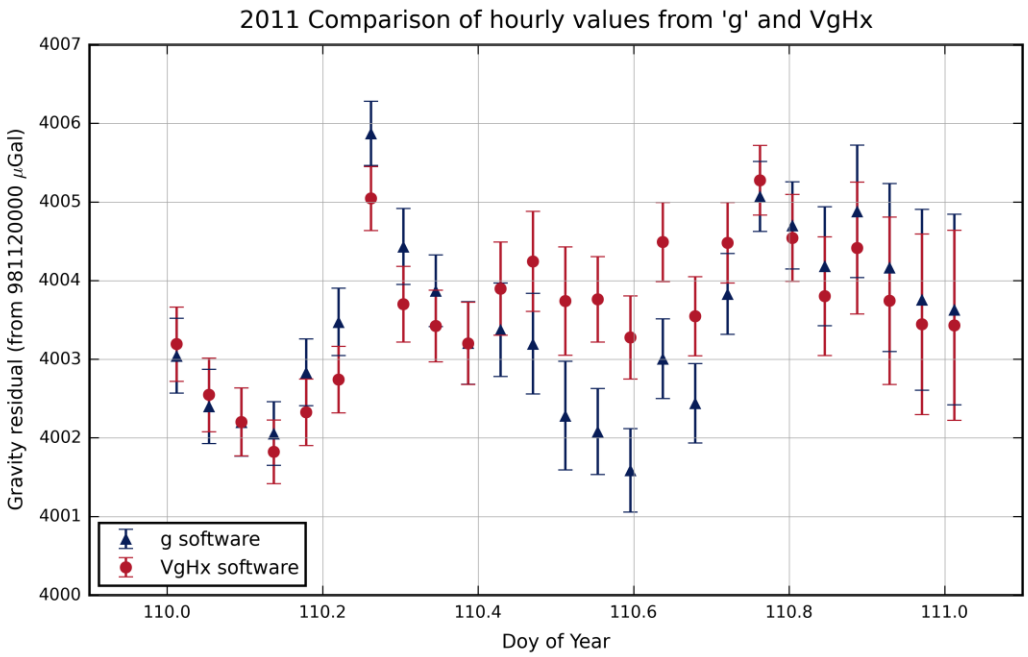

Figure 9.4 Hourly data obtained using 'g' and the VgHx software. The two are plotted together to show validity of the VgHx result. Signals seen within the data are discussed further in Chapter 12.

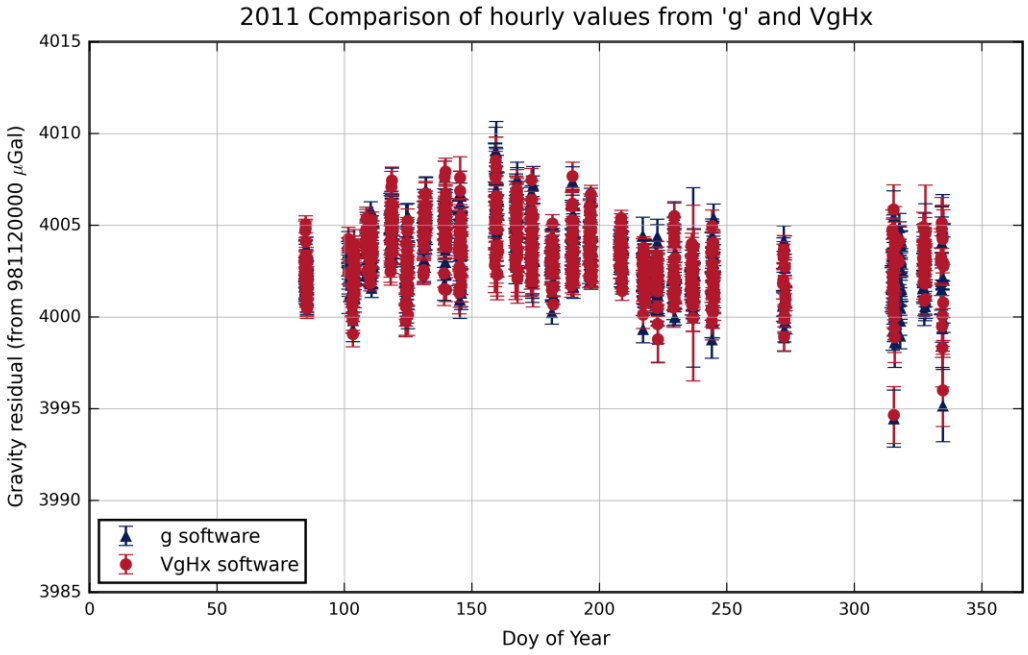

Figure 9.5 A comparison of the hourly output from 'g' and VgHx software over the period of a year.

The results of the plot show that the derivation of hourly values by the VgHx software works well with values and standard errors of the measurements in good agreement.

Minimal differences are seen for the majority of hours although a difference of up to 2 µGal can be seen.

9.3.2.3. Project Data

The project gravity and associated errors are also derived using the same equations as 'g'. The final determination of the gravity value is found using a weighted mean where:

$$\bar{g} = \frac{\sum_{i=1}^{n} \frac{g_i}{\sigma_i^2}}{\sum_{i=1}^{n} \frac{1}{\sigma^2}} \quad and \;\; \sigma = \sqrt{\sum_{i=1}^{n} \frac{(g_i - \bar{g})^2}{n-1}}$$

Validity checks on the final project results were performed on a selection of projects, to show not only that the project values are in line with those obtained from the two established programs but also as a final check that the hourly results are reasonable. An example of the comparison of the final gravity value with the standard deviation and standard error is shown in Table 9.2. The results in Table 9.2 and Figure 9.4 originate from the same data.

Table 9.2 Project Gravity from 'g', 'gap' and VgHx, for day 2011 (DOY 110)

Processing	Gravity	Standard Deviation	Standard Error $\left(\frac{Std\ Dev}{\sqrt{no\ of\ drops\ per\ set}}\right)$
'g'	981124003.37	1.14	0.23
VgHx	981124003.51	0.84	0.17
'gap'	981124003.59	1.02	

9.3.2.4. Critical Analysis of VgHx Processing Software

Although the results shown in the previous sections show that the VgHx processing works well to generate the hourly and project values it is not yet a complete package as it is not perfect. Known problems include the fact that it does not take laser peak jumps into account

and correct for them. While peak jumps do not affect the vast majority of data at the SGF they have occasionally occurred and therefore require correction in the hourly results. To correct this problem the software should check the ‘gap’ ‘preproc’ file, in which peak jumps must be included for correct processing using ‘gap’, and correct affected drop data accordingly.

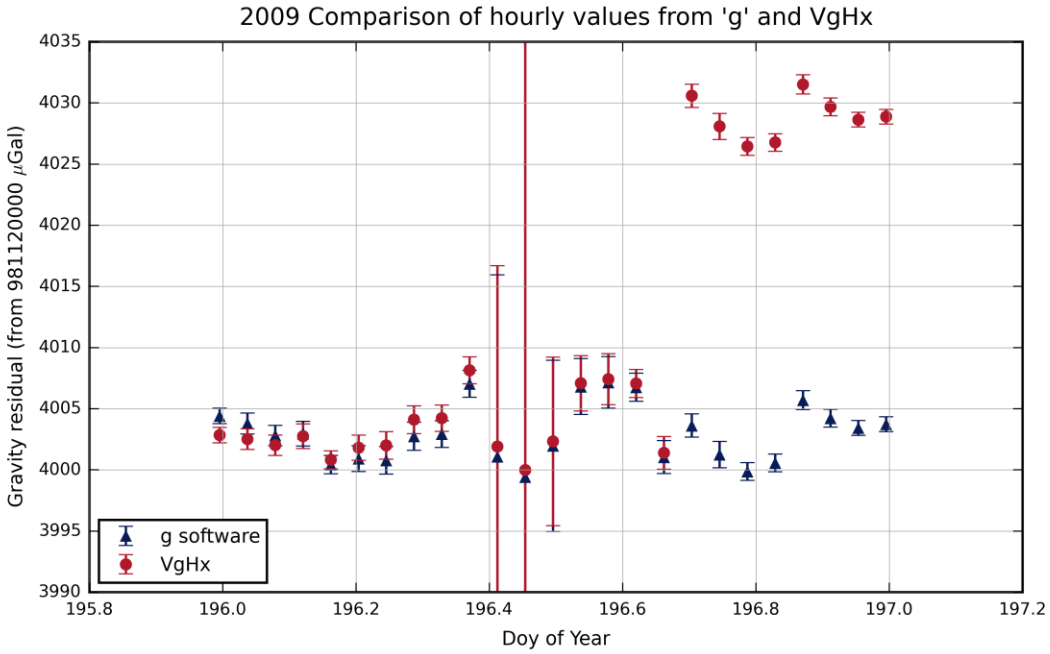

Figure 9.6 Hourly data from ‘g’ and VgHx: uncorrected peak jumps with the VgHx results

Additional problems can be clearly seen when the data is collected with an incorrect timestamp. Figure 9.6. shows a slice of time in 2010 where five projects have been successfully processed but the results from one project are clearly incorrect. The problem with this project is suspected to be the fact the computer which ran ‘g’ was found to be have been set to British Summer Time instead of UTC, which would result in incorrect application of polar motion and tidal corrections.

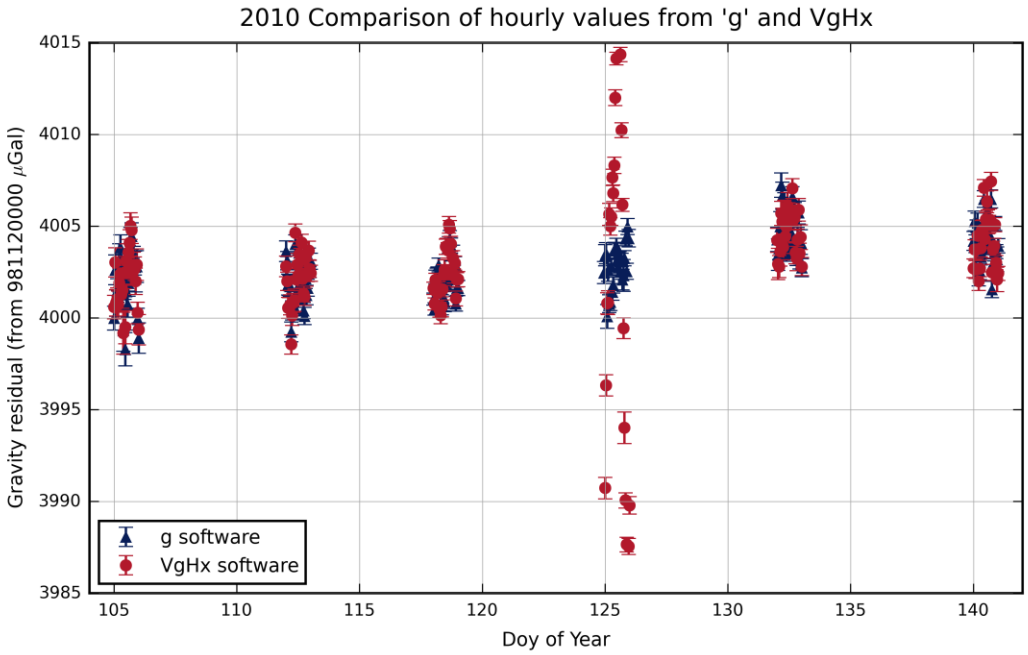

Figure 9.7 An example of problems with the VgHx data processing.

9.3.3. Tide Gauge Data Extraction

Tide gauge data extracted from the British Oceanography Data Centre (BODC) was processed using additional VgHx software. Since the BODC tide gauge data is in ASCII format with quality control flags on each data line. The flags are listed in a separate column and used to represent four values:

- \- (blank in the flag column) means the given value is good
- M - means the value is improbable
- N - means a null value
- T - means the value is interpolated

The software was used to separate the data by each flag, storing a file for each. Only the data with no associated flag (which contained a blank in the flag column) was used to later marry the data with the epochs of gravity data. The results are given in later Chapters.

9.4. Conclusions

Both software packages proved useful for reprocessing the software, both have advantages and disadvantages. The advantages and disadvantages of each include:

Table 9.3 An assessment of the existing reprocessing software, 'g' and 'gap'

'g'		'gap'	
Advantages	Disadvantages	Advantages	Disadvantages
Graphical displays	Lack of ability to batch reprocess	Ability to do fast reprocessing of multiple projects	Number of input files required
Automatic laser peak detection/correction	Limited available tidal model selection	Tidal model selections	Difficult to use for uninitiated
Ease of use		Automatic polar rotation	Lack of hourly values
			Is dependent on 'gsf' file structure, needs adjustment for changes

The VgHx software written for hourly and project gravity determination:

- Works well for hourly values and project values
- Has good agreement with 'g', differences between the two are usually sub micro-Gal but can be up to 2 µGal.
- VgHx (and gap) are dependent on epochs being correctly supplied by 'g'
- Laser peak jumps need to be tested for and corrected
- Is used in later chapters to examine periodic functions within the daily data

Chapter 10

Measurement Precision at Herstmonceux

10.1. Introduction

The super-spring of the gravimeter is sensitive to natural and anthropogenic noise sources as it essentially acts as a seismometer within the FG5. As a result the precision of the gravimetry measurements at Herstmonceux are highly variable and tend to be seasonally dependant, with spring/summer months giving the most precise data. Low precision data is liable to swamp residual signals in the gravity data which are the principle cause for the gravimetry work in the first place. The data clearly shows where the highest precision data is more valuable. This chapter discusses the author's interpretation of the driving factors in the variation in precision at the SGF, Herstmonceux.

10.2. Investigation of Natural Noise Sources

Very early in the data collection it became clear that a statistical correlation between the precision of the gravity measurements and the local wind speed was likely, with the standard deviation of each hourly data set, as determined by 'g', varying between 5 μGal - 35 μGal. To determine if a correlation was present the precision of the gravity data was compared to local wind speed, obtained from a UK Meteorological Office station situated three kilometres to the North East of the SGF.

Six months of data was analysed. The standard deviation of set values, containing between 100 to 200 drops per set, were taken to three decimal places whilst the wind speed data, obtained from the Met Office, was given in units of knots and converted into SI units for consistency, using a standard conversion factor of 0.514444. The times of the two data sets

were married to the nearest minute and standard errors were calculated for the precision of the gravity measurements, giving a precision and wind speed increment pair. This work was presented at the IAG* commission 2: Gravity field conference held in Greece in 2008 (Appleby, 2010) .

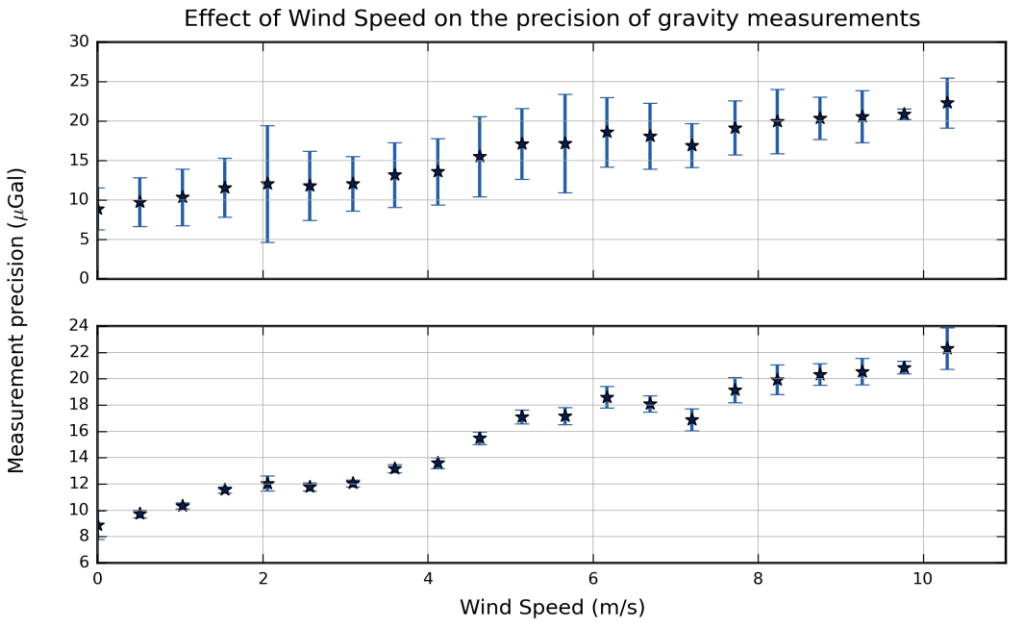

Figure 10.1 The precision of the gravity measurements plotted against local wind speed. The top graph is shown with error bars in standard deviation; the lower shows the standard error of the gravity measurements.

It can be seen in Figure 10.1 that there is some degree of correlation between local wind speed and precision. The mechanism for the interaction is theorised to be due to several factors; vibration transmitted through tree roots due to wind interaction with tree branches, and also, since the SGF is in close proximity to the English Channel, sea state.

The correlation, of wind speed with decreased precision of gravimetry measurements, is further shown in Figure 10.2. Which shows the hourly, or set, precision obtained from varying directions and wind speeds. It shows that the predominate wind direction at the SGF is from the Southwest (215°) and the correlation shown in Figure 10.1 is generally true with a hint that there may be a greater impact on the precision when the wind comes from the North to North-northeast, around 10-22°.

* International Association of Geodesy

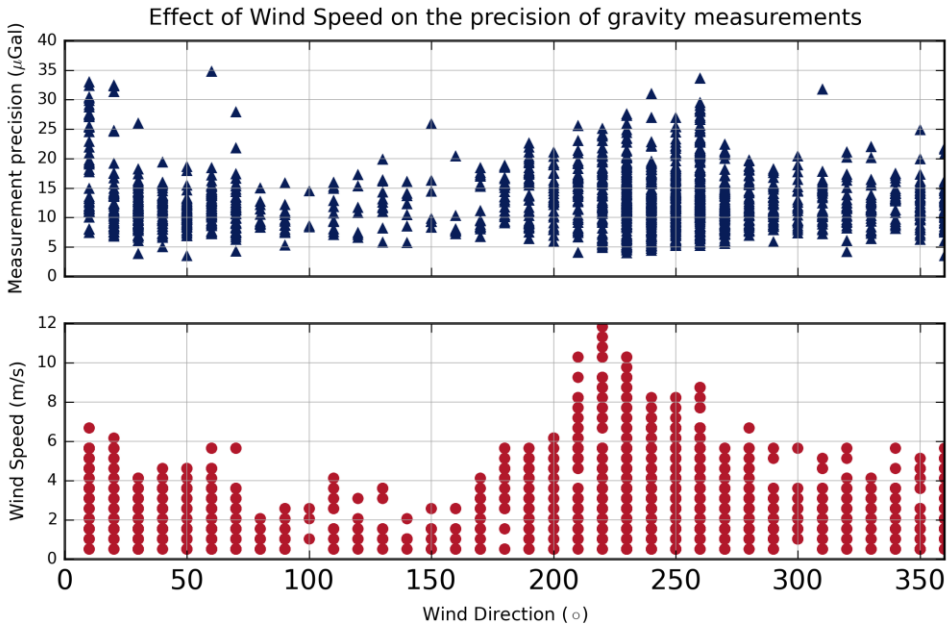

Figure 10.2 Precision of gravity measurements plotted with local wind speed. North = 0°.

Following this early investigation the operation schedule for the FG5 was altered in an effort to reduce the noise seen in the measurements. The operational day was determined by Met Office weather predictions; if no suitable day was obvious the gravimeter was run for one day of measurements regardless of predictions.

Fast moving weather systems also impact the gravity data. The plot shown in Figure 10.3 represents one example of a low pressure weather front which passed directly overhead of the SGF in 2009. The plot indicates an decrease in the precision of gravimetry measurements as the system passes overhead, in the first half of day 98.

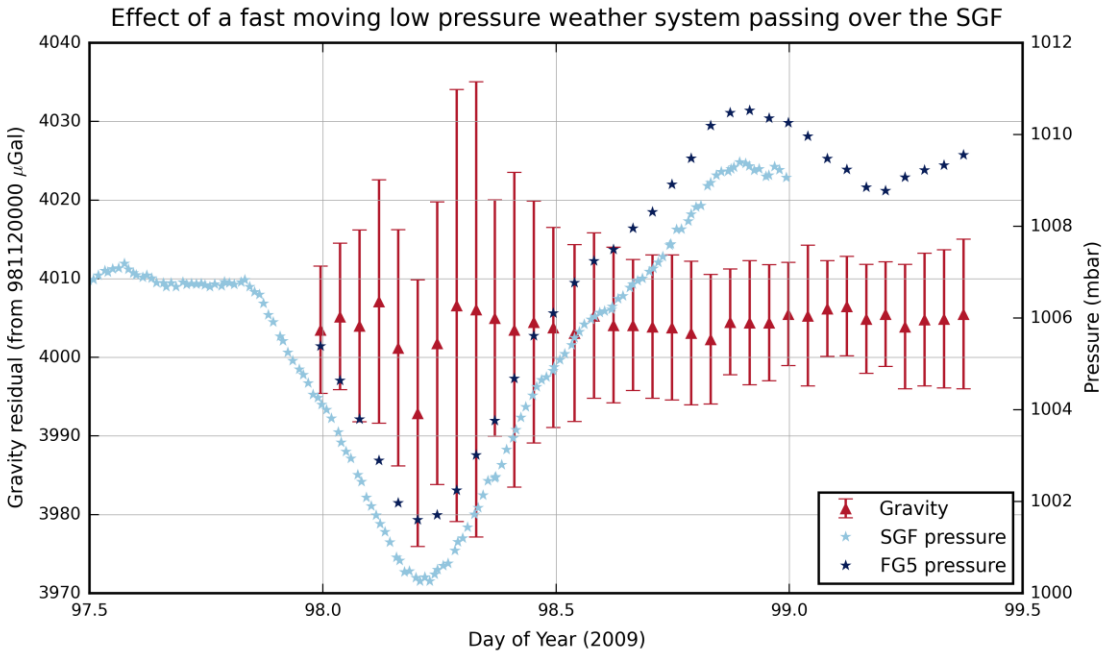

Figure 10.3 The impact of a rapidly moving low pressure system on the gravity measurements. The gravity measurements are plotted against the SGF pressure sensor record and the FG5's internal barometer readings. The offset between the two pressure readings is due to the difference in height between the sensors.

Satellite images showing the passage of the weather front are shown in Figure 10.4. The images were obtained from the NERC Earth Observation Data Acquisition and Analysis Service (NEODASS) .

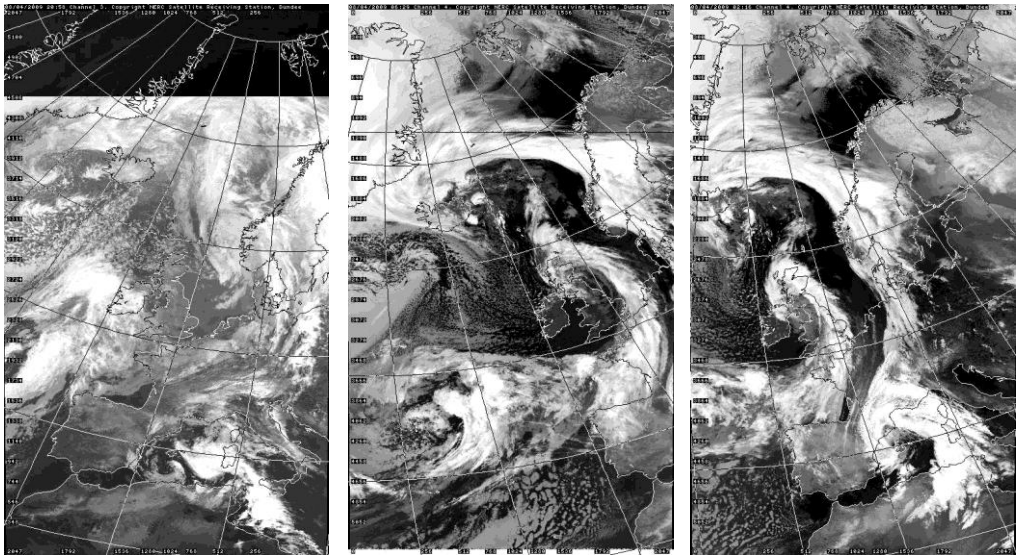

Figure 10.4 A rapidly moving weather front passes overhead at the SGF. The images shown are separated by a four hour interval. Images courtesy of the NERC Earth Observation Data Acquisition and Analysis Service (NEODASS) and the University of Dundee

Following the initial wind speed investigation in 2007 it became evident that local wind speed was not the only cause of decreased precision in the gravity measurements. It was occasionally observed that the precision of the gravity measurements could be poor, and below the average for the period, on perfectly still days at the SGF, with no breeze.

It was seen that storms in the North Sea and North Atlantic had a large impact the gravity data. It was determined that the sea state, both locally and around the UK, was the cause of some of the loss of precision. To support this theory shipping forecast data containing sea state information was recorded for a year. However although a link was made it has not been investigated in this work.

Since the SGF is close to the English Channel and the UK is an island close to the Gulf Stream ocean current it is perhaps unsurprising that there might be more vibrations in the winter months. The variation in the gravimeter precision is shown in Figures 10.6 and 10.7, where the precision is the standard error in the hourly gravity measurements. Both plots show a general improvement in the precision from around the 80th day of the year, around the spring equinox.

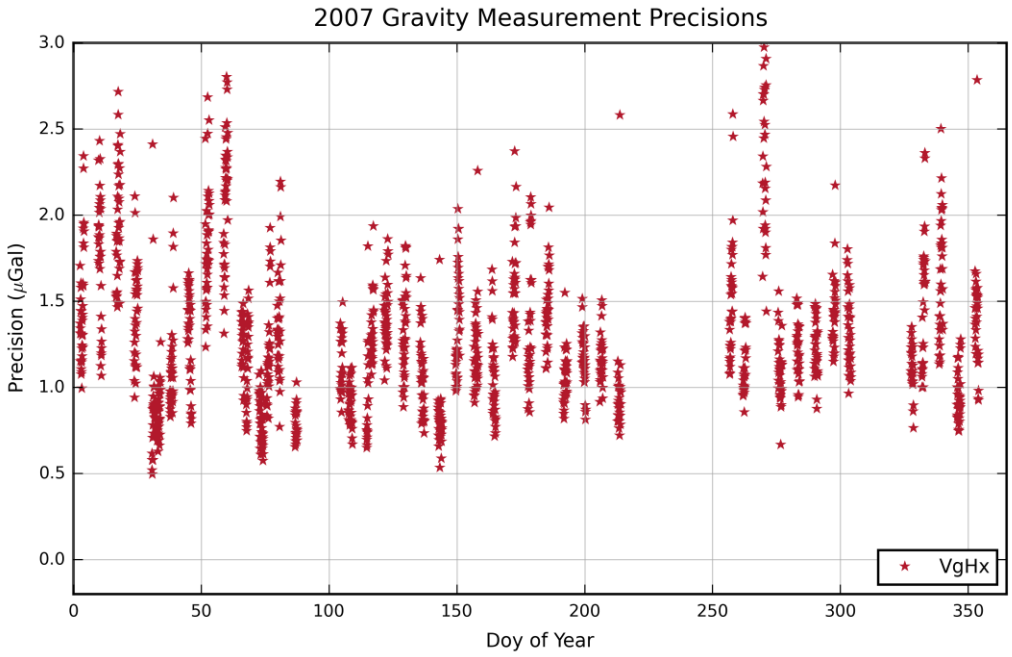

Figure 10.5 The standard error of the hourly gravity measurements in 2007, processed with the VgHx hourly product software.

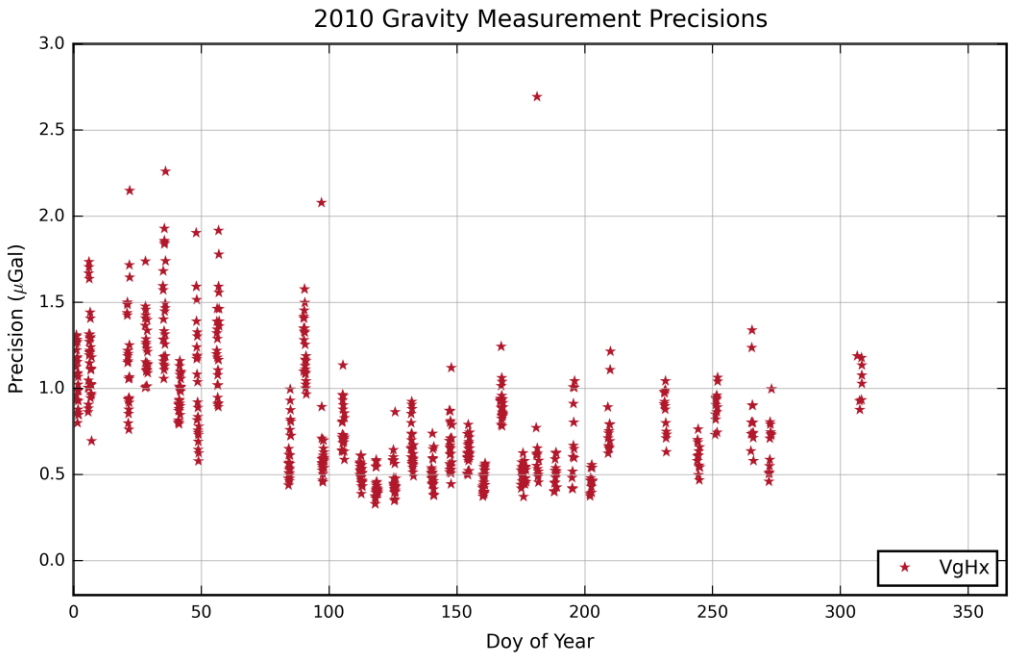

Figure 10.6 The standard error of the hourly gravity measurements in 2010 from VgHx software

From these plots it is clear that the FG5 is easily capable of sub-microgal precision which is seasonally affected and that the data in 2007 is of lower precision than that of 2010. Precision plots for each year are shown in Appendix 5. As mentioned in Chapter 2 the precision of the gravity measurement is reliant on the super-spring tuning as well as the environment. The average precision for each full year of operation is shown in Figure 10.7 and highlights the decreased precisions in the recent years.

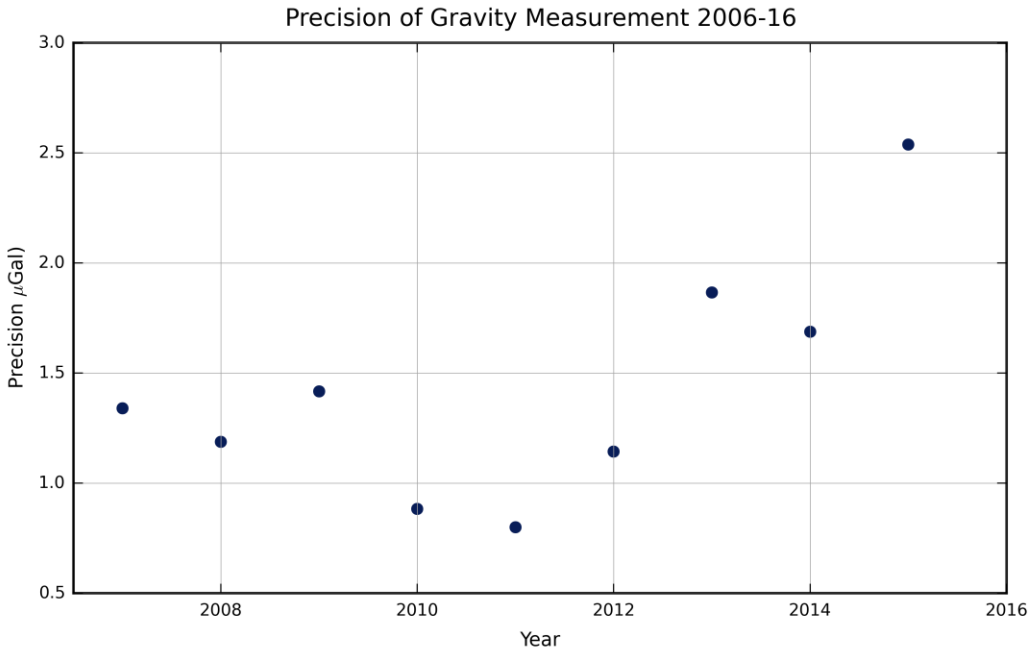

Figure 10.7 Yearly averages of measurement precisions from 2006-15.

Although tempting to associate this change with the FG5X upgrade it can be seen in Figure 10.8 that this is untrue. Although the precisions are generally worse the summer months show that there is nothing wrong with the instrument and it is still capable of sub-microgal precision.

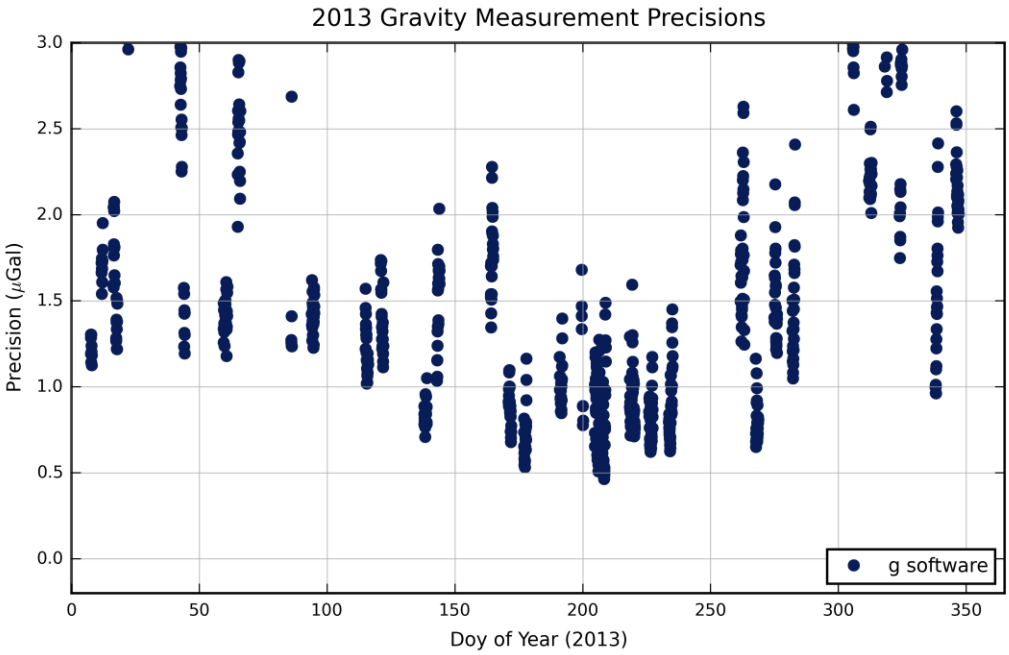

Figure 10.8 Precisions from the FG5X in 2013, showing a clear seasonal variation.

10.3. Earthquake Detection

Due to the behaviour of the super-spring, earthquakes show clearly in the gravity data. However, since the gravimeter is only taking measurements for around five hours a week the majority that are recorded by the BGS seismometer, situated in the North end of the SGF basement, are not seen in the gravity data.

An example of an earthquake being recorded by the gravimeter is shown in Figure 10.10. This earthquake was traced to have originated near the Kingdom of Tonga and was 7.9 on the Richter scale.

Figure 10.9 Earthquake location in 2009. The location of the SGF is marked by a red marker and the location of the Earthquake by a blue spot inside a blue circle Image obtained from the BGS Earthquake Location finder: http://www.bgs.ac.uk/schoolSeismology/schoolSeismology.cfc?method=selectQuake

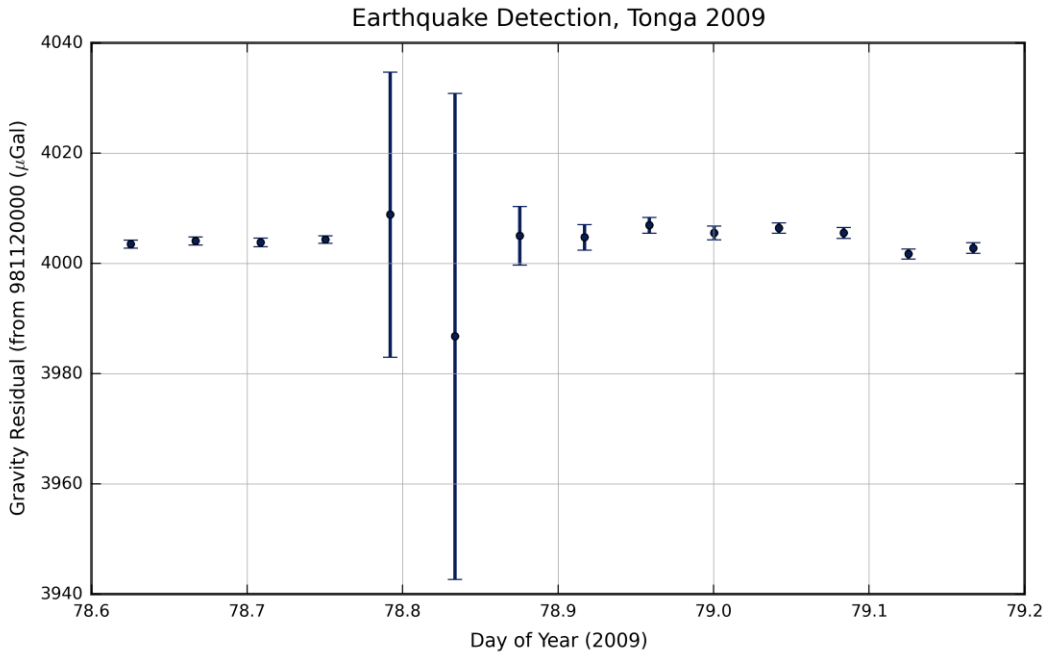

Figure 10.10 Detecting an earthquake in the gravity measurements.

10.4. Anthropogenic Noise Sources at the SGF

Due to the fact that the SGF is located within the grounds of Herstmonceux Castle and is remote from any major industrial units, motorways or cities the anthropogenic noise sources are limited to local road traffic and more unusual events. These rare disruptions have been traced to such things as:

- Clearance of the reed beds which are situated approximately 200 metres to the East of the SGF in a field in front of the castle.
- Concrete slab destruction and removal work taking place on the farm, approximately 200 m to the West of the SGF
- Drain clearance work to the drains within the castle estate using high pressure water.

10.5. Conclusions

The precision of the gravity measurements are seasonally driven and influenced by multiple natural sources. Sources of noise originate from wind, sea-state, earthquakes as well as the anticipated anthropogenic noise.

Chapter 11

Environmental Calculations

11.1. Introduction

Understanding the hydrological processes which affect a high accuracy, long time series gravity station can be a complicated process, as already shown in the relevant section of Chapter 6. Indeed, understanding the hydrological implications upon the time series of data from the gravimeter at the SGF has not proved straightforward. The complexity is largely driven by the fact that the SGF gravimetry laboratory is situated upon compacted clay and is located within a semi-sunken bunker with approximately one metre of soil above it. In addition to these local hydrological calculations the fact that the SGF is in close proximity to the English Channel adds another aspect to environmental influence on the gravimetry data. The subsurface soils play a large role in understanding the hydrological processes. The absorption and runoff rate of rainfall and precipitation is dictated by the topography of the area and the soil composition.

11.2. Subsurface Investigation by the Royal Greenwich Observatory

When the Royal Greenwich Observatory originally planned the move to Herstmonceux castle in the 1940's they carried out investigations into the geological formation by drilling a number of boreholes inside the grounds of the castle. The data from these boreholes were recorded in the archives, which are now held by the British Geological Survey and are accessable via their website through the Onshore Borehole Records, found at: http://www.bgs.ac.uk/data/boreholescans/home.html, or via the 'Geology of Britainviewer' http://www.bgs.ac.uk/discoveringGeology/geologyOfBritain/viewer.html by selecting the 'Borehole Scans' button. Figure 11.1 shows the results when the viewer is centred on the

SGF. Two particular boreholes are of interest; the first, taken in close proximity to what is now the SGF, drilled to a depth of approximately 15m, whilst the second, taken to a depth of approximately 40 m was located in front of Herstmonceux castle itself. Both borehole scans are instructive and are shown in Figures 11.2 and 11.3.

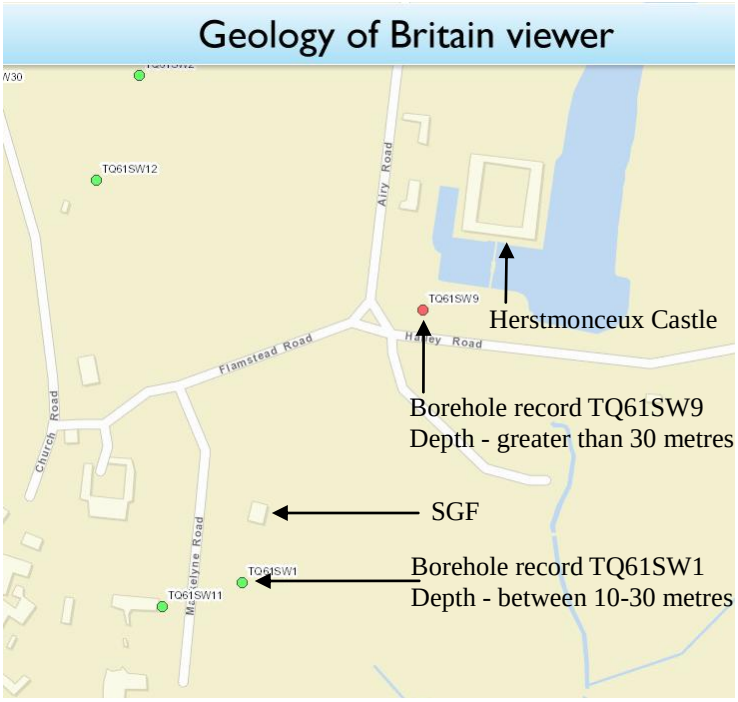

Figure 11.1 Screen shot of the boreholes around the SGF, taken by the RGO from 1940-60.

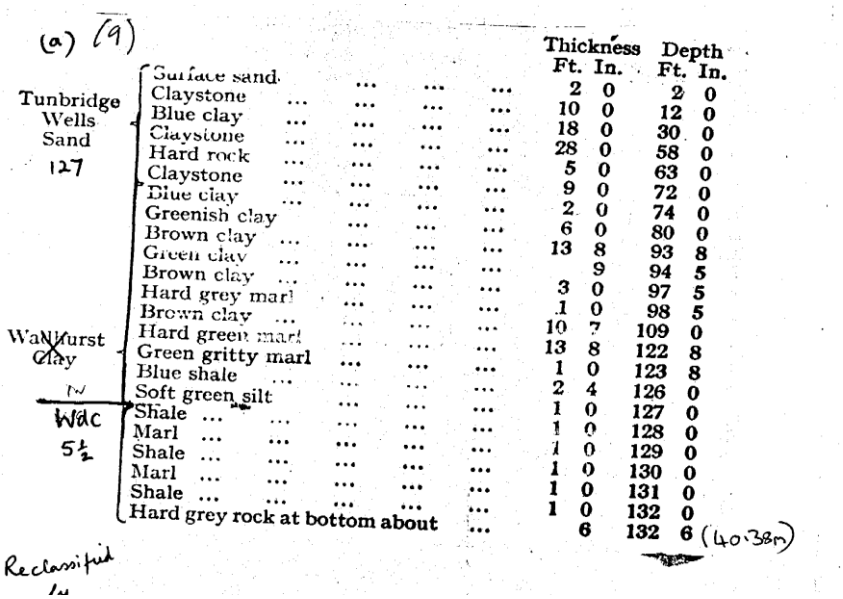

		Thickness Ft.	In.	Depth Ft.	In.
Tunbridge Wells Sand	Surface sand	2	0	2	0
	Claystone	10	0	12	0
	Blue clay	18	0	30	0
	Claystone	28	0	58	0
	Hard rock	5	0	63	0
	Claystone	9	0	72	0
	Blue clay	2	0	74	0
	Greenish clay	6	0	80	0
	Brown clay	13	8	93	8
	Green clay		9	94	5
	Brown clay	3	0	97	5
	Hard grey marl	1	0	98	5
	Brown clay	10	7	109	0
Wadhurst Clay	Hard green marl	13	8	122	8
	Green gritty marl	1	0	123	8
	Blue shale	2	4	126	0
	Soft green silt	1	0	127	0
Wac	Shale	1	0	128	0
	Marl	1	0	129	0
	Shale	1	0	130	0
	Marl	1	0	131	0
	Shale	1	0	132	0
	Hard grey rock at bottom about		6	132	6

Figure 11.2 Borehole record TQ61SW9 .In front of Herstmonceux castle. Both figures are taken from the BGS Onshore Borehole Records*.

* Contains British Geological Survey materials © NERC [2016]

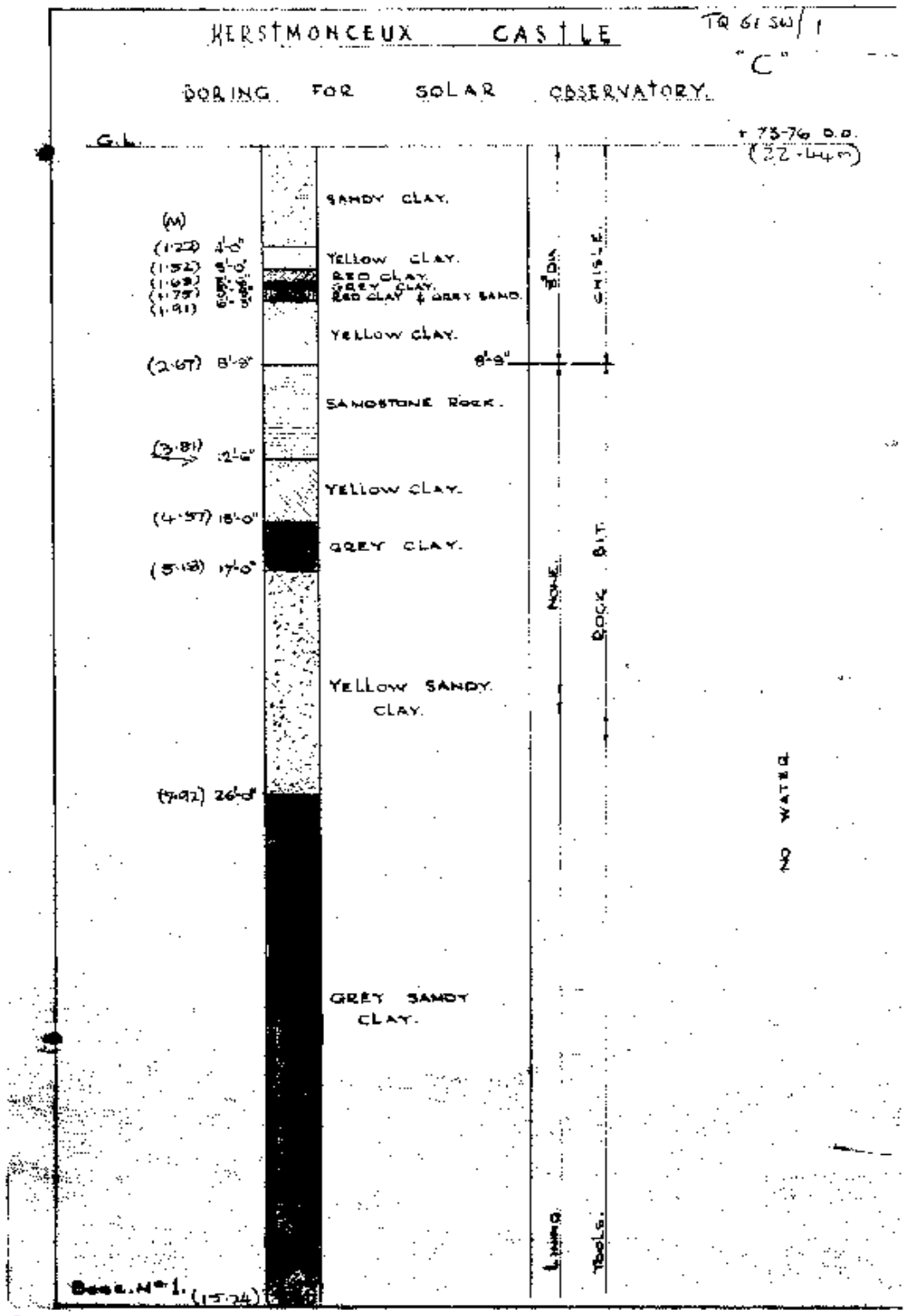

Figure 11.3 Borehole record TQ61SW1*.

* Contains British Geological Survey materials © NERC [2016]

Whilst these borehole records are not in absolute agreement about the exact descriptions of the soils it is worth noting that the entire 'Solar Dome' borehole record, in front of the SGF at 15 metres depth, is encompassed in the first four lines of the deeper borehole, shown in Figure 11.2. From this record it can be seen that the vast majority of substrate beneath the SGF is comprised of various clay and marl materials.

From this information, and using the Bouguer equations explained in Chapter 3, the hydrological influence of the soil above the basement and the groundwater variations below the basement can be approximated. All approximations are based upon using clay as the dominant substrate material and make no allowance for various types of clay or for any other layer found down to a depth of twenty metres.

11.3. Bouguer Approximations

In Chapter 3 gravity anomalies and the use of the Bouguer plate approximations were introduced, to recap:

From the standard Bouguer infinite slab correction we know that:

$$\Delta g = 0.0419\rho h$$

Where ρ is the density of the disturbing mass in Kgm^3 and h is the distance to the slab in metres. Δg will be obtained in µGal.

This gives a first approximation for flat plate changes in a homogeneous layer but this can be altered slightly when considering either a change in gravity due to soil moisture level or by a change in the thickness of the groundwater layer. Such that: The effect on the gravity value for a change in *soil moisture* is:

$$\delta g_{sm} = 2\pi G H \rho_w \delta P = 4.2 H \delta P$$

And, the effect on the gravity value for a change in the thickness of the *ground water* is:

$$\delta g_{gw} = 2\pi GP\rho_w \delta H = 4.2P\delta H$$

where: δg_{gw} is the change in gravity due to a change in ground water, G is the gravitational constant, δH is the thickness of the groundwater layer, $\rho_w$is the density of water, P is the water filled pore space and δP is the change in the water content. δg_{sm} is the change in gravity due to soil moisture, H is the thickness of the soil moisture layer, (Torge, 1989), the units for both δg terms are in μGal.

It should be noted that all of these Bouguer approximations are based upon the premise that the observing station does not move in height in the time frame of the assessments. This is perhaps a flawed argument, especially at the SGF as the swelling and contraction of clay is a well known property of the soil and has the potential to induce a height change of the observation point.

The user wishing to implement these Bouguer approximations must first have some knowledge of the subsoil's around the gravity observation point.

11.4. Estimating the Properties of the Clay Soil Around the SGF

The borehole scan information shown in section 11.2 & 11.3 has shown that the dominant subsoil is clay. It is now necessary to obtain some more information about the properties of the clay to make use of the Bouguer equations.

One problem in this case is that the porosity of clay is known to be variable due to the fact that clay is not a stable substance and is liable to swell or shrink as it gets wet or dries out (The Royal Horticultural Society, 2016). The level of compaction of the clay is also a factor as it will affect the available pore spaces and will likely be variable depending on how undisturbed the soil has been, the depth of the layer as well as the purity of the clay (the upper layers around the SGF are clay whereas deeper down the clay has a sand content).

Since we can estimate the depth of both soil above gravimetry laboratory and the distance between the laboratory and the depth of the water table, with reasonable accuracy (approx. ± 0.25 metres) the focus falls upon estimating the density of the clay soil.

Clay soils have a known variation in density between 1073 kgm^3 and 1826 kgm^3 between 'wet' and 'dry' clays, shown in Table 11.1, but also has variation dependant on the level of compaction of the clay. The compaction level will directly affect the size and number of pore spaces available within the clay, and therefore the water retention capability.

Table 11.1 Density levels of clay (Walker, 2016).

SOIL DESCRIPTION	DENSITY (kgm^3)
DRY CLAY LUMP	1073
WET CLAY LUMP	1602
DRY CLAY (EXCAVATED)	1089
WET CLAY (EXCAVATED)	1826
COMPACTED CLAY	1746

The clay around the SGF has been generally undisturbed since the 1940's, with the notable exception of the soil around the gravity laboratory which was heavily worked during the renovation work mentioned in Chapter 5. An indication of the compaction of the soil was obtained during installation of the UK Ordnance Survey's GeoNet receiver in front of the SLR. Prior to installation OS expected to drill the legs of the monument into the soil to a depth of around 3 metres but in reality only managed an estimated depth of 2 metres due to repeated problems with the drilling rig shearing through the top of the steel legs during installation. The amount of force required to drive the leg into the soil was higher than the shearing tolerance of the steel.

Figure 11.4 The UK's Ordnance Survey reference receiver 'HERO'. The photograph on the left shows the installation of the monument, the photograph on the right is the installed unit.

11.5. Soil Sample Measurements

In an attempt to obtain more information about the density and porosity of the soil a small soil sample, taken from behind the South West office of the SGF, from an area considered to have had the least disturbance over the last decade (at the very least) was taken to obtain a rough estimation of the density and porosity of the soil.

The sample was taken from a depth of 30 cm below the surface by driving a small diameter 12 cm long pipe into the soil and then carefully extracting it. The soil sample did not fill the entire length of pipe, but was 11 cm of the length. The dry soil weight was obtained by removing the soil from the pipe into a container and using a microwave for ten minutes to dry the sample.

Table 11.2 Results from soil sample 1.

	Pipe
Pipe Inner Diameter	2.1 cm
Sample Length	11 cm
Volume	38.01 cm^3
Weight (dried)	50 g
Density	1.315 g/cm^3 or 1315 kg/m^3

From the volume and dry weight the density of the sample was determined using:

$$\rho_{sample} = \frac{Dry\ soil\ weight}{Soil\ volume}$$

In turn the porosity of the sample can be determined if the particle density, $\rho_{particle,}$ is known. If this is assumed to be 2.837 g/cm^3, (Agriculture Information Bank, 2015):

$$P_{dry} = \left(1 - \frac{\rho_{sample}}{\rho_{particle}}\right) \cdot 100 = \left(1 - \frac{1.315}{2.837}\right) \cdot 100 = 54\%$$

An error in sample length measurement of 0.5 cm would give a calculation error of approximately 5% for sample density and porosity.

Since the soil samples were taken at the end of a summer season a ‘wet’ clay sample was simulated by extracting another clay sample and saturating it with water over a period of several days, the sample was also used for estimating the specific yield of the clay. The soil was hydrated within the sampling pipe by standing the pipe upright in a container and allowing the clay to draw water up the pipe, allowing the air to escape upwards, to become fully saturated. The density of the wet clay is then the weight of the clay minus the weight of the pipe divided by the soil volume, giving:

Table 11.3 Results from soil sample 2.

	Soil Sample 2
Pipe Inner Diameter	2.1 cm
Sample Length	10 cm
Volume	34.64 g/cm^3
Weight (wet)	57 grams
Density	1.646 g/cm^3 or 1646 kg/m^3

$$P_{wet} = \left(1 - \frac{\rho_{sample}}{\rho_{particle}}\right) \cdot 100 = \left(1 - \frac{1.646}{2.837}\right) \cdot 100 = 42\%$$

When the sample was fully saturated it was then left to drain for a period of two weeks. Since the porosity of soil is equal to the volume of water that the soil will yield by gravity drainage (S_y) and the volume held by surface tension (S_r), (Wilson, Unknown) and is given by:

$$P = S_y + S_r$$

The specific yield can be obtained from the amount of water which drains from the sample. In reality no detectable water drained from the sample but a small change in weight was detected. The weight of 55 g gave a calculated porosity for this 'drained' sample of clay soil to be 44%. Therefore we can estimate the specific yield for the sample to be 2%.

The results of these tests give density, porosity and specific yield values which are in line with expected for clay (Wilson, Unknown), (Walker, 2016).

11.6. Environmental Influences Above and Below the Gravity Laboratory

The gravity anomalies above and below the gravity laboratory will be considered separately. The water retention of the soil on top of the basement is considered a different case to that below the gravity laboratory as it will be affected by such things as water runoff and vegetation root depth to a higher degree than the soil below.

Figure 11.5 A view of the semi-sunken basement from the South East corner of the SGF.

On the very top of the soil the vegetation root depth, which will affect the water retention of the soil, is assumed to be 25 cm since the only vegetation of note is an assortment of different types of grasses and this value is the average of the estimated depth obtained when the soil sample was obtained. Due to the topography of the basement in the local environment the water runoff, due to rainfall, from the area on top of the laboratory is likely to be high.

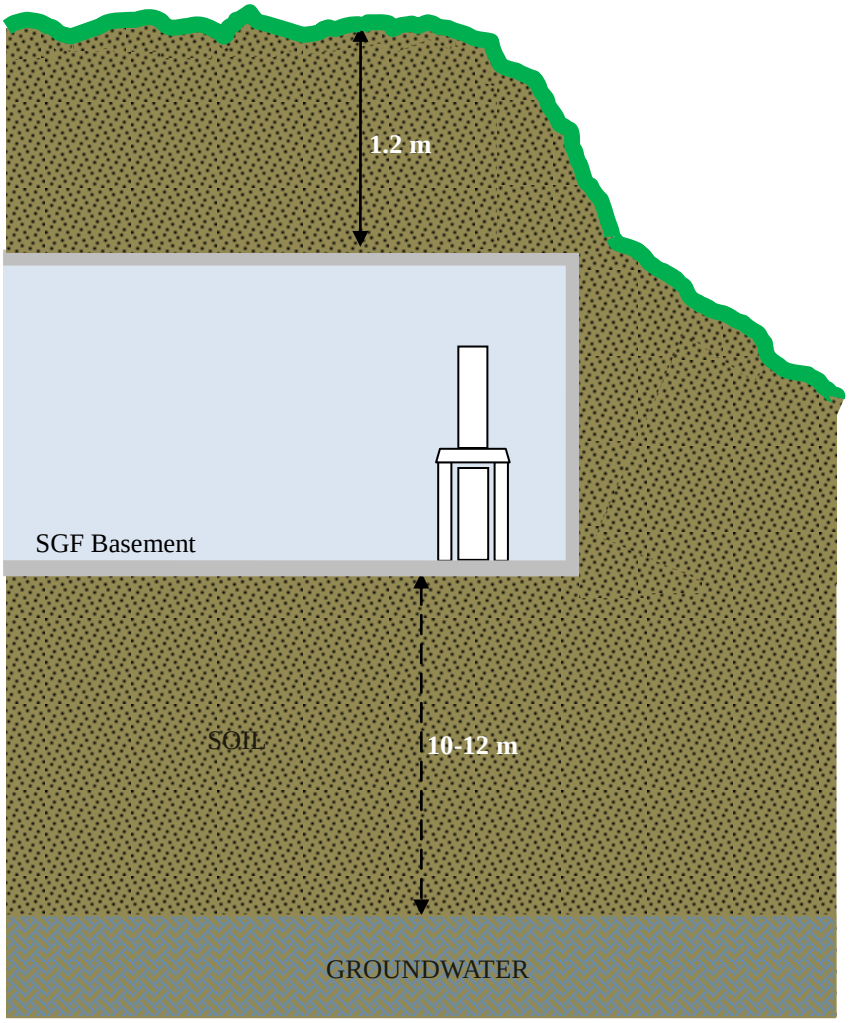

Figure 11.6 Representation of the soil immediately surrounding the gravity laboratory.

Below the root depth the remaining metre of soil above the gravity laboratory will likely be dryer than the soil below the gravity laboratory. In addition, since this soil was also disturbed in the past it may be less compacted.

11.7. Above the Laboratory

To estimate the total effect of the changing soil moisture in the 1.2 m of soil above the gravity laboratory the equation given in section 11.3 can be used.

$$\delta g_{sm} = 4.2H\delta P$$

In this case H is the depth of the soil moisture layer and δP is the change in porosity from dry to wet clay. To obtain the maximum variation which might be possible from this soil the entire 1.2 m depth of soil, from the grass top layer to the top of the gravity laboratory, is considered here. So, if H is 1.2 m and δP is the change in porosity from wet to dry clay, where the test samples gave dry as 54% and wet as 42%:

$$\delta g_{sm} = 4.2 H \delta P$$
$$\delta g_{sm} = 4.2 \cdot 1.2 \cdot 0.12$$
$$\delta g_{sm} = 0.61\ \mu Gal$$

However, although the soil above the laboratory is exposed, and the rainfall run off is likely to be much higher than soils in normal topography, it is unlikely the entire depth of soil will completely dry out. However since 0.61 μGal is a small value, and considerably lower than anticipated for this soil, it will therefore be taken as the best approximation.

11.8. Below the Laboratory

When considering gravity anomalies which might be due to influences beneath the SGF the varying groundwater level is the most significant. The height of the water table, or groundwater level, has been recorded at the SGF since 1996. Since 2002 the measurements are taken via an automatic electronic pressure sensor at five minute intervals.

Since the borehole measurement heights are related to the base of the SGF main building a correction to the water table height can be made to account for the fact that the gravimeter is in the semi-sunken basement. Precise levelling data gives the height between the floor of the gravimetry laboratory to a levelling stud in close proximity to the top of the borehole to 3.27 ± 0.01 m. Since this stud is approximately level with the top of the borehole a height correction, from borehole to gravimetry room floor, of 3.2 ± 0.1 metres will be applied to the water table data. Hence, in the period between the January 2006 and January 2016 it can be seen that the corrected height of the water table has a variation between 10.01 m and

11.79 m below the gravimetry laboratory, giving a range in the water table depth of 1.78 metres.

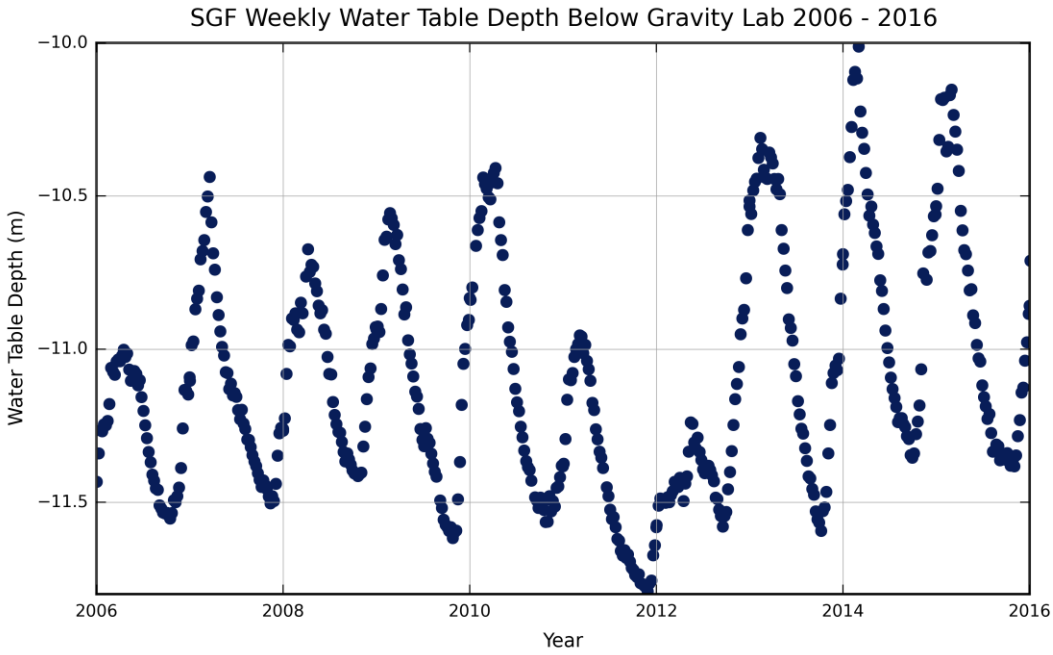

Figure 11.7 Water table depth below the gravity laboratory.

If a first order estimate is attempted, using the basic Bouguer infinite slab correction approximation given in section 12.3, assuming that the density of clay is homogeneous until the water table is reached and that it varies between the 'wet' and 'dry' values that we have already measured, ρ_{wet}= 1315 kgm^3 ρ_{dry}= 1646 kgm^3 and δh = 1.78 m, then:

$$\Delta g = 0.0419\left(\rho_{wet} - \rho_{dry}\right)\delta h = 0.0419 \cdot (1646 - 1315) \cdot 1.78 = 24.75\ \mu Gal$$

This gives a maximum estimated value which might be expected for the effect of the changing water table on the gravity measurements. However this value can be considered unreasonable as the clay at the water table depth is exceedingly unlikely to dry out entirely, as the water retention of the soil will likely be very high.

Therefore, whilst this first approximation can be considered 'worst case' it is unrealistic. If the modified Bouguer equation for ground water equation is used instead, where:

$$\delta g_{gw} = 2\pi G P \rho_w \delta H = 4.2 P \delta H$$

Remembering: P is the porosity and δH is the change in height of the groundwater:

$$\delta g_{gw} = P\delta H = 4.2 \cdot 0.42 \cdot 1.78 = 3.14\ \mu Gal$$

This lower number is considerably closer to the anticipated figure for this effect by looking at the scatter in the time series. The time series of gravity measurements taken during this study and the application of this anticipated variation in gravity due to the water table depth is shown in detail in Chapter 13.

11.9. Changes Affecting the Gravity Laboratory in 2015

The environment above the gravimetry room underwent a large change in December 2015 with a telescope dome installed directly above it. A significant amount of soil was excavated and the resulting hole then in filled with concrete. Above the concrete a single skin of brick was laid around the outside to support a fibre-glass telescope dome.

The details for calculating the gravity anomaly from a buried sphere is detailed in Chapter 3. If we apply this calculation and invert the result will be a simple estimation of the effect of building on top of the laboratory.

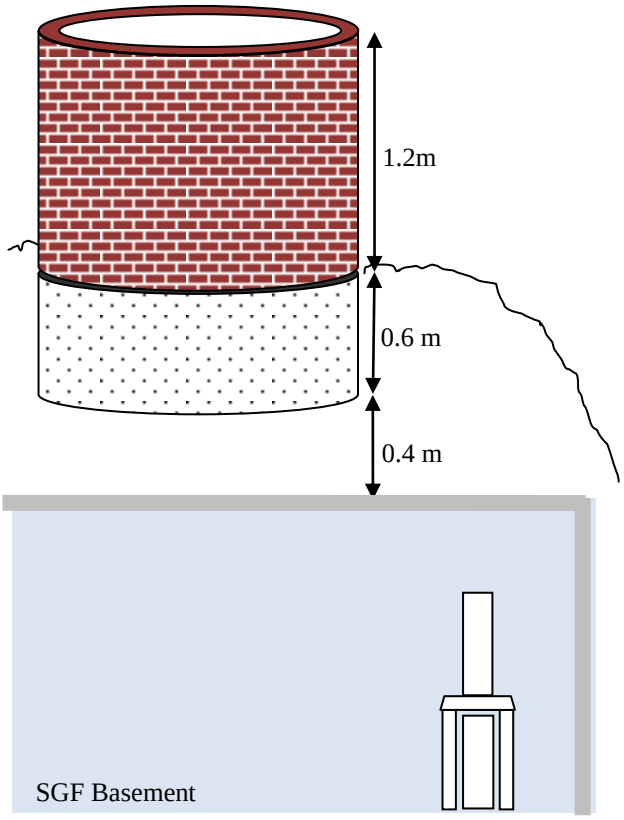

Figure 11.8 Representation of the new dome above the gravity laboratory.

Similarly to the case for a buried sphere, shown in Chapter 3, the calculation for the new dome can be made by substitution of V in the following equation:

$$\Delta g = \frac{G\Delta\rho V}{r^2}$$

But since the volume of the new building is comprised of a cylinder of concrete topped with a hollow brick shell the mass should be considered to consist of two components, where $V_{concrete} = \frac{G\Delta\rho\pi \mathrm{R}^2 \mathrm{h}_{\mathrm{concrete}}}{r^2}$ and$V_{brick} = \frac{G\Delta\rho h_{brick}(2R-t)}{r^2}$, where R is the radius of the brick and concrete, t is the thickness of the brick, and r is the distance between the centre of the new mass and the gravimeter. Hence the equation becomes:

$$\Delta g = \frac{G\Delta\rho\pi \mathrm{R}^2 \mathrm{h}_{\mathrm{concrete}}}{r^2} + \frac{G\Delta\rho h_{brick}(2R-t)}{r^2}$$

This gives the equation for the dome directly above the gravimeter. However, as Figure 11.8 shows, the dome is not directly above the primary gravimetry pier, pier 1, therefore the cosθ component must be also considered.

Again since $cos\theta = \frac{z}{r}$:

$$\Delta g = \frac{G\Delta\rho_{concrete-clay}\pi \mathrm{R}^2 \mathrm{h}_{\mathrm{concrete}}}{r_{concrete}^2} \cdot \frac{z}{r} + \frac{G\Delta\rho_{brick-clay} h_{brick}(2R-t)}{r_{brick}^2} \cdot \frac{z}{r}$$

The density of concrete is 2243 kg/m^3 and the density of brick is 1922 kg/m^3 (Walker, 2016). It has been shown that the density of the clay is between 1315 and 1646 in section 12.4.1, if an average value of 1480 kg/m^3 is used for the clay $\Delta\rho_{concrete-clay}$= 763 kg/m^3 and $\Delta\rho_{brick-clay}$= 442 kg/m^3. Also $r_{concrete} = 1.91\ m$, $r_{brick} = 2.99m$, $z_{concrete} = 1.33\ m$, $z_{brick} = 2.53m$ and t = 0.1 m.

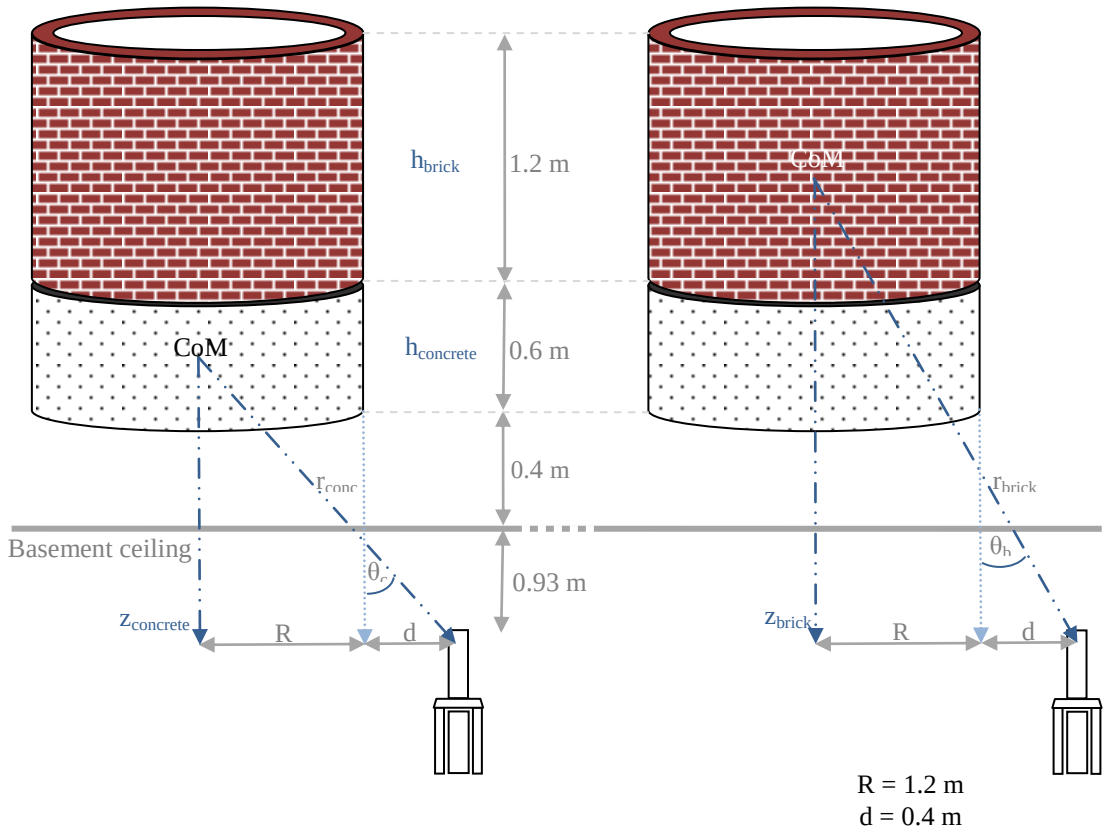

Figure 11.9 Calculating the effect of the dome above the primary pier (HERG) in the gravity laboratory.

$$\Delta g = \frac{6.674 \times 10^{-11} \cdot 763 \cdot 3.142 \cdot 1.2^2 \cdot 0.6}{3.648} \cdot \frac{1.33}{1.91} + \frac{6.674 \times 10^{-11} \cdot 442 \cdot 3.142 \cdot 2(1.2 - 0.1)}{8.94} \cdot \frac{2.53}{2.99}$$

$$\Delta g = 16.86 \times 10^{-9} + 19.28 \times 10^{-9} = 36.14 \times 10^{-9}\, ms^{-2}$$

$$\Delta g = 3.61\, \mu Gal$$

Although there have been measurements taken on pier 1 since the dome was built an average change has not yet been calculated, however the predicted change of 3.61 µGal is roughly in line with observational evidence.

11.10. Conclusions

The information obtained about the soils provide a valuable insight into corrections which can be made to the time series of gravity data. The borehole data provides confidence that treating soils down to the groundwater depth as consistent is a reasonable basis for the simple calculations made. The soil sampling has provided interesting information and a first approximation of the soil density, porosity, specific yield and specific retention, and provided the basis for the calculated approximations on the impact on gravity due to the variation in ground water depth and the weather driven change in density of the soils. The calculated value of 3.14 μGal gives the maximum for a change in gravity due to the variation in ground water depth and will be used to correct the gravity time series in Chapter 13.

However, the results obtained are only approximations and further investigations are recommended to provide a more accurate temporal corrections to the gravity time series. The author would recommend:

- Repeating the soil sampling using larger core sizes
- Obtaining further ancillary instruments to monitor the environment around the SGF

The small core sizes used in this study were not ideal as any error in the weight or size measurements will have had a large impact on the resulting calculations. It is recommended that the soil sampling is reiterated with larger core samples to provide more accurate data. Ideally a sample would also be taken from a greater depth below the surface.

Monitoring instruments would provide direct information about the moisture content and the movement of water through the soils around the gravity laboratory and allow the effect on gravity to be accurately determined. A combination of multiple soil moisture probes and a rainfall detector situated around the laboratory would provide direct temporal information. The data could then be used to calculate the effect of the movement of water and water content within the soil, and the direct effect upon the gravity time series. Without

rainfall and soil moisture data only approximations of the overall effect of the soil above and below the laboratory can be calculated.

Chapter 12

Periodic Signals within the data

12.1. Introduction

The presence of periodic signals in the gravity data implies some an un-modelled influence on the gravity measurements. If the signal source can be determined removal from the gravimetry data is possible, and may be feasible to also be removed from the satellite laser ranging data.

Periodic signals have been intermittently visually obvious in plots of the hourly data provided by the 'g' software. This chapter investigates typical examples of this periodic signal seen, to determine if it is tidal in nature and whether it corresponds with tide gauge data taken from the Newhaven tide gauge, which approximately 22 km from Herstmonceux. Since the signal appears similar to the semi-diurnal tidal constituent investigations also include comparison of several ocean-loading models.

12.2. Short Period Signals

The principle, short period signal in the hourly data sets are visible on an intermittent basis, sometimes showing clearly, with some dependency on precision of the measurements. An example of the set data produced by the 'g' software is shown in Figure 12.1. in which displays a periodic signal with amplitude of around 5 μGal.

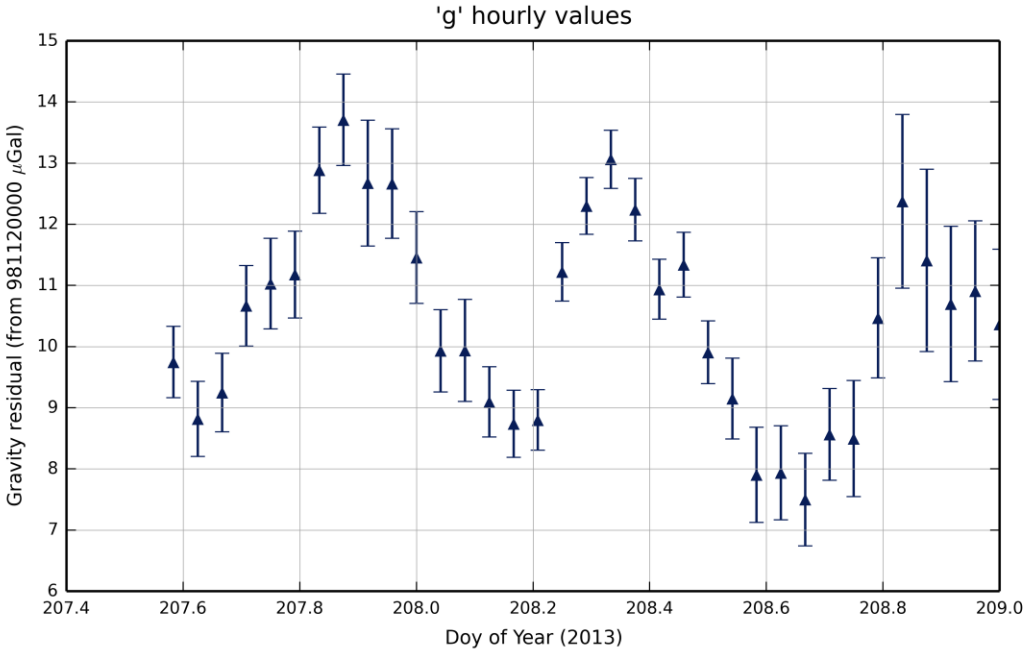

Figure 12.1 . Hourly data from g9 from 2013. Which shows a typical periodic signature seen in the data from 2006 - 16. The amplitude of this signal is approximately 5 μGal.

Since this signal frequency appears diurnal in nature an analysis of the ocean-loading models, chosen from ‘g’ or ‘gap’ are investigated.

12.2.1. Ocean-Loading Model Selection

From the inception of the absolute gravimetry programme at Herstmonceux the data processed by ‘g’ has used the Schwiderski ocean-loading model. This model is known to be less accurate than many other ocean-loading models (Bos, 2011) therefore the differences between the four additional models for Herstmonceux was investigated with the aim of choosing one model to be used in reprocessing using ‘gap’.

The initial investigation was carried out by reprocessing gravity data with the ocean-loading model turned off (in ‘gap’) and then reprocessing again with an ocean-loading model applied. The later was then subtracted from the former to extract the ocean-loading model.

$$Data\ processed\ without\ OL - Data\ processed\ with\ OL\ model = model$$

This applied using a unique ten day data set, where data was obtained for every hour for a ten day period. Figure 12.2 shows results of the extraction. The four ocean-loading models* used within 'gap' were models: GOT00.2, FES2004, TOPEX 7.2 and CSR 4.0. In addition the results from 'g' (versions 7-9 using Schwiderski) were also extracted.

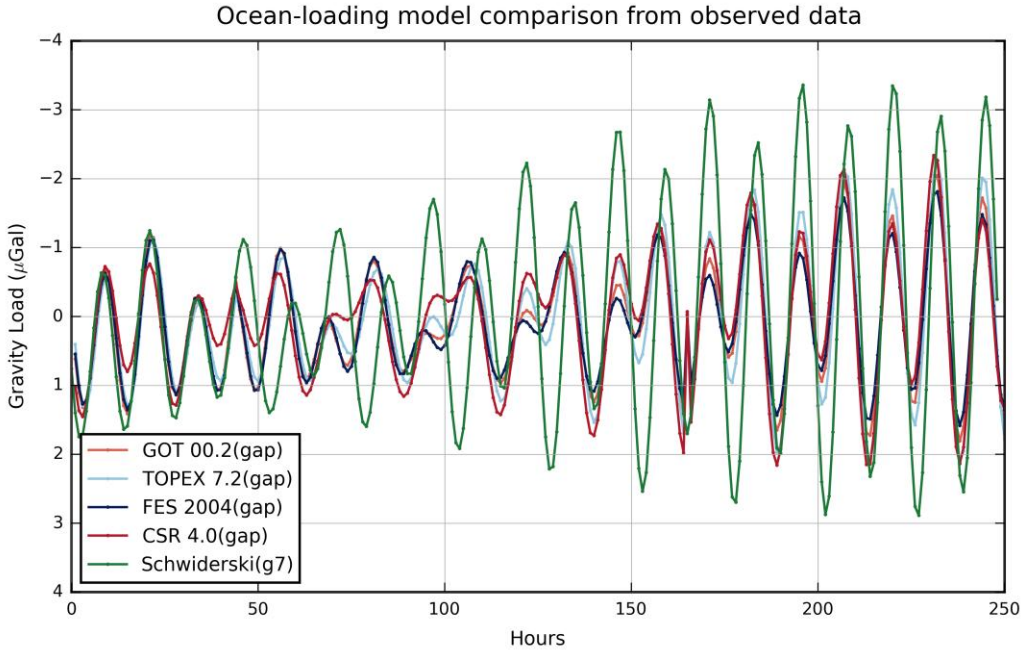

Figure 12.2 Comparison of five ocean-loading models, obtained from extraction using 'gap'

To test this extraction method, using 'gap', the models were also generated using the amplitude and phase constituents for each. The constituent values for each model are given in Appendix 5.

Figure 12.3 shows the comparison of the models using the constituent values, however the amplitude of the Schwiderski model from the two different methods are at odds; Figure 12.2 shows a maximum amplitude of over 3 µGal whilst 12.3 shows less than 3 µGal. In

* The constituents for each model were obtained from the Chalmers free ocean tide loading provider: http://holt.oso.chalmers.se/loading/

fact although Schwiderski is known as a less accurate model it is clear ‘g’ uses a different version of Schwiderski than was obtained from the Chalmers University of Technology ocean loading provider , no version information is available to confirm this theory however. Figure 12.4 shows the differences between Schwiderski models.

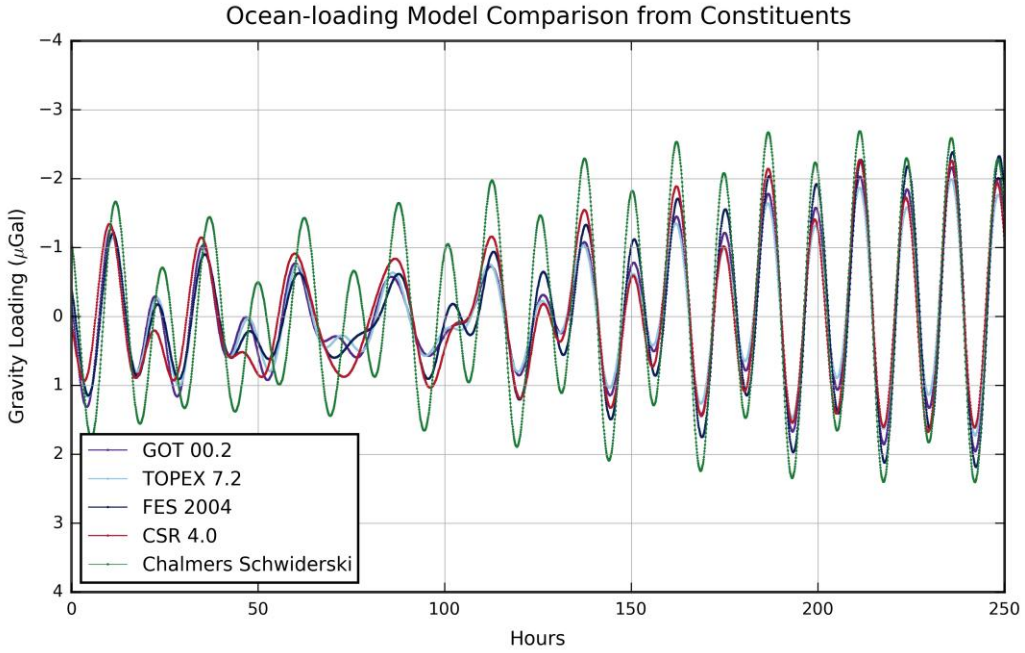

Figure 12.3 Ocean-loading comparison from Chalmers free ocean tide loading provider.

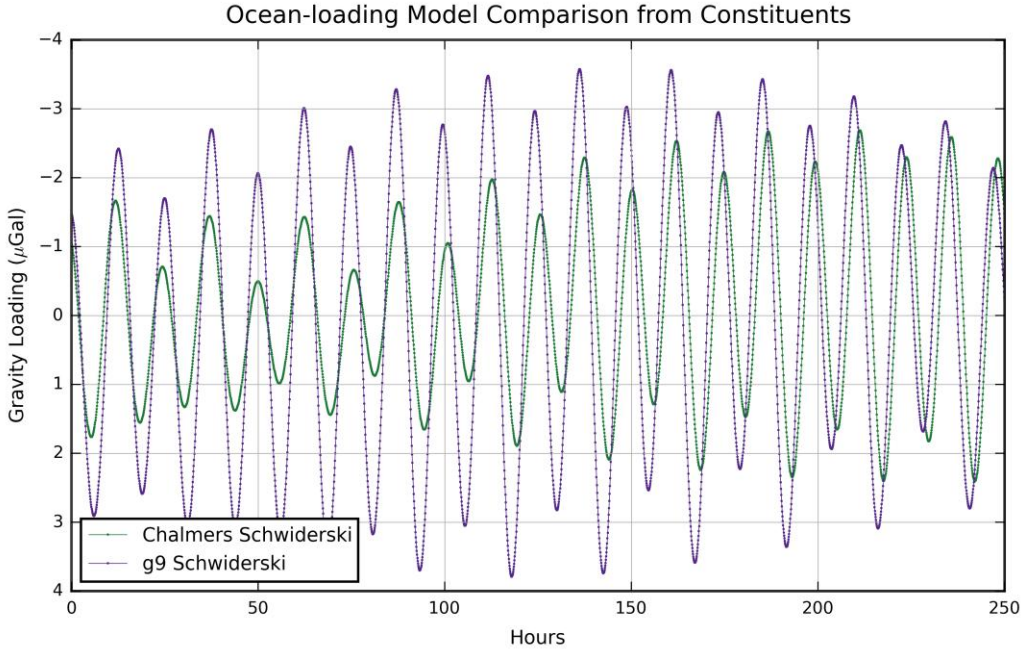

Figure 12.4 Comparison of the Schwiderski ocean-loading models. from Chalmers and ‘g’.

The results of this investigation clearly shows Schwiderski is the least accurate model to use at Herstmonceux, but further that the values used in ‘g’ are clearly even less accurate than could be expected.

If the models are reassessed without Schwiderski it can be see that they are all in close agreement with a maximum deviation which is less than 0.5 µGal.

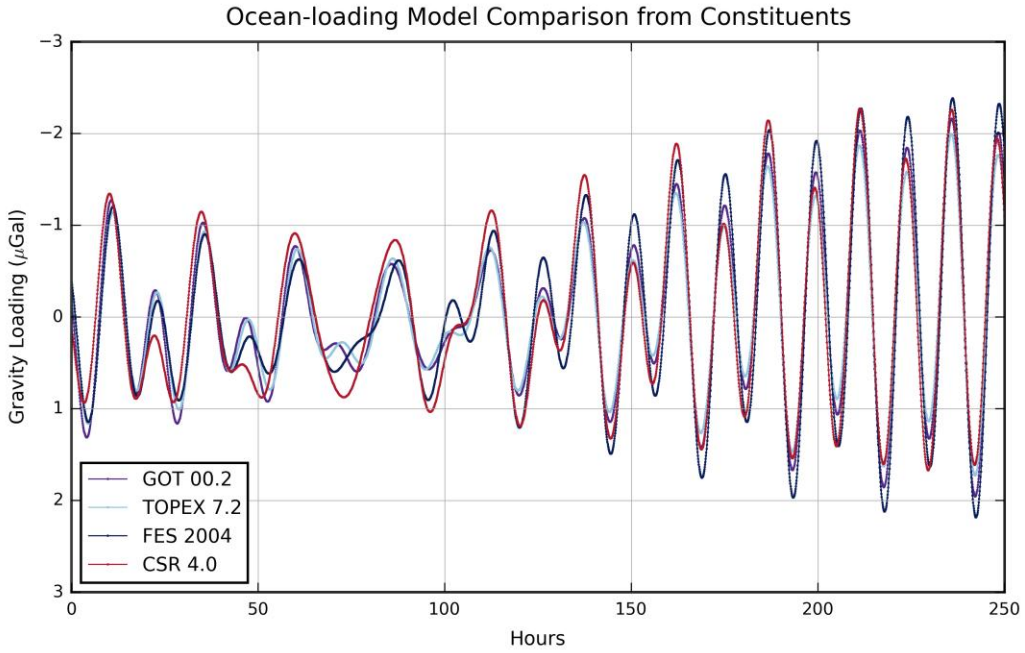

Figure 12.5 Ocean-loading model comparison between four models

Since there is such little difference between these four models and the GOT00.2 ocean-loading model is used in the SGF satellite laser ranging analysis it was determined that the SGF gravity data would also be processed using GOT00.2

12.2.2. Tidal Investigation

To determine if the residual signal seen in the data could be due to tidal influence the measurements from a tide gauge. The closest tide gauges to Herstmonceux are currently found at Newhaven and Dover. Newhaven is around 22km Southwest, whilst Dover is

approximately 72 km Southeast, of the SGF. Due to the distances involved only the data from Newhaven tide gauge was obtained from the BODC*.

As previously mentioned in Chapter 9 the tide gauge data obtained from BODC is supplied with data flags to indicate the status of the measurements, the values M,N or T indicate the data has some quality control from BODC. Data without a flag indicates the value has been assessed as 'good' (NERC, 2015) . The data obtained from BODC for the Newhaven tide gauge was filtered to use only the data flagged by BODC as 'good'.

One gravity project with a distinct residual was selected at random and the tide gauge data was then scaled and plotted with the hourly data from VgHx. The result is shown in Figure 12.6, where the tidal data is inverted. The signals appear to be related. The inversion of the tidal signal may indicate that the gravitational attraction of the changing tidal mass is dominant (Bos, 2011).

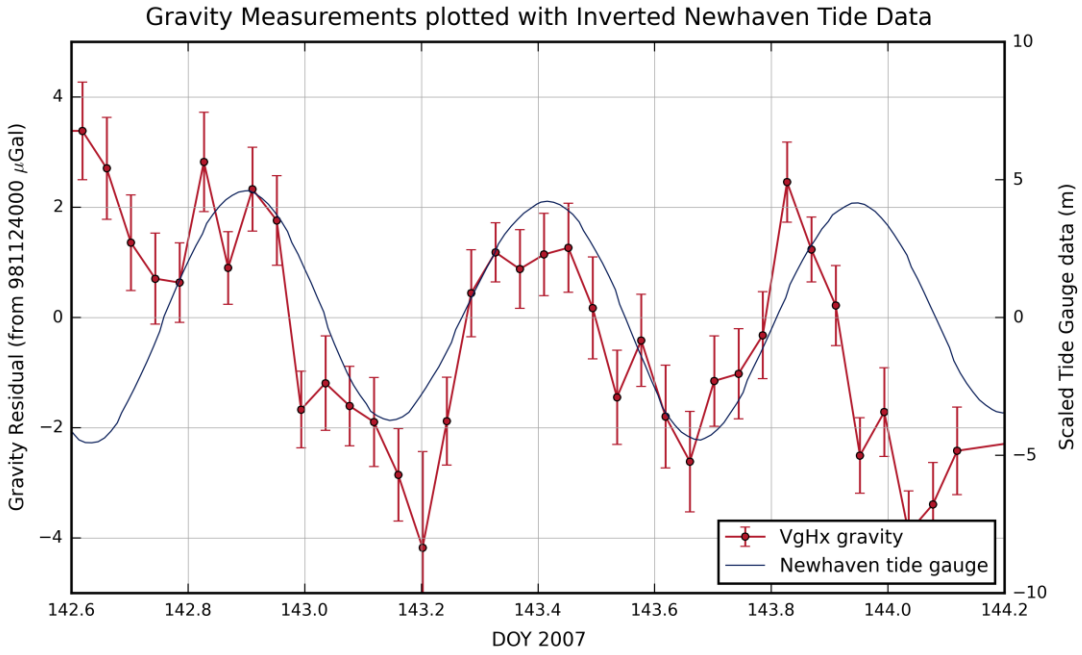

Figure 12.6 Hourly gravity residuals with standard errors plotted with tide data from Newhaven tide gauge

* British Oceanographic Data Centre

A Pearson product-moment correlation, to measure the strength of a linear association between two variables, was carried out for the data shown in Figure 12.5, gives a minimal correlation of 0.26 between the tide and the gravity data.

As a final correlation test the hourly gravity measurements for an entire year were tested. The gravity measurements were first filtered to remove outliers and hourly data with an associated standard deviation greater than 25 μGal. The remaining gravity measurement epochs were then matched with tidal data and any gravity data with no matching tidal data removed. A Pearson correlation was then obtained for the remaining data. For 2009 this resulted in a total of 30 matched gravity sets of hourly project data with hourly tidal data. The Pearson correlation values of the 30 data sets fell between +0.61 and -0.25, with 17 values between ±0.2.

Since the Pearson correlation tests show no conclusive correlation between the tide and the gravity measurement residuals, a ten day hourly data set was obtained. The result of this data plotted with the scaled tidal data from the Newhaven tide gauge is shown in Figure 12.6. The Pearson correlation value for this ten day data set was only -0.11. Although the correlation tests show little correlation between the two the plot shows compelling evidence of some relationship between them. While the phases of the two set of data are reasonably matched in the first two days they can be seen to go out of phase around DOY 81 and remain so until nearly DOY 87.

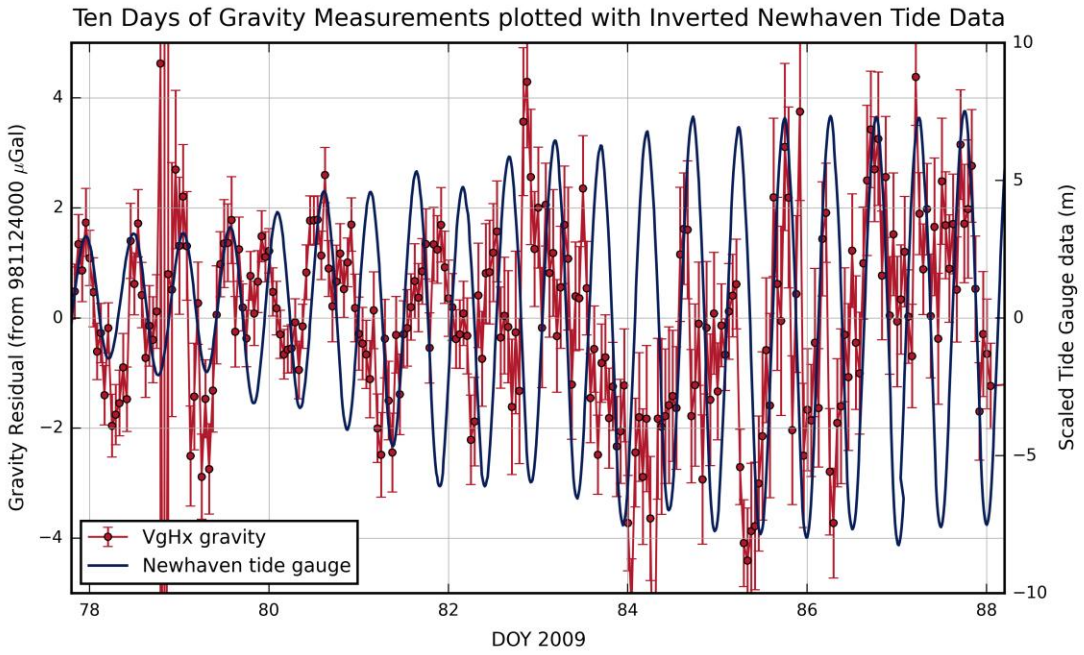

Figure 12.7 Ten day data set of hourly gravity values, with standard errors plotted with corresponding tide gauge data, scaled for best fit around day 86. The large error bars shown late in DOY 78 correspond with an Earthquake event, for more detail see Figure 10.10 in Chapter 7.2.1.

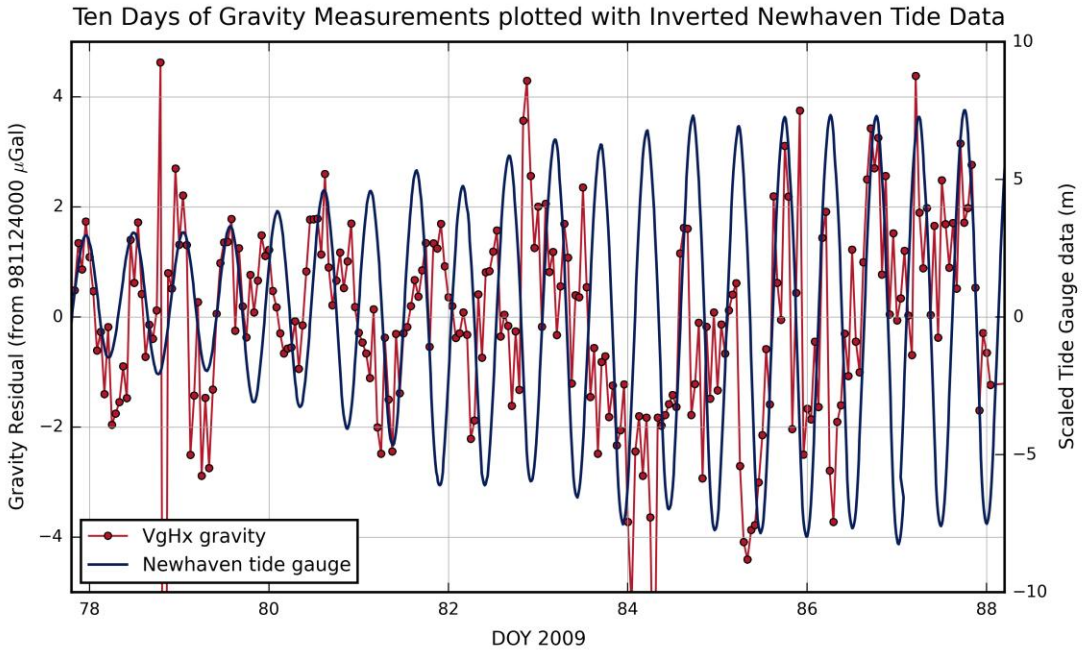

Figure 12.8 Ten day data set of hourly values only, with corresponding tide gauge data.

However the amplitude of the two signals is seen to be fairly consistent throughout, which suggests a relationship between the tidal loading and the gravity residuals exist. The gravity

data from day of year 82 may diverge from the tidal signature due to rainfall in the period. The attraction of the extra mass above the gravity laboratory is shown to reduce the gravity values in this period in Figure 12.9.

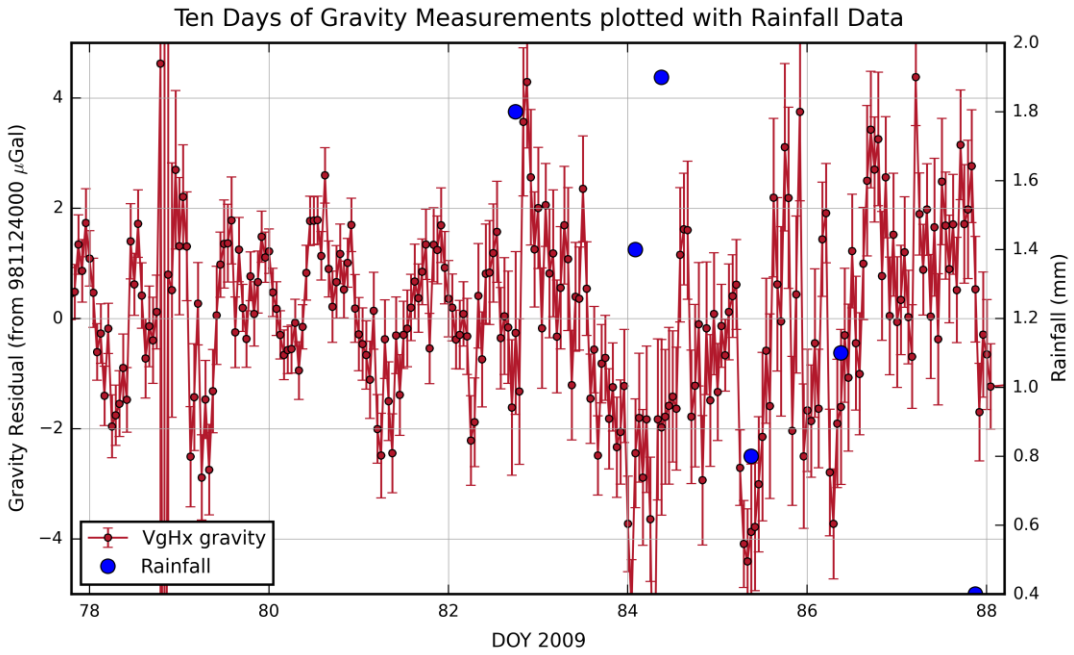

Figure 12.9 Ten day data set of hourly values plotted with rainfall data from the UK Met Office station at Herstmonceux.

12.3. Conclusions

The periodic signals seen in the gravity results at the SGF are identified in both the 'g' processing and the VgHx hourly processing data. The ocean-loading models of GOT00.2, TOPEX7.2, FES2004 and CSR4.0 are all in close agreement for Herstmonceux whilst Schwiderski has been shown to be at variance to the other models.

Since little difference between four models of GOT00.2, TOPEX7.2, FES2004 and CSR4.0 are seen, and it is used for SLR processing, GOT00.2 was adopted for all data processing using 'gap' and VgHx. Residual tidal signatures are identified using GOT00.2 as well as Schwiderski confirm the model is not accurate enough at Herstmonceux. GOT00.2 is based on a 0.5°X 0.5°grid.

Whilst the periodic signals appear to be closely related to tidal signatures they do not have a high correlation with the tide gauge data from Newhaven, however some relationship is shown to exist. The Dover tide gauge is too remote to be likely to be correlated, however the analysis could be expanded in future to include this data. Installation of a tide-gauge in closer proximity is unlikely to occur due to lack of suitable locations and prohibitive cost.

The correlation between the tide gauge data and the gravity measurements is affected by precipitation/soil moisture content, which drives the gravity value low.

This suspected tidal anomaly could be resolved by either:

- The installation of a gPhone gravity meter, manufactured by Micro-g LaCoste, at the SGF. The g-phone is based upon a relative gravimeter but is designed for long period installations rather than for high mobility. The gPhone applications list includes Earth tide monitoring, ground water monitoring as well as ocean-loading studies (Micro-g LaCoste, 2014)
- Working with oceanographers to supply a high resolution coastline model for Herstmonceux which could be incorporated into a global grid (Bos, 2011).

Chapter 13

The Time Series of Gravity Measurements at the SGF, 2006-2016

13.1. Introduction

Quantifying the time period required to make a useful gravity time series is at best difficult, but what is generally accepted however is the fact that a 'few years' of data will be required at minimum before any serious investigations may be carried out into any constituent influences which might affect the measurement value. Indeed, the first few years of data from the absolute gravimeter at the SGF, Herstmonceux, yielded no discernible information which could be used to extract any estimation on the long term influences on the gravity measurements.

In this chapter the entire, ten year, time series of gravity data is presented. Corrections and offsets to be made to the data are applied and discussed. The data are also presented as vertical height displacements for comparison with the vertical height coordinate product of the satellite laser ranging station at Herstmonceux. Finally a single project value is taken from the time series on an annual basis to simulate the results of a 'campaign style' measurement; where a gravity station is occupied once a year.

13.2. Introducing the Time Series of Gravity data 2006-2016

The time series of data presented here has been generated using the 'gap' software using the ocean-loading model GOT00.2, discussed in Chapter 12. Unfortunately 'gap' could only be used until 2012 as it has not yet been adapted for use with new formatting, of the 'gsf' files, generated by the 'g9' data acquisition program. Therefore the data from 2012-2016 is

directly obtained from ‘g’, using the Schwiderski ocean-loading model. However, the variation in ocean-loading model used does not significantly impact the project values, since the effect will be largely smoothed over the normal 25 hour period of operation. All polar rotation values are the measured values obtained from the IERS* or, where predicted values have been kept, they have been deemed close enough to the measured that reprocessing is not required. The gravity time series shown in the plots in this chapter are comprised of the daily project data and shown with the associated standard deviation.

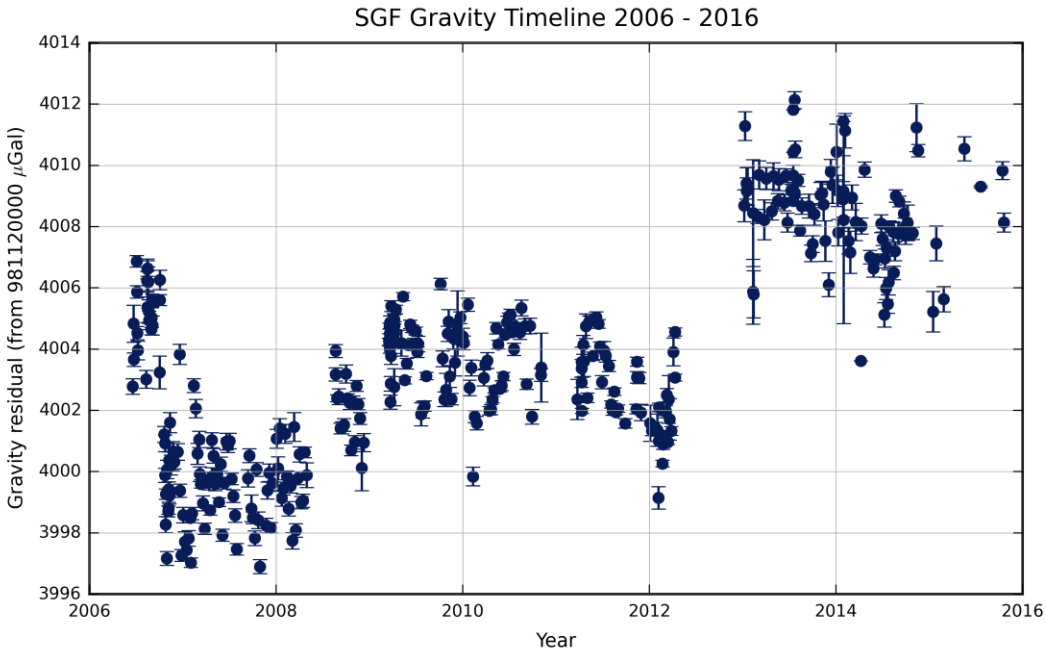

Figure 13.1 The time series of gravity data at the SGF, shown with standard deviations

On introduction to the time series it can be seen that the measurements are contained within a 16 µGal range. If taken superficially it might appear as though some long period influence is affecting the data.

However, when major instrumental events are shown, and each data collection period between events is highlighted, as shown in Figure 13.2, the structure of the time series reveals a different aspect to the data.

* IERS - International Earth Rotation and Reference Systems Service

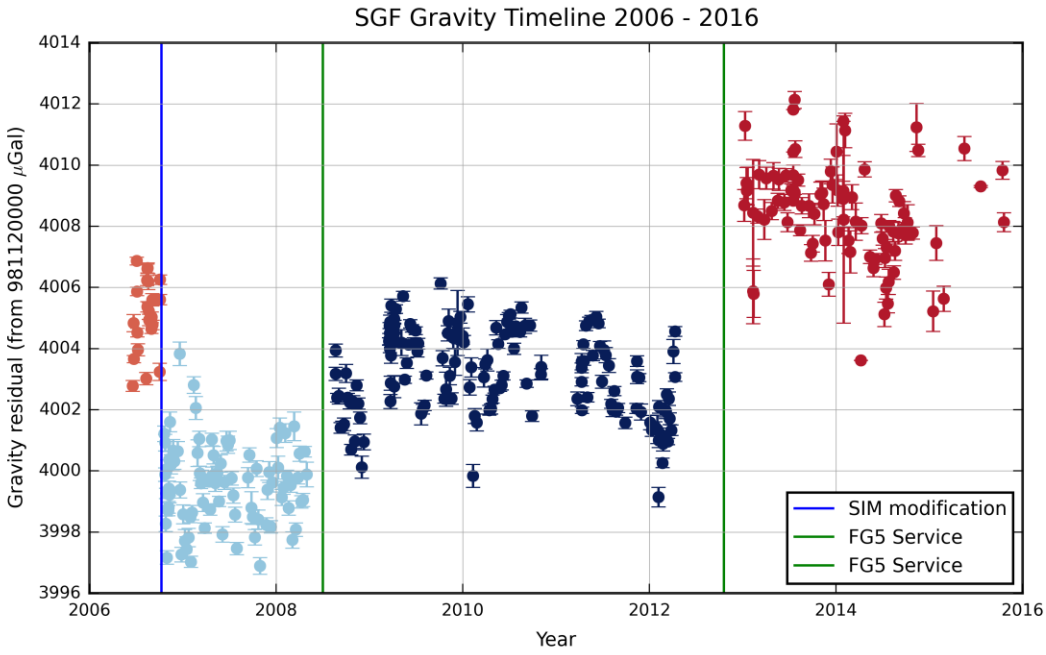

Figure 13.2 Major instrumental changes are highlighted within the gravity time series.

The instrumental changes in 2006, 2008 and 2012, where the instrument underwent service at Micro-g LaCoste, reveal clearly delineated regimes within the data, which are identified by colour changes in Figures 13.2 and 13.3. The time series is split into the different regimes in Figure 13.3 to highlight the consistency between the regimes of data. Each regime is banded within a 10 µGal range, but offset in value.

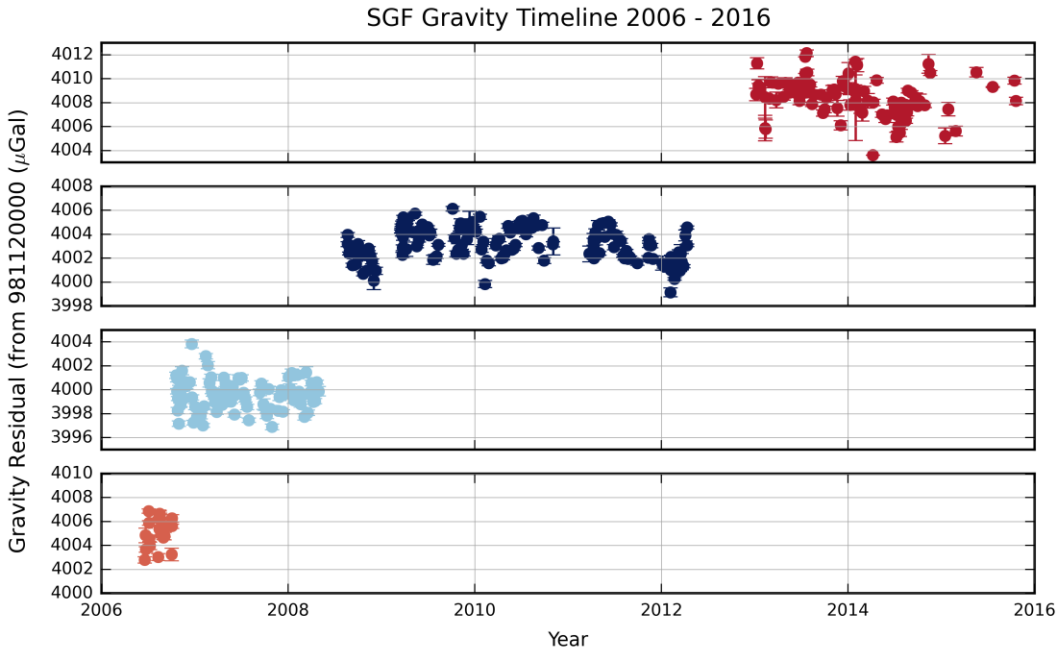

Figure 13.3 The gravity time series split into four regimes, showing similar scatter in each regime of data.

Regime 1 encompasses the period April - September 2006, when the FG5 suffered electrical synchronisation issues described in Chapters 7 and 8. Regime two encompasses October 2006 - May 2008. Regime 3 encompasses August 2008 until September 2012. Regime four encompasses January 2013 - January 2016. It should be noted that only one service at Micro-g LaCoste highlighted a factor of concern; the service in 2008, between regimes 2 &3, reported a cracked corner cube in the dropping chamber, which may account for the slightly low value as given in the international comparison the preceding year (2007).

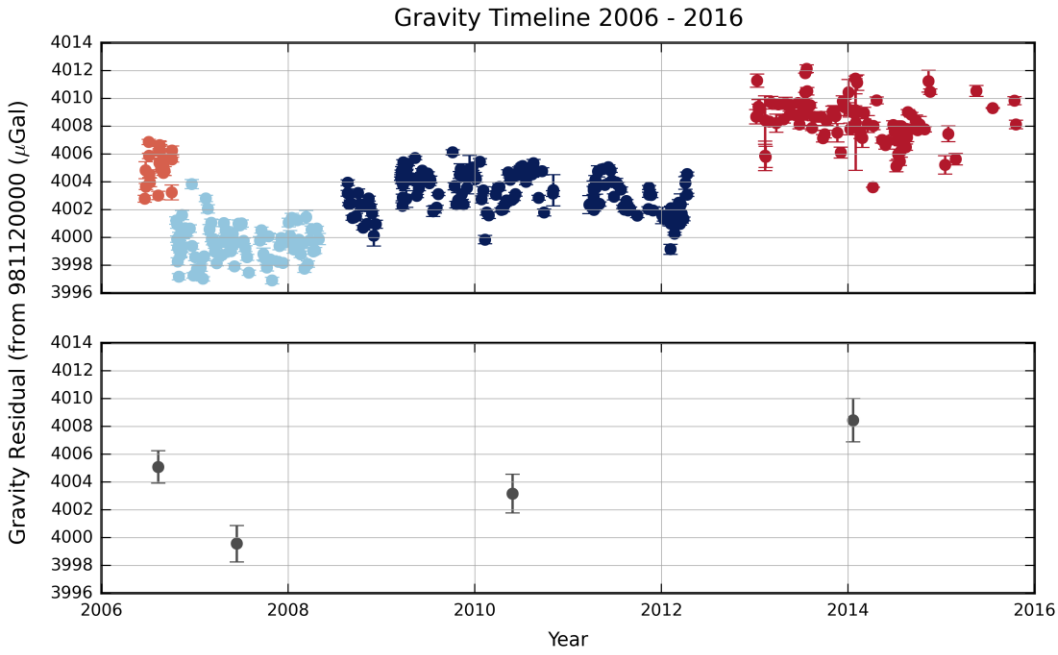

Figure 13.4 Each regime of data has an offset from the last

The mean of each regime of gravity measurements have consistent standard deviation values of 1.17, 1.31, 1.39 and 1.56 µGal, shown in Figure 13.4. The slightly higher variation in the later data may be due to environmental changes on site in 2014-15; dozens of fir trees in close proximity, from 10 m and beyond, to the gravity laboratory were removed.

It is clear that the accuracy of the instrument (±2 µGal) does not account the offsets between every regime change. The average value of each regime is 4005.08, 3999.57, 4003.17 and 4008.45 µGal (from 9811240000). Only the data from late 2006 until 2012 falls within the ±2 µGal accuracy boundary.

To help interpret the data successfully two factors must be considered, including:

1. Local influences, which might affect the gravity data; via hydrological changes etc.
2. Application of bias offsets in the time series between regime changes

Local influences are known to have the potential to influence the gravity data by 20 μGal (Longuevergne, et al., 2009), however the findings in Chapter 12 have indicated that the total influence of the ground water height changes will have less than a 4 μGal effect on the data. The application of the groundwater influence on the gravity data is discussed in the next section.

Bias offsets are considered valid but a scientific foundation must ideally be presented for an bias to be applied. The comparison data presented in Chapter 7 are applied and discussed in section 13.2.2.

13.2.1. Application of the Groundwater Correction

Hydrological influences are well known to have large effects on absolute gravity data, as discussed in Chapter 6. However, the calculations shown in Chapter 11 (section 11.5.2) have determined the change in gravity due to vertical depth changes in the ground water, $\delta g_{gw.}$, to be only 3.14 μGal. Even though this is a small correction its application to the time series can only be determined when any phase lag, between gravity and the groundwater response, has been approximated. Figure 13.5 shows the time series, from 2006-2013, plotted with the groundwater .

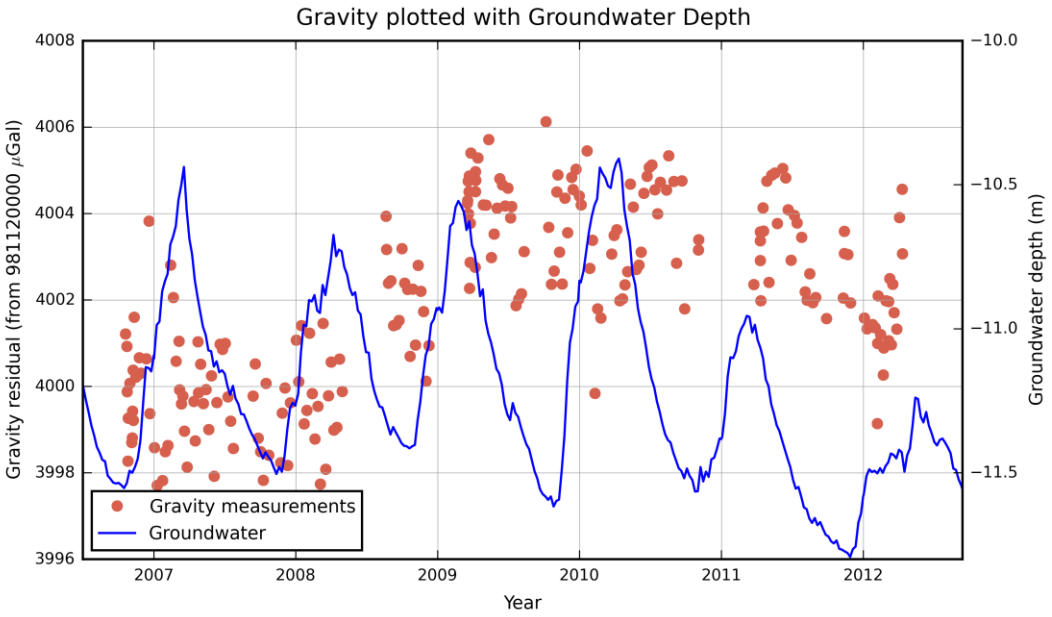

Figure 13.5 Gravity data plotted with groundwater depth.

No correlation between the two was clearly identified until 2011, when South East England suffered a drought. The correlation shows a phase lag between the gravity measurements and the water depth.

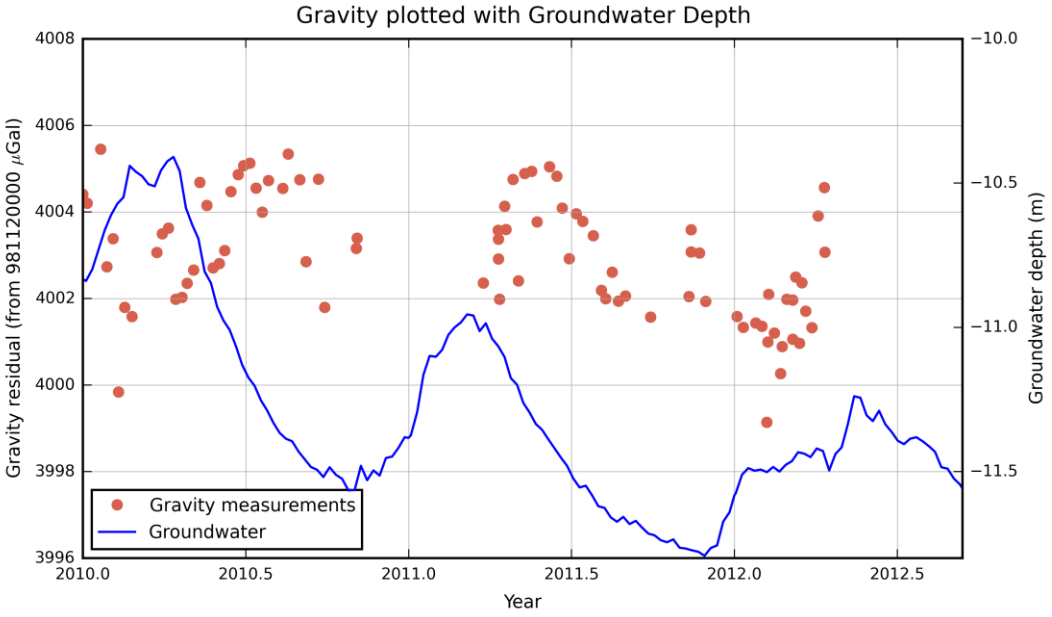

Figure 13.6 A phase lag between the gravity and groundwater depth is identified

Figure 13.6 shows the period of agreement between the signals. The phase lag between the gravity signal and the groundwater was estimated in Figure 13.7 by applying a lag to the ground water data. The lag determined by best fit is found to be as 0.23 years or 84 days.

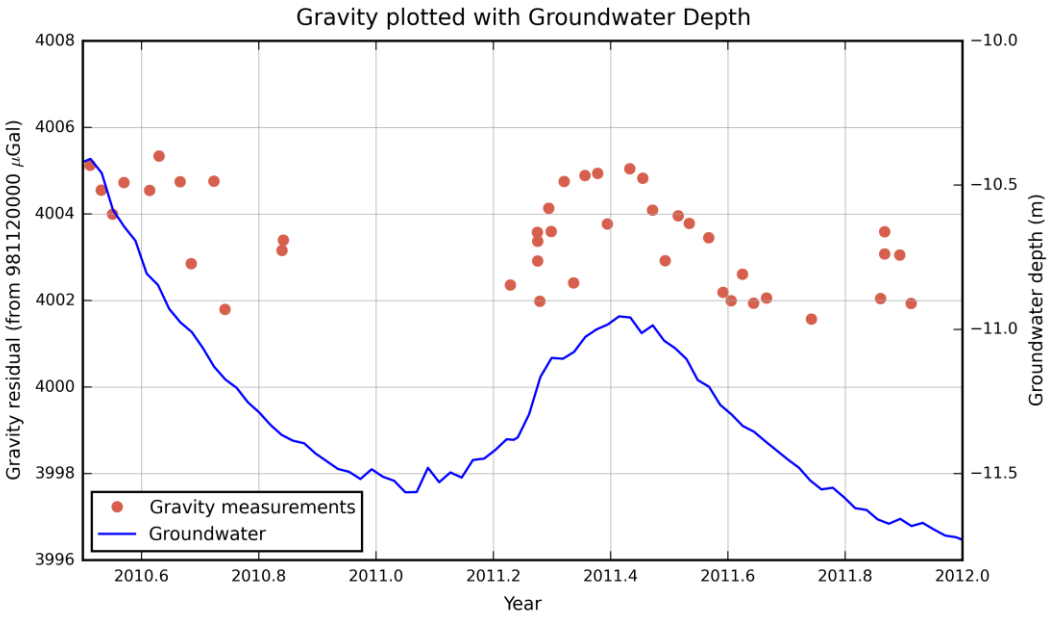

Figure 13.7 Groundwater depth with a phase lag applied

If, instead of plotting with the groundwater depth, the gravity results are now plotted with the $\delta g_{gw,}$ determined in Chapter 11, it is clear the calculated value will not smooth the signal in the gravity data and is unlikely to be accurate.

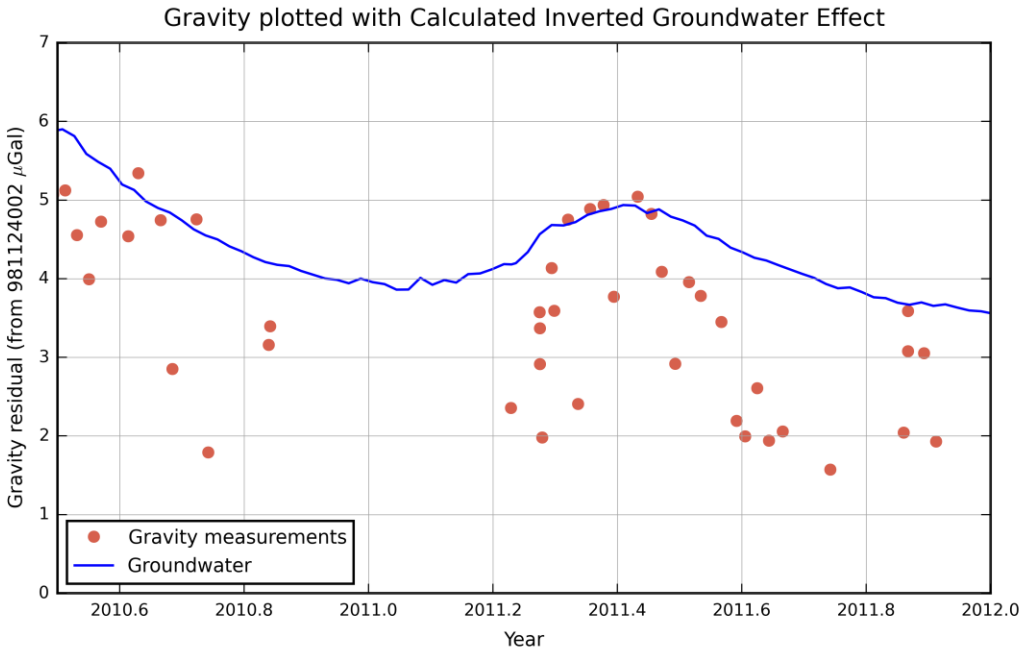

Figure 13.8 The calculated groundwater effect on gravity plotted with gravity measurements. The groundwater effect is adjusted to the scale of the gravity measurements.

If the calculated groundwater effect is increased by a factor of 2, the signal in the gravity data fits to the groundwater. This implies that the groundwater effect calculated in Chapter 11 is unrealistic. When the calculated δg_{gw} is applied to the entire time series, in Figure 13.10, little impact is made to the series.

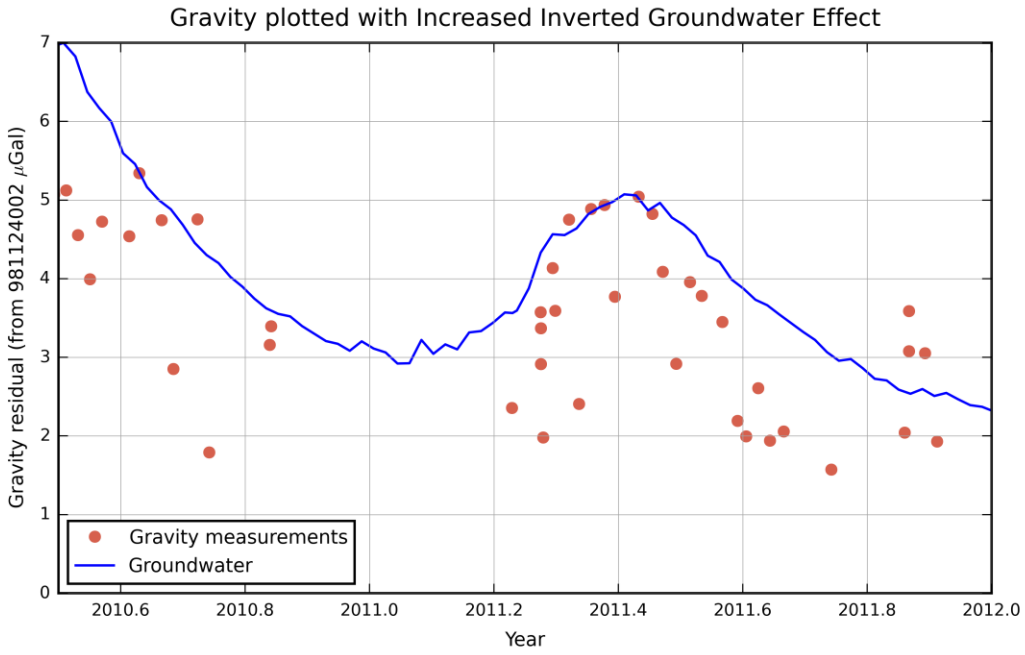

Figure 13.9 The gravity data plotted with an amplified groundwater effect during the 2011 drought period

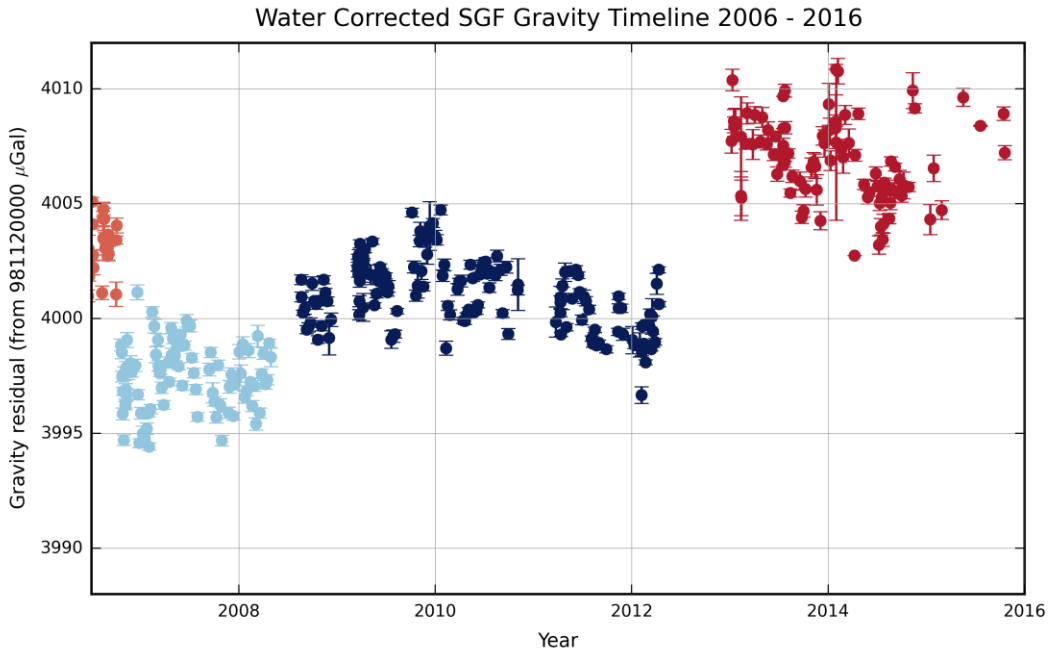

Figure 13.10 Gravity time series with calculated ground water effect removed

However, if the groundwater effect is increased by a factor of two and applied to the gravity time series the scatter of the data in regime three (2008.5 - 2013) is decreased but the data in regime 4 (2013-16) is forced to emulate the groundwater signal.

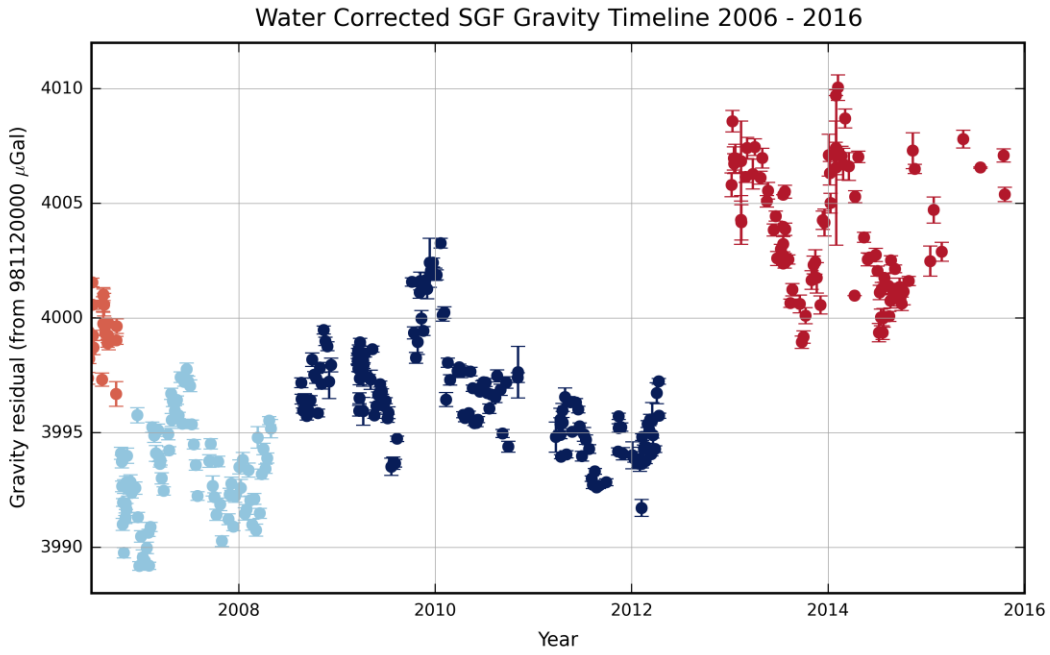

Figure 13.11 Gravity time series with the calculated gravity effect increased by a factor of two removed.

The result of this analysis tends to imply that the groundwater signal cannot be considered in isolation from the soil moisture on top of the basement. In the drought conditions in 2011 the soil on top of the basement is likely to have dried considerably allowing the clarity of the groundwater to become apparent in the gravity data. The influence of the groundwater and soil moisture signals have opposite signs and therefore have a cancelling effect within the time series.

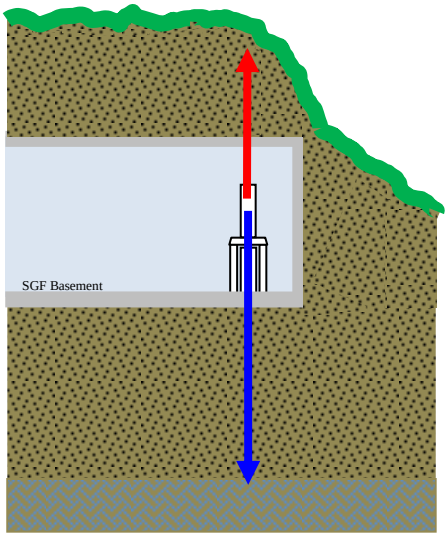

Figure 13.12 The opposite attraction of influences

It is evident that more investigations and greater knowledge of the site is required to accurately apply a correction to the gravity data for hydrological influences.

13.2.2. Interpretation Using Comparison Data

Another way of interpreting the data accurately is to apply bias offsets between each regime. However, to apply an offset a rationale should be employed. The implementation of the offsets found during the international comparisons, the results of which are presented in Chapter 7, provides one correction method. To apply the offsets, of +1.5, -2.0 and -0.08 µGal for each comparison respectively, may be somewhat open to debate since the instrument was found to be operating within accuracy specification on each occasion. However since offsets are known to occur for instrumental issues such as miscalibration of the clock or barometer (Nicolas, 2006) the rationale is considered fair.

Whilst Figure 13.2 implies an offset between each regime, Figure 13.13 shows the comparison-corrected time line. The data in regime 1 and prior to the SIM repair in Oct 2006, is removed due to the fact that it has no comparison data associated with it and the instrument had synchronisation issues.

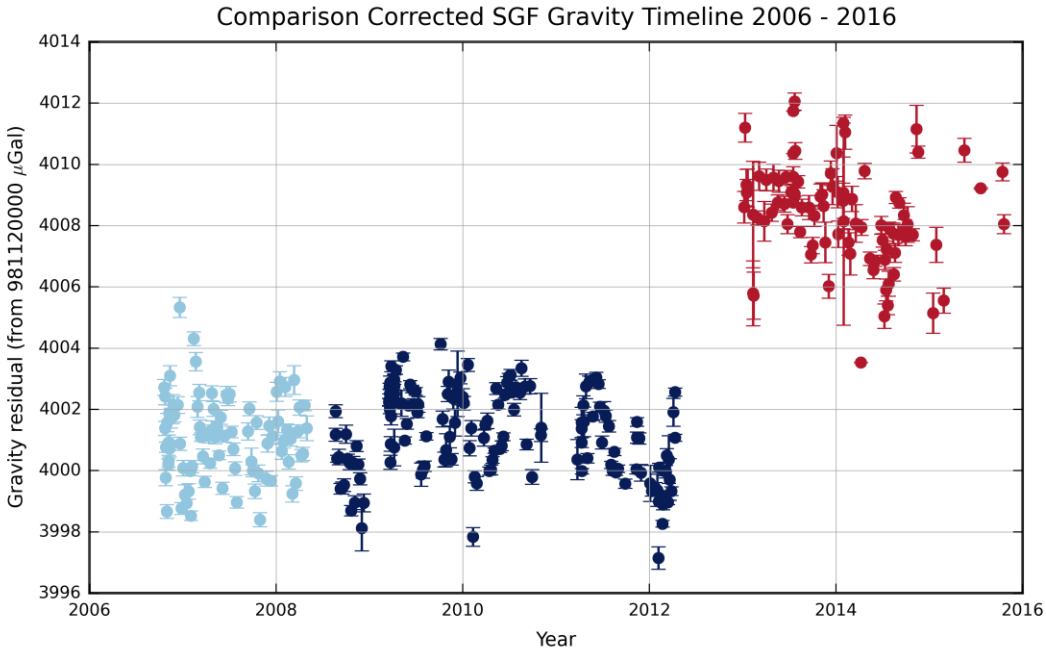

Figure 13.13 The comparison corrected time series, without groundwater correction.

It is seen that the application of the offsets in 2007 and 2012, where the FG5 was found to be 1.5 µGal low and 2.0 µGal respectively, smoothes the time line. However since the

offset found in 2015 was only 0.08 μGal the discontinuity which occurred in 2013 remains. This jump in the mean gravity value from 2012 to 2013 coincided with the upgrade of the FG5 to the FG5X.

Prior to the comparison in 2015, in order to investigate the step in gravity value, tests were conducted at the SGF to eliminate two known sources of offset error; the clock and the laser. FG5X was operated with two different WEO-100 lasers and two different clock sources (its onboard rubidium and the SGF H-MASER). No change in the gravity value was discernible. Following this Micro-g LaCoste had the instrument returned to Colorado to be investigated. The results found a possible electrical fault within the SIMX, stemming from the mains electrical voltage used (the UK uses 240 V, whilst the USA uses 120 V). Micro-g LaCoste installed corrective electrical protection into the electronics rack of FG5X-229 to correct any electrical problem. The FG5X then continued to operate perfectly at Micro-g LaCoste in Colorado, USA. The electrical protection did not result in a change in value at the SGF. Following this the instrument was taken to the comparison at Belval, Luxembourg, which also indicated the gravimeter was working perfectly.

Following these results an investigation was also carried out at the SGF comparing the measurements of the classic design FG5-222 with those of the FG5X. A 6-8 μGal differential between the measurements was found, with the FG5X reading higher than the classic FG5. The measurements from FG5-222 are consistent with the gravity time series from 2006-12. The difference suggests that the classic FG5 reads lower than the X at the SGF. However, the results from FG5-222 cannot be taken as definitely correct due to several factors:

- The gravimeter has not attended a comparison since 2011
- Major repairs have been carried out within the dropping chamber between 2012-15
- The laser beam in the interferometer was heavily diffracted, implying an internal problem in the beam path. This problem will drive the measured gravity lower than would otherwise be anticipated.

The data pre and post 2013 has been thoroughly checked for discrepancies. The latitude. longitude, elevation, ocean-loading, gravity gradient, nominal pressure are all identical in both. The fringe window, factory height, laser peak detection, and internal control card parameters are all the same at comparisons and the SGF. Therefore if the results from FG5-222 are ignored the implication is that it is SGF specific. However none of the physical or environmental investigations carried out to date have provided a satisfactory explanation.

Therefore, since these investigations have shown that the instrument has been operating correctly from 2013 the issue of implementation of the comparison offsets is continued. To analyse the impact of the application of the comparison offsets, yearly regime averages were produced. Figure 13.14 shows the results, with both corrected and uncorrected data.

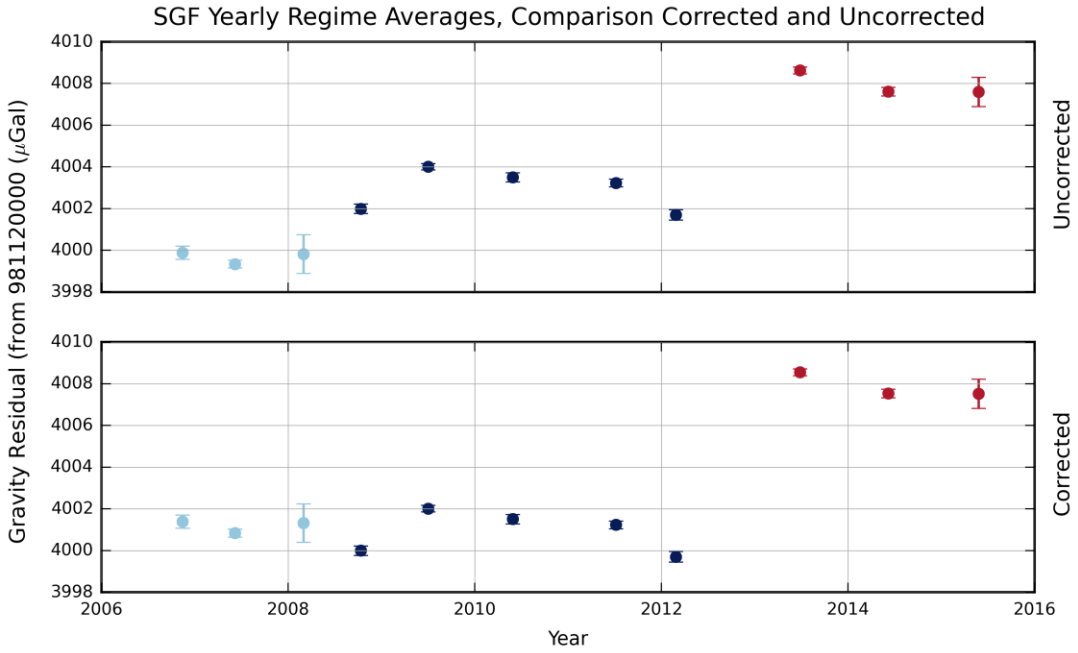

Figure 13.14 Uncorrected (top) and corrected (bottom) gravity time series of yearly regime averages

Both Figures 13.13 and 13.14 offer evidence in support of the application of the offsets, determined at the comparisons, but clearly do not explain the offset in the 2013-2016 data. To assess this 2013 bias, a residual bias value was calculated. The mean of the data from 2006-2012 was subtracted from the mean of the data from 2013-16 (all with comparison offsets applied). This residual bias was found to be 7.25 µGal. The calculated bias is applied in addition to the comparison offsets to the time series in Figures 13.15 & 13.16.

The scatter of the yearly averaged data is reduced by four fold, from ~10 µGal to ~2.5 µGal, whilst the scatter of the weekly project data is reduced by a third, from ~15 µGal to ~10 µGal.

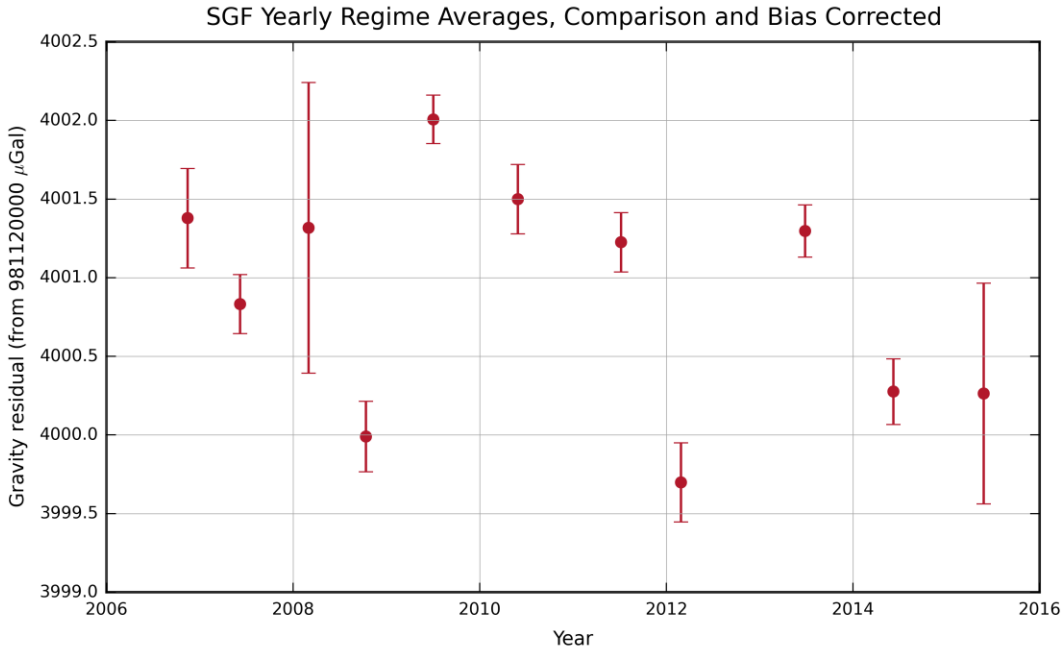

Figure 13.15 Yearly time series averages corrected with comparison results, and a bias 7.25 µGal for the 2013-16 data.

The bias applied to the entire time series results in a clearly anticipated alteration in the appearance of the time series. Showing excellent agreement throughout the ten years of measurements.

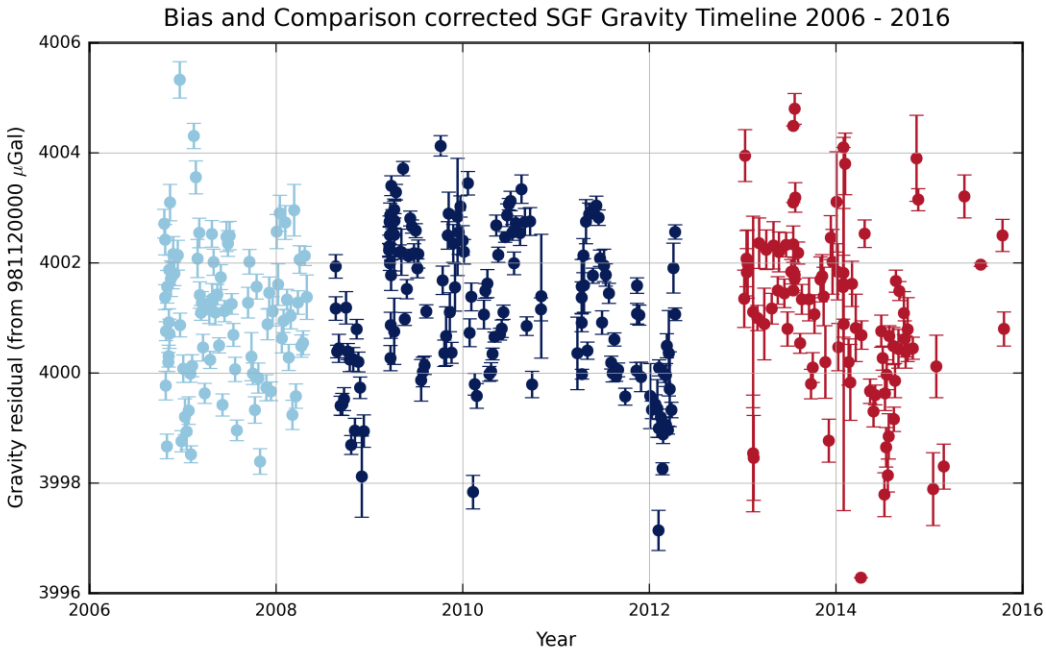

Figure 13.16 Gravity time series, of weekly project data, with comparison corrections and bias applied

13.3. Comparison of the Gravity Time Series with the SLR Coordinate Heights

An additional check on the bias application is to convert the gravity time series into temporal height changes. Various papers have been published including references to height changes, by (Richter, 2004) (Bilham, 2016), (Van Camp, 2003) for instance, using a conversion of -2 µGal/cm. The comparison of the two time series should strictly be conducted using the same treatment for atmospheric loading. However, in the data shown below the gravity data has the standard atmospheric corrections applied whereas the SLR has no atmospheric loading applied. Even so it is believed to be a valid comparison since previous studies, conducted at the SGF, using atmospheric loading in the SLR data have shown less than a 4mm change to the SLR heights with and without loading model.

If the height series of both techniques are started at an arbitary zero point and plotted together, the results are as shown in Figure 13.17. Of important note is that the bias offset is not seen in the SLR data from 2013 onwards and the comparison of the two techniques offers additional evidence in support of application of a mean, unaccounted for bias to the SGF AG data.

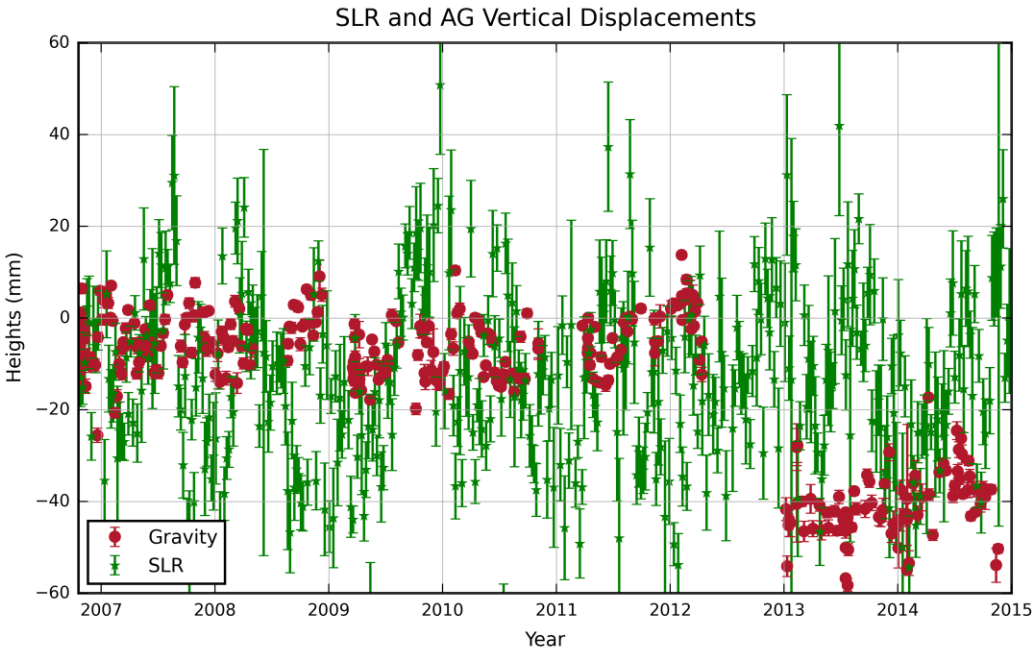

Figure 13.17 Vertical displacements from satellite laser ranging (green) and absolute gravity (red). Comparison offsets have been applied to the gravity data

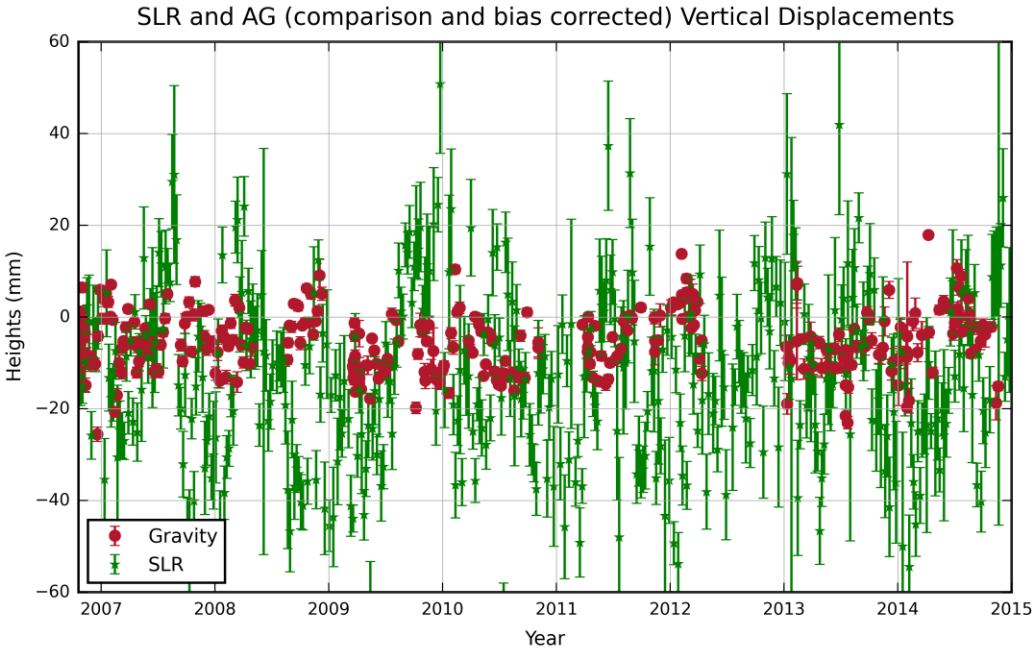

Figure 13.18 Vertical displacements from gravity measurements corrected for comparisons and bias plotted with the SLR vertical displacement product.

If the gravity data is corrected with the 7.25 μGal bias it is clear that the application of the bias is substantiated.

With additional geodetic techniques, or long term high frequency data it is clear the comparison offsets should be applied and, until a satisfactory physical explanation is found, a bias applied to the 2013-2016 data.

13.4. Simulation of Yearly Campaign Measurement at the SGF

The majority of FG5 gravimeters are employed in regular campaign measurements, where a measurement site is visited for a few days at a time. To simulate this data one project value, for the same month each year, was extracted from the SGF gravity time line. No data was obtained for the yearly epoch in 2012.

In this simulated scenario comparison corrections have been ignored as the instrument was found to be working correctly, and within accuracy tolerance, during international comparisons. The trend line shown in Figure 13.19 gives one interpretation of the data which may have been made at a site with only one occupation a year. The estimated rate of change in gravity obtained from Figure 13.19 is approximately 1.2 μGal/yr, or -0.60 mm/yr. Which is comparable to the GIA* rate obtained from SLR of -0.46 ±0.1 mm/yr (obtained by solving the SLR data for 1993 - 2016 for slope, annual and semi-annual terms) (Appleby, 2016).

However when the comparison offsets are applied, a trend line should not be applied, as the yearly values from 2006 - 2012 clearly flatten. Whilst the bias offset in 2013 remains, as shown in Figure 13.20.

* Glacial Isostatic Adjustment

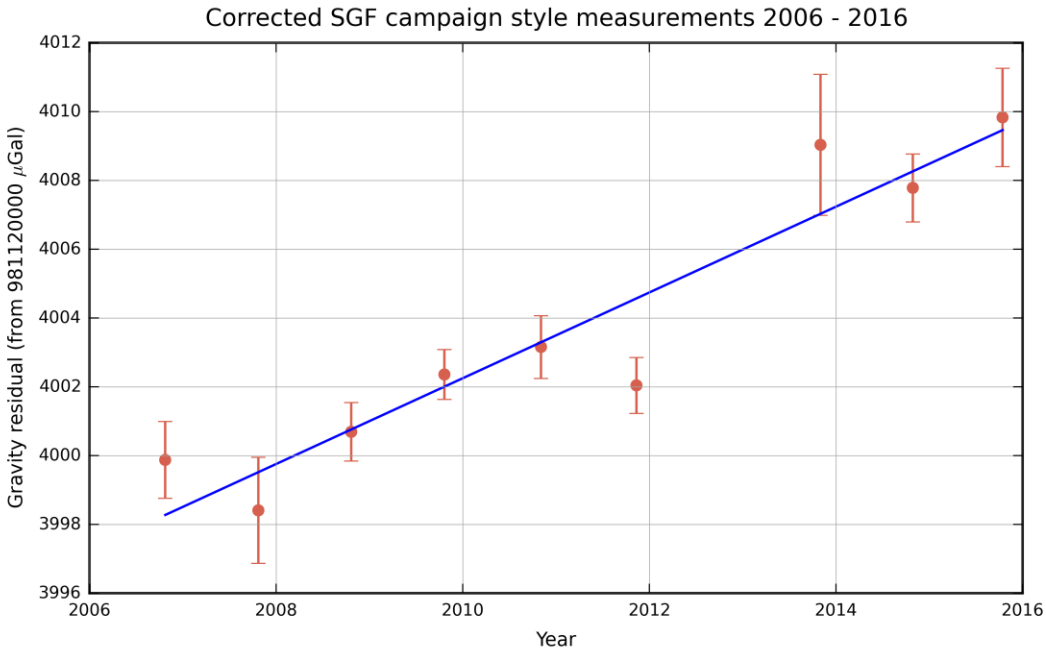

Figure 13.19 Simulation of yearly campaign type measurements for the SGF

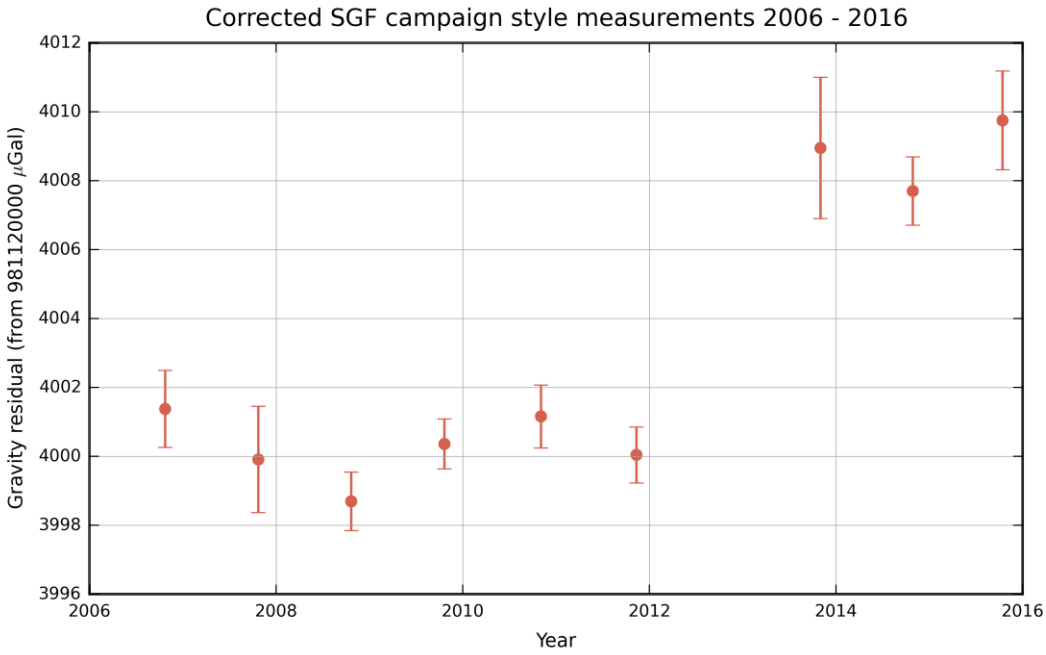

Figure 13.20 Campaign simulation with comparison offsets applied. Showing a linear term is clearly an incorrect interpretation of the data.

This simulation shows that if the comparison results are ignored the data may be interpreted incorrectly. These results could be used to support the more rigorous use of comparison

results in the geodetic community, which is a view currently only supported by the metrological community of AG users.

13.5. Conclusions

The high frequency, weekly data at the SGF has enabled environmental and instrumental changes to be identified. The phase lag between the changing depth of groundwater and the identification of the signal in the gravity data is unclear except in drought conditions were the soil above the gravity laboratory is thought to be dry. The phase lag is identified as 84 days. Implementation of the calculated effect on gravity shows minimal correction to the time series, however if the calculated value is increased by two fold the data from 2008-2012 is smoothed whilst the data from 2013-2016 is forced to resemble the groundwater signal. The implication of this is that the soil moisture is confirmed to be an essential measurement to enable the proper environmental corrections to be applied to the gravity time series. It is also surmised that differing lag values may be operating, depending on whether the ground water is rising or falling, for instance.

The time series of gravity measurements is clearly defined into four regimes of data, which are split by instrumental changes. One regime is ignored since it contains very early data with ongoing instrumental problems. Two regimes are smoothed by the application of offset corrections obtained by international comparisons (explained in Chapter 4 with results in Chapter 7) and one regime is corrected but still stands off by a bias of 7.25 μGal.

The project data and yearly averages of the project data confirm that the application of comparison offsets are justified and essential for the data between 2006 and 2012.

The geodetic technique products from the SLR and the AG show support for the idea that the 2013-2016 AG data has a bias offset, since the data are comparable until this event. The bias offset of the 2013-2016 data is of unknown origin, and is likely to remain unidentified until either a comparison with another gravimeter is performed at the SGF or an environmental cause is identified.

If the SGF site were occupied for one project only on an annual basis the data is open to misinterpretation. An subsidence rate of 0.60 mm/year is obtained if the uncorrected data is used. If comparison offsets are applied no rate can be inferred from the ten years of data available.

Chapter 14

Discussion

14.1. Introduction

This chapter explores the findings of the study, reiterates some of the strengths and weaknesses of the investigation and offers thoughts on the following:

- Development of absolute gravity resource at the SGF
- Benefits from long term, high frequency data
- Offset and bias corrections

14.2. Development of the Absolute Gravity Resource at the SGF

The establishment of the absolute gravity resource at the SGF has not been without its challenges, from exploiting and upgrading an existing suboptimal basement area, attaining the in depth knowledge to enable instrumental repair without addition of errors, through offsets or misalignments. However the multi-dimensional aspect of the gravimeter makes it an attractive instrument to learn. Having developed the expertise the SGF now offers the UK an absolute gravity resource, offering a long-term occupation of the SGF as a fundamental site and, with the addition of the NOC gravimeters, capability to provide gravity base stations for users. In fact, the SGF conducted the first campaign mission of this type in early 2012 in the Caribbean.

14.3. Benefits From Long-Term High Frequency Data

The long-term high frequency data obtained at the SGF is a unique data set, believed to be the first occupation of its kind in the world. The foray into gravity measurement and the

resulting time series of data has revealed previously unknown influences affecting the site at Herstmonceux.

A useful test of the periodic/tidal finding of this study will be the removal of the suspected tidal mis-modelling from the products of the space geodesy techniques and therefore the ITRF. Further work will be required to achieve this but the ten day data set offers compelling evidence which, once the data is filtered by removing the soil moisture signal, may prove conclusive and may provide enough information to obtain an estimation of a corrective model.

This work, if correct, substantiates corrections to be assessed and made to geodetic techniques at other geodetic stations. Improvements of the products of SLR and GNSS may be made through determination of any mis-modelled tidal loading constituents, which would impact on the accuracy of the ITRF. It would also offer support to the premise that gravity measurements should be taken at geodetic observatories, either by long-term relative or absolute means. This is especially for coastal sites or any observatories.

14.4. Offset and Bias Corrections

Historically, the SGF at Herstmonceux has been considered, by some, to be less than ideally located, since there the observatory rests upon a clay subsurface with no bedrock within 50 m below it. Local high-accuracy inter-technique levelling and the results of analyses of SLR and GNSS observation suggest that the site is extremely stable, but the gravity data may provide additional, independent evidence that the site is far better, or far worse, than perceived and as estimated from those techniques. If the offsets and bias in the AG series are assumed to be of instrumental origin and applied to the observations, then the short term station stability may be better than anticipated. However if the opposing interpretation is considered, the results suggest that there are large mass disturbances which may affect the site in unknown ways, perhaps driving a larger un-modelled motion in the station positions.

If the application of comparison offsets and bias correction is a correct assessment of how gravity data should be treated, this casts a worrying shadow over how data may be used in campaign measurements. In particular, as highlighted by this study, it is suggested that the entire AG community should look very carefully at the geophysical conclusions reached from campaign use of absolute gravimeters.

Chapter 15

Conclusions

15.1. Introduction

This study undertook to determine how the addition of an absolute gravimeter might improve knowledge of vertical displacements taking place at a fundamental geodetic station. The objective was to determine the benefit which might be gained, in line with the GGOS objectives, from a unique high frequency time series of absolute gravity data. The work contained in this thesis has encompassed installation of the gravimeter through to the establishment of operational criteria and data analysis of the measurements.

15.2. Principal Conclusions

The principal conclusions drawn from this study are as follows:

1. High frequency gravity data has highlighted:
    a. the need to apply offsets obtained from international or European comparison of gravimeters, to give greater consistency of results and provide more accurate interpretation.
    b. possible disadvantages to measurement campaigns and a low frequency of site occupation. Infrequent measurements would have resulted misinterpretation of the results in this specific case.

2. Residual systematic bias is possible in absolute gravity data even after removal of comparison offsets.

3. Comparison with additional geodetic techniques, mainly satellite laser ranging, has proved beneficial in this case, primarily due to the residual discontinuity in the gravity data which occurred between 2013 and 2016.

4. The ground water calculations do not provide enough information to correct for hydrological processes: soil moisture measurements are essential.

5. Residual, clearly tidal related, signatures in the hourly data may be an un-modelled tidal constituent, but are not entirely consistent with data taken from a local tide gauge. It is conjectured that the existing ocean-loading models are insufficient. The cause of this signal is still unknown. However if it is resolved sufficiently it could be applied to the SLR and GNSS data to study the impact.

The supporting evidence for the primary conclusions can be summarised:

The high frequency data can be used to show that offsets should be applied to the time series of data in sites with permanently installed gravimeters. The data could have been easily misinterpreted if infrequent measurements had been taken, this is supported by the evidence shown in Figures 15.1 and 15.2 where the time series is shown; in its entirety and with averages for each ‘regime’ of data and finally by simulating campaign style measurements, by selecting one data set per year at a similar epoch each year.

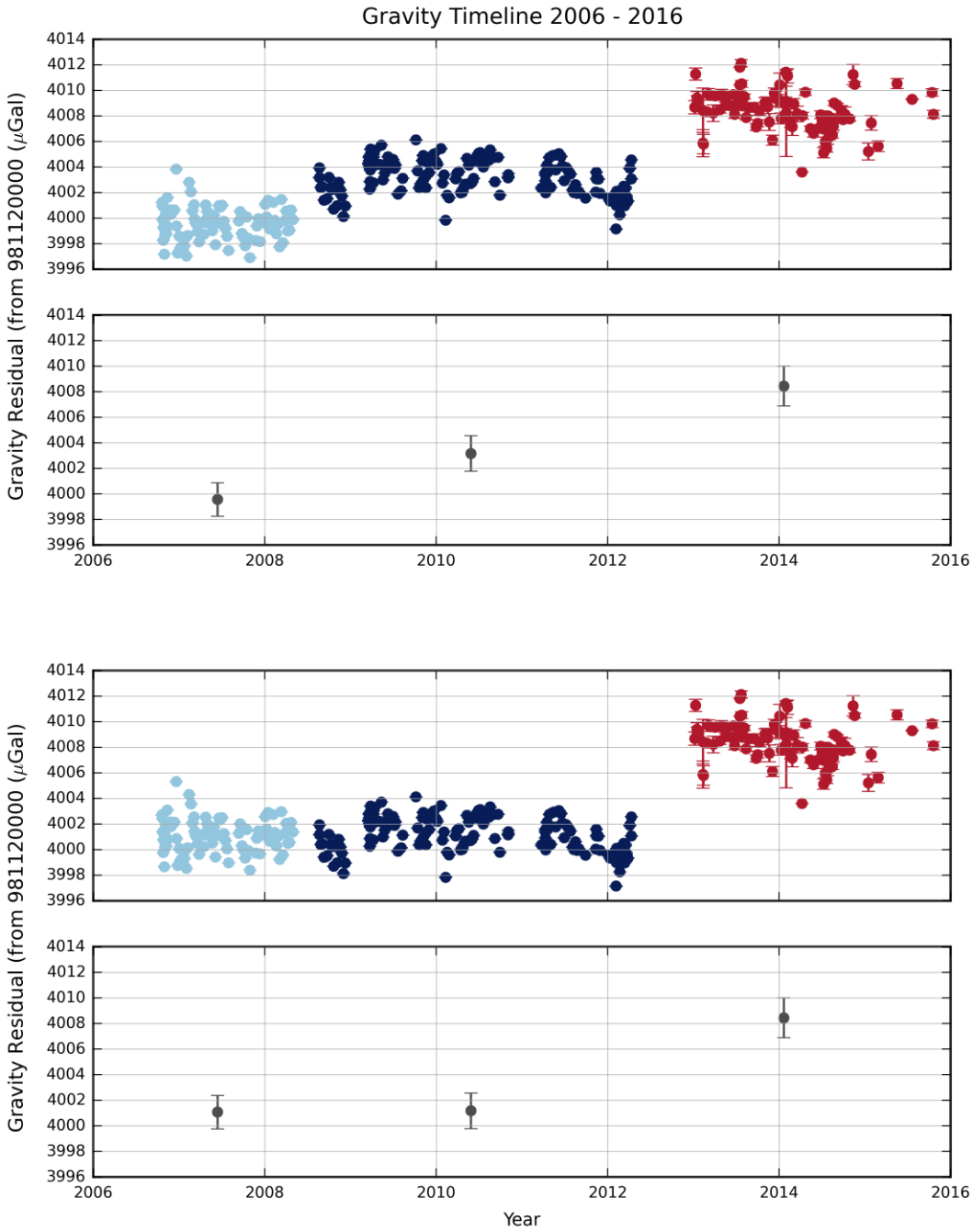

Figure 15.1 The SGF absolute gravity time series from 2006-16 with (lower) and without (upper) comparison offset corrections applied.

The offset-corrected data from 2006-2012 is shown to remove discontinuities in the data completely with excellent agreement both in value and associated standard

deviation. If the offsets are not applied single project data extracted on an annual basis leads to possible misinterpretation.

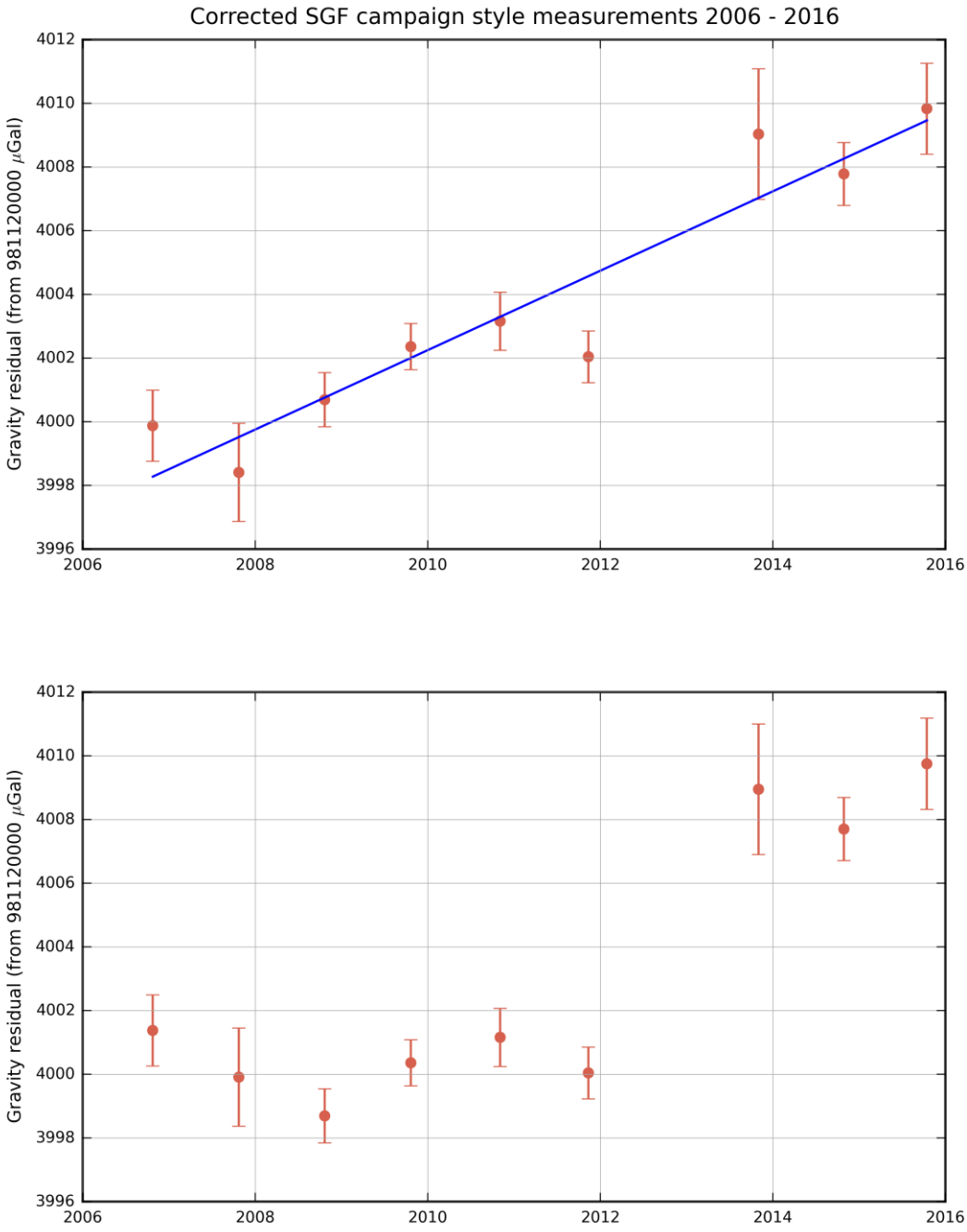

Figure 15.2 Campaign simulation gravity data, with and without comparison offsets applied. The top plot shows data without correction, bottom plot shows the data with comparison offsets applied.

1. A bias correction for the data from 2013-2016 removes discontinuities in the data and makes it consistent throughout the ten years of occupation at the SGF.

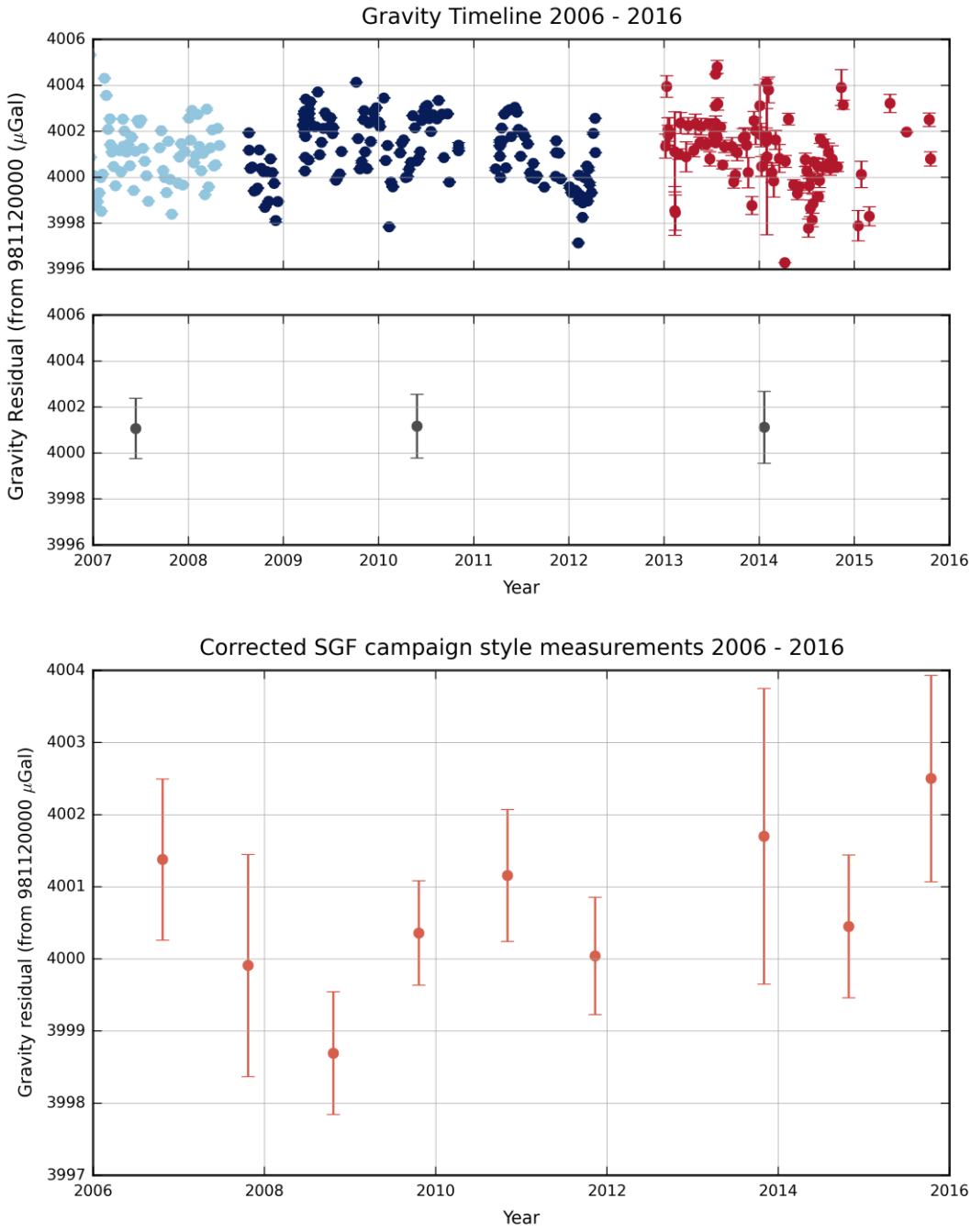

Figure 15.3 Corrected time series of absolute gravity data. The entire corrected series, with corrected regime averages, is shown in the upper plot. The lower plot is the corrected campaign simulation data.

2. The capacity to compare the AG time series with another geodetic technique enables the rational for the application of a bias to the 2013-2016 data. Since the comparison in Belval in 2015, showed the gravimeter to be working within expectations the offset in the data would have been considered as due to environmental factors. However whilst theory this cannot be entirely ruled out it is considered unlikely since the SLR data shows no indication of a similar signature in the data. No noticeable environmental changes occurred at the SGF between 2012-2013 to account for a mass change of a magnitude sufficient enough to change the gravity measurement by the 7.25 µGal in question.

3. The influence of ground water on the gravity data at the SGF is lower than anticipated. The ground water signal was not visible in the gravity data until a drought in 2011, where the soil on top of the basement is likely to have dried out significantly. This period would reflect minimisation of soil moisture counteracting the groundwater.

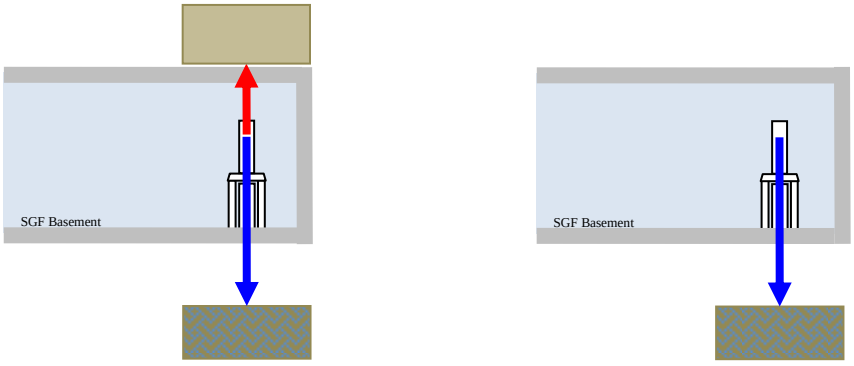

Figure 15.4 Opposing attraction from the changing water content of the soils above and below the gravimeter. (left), and the attractive mass which calculations have compensated for during this work (right).

4. The residual periodic signal in the hourly gravity data proves that the ocean-loading model for Herstmonceux requires adjustment. A detailed regional model is required to be fitted into the global model. An improved model would be utilised in SLR analysis also.

15.3. Secondary Conclusions

Secondary conclusions include:

1. Comparisons of gravimeters are hugely important and should be carried out on a frequent basis. Sites, such as the SGF, require data from more than one gravimeter to rule out bias errors.
2. A non perfect near coastal site without isolated pier to bedrock is capable of giving valuable and high precision, data.

3. The AG precision at the SGF is affected by seasonal variation.

4. High sensitivity interpretation of gravity results requires additional sensors, such as groundwater, soil moisture and rainfall.

5. Measurement precision at the SGF is affected by local weather as well as wave interaction both locally and from the Atlantic / North Sea.

6. Environmental controls are required for permanent locating an FG5, consistent or rapidly changing humidity negatively affects the FG5.

7. The FG5 is a highly sensitive instrument which requires expertise to operate successfully and avoid unnecessary problems with a time series of data
   .
8. When designing a new measurement site comparison capability, as well as the capability to house different types of gravimeter should be built in.

15.4. Future Research

This study can be expanded in future studies by:

- Inclusion of an Earth tide meter at the station, to accurately measure the tidal constituents at Herstmonceux and thereby remove reliance on predictive models. Or a involvement from an oceanographer to generate a detailed ocean-loading model.
- A thorough hydrological investigation should be carried out at the SGF, to include the installation of soil moisture probes at multiple depths and other additional meteorological sensors. BGS hydrology experts should be consulted in the attempt to thoroughly characterise the hydrological and subsurface factors which influence the gravity data.
- The three UK gravimeters should be employed to expand UK gravity knowledge by:
    - the continuation of the SGF data
    - FG5-103 should be used for another permanent installation, perhaps at BGS Eskdalemuir.
    - FG5-222 should be used as a comparison machine at the two permanent installations and as a campaign machine when required.
    - The ‘gap’ software should be modified to enable the 2013-2016 data to be processed.

Appendix 1

Economic Appraisal for RTP of Absolute Gravimeter at SGF, Herstmonceux.

Background. The NERC Space Geodesy Facility (SGF) has a national and international reputation for observational and developmental excellence in the field of space geodesy. In the 2002/03 NERC Services Review, the Facility was awarded maximum scores in all categories. In particular, its satellite laser ranging (SLR) system is among the most prolific and stable in the world. The SLR technique is complemented at Herstmonceux by continuously operating Global Navigation Satellite System (GPS and GLONASS) receivers as well as automated meteorological and groundwater-level recording systems. An Absolute Gravimeter from the Proudman Oceanographic Laboratory (POL) has been placed on-site at Herstmonceux twice in recent years for calibration and benchmarking purposes (Williams, *et al*, 2001).

This proposal seeks to broaden the scientific benefit to the UK and international communities by making available, on a regular basis, precise measurements of absolute gravity at this unique fiducial site in the UK. The Facility Steering Committee, the NSGSC, at its annual meeting on 25th May 2004, endorsed this proposal. Funds to purchase the gravimeter during 2004/05 have been made available from Services and Facilities Capital Budget (attached letter from Dr Lin Kay).

Science Case. This proposal to expand the scope of the observational capability of the SGF into very accurate gravity monitoring is particularly timely. Key to Earth-system monitoring is maintenance of a terrestrial reference system with accuracy in global scale of 1 part per billion. In order to develop such a capability within the European and global community, an initiative to establish a European Combined Geodetic Network (ECGN, Ihde, Baker, *et al*, 2003) is underway within the auspices of EUREF, a European sub-

commission of the International Association of Geodesy. One of the objectives of ECGN is to establish core sites where geometric positioning (GPS/GLONASS/SLR), physical height and gravity field components are all measured to sub-cm accuracy. Given the SGF long record of precise space geodetic and ancillary measurements, a UK consortium comprising researchers from POL, the OS, the University of Nottingham and the SGF itself have proposed to ECGN that the Herstmonceux site be accepted as a 'station' within ECGN. However, the current weakness in this proposal is the very sparse absolute gravity measurements obtained at the site (only two one-week visits in 8 years). The proposed absolute gravimeter for permanent operation at Herstmonceux would address this weakness and would be able to contribute to the community frequent absolute gravity measurements from this site of precisely known location within the international terrestrial reference frame. In addition, the site would be very valuable for side-by-side inter-comparison of the POL, and other European absolute gravimeters, an essential, on-going requirement for this precise work. This proposal would make the SGF into one of the leading observational facilities worldwide, because of the range of different techniques that would be available, precisely inter-linked through local survey, on one site. In collaboration with POL, it will undoubtedly strengthen absolute gravimetry work within the UK.

Specifically, the absolute gravimeter observations will be used to determine the vertical crustal movements at Herstmonceux to better than 1 mm/year (Williams *et al*, 2001). The absolute gravimetry technique is completely independent of the space geodesy measurements and will therefore provide an important check on any systematic errors in those measurements or in their interpretation. According to post-glacial rebound models, southern England is undergoing subsidence as the Earth's mantle flows back under the areas previously covered by the ice sheets. The rate of the 'fore-bulge' collapse is estimated to be 1mm/year, but its determination through space geodetic observations is compromised by the existence of 10mm-level seasonal height variations. These seasonal height variations are due to large-scale surface loading deformations of the Earth caused by hydrological, atmospheric pressure and ocean mass redistributions as well as, almost certainly, local hydrological loading effects. Such seasonal mass variations cause seasonal variations in the Earth's centre of mass, which is the origin of the reference frame for space

geodetic measurements. The availability of the absolute gravity data will provide important information on these global seasonal signals, as well as higher frequency local deformations from the seasonal to the tidal bands.

Options Appraisal.

A discussion of options is set out below, but we argue that the only option that will significantly address the science case made above is that an absolute gravimeter be purchased for permanent installation at Herstmonceux.

1. Do nothing. Since we are arguing for new equipment to expand the capability and value of the SGF site, to do nothing would save the capital costs and ongoing maintenance costs detailed below. It would however, in our opinion, be a lost opportunity for expansion of the capability of the SGF site.
2. Hire the instrument from the manufacturers. We understand from the only suppliers worldwide of this instrument, that hiring is not an option. The other option that we seriously considered was more frequent occupations at Herstmonceux by the POL instruments. However, despite best efforts to make regular visits to Herstmonceux, the busy schedule dictated by the POL science plan has meant only two visits during the last eight years. This is not sufficient to engage in long-term monitoring of the site, particularly since understanding of and subtraction from real signal of local environmental changes (groundwater, ocean loading, local interference, etc) will need gravity observations on a range of timescales, from seasonal to tidal.
3. Purchase an absolute gravimeter and operate at Herstmonceux. This option will provide the flexibility required to address the science objectives discussed. Ready access to the instrument will allow operations to be scheduled, in a cost-effective way alongside laser ranging operations, to build up a detailed picture of the environmental effects that will have to be understood to realise the long-term monitoring goal. The costs of purchase and on-going maintenance, calculated over the next ten years, may be summarised:
    a. Purchase, delivery and on-site training of instrument from Micro-G Solutions Inc in year 0. $335,000 + VAT/10 yr = £221,300 /10 yr

b. Running costs, to include 2-year return to manufacturer = £25,000/ 10yr
c. Refurbishment of basement at SGF in year 0 = £10,000/ 10 yr

Net cost of Option 3 £256,300/ 10 yr

Project Management

Purchase of the system will be managed by the Head of Service, Dr Graham Appleby and support engineer/scientist Victoria Smith. David Benham, Facility Mechanical Engineering Manager will oversee the refurbishment of the SGF basement, working with Victoria Smith to prepare a suitable and safe environment in which to set up and operate the gravimeter. She will advise the HoS on the final acceptance of the instrument, after the chosen manufacturer sets it up on site. Ideally, she will also attend a pre-delivery training session at the manufacturer's premises. In the longer term, Victoria Smith will manage the operation of the gravimeter, in consultation with SGF Operations Manager Philip Gibbs, and train SGF staff in the effective and safe use of the equipment. She will be responsible for the accuracy of the initial results and be encouraged to work towards a further degree by making a unique contribution to setting up and making available this new facility.

Appendix 2

Ordnance Survey Gravity Laboratory Survey Report

The table below gives coordinates of the four absolute gravimeter location studs in the gravity laboratory. Data obtained from the Ordnance Survey report "Coordination of RGO Absolute Gravimeter at Herstmonceux"

Final ETRS89 Coordinates			
Station	Latitude (dms)	Longitude (dms)	Elip-Height (m)
101	N 50 52 1.84836	E 0 20 10.49036	64.499
102	N 50 52 1.91441	E 0 20 10.49271	64.499
103	N 50 52 1.97248	E 0 20 10.49195	64.500
104	N 50 52 2.01309	E 0 20 10.49236	64.499

Table 4. Final ETRS89 Coordinates

More information about the UK's Ordnance Survey can be found at:
https://www.ordnancesurvey.co.uk/

Appendix 3

Example of Project text file and Set text file, as produced by ‘g’

Project file

Micro-g Solutions g Processing Report
File Created: 06/17/10, 15:20:33

Project Name: herg1120.10
g Acquisition Version: 4.041500
g Processing Version: 7.070307

Company/Institution:
Operator: vs

Station Data
Name: Grav Room
Site Code: Pier 1
Lat: 50.86718 Long: 0.33625 Elev: 19.38 m
Setup Height: 13.40 cm
Transfer Height: 130.00 cm
Actual Height: 130.03 cm
Gradient: -3.080 µGal/cm
Nominal Air Pressure: 1005.70 mBar
Barometric Admittance Factor: 0.30
Polar Motion Coord: -0.0694 " 0.3694 "
Earth Tide (ETGTAB) Selected
Potential Filename: C:\Program Files\Micro-g Solutions Inc\gWavefiles\ETCPOT.dat

Delta Factor Filename: C:\gData\OceanLoad-Grav Room.dff

Delta Factors

Start	Stop	Amplitude	Phase	Term
0.000000	0.002427	1.000000	0.0000	DC
0.002428	0.249951	1.160000	0.0000	Long
0.721500	0.906315	1.154250	0.0000	Q1
0.921941	0.974188	1.154240	0.0000	O1
0.989049	0.998028	1.149150	0.0000	P1
0.999853	1.216397	1.134890	0.0000	K1
1.719381	1.906462	1.161720	0.0000	N2
1.923766	1.976926	1.161720	0.0000	M2
1.991787	2.002885	1.161720	0.0000	S2
2.003032	2.182843	1.161720	0.0000	K2
2.753244	3.081254	1.07338	0.0000	M3
3.791964	3.937897	1.03900	0.0000	M4

Ocean Load ON, Filename: C:\gData\OceanLoad-Grav Room.olf

Waves:	M2	S2	K1	O1	N2	P1	K2	Q1	Mf	Mm	Ssa
Amplitude (µGal):	2.262	0.724	0.517	0.257	0.347	0.130	0.241	0.055	0.244	0.117	0.065
Phase (deg):	174.6	122.9	67.4	168.7	-86.9	85.6	139.3	-161.1	2.6	21.0	100.7

Instrument Data

Meter Type: FG5

Meter S/N: 229

Factory Height: 116.63 cm

Rubidium Frequency: 10000000.00000 Hz

Laser: WEO100 (000000)

ID: 632.99117754 nm (1.19 V)

IE: 632.99119473 nm (0.73 V)

IF: 632.99121259 nm (0.34 V)

IG: 632.99123023 nm (-0.04 V)

IH: 632.99136890 nm (-1.24 V)

II: 632.99139822 nm (-1.21 V)

IJ: 632.99142704 nm (-1.23 V)

Modulation Frequency: 8333.330 Hz

Processing Results

Date: 04/22/10

Time: 12:12:39

DOY: 112

Year: 2010

Time Offset (D h:m:s): 0 0:0:0

Gravity: 981124002.01 µGal

Set Scatter: 1.23 µGal

Measurement Precision: 0.25 µGal

Total Uncertainty: 1.88 µGal

Number of Sets Collected: 25

Number of Sets Processed: 25

Set #s Processed: 1,2,3,4,5,6,7,8,9,10,11,12,13,14,15,16,17,18,19,20,21,22,23,24,25

Number of Sets NOT Processed: 0

Set #s NOT Processed:

Number of Drops/Set: 150

Total Drops Accepted: 3739

Total Drops Rejected: 11

Total Fringes Acquired: 700

Fringe Start: 19

Processed Fringes: 601

GuideCard Multiplex: 4

GuideCard Scale Factor: 250

Acquisition Settings

Set Interval: 60 min

Drop Interval: 10 sec
Number of Sets: 25
Number of Drops: 150

Gravity Corrections
Earth Tide (ETGTAB): -31.79 µGal
Ocean Load: 0.07 µGal
Polar Motion: 1.34 µGal
Barometric Pressure: 3.18 µGal
Transfer Height: 0.09 µGal
Reference Xo: -0.00 µGal

Uncertainties
Sigma Reject: 3.00
Earth Tide Factor: 0.001
Average Earth Tide Uncertainty: 0.03 µGal
Ocean Load Factor: 0.10
Average Ocean Load Uncertainty: 0.01 µGal
Barometric: 1.00 µGal
Polar Motion: 0.05 µGal
Laser: 0.05 µGal
Clock: 0.50 µGal
System Type: 1.10 µGal
Tidal Swell: 0.00 µGal
Water Table: 0.00 µGal
Unmodeled: 0.00 µGal
System Setup: 1.00 µGal
Gradient: 0.00 µGal (0.03 µGal/cm)
Comments
None

Set file

Source Data Filename: herg1120.10

g Acquisition Version: 4.041500

g Processing Version: 7.070307

Set	Time	DOY	Year	Gravity	Sigma	Error	Uncert	Tide	Load	Baro	Polar	Trans	Refxo	Temp	Pres	Acc	Rej
1	00:12:32	112	2010	981124003.684	6.890	0.564	1.947	-63.664	0.578	3.997	1.341	0.092	-0.002	30.064	1019.027	149	1
2	01:12:35	112	2010	981124003.169	6.145	0.502	1.930	-77.806	0.466	3.876	1.341	0.092	-0.002	30.101	1018.623	150	0
3	02:12:40	112	2010	981124001.866	7.012	0.573	1.949	-84.245	0.165	3.752	1.341	0.092	-0.002	30.121	1018.212	150	0
4	03:12:40	112	2010	981124001.823	6.955	0.568	1.948	-83.477	-0.221	3.689	1.341	0.092	-0.002	30.145	1018.001	150	0
5	04:12:40	112	2010	981124001.776	6.715	0.548	1.943	-77.230	-0.572	3.612	1.341	0.092	-0.002	30.163	1017.744	150	0
6	05:12:34	112	2010	981123999.284	6.483	0.533	1.939	-67.987	-0.772	3.583	1.341	0.092	-0.002	30.154	1017.648	148	2
7	06:12:40	112	2010	981124000.456	6.410	0.523	1.936	-58.322	-0.745	3.656	1.341	0.092	-0.002	30.149	1017.891	150	0
8	07:12:40	112	2010	981124000.775	6.397	0.522	1.935	-50.478	-0.471	3.685	1.341	0.092	-0.002	30.164	1017.987	150	0
9	08:12:37	112	2010	981124000.600	7.494	0.614	1.961	-45.715	0.011	3.655	1.341	0.092	-0.002	30.172	1017.887	149	1
10	09:12:46	112	2010	981124004.076	6.001	0.493	1.927	-44.103	0.607	3.563	1.341	0.092	-0.002	30.180	1017.582	148	2
11	10:12:40	112	2010	981124001.438	7.468	0.610	1.963	-44.538	1.189	3.416	1.341	0.092	-0.002	30.187	1017.090	150	0
12	11:12:40	112	2010	981124002.272	7.517	0.614	1.967	-45.019	1.632	3.289	1.341	0.092	-0.002	30.190	1016.667	150	0
13	12:12:40	112	2010	981124001.772	5.940	0.485	1.933	-43.226	1.835	3.122	1.341	0.092	-0.002	30.211	1016.112	150	0
14	13:12:40	112	2010	981124002.965	6.281	0.513	1.939	-37.227	1.745	2.947	1.341	0.092	-0.002	30.180	1015.527	150	0

15	14:12:37	112	2010	981124002.918	4.770	0.391	1.907	-26.161	1.371	2.775	1.341	0.092	-0.002	30.195	1014.956	149	1
16	15:12:40	112	2010	981124003.563	5.559	0.454	1.918	-10.628	0.782	2.647	1.341	0.092	-0.002	30.211	1014.529	150	0
17	16:12:40	112	2010	981124001.441	6.207	0.507	1.929	7.141	0.092	2.667	1.34 1	0.092	-0.002	30.196	1014.596	150	0
18	17:12:37	112	2010	981124000.452	5.326	0.438	1.913	23.781	-0.567	2.624	1.3 41	0.092	-0.002	30.221	1014.452	148	2
19	18:12:40	112	2010	981124000.151	5.731	0.468	1.923	35.579	-1.074	2.682	1.341	0.092	-0.002	30.203	1014.643	150	0
20	19:12:40	112	2010	981124002.205	6.833	0.558	1.948	39.320	-1.339	2.696	1.341	0.092	-0.002	30.225	1014.692	150	0
21	20:12:40	112	2010	981124001.289	6.574	0.537	1.942	33.297	-1.328	2.800	1.341	0.092	-0.002	30.225	1015.036	150	0
22	21:12:40	112	2010	981124001.689	5.576	0.455	1.919	17.781	-1.068	2.772	1.341	0.092	-0.002	30.202	1014.944	150	0
23	22:12:40	112	2010	981124003.338	6.280	0.513	1.932	-4.924	-0.633	2.684	1.341	0.092	-0.002	30.197	1014.650	150	0
24	23:12:40	112	2010	981124002.725	5.805	0.474	1.921	-30.962	-0.136	2.714	1.341	0.092	-0.002	30.210	1014.751	150	0
25	00:12:45	113	2010	981124003.136	5.325	0.438	1.913	-55.813	0.308	2.655	1.341	0.092	-0.002	30.217	1014.555	148	2

Uncert - uncertainty

Baro - barometer correction

Trans - Transfer (between instrument height and measurement height)

Temp - Temperature

Pres - Pressure

Acc - Accepted (number of drops)

Rej - Rejected (number of drops)

Appendix 4

Hourly Precision Plot Comparisons Between VgHx and ‘g’, 2006-2016

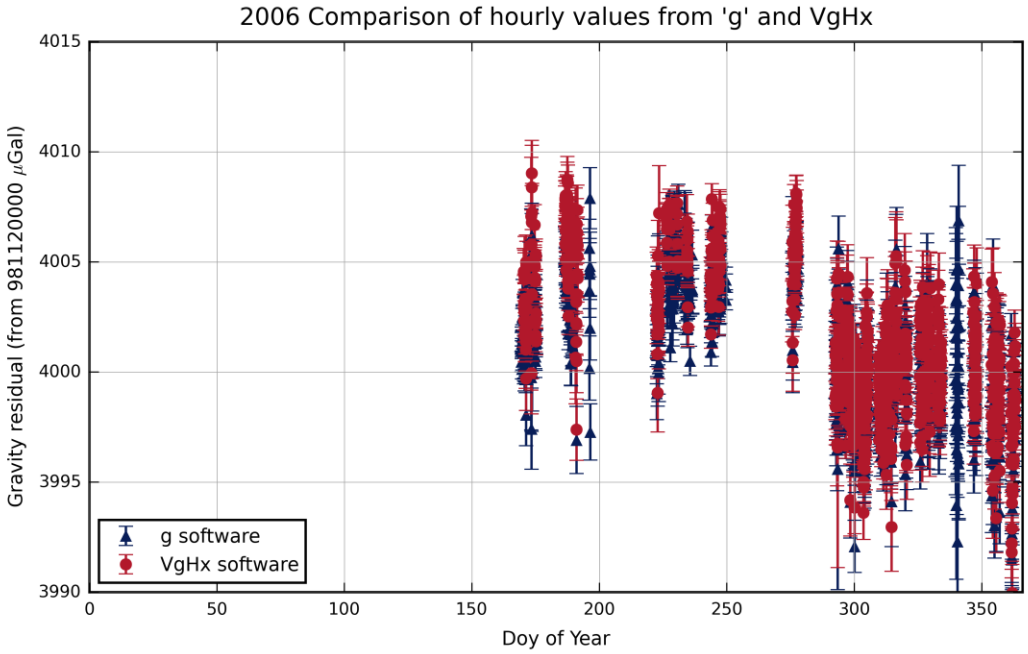

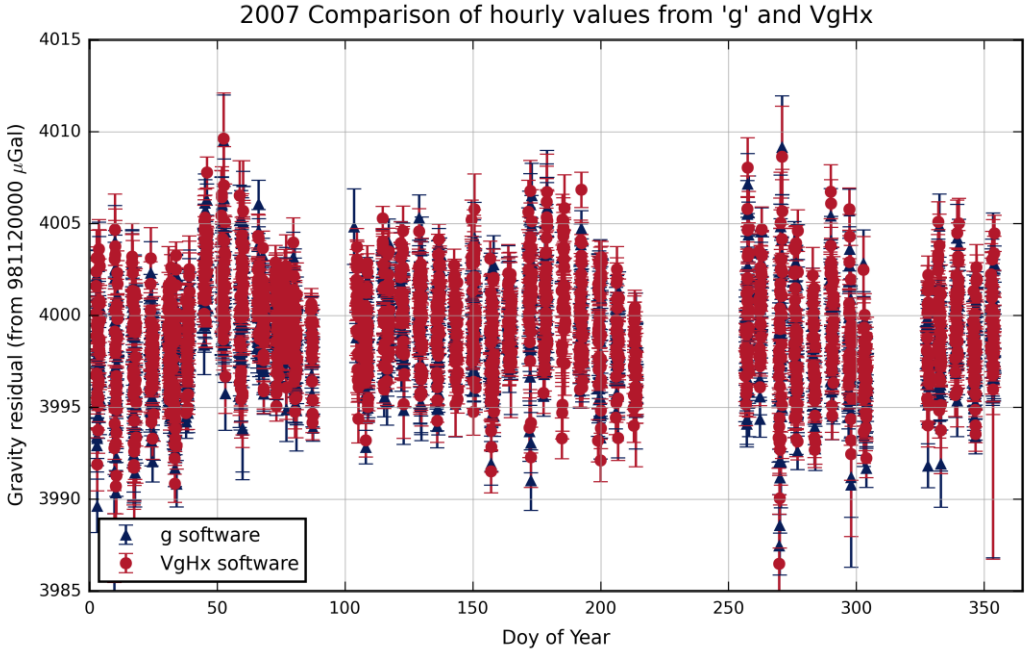

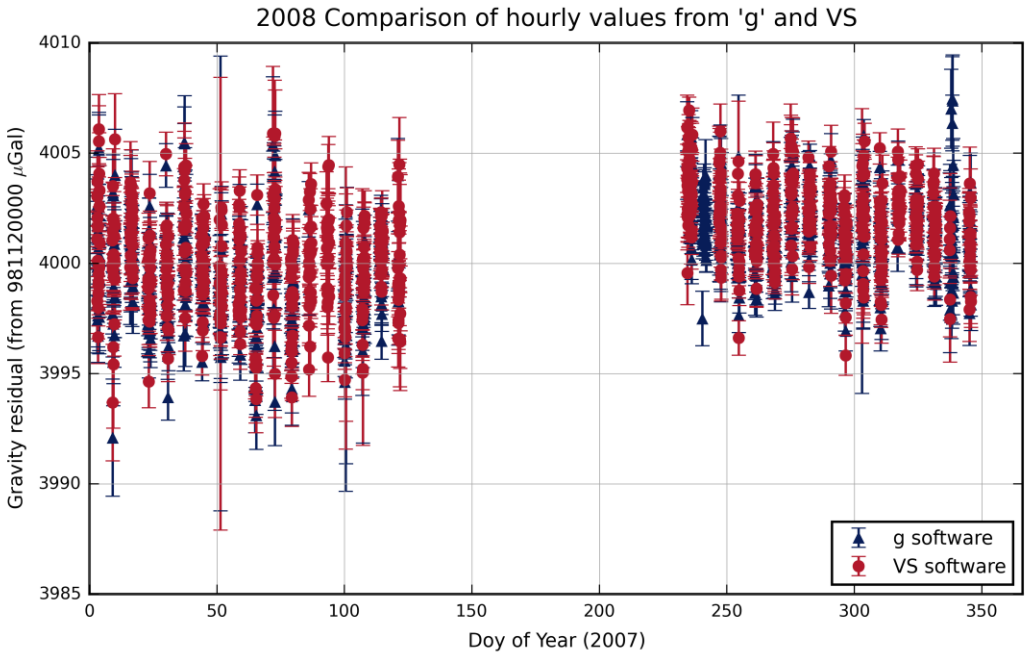
2008 Comparison of hourly values from 'g' and VS
Gravity residual (from 981120000 μGal)
Doy of Year (2007)
g software
VS software
4010
4005
4000
3995
3990
3985
0
50
100
150
200
250
300
350

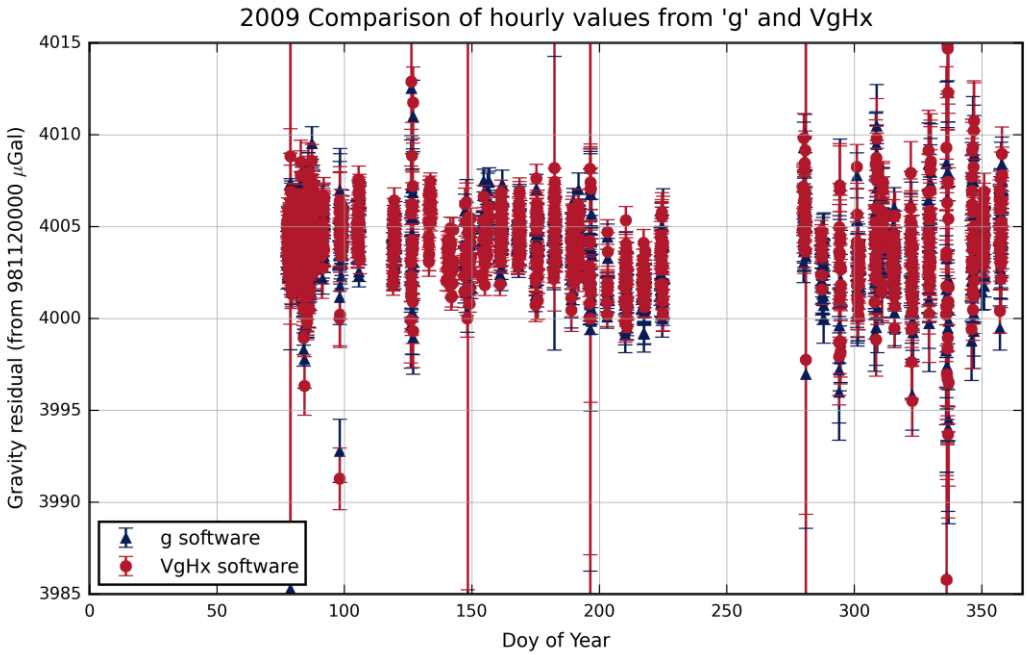
2009 Comparison of hourly values from 'g' and VgHx
Gravity residual (from 981120000 μGal)
Doy of Year
g software
VgHx software
4015
4010
4005
4000
3995
3990
3985
0
50
100
150
200
250
300
350

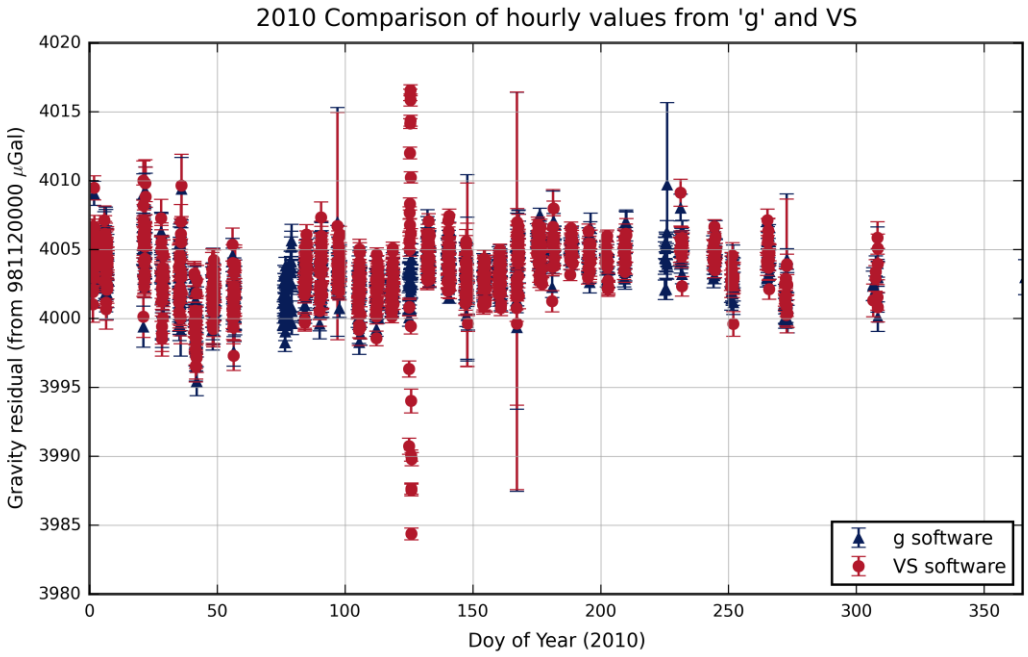
2010 Comparison of hourly values from 'g' and VS
Gravity residual (from 981120000 μGal)
Doy of Year (2010)
g software
VS software
4020
4015
4010
4005
4000
3995
3990
3985
3980
0
50
100
150
200
250
300
350

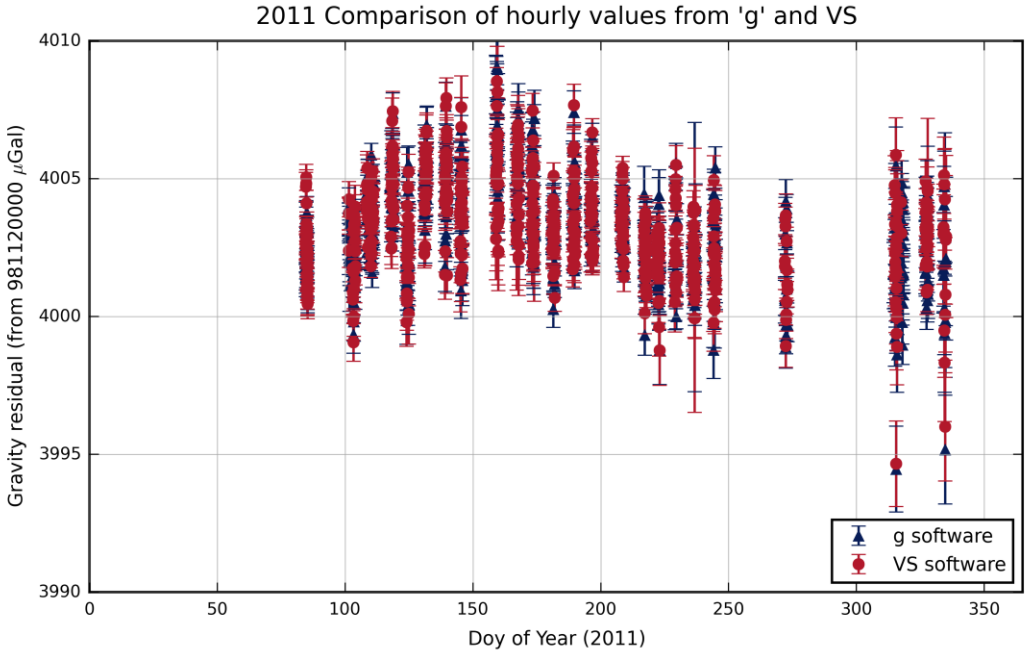
2011 Comparison of hourly values from 'g' and VS
Gravity residual (from 981120000 μGal)
Doy of Year (2011)
g software
VS software
4010
4005
4000
3995
3990
0
50
100
150
200
250
300
350

Appendix 5

Yearly Precision Plots from VgHx (2006-2012) and ‘g’ (2013-2016)

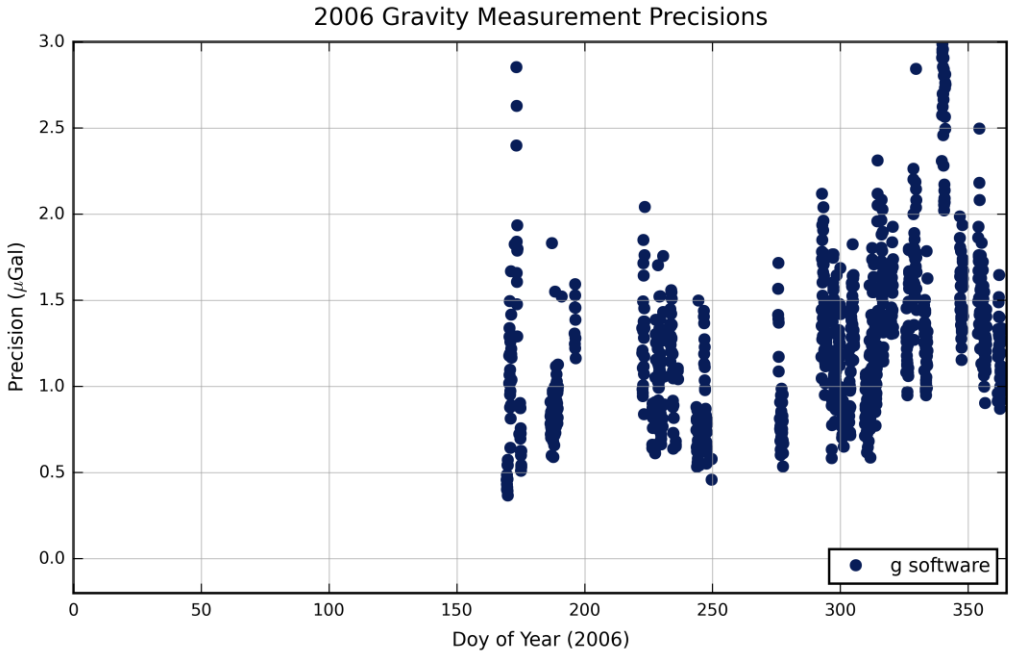

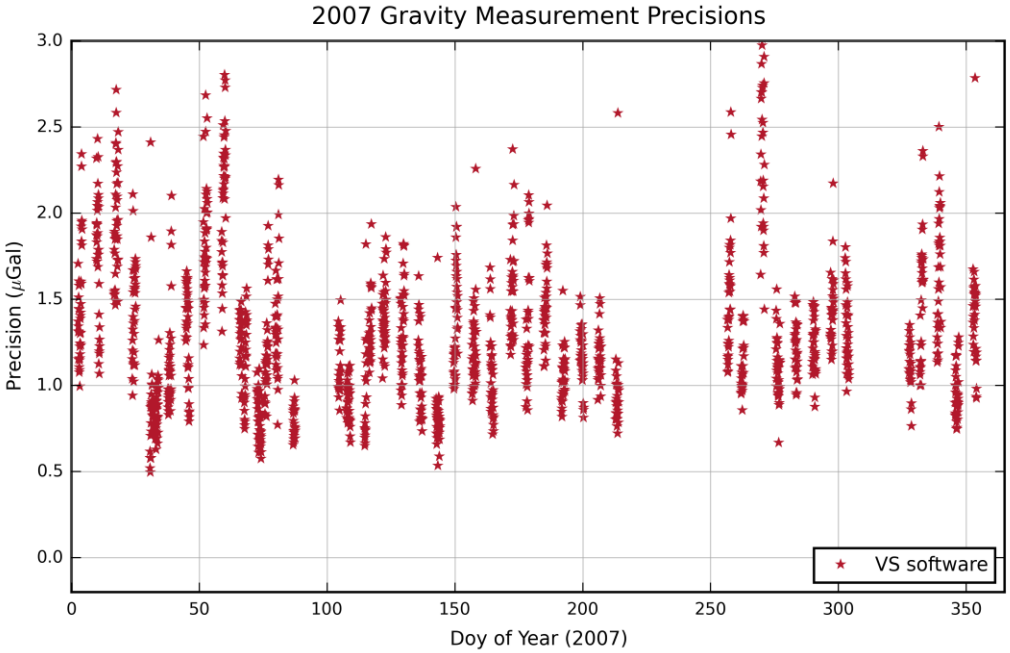
2007 Gravity Measurement Precisions
Precision (μGal)
Doy of Year (2007)
VS software
0.0
0.5
1.0
1.5
2.0
2.5
3.0
0
50
100
150
200
250
300
350

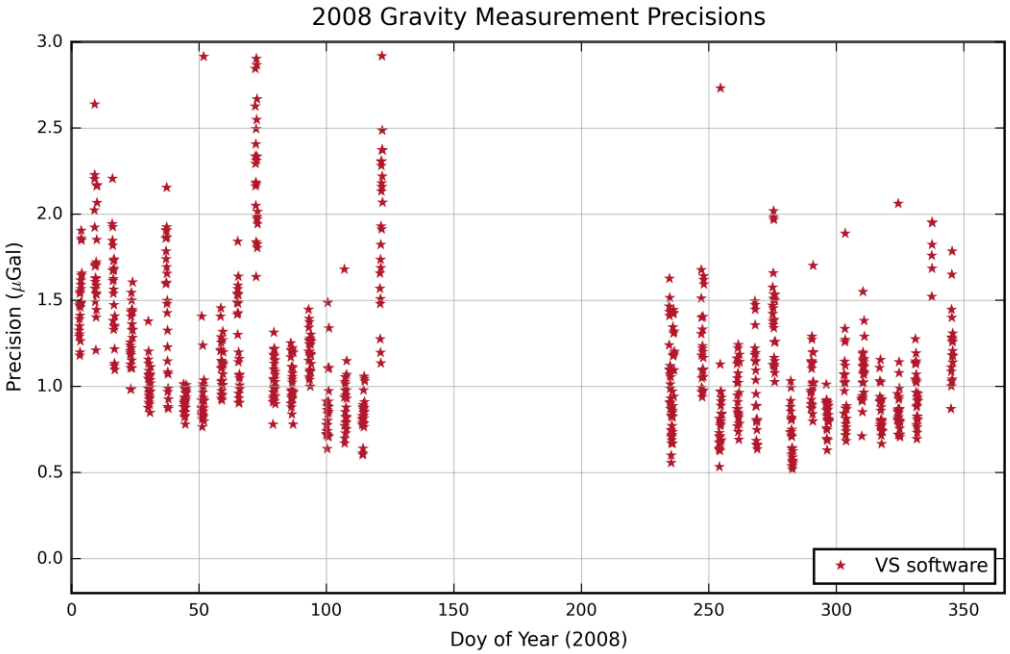
2008 Gravity Measurement Precisions
Precision (μGal)
Doy of Year (2008)
VS software
0.0
0.5
1.0
1.5
2.0
2.5
3.0
0
50
100
150
200
250
300
350

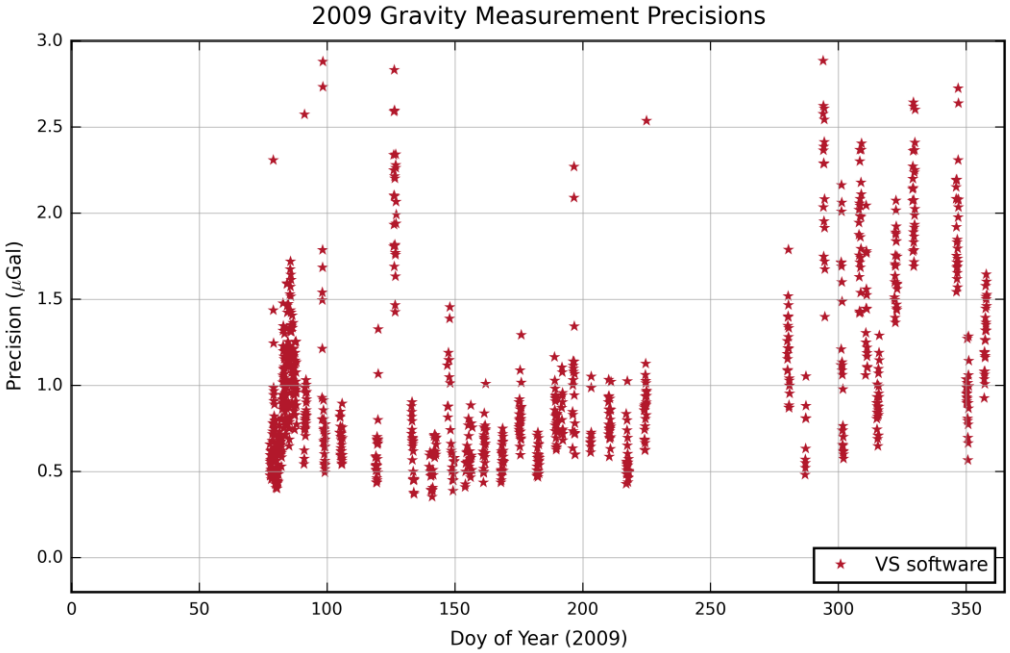
2009 Gravity Measurement Precisions
Precision (μGal)
Doy of Year (2009)
VS software
0.0
0.5
1.0
1.5
2.0
2.5
3.0
0
50
100
150
200
250
300
350

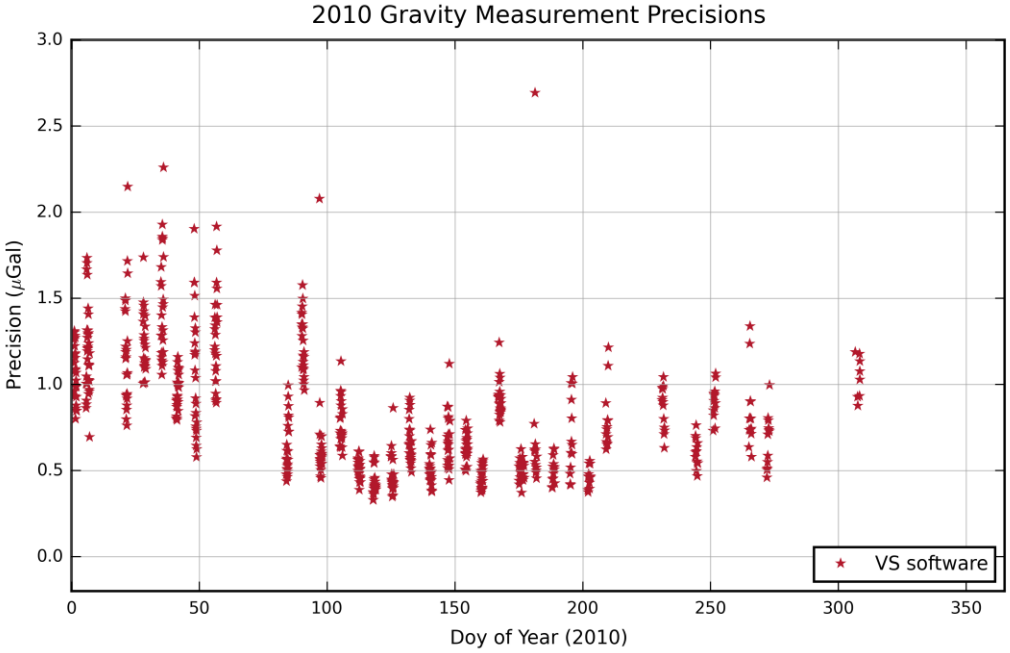
2010 Gravity Measurement Precisions
Precision (μGal)
Doy of Year (2010)
VS software
0.0
0.5
1.0
1.5
2.0
2.5
3.0
0
50
100
150
200
250
300
350

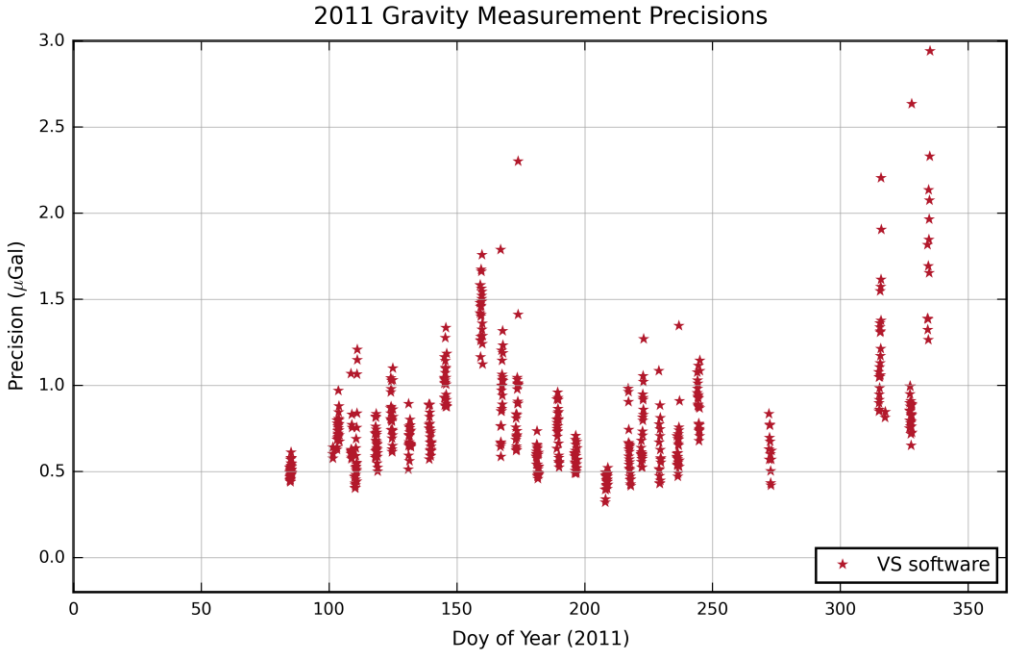
2011 Gravity Measurement Precisions
Precision (μGal)
Doy of Year (2011)
VS software
0.0
0.5
1.0
1.5
2.0
2.5
3.0
0
50
100
150
200
250
300
350

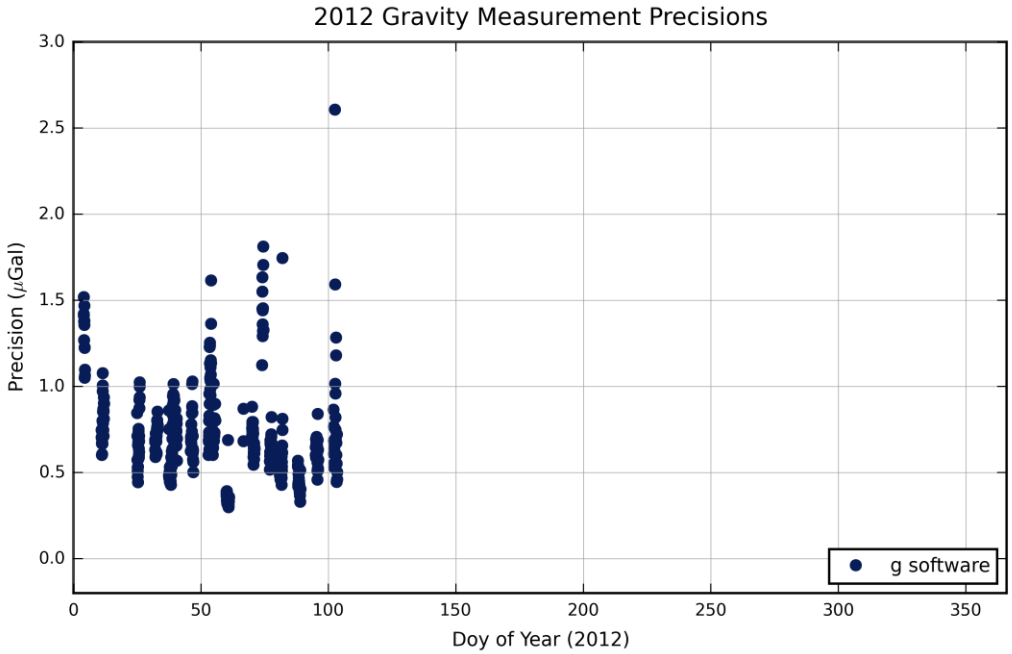
2012 Gravity Measurement Precisions
Precision (μGal)
Doy of Year (2012)
g software
0.0
0.5
1.0
1.5
2.0
2.5
3.0
0
50
100
150
200
250
300
350

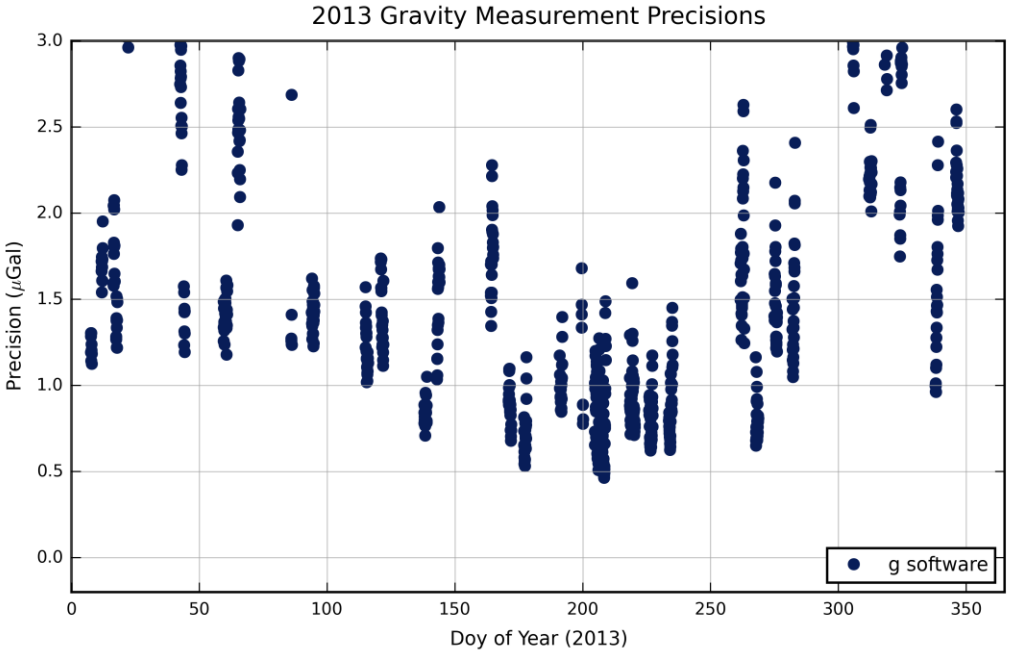
2013 Gravity Measurement Precisions
Precision (μGal)
Doy of Year (2013)
g software
0.0
0.5
1.0
1.5
2.0
2.5
3.0
0
50
100
150
200
250
300
350

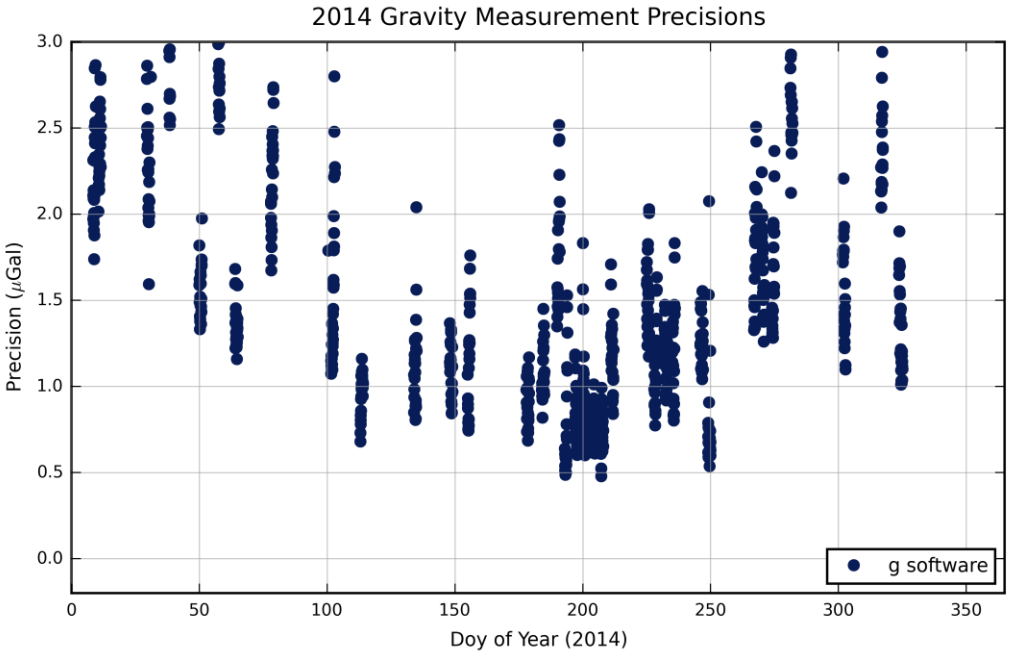
2014 Gravity Measurement Precisions
Precision (μGal)
Doy of Year (2014)
g software
0.0
0.5
1.0
1.5
2.0
2.5
3.0
0
50
100
150
200
250
300
350

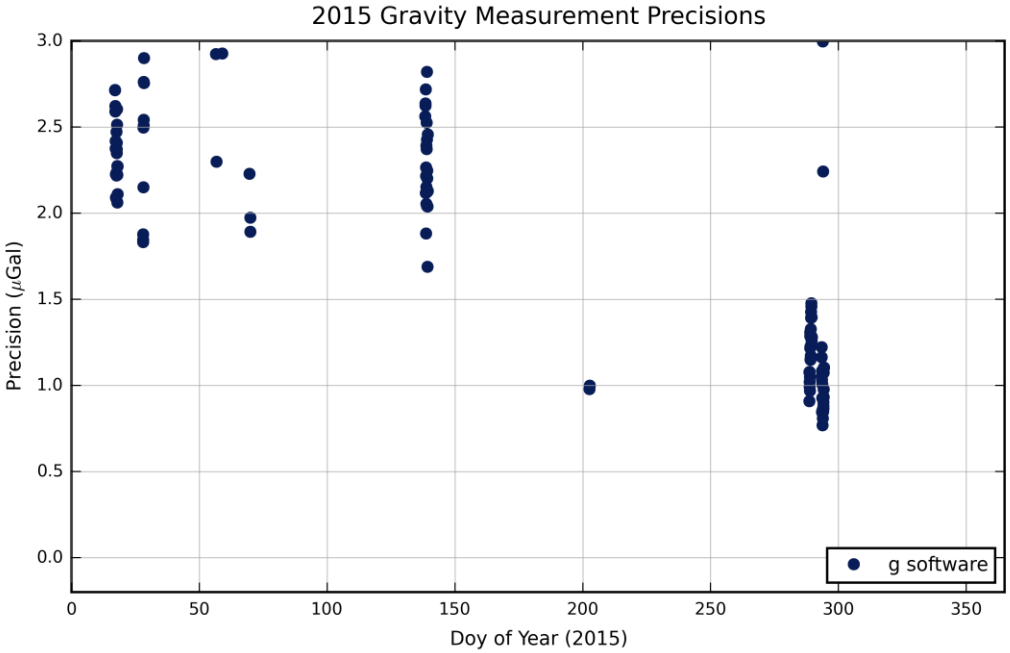
2015 Gravity Measurement Precisions
Precision (μGal)
Doy of Year (2015)
g software
0.0
0.5
1.0
1.5
2.0
2.5
3.0
0
50
100
150
200
250
300
350

APPENDIX 6

Ocean loading model constituents

From the Chalmers free ocean tide loading provider: http://holt.oso.chalmers.se/loading/index.html

For the Herstmonceux site latitude and longitude

	M2	S2	N2	K2	K1	O1	P1	Q1	Mf	Mm	Ssa
Schwiderski											
	1.793	0.583	0.265	0.209	0.479	0.245	0.123	0.051	0.187	0.045	0.105
	-165.6	-115.5	90.4	-142.5	-68.7	-166.7	-83.9	154.1	-9.7	-46.8	-63
	194.4	244.5	-269.6	217.5	291.3	193.3	276.1	-205.9	350.3	313.2	297
GOT00.2											
	1.035	0.593	0.189	0.171	0.512	0.249	0.157	0.115	0.137	0.067	0.075
	-167.7	-103.4	-149.9	-97.1	-65.8	-154.8	-69.1	151.6	19.8	13.2	3.1
	194.4	256.6	210.1	262.9	294.2	205.2	290.9	-208.4	-340.2	-346.8	-356.9
FES2004											
	1.015	0.449	0.195	0.171	0.494	0.242	0.159	0.088	0.131	0.083	0.083
	-168.3	-105.3	-169.9	-85.5	-58.9	-157.4	-58.7	156.9	21.5	16.8	3
	194.4	254.7	190.1	274.5	301.1	202.6	301.3	-203.1	-338.5	-343.2	-357
Topex 7.2											
	1.222	0.599	0.21	0.234	0.459	0.226	0.127	0.081	0.126	0.088	0.082
	-154.4	-106.9	-151	-92.6	-68.6	-157.9	-70.6	139.7	25.5	15.7	3
	194.4	253.1	209	267.4	291.4	202.1	289.4	-220.3	-334.5	-344.3	-357
CSR 4.0											0.98
	0.591	0.197	0.175	0.489	0.548	0.168	0.077	0.137	0.066	0.075	
	-166.8	-117.1	-145.8	-112.1	-72	145.9	-79	128.8	19.9	13.2	3.1
	194.4	242.9	214.2	247.9	288	-214.1	281	-231.2	-340.1	-346.8	-356.9

Schwiderski ocean loading model, used in ‘g’ versions 7-9

M2	S2	N2	K2	K1	O1	P1	Q1	Mf	Mm	Ssa
2.262	0.724	40.347	0.241	0.517	0.257	0.130	0.055	0.244	0.117	0.065
174.6	122.9	85.6	139.3	67.4	168.7	85.6	-161.1	2.6	21.0	100.7

Appendix 7

Early Operation of the FG5 prior to the Completion of the Gravity Laboratory in 2006

Due to the over run of the renovation work, the FG5 was delivered to the SGF in May 2005, 9 months before the basement gravimetry room was finally completed. During which time attempts were made to install and run the gravimeter in alternative locations. None of the data collected within those 9 months has been used in this work, due to issues explained later in the chapter.

In June 2005, the initial attempt made use of a disused building, property of Queens University Canada International study centre, less than 100 m and to the East of the SGF. The building formed the physics block during the years of Royal Greenwich Observatory (RGO) occupation, but had lain disused for around 15 years. Although it was thought that the site offered a reasonably low level of seismic activity and the least decayed room was chosen, the attempt had to be aborted due to a significant build-up of condensation, particularly beneath the FG5.

A hole in the upper layer of the SGF office flooring.

The second attempt was made within the SGF perimeter, in one of the office buildings that were added to the site in the mid 1990s. Although they were largely made of timber, and could be considered of a temporary construction, the office buildings were laid on a thick concrete base, and therefore it was thought that they could offer a valid temporary home for the FG5. In late June 2005, the gravimeter was moved into the South East office, where a hole was cut in the polystyrene upper of the flooring to provide access to the building's concrete base, thus giving an adequate floor for absolute gravity measurements.

A lack of knowledge and understanding of the behaviour characteristics of the gravimeter laser meant that a there was a delay of approximately 2 weeks before an attempt was made to operate the gravimeter. It is now known that the WEO-100 laser is susceptible to humidity changes and can require a significant time period to stabilise and produce laser light. Unfortunately, in 2005 there was insufficient knowledge available, which resulted in attempts to align the cavity of the laser, a course of action which was ill-fated and should have been avoided. Some of the characteristics and lessons learnt about the WEO-100 are discussed thoroughly in Chapter 8.

Because of issues caused by the attempt to align the cavity of the laser, it was sent to Micro-g LaCoste for repair. Following the return of the laser from Micro-g LaCoste, after alignment and optimisation, although the laser power output was good, the power output at the collimation assembly, on the end of the fibre optic (see Chapter 2 for a description of the laser and coupling into the interferometer), was minimal. Thus, adjustment to the alignment of the five axis mount, the coupling from the laser bed into the fibre optic, had to be made to optimise the transmission of the laser through the fibre optic and obtain sufficient power for the FG5 to operate.

The next complication to arise was an inability of the cart to either drop or oscillate successfully within the dropping chamber. This was caused by two problems located within the system interface module (SIM)*: a connectivity problem of the EPROM† cards, which were not connecting correctly and therefore was cured by a simple readjustment of the cards within their housings; and incorrect tuning of the dropping chamber motor controls. This latter fault caused both the oscillate mode (required for measurement of the fringe signal) and the drop mode (used to measure ‘g’ or to conduct tests) of the cart to fail. The failure in either caused abnormal noise (a knock or hum) or complete cessation in the control of the cart. The solution to faults of this type requires retuning of the dropping motor controls, which is achieved through the adjustment of five potentiometers (pos-gain, pos-damp, s-gain, s-damp and ff-gain) on the dropping card control board. Where:

---

* SIM - System Interface Module within the electronics rack of the FG5

† EPROM - Erasable programmable read-only memory

- pos-gain is the position servo, which keeps the cart on trajectory held in the EPROM cards
- s-gain is the sphere servo, which keeps the test mass assembly a set distance from the cart during freefall.
- ff-gain is the main control signal, which drives the cart

The motor tuning dictates the power and control of the cart during the lift, the hover, and the drop of the cart. In this instance, the poor tuning caused:

- Insufficient power to lift the cart, so it could not be lifted at all, or by a fraction only
- Vibration at the 'hover' phase
- Failure to control the drop (the cart would impact the base plate)

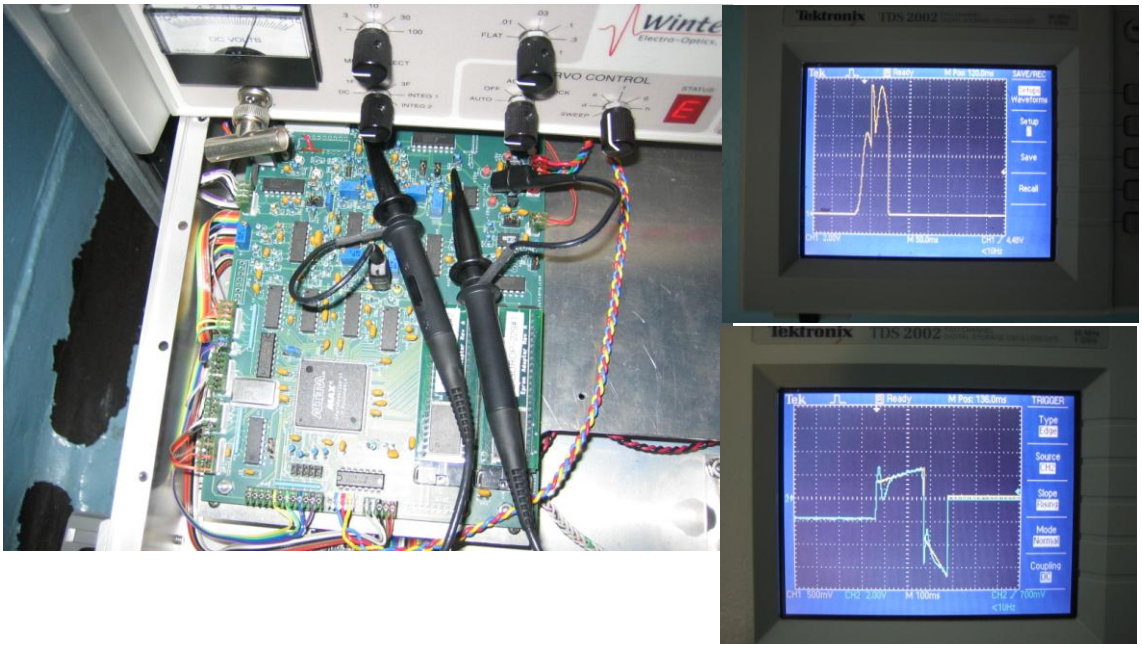

Testing the dropping chamber controller board, with oscilloscope traces. The motion of the cart is shown on the on the upper oscilloscope trace in yellow, whilst the lower trace shows the model drop in yellow and the actual drop, after some tuning, in blue.

The retune of the dropping controller board was undertaken on successive days for approximately a week; each attempt appeared successful but the gravimeter was found to

be inoperable several hours later. The cause of the repeated tuning failure was attributed to a 24-hour, 15-degree (Celsius) temperature fluctuation in the office building. This level of temperature variation resulted in an instability in the electronic drive card tuned to provide sufficient power to drive the mechanical components within the dropping chamber, such that when the dropping chamber was tuned to operate at the higher temperature, it was later found to be insufficient at the lower temperature and therefore manifested the problems described above.

Additionally however, following the return of the electronics rack and dropping chamber, Micro-g LaCoste reported (van Westrum, 2005) that the dropping controller circuit board was badly corroded (on the reverse of the board); the electrical pathways were so badly oxidised that the board was replaced entirely. The oxidation of the board may have also contributed to the tuning problems. Therefore no further attempts were made to operate the FG5 in this location.

With the elimination of these two sites, the former physics block opposite the SGF and the South East office, as viable locations in which to operate the FG5 all other possible locations were rejected at this point. Consequentially the FG5 was mothballed to await the completion of the gravity laboratory.

Installation in the Gravity Laboratory

In April 2006, the FG5 was moved into the newly finished gravimetry room in the basement. During the warm-up of the gravimeter, after a vacuum had been established in the dropping chamber and whilst waiting for the laser to stabilise, the temperature of the laboratory was measured to be 13°C and the humidity was found to be 98%; neither were considered beneficial to the FG5 and so a dehumidifier was installed (and the laser switched off), which stabilised to a respectable 19 °C and 69.5% over a 7-day period.

The chart recorder trace shown in Figure 8.6 shows several weeks of measurements starting 2nd May 2006. The measurements are not continuous and have breaks in the data. The

green line shows the overall decrease in relative humidity over the time period, whilst the red line shows the temperature increasing from 13 to 21°C.

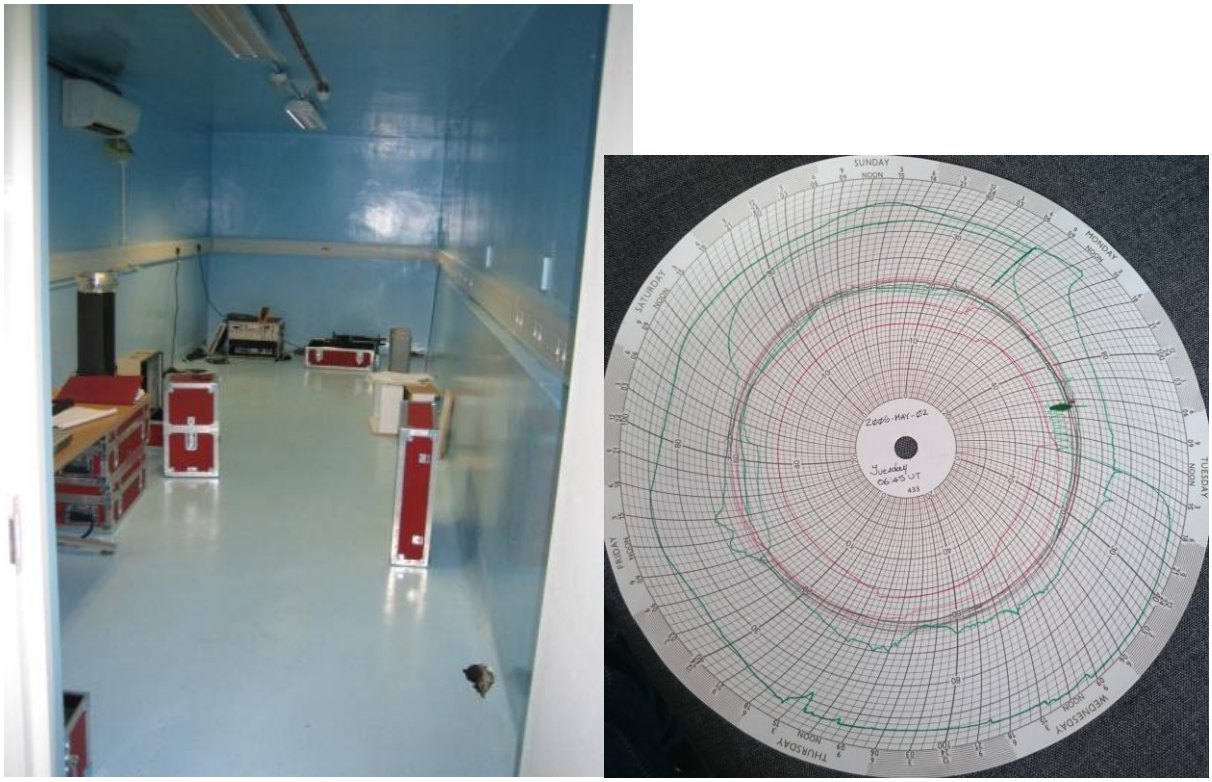

The new gravity laboratory in 2006 with a chart recording, to show temperature and humidity from the period.

Operation Following Completion of the Gravity Laboratory

The first measurement projects which were run in the gravity laboratory suffered a large proportion of failures; on each occasion, the project was automatically stopped by the software due to a displayed error that read: "Time out - check trigger, fringe amplitude or TTL. Guide Error: 3002 Program Stopping". Each failure was accompanied with no discernible variation in the value of g from that obtained from completed projects, and a colossal noise value (500927.9 µGal, for example).

Official installation of the FG5 by the manufacturers (Micro-g LaCoste, based in Colorado, USA) took place in mid May 2006, during which the same synchronisation fault occurred

numerous times. This type of fault can be described such that the dropping chamber rise and fall become out of phase with the expected position of the cart by the computer, i.e. when the computer instructs the cart to drop, and therefore takes a gravity measurement, the cart is actually in the raised position the top of the chamber. Due to the large variance in the observed and calculated fringes, the computer interprets this as a fault and a general error message is shown.

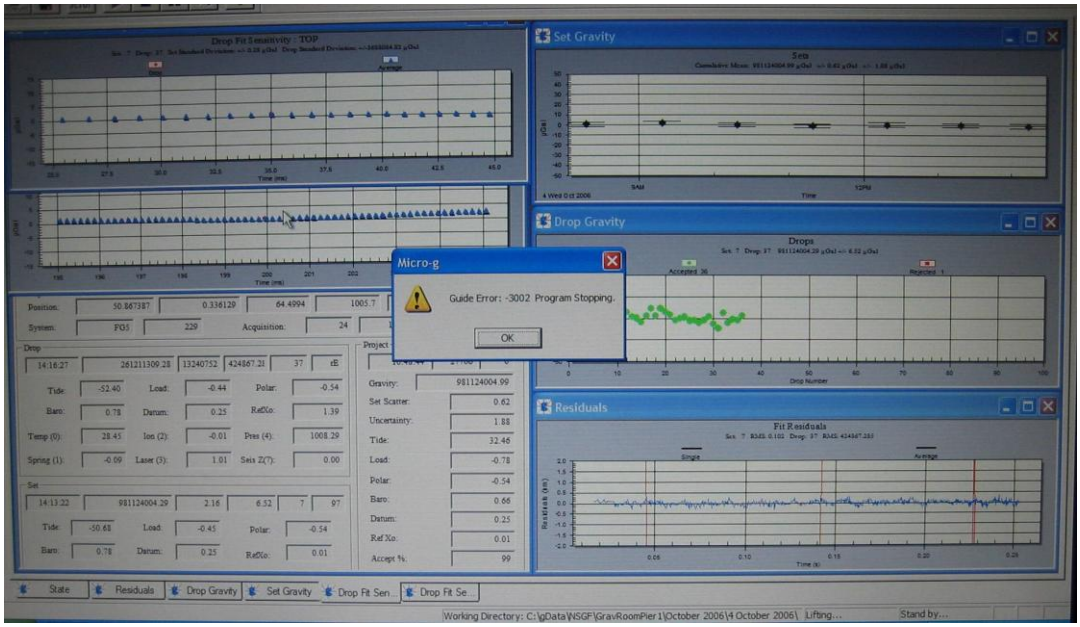

Screen shot of the gravimeter control software ‘g6’.

The fault was diagnosed to be due to the electrical Earth, such that voltage spikes travelling through the earth can ‘jump’ to the Neutral and Live. A demonstrable effect on the FG5 was caused by such equipment as the heater and chart recorder in the room.

In response to the problem Micro-g LaCoste asked for the return of the system interface module of the electronics rack to enable them to increase a pulse width requirement, which would theoretically result in a reduction of susceptibility of the FG5 to ‘spikes’ on the Earth line. However after a validation period of very frequent running to test the new the effect of the alteration in the SIM it was quickly established that this solution had not been successful; the FG5 was still demonstrating the same failure characteristics.

During a gravimeter technical workshop held at Micro-g LaCoste in Colorado, the results from the failed attempts to run the gravimeter were discussed in length with the technical staff. The result included full agreement that the local electrical supply could not be at fault and that some investigative checks should be performed upon the electronics rack. Following this meeting, and with a list of checks to do, the source of the error was found to originate from the SIM. It was traced to a combination of a faulty output signal (trig-out) from the SIM and from new corrosion of the EPROM cards. Micro-g LaCoste responded to the test results with a new SIM, which was installed by Dr D. Van Westrum from Micro-g LaCoste in October 19th 2006, after which the gravimeter operated successfully.

The underlying cause of the synchronisation problem was solved in the FG5X, the software in this variant communicates with the hardware to determine where the cart is before a drop.

Environmental Conditions within the Gravity Laboratory

After installation of a dehumidifier during the conversion of the basement, see Appendix 3, the stability of the temperature and humidity within the gravity laboratory proved to have a seasonal variation. The addition of a heater into the room, in early 2007, resolved the issue and since 2007 the temperature within the laboratory proved to be reasonably stable at 20 ± 2 °C. The chart recorder traces shown in Figure 7.4 from 2007 and 2009 show the stability of the temperature whilst the humidity is seen to be more variable.

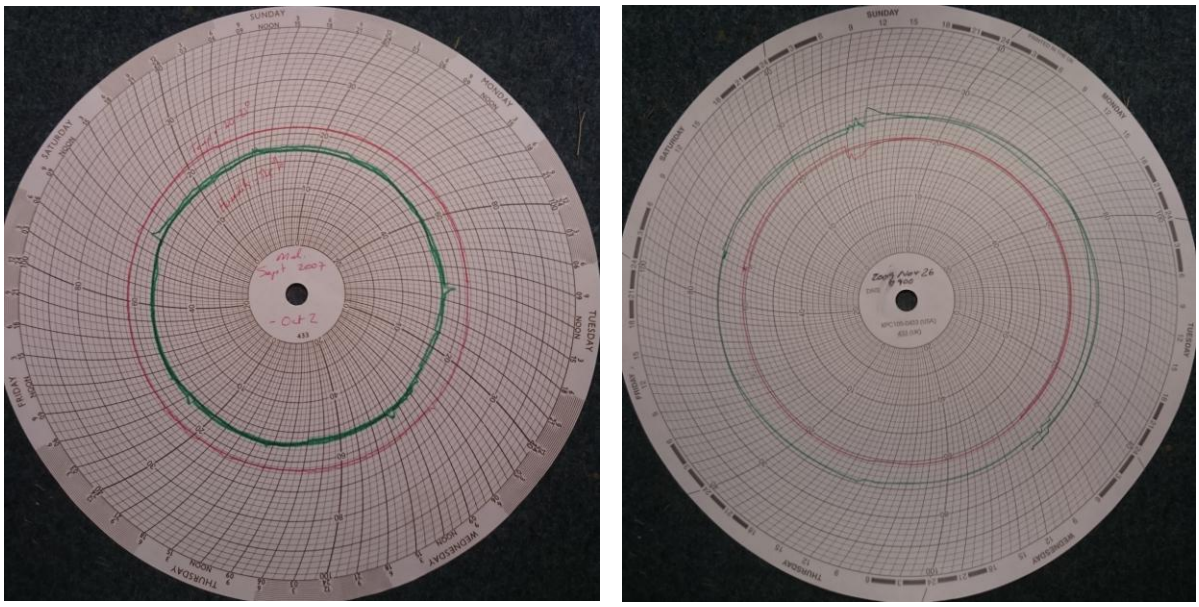

Chart recorder traces from 2007 (left) and 2009 (right) showing the temperature and humidity within the gravity laboratory. Red indicates temperature and green indicates the humidity. In 2007 the temperature is shown to be 20-21 °C with a relative humidity of 54%, whilst in 2009 the temperature was similar whilst the humidity had increased to 70%.

Appendix 8

Discussion of the FG5 Timing Frequency Source

Background

Micro-g Lacoste incorporates a Rubidium 10 MHz clock source into the electronics rack of the FG-5 gravimeter to provide the time interval component of the time distance pairs used in the equation of motion, as discussed in Chapter 2, section 2.3.5.

Rubidium oscillators are known to have good short term stability, making it a good choice for the clock frequency in the gravimeter. However they are also known to have a frequency drift over long time periods and therefore either require calibration, or at least regular checks to ensure the oscillation frequency has not changed.

The rubidium source frequency should be checked in FG5's on a regular basis, and as no two clocks are quite the same some clocks are known to drift faster than others. A fact which is evident when discussing the frequency stability of rubidium clocks used in FG5's with other members of the AG community (i.e. during inter comparisons). Following a frequency measurement the frequency value held within the Micro-g LaCoste 'g' software should be adjusted to ensure it is accurate.

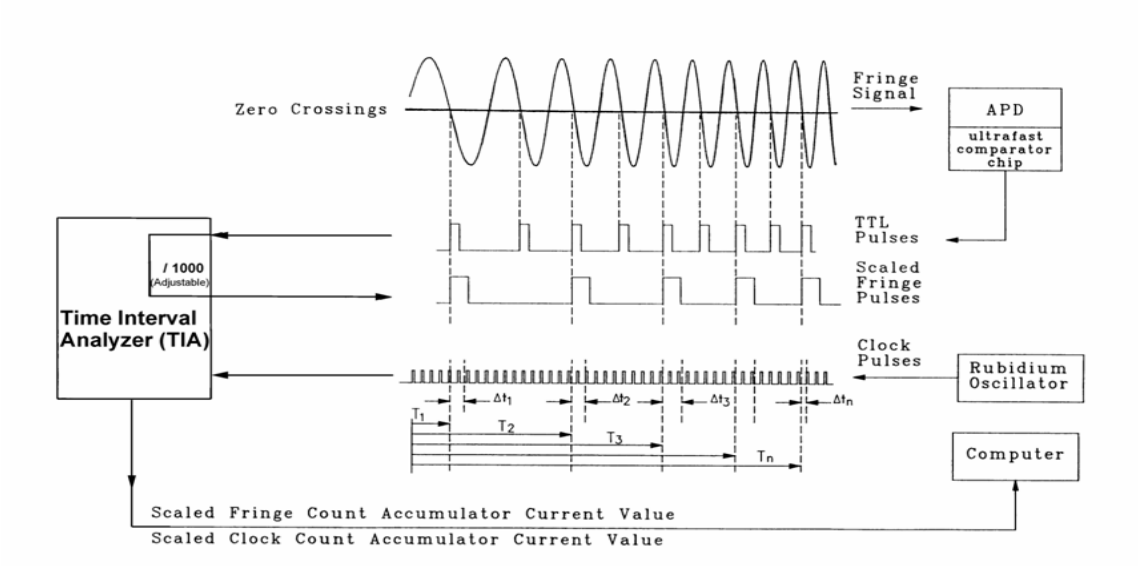

Generation of the time component for the determination of gravity (diagram courtesy of Micro-g LaCoste)

In 2005 Micro-g LaCoste set the frequency of the frequency source in FG5-229 to be 10 MHz, within the 'g' software programme. In 2007 the frequency was measured to be 10,000,000.00385 Hz (no formal uncertainty was provided) by the Czech FG-5 operators during the European Comparison of Absolute Gravimeters (ECAG-2007)* meeting in 2007. The implication of the frequency shift is explored in the next section.

Testing the Frequency

The SGF moved from reliance on the GNSS 10 MHz carrier signal to using the 10 Mhz frequency generated by an active Hydrogen Maser during 2010. The H-Maser has excellent short term stability, 20 femtoseconds per day, and a low long term drift of 50 nanoseconds after 30 days (NERC Space Geodesy Facility, 2016). The maser is situated in the basement of the SGF at the opposite end to the gravimetry room.

Since the maser is in close proximity to the gravimeter a 10 MHz supply was installed into the gravimetry room in 2011. Having access to such a stable frequency source allows the true oscillation frequency of the rubidium clock within the gravimeter to be

* ECAG = European comparison of absolute gravimeters

determined. In addition the gravimeter can be run directly from the maser frequency, adjusting the value within the software, eliminating any error which may be induced by incorrect characterisation of the rubidium frequency.

The rubidium frequency can be maintained at 1 part in 10^{10} with frequent calibration the FG5 instrumental error budget from this effect is 0.2 µgal (Hopewell, 1999) (Niebauer, 1995) , which effectively means that the frequency should be maintained to 1mHz.

Prior to the ECAG meeting of 2011 characterisation of the rubidium was carried out at the SGF. The rubidium clock drift can be measured simply by inputting the two frequency sources into an oscilloscope displaying either;

a) The two 10 MHz sine waves and measuring the time taken for the secondary source to move a full wavelength through the primary, using the maser as the oscilloscope trigger source

   or

b) Using the oscilloscope in X-Y mode, where the result of the two inputs produces a phasing elliptical which sweeps through a ‘zero’, effectively displaying the half wavelength, or half the beat frequency.

Method a) suffers higher probability of measurement error due to the subjective definition of the zero point of the sine wave on the moving peak. Both methods rely knowing which clock is triggering the oscilloscope and whether it is faster or slower that the other clock.

Three sets of testing were conducted in the attempt to characterise the rubidium within the FG5. The first two tests used a fast oscilloscope with one set of tests (three measurements) for either method described above and the third test used the slower oscilloscope supplied in the standard toolkit of the gravimeter. Such that;

- Test 1 - Fast oscilloscope to look at the time taken for the 10 MHz sine wave of the Rubidium clock to travel one full wavelength along the sine wave from the H-Maser (which used as the trigger source).
- Test 2 - Fast oscilloscope in X-Y mode, as above

- Test 3 - Standard oscilloscope also set to X-Y mode

For each test the time (T) was measured with a simple hand triggered stopwatch. Each test consisted of three measurements.

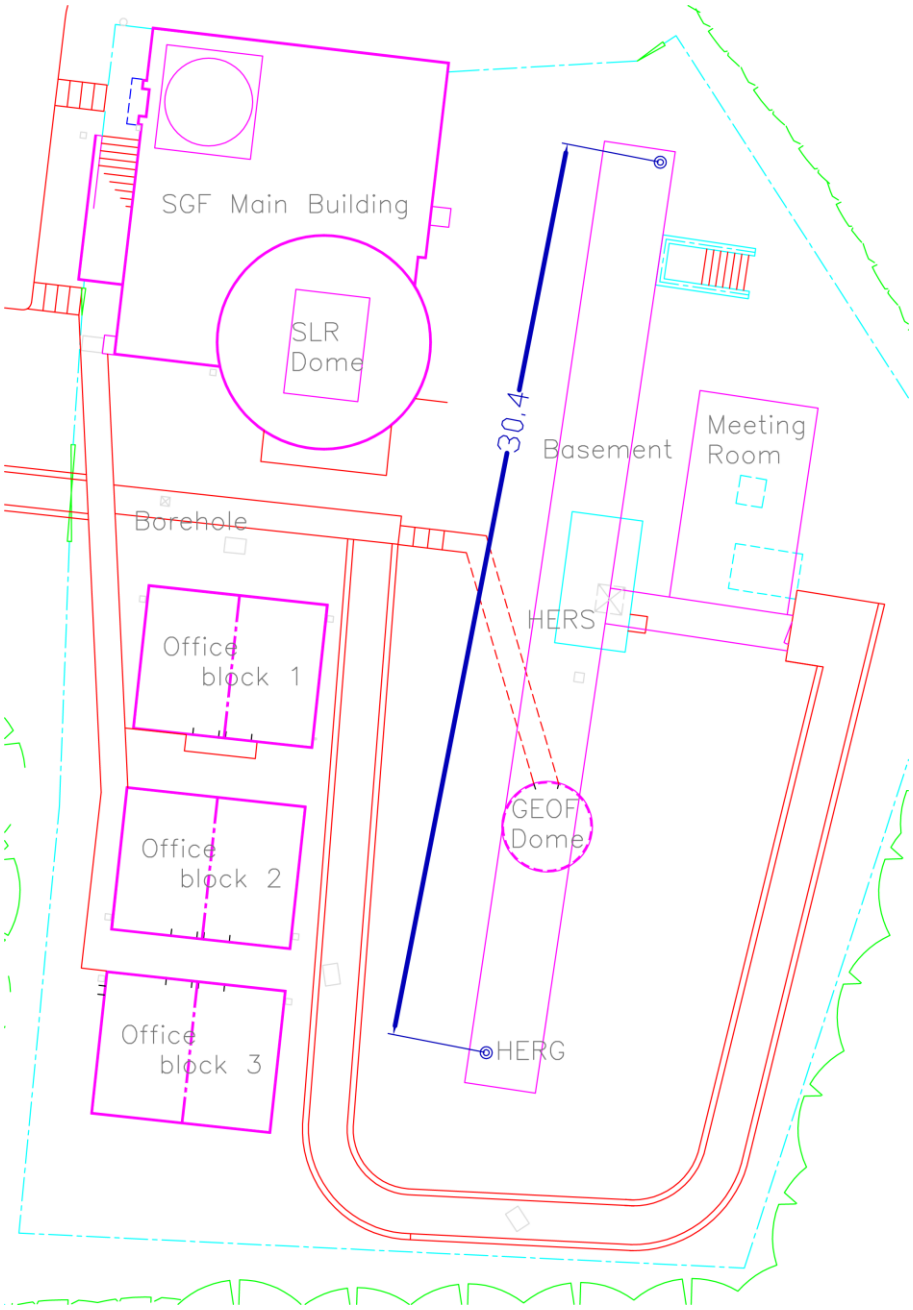

Distance from the primary gravity pier, HERG, to the H-MASER. Drawing courtesy of the SGF.

The frequency change between the clocks, rubidium and maser, is obtained since it is

equal to inverse of the cycle period, which in this case is the time measured between zero crossings on the oscilloscope.

Testing the FG5 clock frequency

	Test 1		Test 2		Test 3	
	Period (s)	Frequency (Hz)	Period (s)	Frequency (Hz)	Period (s)	Frequency (Hz)
Measurement 1	394.6	2.53×10^{-3}	388.4	2.58×10^{-3}	289.8	2.57×10^{-3}
Measurement 2	392.0	2.55×10^{-3}	389.2	2.57×10^{-3}	290.2	2.56×10^{-3}
Measurement 3	392.1	2.55×10^{-3}	387.6	2.59×10^{-3}	390.4	2.56×10^{-3}
Average	392.9	**2.55×10^{-3}**	388.4	**2.58×10^{-3}**	390.1	**2.56×10^{-3}**
Standard Deviation	1.2	7.77×10^{-6}	0.65	4.33×10^{-6}	0.25	1.64×10^{-6}

Therefore for an apparently large (7s) scatter in the average recorded times there is less than 0.03mHz difference in the final frequency. If the average of the three measurements is taken as the difference between the clock sources, and assuming the H-maser is exactly 10 MHz, then the rubidium clock has a frequency offset from the maser of 2.56 mHz ± 4.58 μHz.

As mentioned above, the frequency was determined as having an offset of 3.85 mHz, during ECAG-2007. If we assume the frequency still has the same sign, is above the 10 MHz source, then the change in frequency over 4 years is 1.29 mHz, and if 1 mHz = 0.2 μgal then 1.29 mHz ≈ 0.26 μgal. Thus, although the correction is slightly outside the standard instrumental error budget for the FG5 no correction need be applied to the gravity results between these epochs.

As part of the upgrade of the FG5 into the FG5X a new rubidium clock, therefore the value assigned by Micro-g is assumed to be correct in 2013 (9999999.999167Hz).

The method for determining clock frequency outlined here is not rigorous or the ideal methodology. Ideally the clocks should be tested over a long period and the Allen variance measured.

Bibliography

Agriculture Information Bank, 2015. *Agriculture Information Bank.* [Online] Available at: http://www.agriinfo.in/default.aspx?page=topic&superid=4&topicid=271 [Accessed 16 May 2016].

Altamimi, Z., Rebischung, P., Metivier, L., & Collilieux, X. (2016). ITRF2014: A new release of the International Terrestrial Reference Frame modeling nonlinear station motions. *Journal of Geophysical Research: Solid Earth* , 6109-6131.

Aldiss, D. et al., 2014. *Geological interpretation of current subsidence and uplift in the London area, UK, as shown by high precision satellite-based surveying.* s.l., Elsevier Ltd.

Appleby G.M, G. P. (1999). Achieving and maintaining Sub-cm accuracy for the Herstmonceux single-photon SLR Facility. *Laser, Radar and Atmospheric Lidar Techniques II, SPIE , 3865*, 52-63.

Appleby, G. (1996, October). PhD. *Satellite Laser Ranging and the ETALON Geodetic Satellites* . The University of Aston in Birmingham.

Appleby, G. (1998, October). The UK Satellite Laser Ranging Facility. *Spectrum - Newsletter of the Royal Greenwich Observatory* , pp. 44-48.

G Appleby, et al., (2010). Comparison of Height anomalies determined from SLR, Absolute Gravimetry and GPS with high frequency borehole data at Herstmonceux. In I. A. Symposia, *Gravity, Geoid and Earth Observation* (pp. 107-113). Springer.

Appleby, G., 2016. *Personal communication.* Herstmonceux: s.n.

Appleby, G., Rodriguez, J., & Altamimi, Z. (2016). Assessment of the accuracy of global geodetic satellite laser rangning observations and estimated impact on ITRF scale: estimation of systematic errors in LAGEOS observations 1993-2014. *Journal of Geodesy* , 1-18.

Baker, T., 1984. Tidal deformations of the Earth. *Science Progress (1933-),* 69(274), pp. 197-233.

Baker, T. F. & Bos, M. S., 2003. Validating Earth and ocean tide models using tidal gravity measurements. *Journal of Geophysics,* Volume 152, pp. 468-485.

Breili, K. & Pettersen, B. R., 2009. Effects of surface snow cover on gravimetric observations. *Journal of Geodynamics,* Volume 48, pp. 16-22.

Bilham, R. N. (2016). Changes in absolute gravity 2000-2015, South Island, New Zealand. *New Zealand Journal of Geology and Geophysisc , 59* (1), 176-186.

S. Bonvalot, H. W. (2012). AG Working group meeting IAG Gravity meeting Venice. Verbal

Bos, M. S. H.-G., 2011. *Chalmers free ocean tide loading provider.* [Online]
Available at: http://holt.oso.chalmers.se/loading/index.html
[Accessed Jul 2009].

Boucher, C., Pearlman, M., & Sarti, P. (2015). Global geodetic observatories. *Advances in Space Research* , 24-39.

Charles, K., 1995. *High precision relative and absolute gravity in Britain.* Edinburgh: University of Edinburgh.

CCM and WGG, 2013. *Technical Protocol for the 9th International Comparison of Absolute gravimeters ICAG-2013.* s.l.:s.n.

Comparison of Absolute Gravimeters EURAMET.M.G-K2 Key Comparison and Pilot Study: Technical Protocol. s.l.:s.n.

Consultative Committee on Mass and Related Quantities working group on gravimetry, 2015.

Cook, A. H. (1965). A new absolute determination of the acceleration due to gravity at the national physical laboratory. *Nature* , 279.

Cook, A. (1965). The absolute determination of acceleration due to gravity. *Metrologia* , 84-114.

Darling, D. (2006). *Gravity's Arc.* Hoboken, New Jersey: John Wiley & Sons Inc.

Demoulin, A., Ducarme, B. & Everaerts, M., 2007. Seasonal height change influence in GPS and gravimetric campaign data. *Journal of Geodynamics,* Volume 43, pp. 308-319.

Dolan, G. (2014-15). *The Royal Greenwich Observatory where East meets West.* Retrieved 2014 & 15, from http://www.royalobservatorygreenwich.org/articles.php?article=0

Encylopaedia Britannica. (1976). *The New Encylopaedia Brittanica.* Encylopaedia Britannica.

European Centre for Geodynamics and Seismology, n.d. *The Walferdange Underground Laboratory for Geodynamics.* [Online] [Accessed June 2012].

Faller, J. E. (1967). Precision Measurement of the Acceleration of Gravity. *Science* , 60-67.

Forsberg, ., et al., (2005). The gravity field and GGOS. *Journal of Geodynamics , 40*, 387-393.

Francis, O. & vanDam, T., 2010. *Results of the European Comparison of Absolute gravimeters in Walferdange (Luxembourg) of November 2007. Gravity, Geoid and Earth Observation, Internation Association of Geodesy Symposia* (pp. 31-35). SpringerLink.

Francis, O. et al., 2013. The European Comparison of Absolute Gravimeters 2011 (ECAG-2011) in Waferdange, Luxembourg: results and recommendations. *Metrologia*, pp. 257-268.

Francis, O., Baumann, H. & participants, a., 2014. *International comparison of absolute gravimeters* , s.l.: Metrologia.

Fosberg, R., Sideris, M. G., & Shum, C. K. (2005). The gravity field and GGOS. *Jounal of Geodynamics* , 387-393.

Graham-Smith, F. (1978). *The Royal Greenwich Observatory: Report for the period 1976 October 1 to 1977 September 30.* . London: Royal Astronomy Society, 19, 456.

Harnisch, G. & Harnisch, M., 2006. Hydrological influences in long gravimetric data series. *Journal of Geodynamics,* Volume 41, pp. 276-287.

Hopewell, H. (1999). Environmental and Instrumental Effects on High Precision Graivmetry - A Case Study in Britain. Edinburgh, Great Britain: University of Edinburgh.

Hosmer, G. (1919). *Geodesy, including astronomical observations, Gravity measurements, and method of Least Squares* (First ed.). John Wiley and Sons.

Hwang, C., Cheng, T.-C., Cheng, C. C. & Hung, W. C., 2010. Land subsidence using absolute and relative gravimetry: a case study in central Taiwan. *Survey Review,* 42(315), pp. 27-39.

Imanishi, Y. et al.,, 2006. Effect of underground water on gravity observation at Matsushiro, Japan. *Journal of Geodynamics,* Volume 41, pp. 221-226., 2006. Effect of underground water on gravity observation at Matsushiro, Japan. *Journal of Geodynamics*, Volume 41, pp. 221-226.

International Association of Geodesy, 2015. *Letter to the working groups and steering committes of the CCM and IAG AG users.* s.l.:s.n.
International Laser Ranging Service. (2013). *ILRS*. Retrieved 2014-15, from http://ilrs.gsfc.nasa.gov/about/index.html

International Laser Ranging Service. (1984). Resolution Three. *5th International Workshop on Laser Rangning Instrumentation* (pp. 525-527). International Laser Ranging Service.

Jiang, Z. et al., 2012. *The 8th International comparison of Absolute Gravimeters 2009: the first Key Comparison (CCM.G-K1) in the field of absolute gravimetry.* s.l., IOP Publishing, pp. 666-684.

Kucharski, D. e. (2015). A method to calculate zero-signature satellite laser ranging normal points for millimeter geodesy - a case study with Ajisai. *Planets and Space* , 34-44.

Lambert, A., Courtier, N. & James, T. S., 2006. Long-term monitoring by absolute gravimetry: Tides to post glacial rebound. *Journal of Geodynamics*, Volume 41, pp. 307-317.

Lampitelli, C., et al., (2010). Hydrological effects on gravity and correlations between gravitational variations and level of the Alzetter River at the station of Walferdange, Luxembourg. *Journal of Geodynamics , 49*, 31-38.

Larson, K. M. & van Dam, T., 2000. Measuring postglacial rebound with GPS and absolute gravity. *Geophysical research letters,* 27(23), pp. 3925-3928.

Llubes, M. et al., 2008. Multi-technique monitoring of ocean tide loading in Northern France. *Geoscience,* Volume 340, pp. 379-389.

Longuevergne, L. et al., 2009. Local and global gydrological contributions to gravity variations observed in Strasbourg. *Journal of Geodynamics,* Volume 48, pp. 189-194.

Makinen, J. & Tattari, S., 1990. *Subsurface water and gravity.* Walferdange , Proceedings of the workshop: non tidal gravity changes.

Marson, I. (2012). A short walk along the gravimeters path. *International Journal of Geophysics* .

Marson, I., & Faller, J. E. (1986). g - the acceleration of gravity: its measurement and its importance. *Journal of Physics: Scientific Instruments* .

Marti, U. R. (2014 11-March). CCN-IAG Stategy for Metrology in Absolute Gravimetry. *Role of CCM and IAG* . BIPM.

Meinesz, W. H. (1958). *The Earth and Its Gravity Field.* McGraw-Hill.

Melchior, P., et al., 2005. About time variations of gravity. In: *Selected papers from Vol 32 of Vychislitel'naya Seysmologiya.* s.l.:American Geophysical Union, pp. 198-207.

Meurers, B., Van Camp, M. & Petermans, T., 2007. Correcting superconducting gravity time-series using rainfall modelling at the Vienna and Membach stations and application to Earth tide analysis. *Journal of Geodesy,* Volume 81, pp. 703-712.

Micro-g LaCoste. (2005). FG5 Gravity Meter. *Sales Brochure* . Micro-g LaCoste.

Micro-g LaCoste, 2005. *FG5 Gravity Meter.* s.l.:Micro-g LaCoste.

Micro-g LaCoste. (2006 July). *g6Help manual*. Colorado, U.S.A.

Micro-g LaCoste. (2006). The FG5 Absolute Gravimeter (Presentation). *FG5 Absolute Gravimeter* .

Micro-g LaCoste, 2007. *Micro-g LaCoste FG5 Manual 2007.* [Online]
Available at: http://www.microglacoste.com/pdf/FG5Manual2007.pdf
[Accessed 2010].

Micro-g LaCoste, 2013. *Introducing the FG5-X,* s.l.: Micro-g LaCoste.

Micro-g LaCoste. (2014 3-November). *Introducing the FG5-X.* Retrieved 2015 10-April from Micro-g LaCoste FG5-X Absolute Gravimeter: http://www.microglacoste.com/pdf/Brochure-FG5-X.pdf

Micro-g LaCoste, 2014. *gPhone Gravity Meter Brochure.* s.l.:Micro-g LaCoste.
NERC, 2015. *National TIdal and Sea Level Facility (NTSLF) format.* [Online]
Available at: https://www.bodc.ac.uk/data/codes_and_formats/sea_level/ntslf_format/
[Accessed August 2015].

Nagornyi, V., 1995. A new approach to absolute gravimeter analysis. *Metrolgia,* Volume 32, pp. 201-208.

Naujoks, M. et al., 2010. Evaluating local hydrological modelling by temporal gravity observations and a gravimetric three-dimensional model. *Geophysical Journal International,* Volume 182, pp. 233-249.

NERC Space Geodesy Facility, 2016. *Keeping Accurate Time.* [Online]
Available at: http://sgf.rgo.ac.uk/work/timing.html
[Accessed 1st June 2016].

Nicolas, J., Nocquet, J.-M., Van Camp, M., van Dam, T., Boy, J.-P., Hinderer, J., et al. (2006). Seasonal effect on vertical positioning by SLR and GPS and on AB at the OCA geodetic station, Grasse, Fance. *Journal of Geophysics* , 1127-1137.

Niebauer, T. M., Hoskins, J. K., & Faller, J. E. (1986). Absolute gravity: A reconnaissance tool for studying vertical crustal motions. *Journal of Geophysical research , 91* (89), 9145-9149.

Niebauer, T. M, Sasagawa, G.S., Faller, J.E., Hilt, R., Klopping, F. (1995). A new generation of absolute gravimeters. *Metrologia* , 159-180.

Niebauer, T. M., Billson, R., Ellis, B., Mason, B., van Westrum, D., Klopping, F. (2011). Simultaneous gravity and gradient measurements from a recoil-compensated absolute gravimeter. *Metrologia ,* 154-163.

Niebauer, T. M. et al., 2013. The self-attraction correction for the FG5X asbolute gravity meter. *Metrologia,* Volume 50, pp. 1-8.

NOAA, 2013. *NOAA tides and currents.* [Online]
Available at: http://tidesandcurrents.noaa.gov/harcon.html?id=9410170 [Accessed 28 Aug2016].

Ophaug, V. et al., 2016. *Absolute gravity observatins in Norway (1993-2014) for glacial isostatic adjustment studies: The influence of gravitational loading effects on secular gravity trends.* [Online]
Available at: http://www.sciencedirect.com/science/article/pii/S0264370716300722
[Accessed 2 October 2016].

Palinkas, V., Francsi, O., Val'ko, M. & participants, a., 2015. *Draft A, V02 Regional comparison of absolute gravimeters. EURAMET.M.G-K2 Kay Comparison and Pilot Study*

Penna, N. T., Bos, M. S., Baker, T. F. & Scherneck, H. G., 2008. Assessing the accuracy of predicted ocean tide loading displacement values. *Journal of Geodesy,* 82(12), pp. 893-907.
Pfeffer, J. et al., 2011. Local and global hydrological contributions to time-variable gravity in Southwest Niger. *Geophysical Journal International,* Volume 184, pp. 661-672.

Plag, H. P., & Pearlman, M. (2009). *Global geodetic observing system: meeting the requirements of a global society on a changing planet in 2020* . Berlin: Springer-Verlag
Plag, H.P., (2009). The Global Geodetic Observing System. *Solid Earth,* 13(Advances in Geosciences), pp. 105-127.

Planet Earth Online. (2009). Space Geodesy Facility locates satellite in lunar orbit. NERC.

Potter, C., Appleby, G., Sherwood, R., (2010). Volcanic Ash Plume Detected over SGF Site, Herstmonceux. NERC SGF.

Richter,B., et al. (2004). Long-term crustal deformation monitored by gravity and space techniques at Medicina, Italy and Wettzell, Germany. *Journal of Geodynamics , 38,* 281-292.

Robertsson, L., Francis, O., vanDam, T. & Faller, J., 2001. Results of the Fifth International Comparison of Absolute Gravimeters ICAG97. *Metrologia,* Volume 38, pp. 71-78.

Robertsson, L., 2007. On the diffraction correction in absolute gravimetry. *Metrologia,* Volume 44, pp. 35-39.

Romagnoli, C., et al., (2003). Influence of soil consolidation and thermal expansion effects on height and gravity variations. *Journal of Geodynamics , 35,* 521-539.

Ruess, D. U. C., 2011. 20 years of international comparison of absolute gravimeters (ICAG) at the Bureau International des Poids et Mesures (BIPM)in Paris with participation of the BEW. *Vermessung & Geoinformation* , pp. 154-161.

Sasagawa, G. S. (1995). Intracomparison tests of the FG5 absolute gravity meters. *Geophysical research letters* , 461-464.

Sato, T. et al., 2012. Gravity and uplift rates observed in southeast Alaska and their comparison with GIA model predictions. *Journal of Geophysical Research; Solid Earth,* Volume 117, p. B01401.

Smith, A. B., Walker, J. P. & Western, A. W., 2006. *Detection of a soil moisture and groundwater signal in ground-based gravity observations.* Hobart, TAS, 30th Hydrology and Water resources Symposium.

Schmerge, D.,. et al., 2012. Results of the first North American comparison of absolute gravimeters, NACAG-2010. *Journal of Geodesy,* pp. 591-596.

Schultz, B. (2007). *Gravity from the ground up* (Fourth ed.). Cambridge Unversity Press.

Seismology, E. C. (n.d.). *Underground Laboratory*. Retrieved June 2012

Sugihara, M., 2003. *Geothermal reservoir monitoring with absolute gravimetry.*

Sapporo, Japan, Springer Berlin Heidelberg, pp. 571-575.

Taylor, C., 1997. *Measuring absolute gravity.* Liverpool: Unknown.

Teferle, F. N. et al., 2007. Sea Level in the British Isles: Combining Absolute Gravimetry and Continuous GPS to Infer Vertical Land Movements at Tide Gauges. *International Association of Geodesy Symposia,* Volume 130, pp. 23-30.

Terferle, F.N. et al., (2009). Crustal motions in Great Britain: evidence from continuous GPS, absolute gravity and Holocene sea level data. *Geophysical Journal International , 178*, 23-46.

The Royal Horticultural Society, 2016. *Clay soils advice webpage.* [Online]
Available at: https://www.rhs.org.uk/advice/profile?PID=620
[Accessed 10 August 2016].

Timmen, L. (2010). Absolute and Relative Gravimetry. In *Sciences of Geodesy - I* (pp. 1-48). Springer-Verlag Berlin Heidelberg.

Timmen, L., Engfeldt, A. & Scherneck, H. G., 2015. Observed secular gravity trend at Onsala station with the FG5 gravimeter from Hannover. *Journal of Geodetic Science,* 5(1), pp. 18-25.

Torge, W. (1991). *Geodesy* (Third ed.). Hannover: Walter de Gruyter Gmbh & Co.

Torge, W. (1989). *Gravimetry.* Berlin: Walter de Gruyter & Co.
University of Luxembourg, 2015. *Moving to Belval.* s.l., University of Luxembourg.

Van Camp, M., et al.,T. C. (2003). The FG5 absolute gravimeter: metrology and geophysics. *Physicalia Magazine, Journal of the Belgian Society , 25* (3), 161-174.

Van Camp, M., 2003. *Efficiency of tidal corrections on absolute gravity measurements at the Membach station.* [Online]
Available at: http://homepage.oma.be/mvc/pdf/ECGS_22_Efficiency_Tides.pdf
[Accessed Feb 2014].

Van Camp, M., Williams, S. D. & Francis, O., 2005. Uncertainty of absolute gravity measurements. *Journal of Geophysical Research,* 110(B05406).

Van Camp, M., et al., (2006). Hydrogeological investigations at the Membach station, Belgiu, and application to correct long periodic gravity variations. *Journal of Geophysical Research , 111*.
Van Camp, M. et al., 2006. Karst aquifer investigation using absolute gravity. *EOS,* 87(30).

Van Camp, M. (2009). COST 0701 AG working group Brussels .

van Westrum, D., 2012. *Pers. Comms.* s.l.:email.

van Westrum. D,et al., 2013. The diffraction correction for absolute gravimeters. *Metrologia,* pp. 35-49.

Vitushkin, L. et al., 2002. Results of the Sixth International Comparison of Absolute Gravimeters, ICAG-2001. *Metrologia,* Volume 39, pp. 407-424.

Walker, R., 2016. *simetric.* [Online]
Available at: http://www.simetric.co.uk/si_materials.htm
[Accessed 3 4 2016].

Williams, S D P., Baker, T. (2001). Absolute Gravity Measurements at UK Tide Gauges. *Geophysical Research Letters , 28* (12), 2317-2320.

Williams, S., 2001. *Effect of Rubidium Clock Drift on the value of "g",* s.l.: s.n.

Williams, S., 2006. *Gravity Difference Between FG5-103 and FG5-222,* s.l.: s.n.

Williams, S., 2009. *Personal Communication.* Liverpool: s.n.

Wilkins, G. (2009). *A personal history of the Royal Greenwich Observatory at Herstmonceux Castle, 1948-1990.* Retrieved from University of Cambridge, Cambridge University Library: http://www.lib.cam.ac.uk/deptserv/manuscripts/RGO_history/

Wilson, E., Unknown. *Environmental Hydrology 302 Lecture 8 Notes, More Porosity, Specific Yield and Specific Retention.* [Online]
Available at: http://www2.nau.edu/~doetqp-p/courses/env302/lec8/LEC8.html
[Accessed 5 September 2016].

Winters Electro-Optics Inc. (2004). *Model WEO-100 Laser.* Retrieved 2016 11-May from Winters Electro-Optics Products Model 100 Laser: www.winterseo.com/m100.html

Winters Electro-Optics, I. (2000). Model 100 Iodine-stabilized HeNe Laser Operator's Manual. Longmont, Colorado, U.S.A.: Winters Electro-Optics, Inc.

Zerbini, S. et al., 2002. Multi-parameter continuous observations to detect ground deformation and to study environmental variability impacts. *Global and Planetary Change*, Volume 34, pp. 37-58.